


Spring August 2014

Molecular Engineering Strategies for the Design and Synthesis of New Organic Photovoltaic Materials

Paul J. Homnick
University of Massachusetts - Amherst

Follow this and additional works at: https://scholarworks.umass.edu/dissertations_2

 Part of the [Materials Chemistry Commons](#), [Organic Chemistry Commons](#), [Physical Chemistry Commons](#), [Polymer and Organic Materials Commons](#), and the [Semiconductor and Optical Materials Commons](#)

Recommended Citation

Homnick, Paul J., "Molecular Engineering Strategies for the Design and Synthesis of New Organic Photovoltaic Materials" (2014). *Doctoral Dissertations*. 95.
<https://doi.org/10.7275/ke5d-9w86> https://scholarworks.umass.edu/dissertations_2/95

This Open Access Dissertation is brought to you for free and open access by the Dissertations and Theses at ScholarWorks@UMass Amherst. It has been accepted for inclusion in Doctoral Dissertations by an authorized administrator of ScholarWorks@UMass Amherst. For more information, please contact scholarworks@library.umass.edu.

**MOLECULAR ENGINEERING STRATEGIES FOR THE DESIGN AND SYNTHESIS
OF NEW ORGANIC PHOTOVOLTAIC MATERIALS**

A Dissertation Presented

by

PAUL J. HOMNICK

Submitted to the Graduate School of the
University of Massachusetts Amherst in partial fulfillment
of the requirements for the degree of

DOCTOR OF PHILOSOPHY

May 2014

Department of Chemistry

© Copyright by Paul J. Homnick 2014

All Rights Reserved

**MOLECULAR ENGINEERING STRATEGIES FOR THE DESIGN AND SYNTHESIS
OF NEW ORGANIC PHOTOVOLTAIC MATERIALS**

A Dissertation Presented

by

PAUL J. HOMNICK

Approved as to style and content by:

Paul M. Lahti, Chair

Dhandapani Venkataraman, Member

Michael D. Barnes, Member

E. Bryan Coughlin, Member

Craig T. Martin, Department Head
Department of Chemistry

DEDICATION

To my wife Katie, and to my friends, family, and mentors. Thank you for providing me with so much love, support, and inspiration.

ACKNOWLEDGMENTS

I would like to thank my advisor, Professor Paul M. Lahti, for his encouragement and mentorship over the past few years. Thank you also to my committee members, Professors Dhandapani Venkataraman, Mike Barnes, and E. Bryan Coughlin, for their insight and guidance. Professor Lahti and my committee were instrumental in my technical and intellectual development, and I am very grateful for all that they have done for me.

I would also like to thank my collaborators and colleagues who have contributed so much to my work: Dr. Akshay Kokil and Professor Jayant Kumar at UMass Lowell for their work on dye sensitized solar cells and squaraine-related devices; Professor Sankaran Thayumanavan, Dr. Andrea Della Pelle, Youngju Bae, and Ambata Poe for inviting me onto their squaraine dye development project; Dr. Supravat Karak for his exciting solar cell work using some of my compounds; Professor Alex Briseño from UMass PS&E for teaching me chemical vapor deposition and single-crystal field effect transistor fabrication techniques; Professor Vincent Meunier and Dr. Eduardo Cruz at RPI for their computational contributions; Dr. John Schleuter, Professor Joel Mague, Dr. Rafael Cassaro, and Professor DV for contributing their XRD crystallography skills and expertise; Dr. J. Matthew Chudomel, Jeff Lucas, Jon Tinkham, Tim Gehan, and other Lahti Group members past and present for their help and camaraderie.

I am also grateful for my financial assistance. My work was supported as part of Polymer-Based Materials for Harvesting Solar Energy (PHaSE), an Energy Frontier Research Center funded by the U.S. Department of Energy, Office of Basic Energy Sciences under Award Number DE-SC0001087. Working within PHaSE was an amazing experience, and I am grateful for all of the opportunities and fruitful collaborations I was provided as a PHaSE member.

Finally, thank you to my wife Katie and to all of my UMass friends. My time at UMass was a lot of fun. Thank you for all the great memories.

ABSTRACT

MOLECULAR ENGINEERING STRATEGIES FOR THE DESIGN AND SYNTHESIS OF NEW ORGANIC PHOTOVOLTAIC MATERIALS

MAY 2014

PAUL J. HOMNICK, B.S., UNIVERSITY OF SCRANTON

M.A., UNIVERSITY OF SCRANTON

Ph.D., UNIVERSITY OF MASSACHUSETTS AMHERST

Directed by: Professor Paul M. Lahti

Dramatic improvements in organic photovoltaic device efficiency can be obtained by optimizing spectral absorbance and frontier molecular orbital (FMO) energies, increasing solid state exciton/charge mobility, and utilizing p-/n-type nanoarchitecture. Combining all of these properties into a new material presents a considerable synthetic challenge because potential commercial applications require materials that are high-performance *and* inexpensive. Thus, it is advantageous to design new materials using a versatile, modular synthetic approach that allows *each* design criterion to be engineered *individually*, in a synthetically efficient manner.

Several strategies were successfully pursued using simple interchangeable electron donor and acceptor components as functional modules, which provided various donor-acceptor chromophores in a synthetically straightforward manner. This approach provided broad functional tunability to the range of materials produced and, as a result, various molecular engineering requirements were systematically addressed. In some cases, these materials were utilized in photovoltaic devices as p-type active layers or redox enhancement additives. In these cases, competitive power conversion efficiencies were obtained or test device performance was considerably enhanced by comparison to control devices.

Fluorenone, fluorenylidene-malononitrile, and squaric acid were utilized as electron acceptor modules, and electron donor module strength was varied using a styrene-based and several di- and triarylamine-based components.



One strategy, published in *Phys. Chem. Chem. Phys.*, (Chapter 2, [DOI-10.1039/C2CP41813D](https://doi.org/10.1039/C2CP41813D)) is to fix the donor-acceptor lowest unoccupied molecular orbital energy using the synthetically versatile fluorenone module. Fluorenone was chosen because of its ready availability and synthetic versatility, and its multiple functionalization sites allow for *selective* FMO engineering. Extrapolation of this approach was published in *J. Phys. Chem. A.* (Chapter 3, [DOI-10.1021/jp407854r](https://doi.org/10.1021/jp407854r)), describing various fluorenylidene-malononitrile derivatives. Chemical oxidation of fluorenone-based triarylamines to produce stable radicals was published in *Tetrahedron Letters* (Chapter 4, [DOI-10.1016/j.tetlet.2012.10.060](https://doi.org/10.1016/j.tetlet.2012.10.060)).

Fluorenone derivatives applied as dye sensitized solar cell redox system enhancement additives was described in *RSC Advances* (Chapter 5, [DOI-10.1039/C3RA40986D](https://doi.org/10.1039/C3RA40986D)). Development of new, functionalized, squaraine-based materials was described in *J. Phys. Chem. C.* (Chapter 6, [DOI-10.1021/jp410362d](https://doi.org/10.1021/jp410362d)) and was extrapolated for use in single-heterojunction photovoltaic cells having 4.8% maximum power conversion efficiency.

The fundamental insights provided by these findings will be valuable for developing new high-performance photovoltaic materials in the future.

TABLE OF CONTENTS

	Page
ACKNOWLEDGMENTS	v
ABSTRACT.....	vi
LIST OF TABLES	xi
LIST OF FIGURES	xii
LIST OF SCHEMES.....	xviii
CHAPTER	
1. GENERAL BACKGROUND AND MOLECULAR DESIGN STRATEGIES.....	1
1.1 Introduction.....	1
1.2 General OPV Operating Principles and Historical Context.....	3
1.3 Molecular Design Requirements and Donor-Acceptor Architecture.....	7
1.4 π -Conjugation	10
1.5 Molecular Design Strategy	13
1.6 References.....	15
2. DIARYLAMINOFLUORENONE PUSH-PULL MOLECULES.....	19
2.1 Introduction.....	19
2.2 Experimental Methods	21
2.3 Results and Discussion	23
2.3.1 Solution Electronic Spectroscopy for D-A Systems	23
2.3.2 Solution Electronic Spectroscopy for D-A-D Systems	27
2.3.3 Comparative Amino Substituent Effects on Fluorenone Acceptors	31
2.3.4 Solid State Absorption Spectroscopy.....	33
2.3.5 Electrochemistry	35
2.3.6 Modular Analysis of Donor Group Tuning of Push-Pull Molecule FMO Energies.....	38
2.3.7 Time Resolved Photoluminescence Spectroscopy for Selected Push- Pull Systems.....	42
2.4 Conclusions.....	43
2.5 References.....	45
3. ENGINEERING FRONTIER ENERGY LEVELS IN DONOR-ACCEPTOR FLUOREN-9-YLIDENE MALONONITRILES VERSUS FLUORENONES	49
3.1 Introduction.....	49
3.2 Background.....	50
3.3 Experimental Methods	52
3.4 Results and Discussion	52

3.4.1 Energy levels of electronic donor and acceptor structural modules.....	53
3.4.2 Monosubstituted D-A type dipolar systems	57
3.4.3 Disubstituted D-A-D dipolar systems	63
3.4.4 Modular electronic analysis of the dipolar molecules.....	65
3.4.5 Strengthening absorption by a connectivity change.....	69
3.5 Conclusions.....	72
3.7 References.....	74
4. RADICAL CATIONS FROM DIARYLAMINO-SUBSTITUTED FLUORENONES	79
4.1 Introduction and Background	79
4.2 Experimental Methods	80
4.3 Results and Discussion	81
4.3.1 Mono(diarylamino)fluorenone oxidations	81
4.3.2 Multiple oxidation steps in FOBDAA	86
4.3.3 Comparisons to other conjugated aminium cation systems	89
4.4 A Radical Cation from an Amine-Substituted Fluorenylidene Malononitrile	91
4.5 Conclusions.....	92
4.6 Acknowledgements.....	92
4.7 References.....	93
5. FLUORENONE-BASED DONOR-ACCEPTOR MOLECULES THAT ENHANCE DYE SENSITIZED SOLAR CELL PERFORMANCE.....	96
5.1 Introduction.....	96
5.2 Background.....	97
5.3 Results and Discussion	100
5.4 Conclusions.....	104
5.5 References.....	105
6. MOLECULAR ENGINEERING OF SQUARAIN-BASED DONOR- ACCEPTOR COMPOUNDS FOR ORGANIC PHOTOVOLTAIC DEVICES.....	107
6.1 Introduction.....	107
6.2 Background.....	108
6.3 Results and Discussion	109
6.3.1 Molecular Design and Synthetic Procedure.....	109
6.3.2 Optoelectronic Properties.....	110
6.3.3 Electrochemical Properties	111
6.4 Summary of Squaraine Dye Physical Chemistry.....	112
6.5 SQ-OH:PC ₇₁ BM BHJ Solar Cell Results.....	113
6.6 Conclusions.....	116
6.7 References.....	117

7. ORGANIC PHOTOVOLTAIC DEVICES USING FMBDAA36 AS A MOLECULAR LOW BAND GAP HOLE TRANSPORTING MATERIAL	120
7.1 Introduction.....	120
7.2 Results and Discussion – FMBDAA36:PC ₇₁ BM BHJ Solar Cells	122
7.3 Conclusions.....	124
7.4 References.....	125
8. FUTURE WORK: π -MACROCYCLES, INDIGO-BASED MATERIALS, AND PANCHROMATIC A-D-A' CHROMOPHORE ENGINEERING	126
8.1 Introduction.....	126
8.2 Preliminary and Proposed Development of Fused Aromatic π -Macrocycles as Self-Assembling Push-Pull Chromophores	127
8.2.1 Background Information for Truxene- and Heterotriangulene-Based π - Macrocycles	128
8.2.2 Molecular Design and Preliminary Work	129
8.2.3 Highly Structurally Tunable π -Macrocycles via Soluble Synthetic Intermediates.....	133
8.3 Proposed Development of Indigo-Based Organic Electronic Materials	137
8.3.1 Experimental Plan and Expectations for Indigo-Based Materials.....	140
8.4 Panchromatic Materials Design	142
8.4.1 Proposed Physical Chemical Model for Panchromatic Absorption Behavior.....	145
8.5 Concluding Remarks.....	147
8.6 References.....	148
9. EXPERIMENTAL AND SYNTHETIC PROCUEDURES	155
9.1 Materials, Abbreviations, Instrumentation, Computational Methods.....	155
9.2 Triarylamine Oxidation Experiments	158
9.3 Field Effect Transistors (FET - Thin Film, Spin-Cast).....	158
9.4 Chemical Vapor Deposition (CVD).....	159
9.5 General Synthetic and Purification Procedures	160
9.6 Specific Synthetic and Purification Procedures	163
9.7 Acknowledgements.....	205
9.8 References.....	206
10. SUPPLEMENTARY DATA	209
10.1 Crystallographic Data	209
10.2 ¹ H-NMR Spectrum for FODAAS.....	221
BIBLIOGRAPHY	222

LIST OF TABLES

Table	Page
2.1: Optical and oxidation properties of fluorenone-diarylamine D-A molecules.....	25
2.2: Absorption solvatochromism from hexanes to acetonitrile, emission Stokes shifts and solvatochromism from hexanes to acetonitrile, in meV.	26
2.3: Solution and neat film band gap onset comparisons.....	34
2.4: Computed ground state dipole moments.....	41
2.5: Fluorescence lifetimes of BDAAFO, DAAFO, and DAAFOV in hexanes, and OFOPV and NB in chloroform.	43
3.1: Redox potentials and HOMO/LUMO energies of donor-acceptor molecules.....	55
3.2: Absorption spectra maxima of donor-acceptor molecules in low versus high polarity solvents.	57
3.3: Solvatochromism data for donor-acceptor molecules, taken in hexane, diethyl ether, and acetonitrile. Solvatochromic shifts reported in meV.....	62
3.4: Frontier molecular orbital energy variations for donor-acceptor molecules.....	68
3.5: Average FMO energy for FO- and FM-based compounds versus their component donor and acceptor modules' FMO energies, obtained by averaging ΔE_{HOMO} and ΔE_{LUMO} values for each FO- or FM-set from Table 3.4. FMO energy variations are the standard deviations of these sets.	69
3.6: TDDFT B3LYP 6-31G(d,p) predicted band positions and oscillator strengths for FO- and FMBDAA 2,7- and 3,6-derivatives using Gaussian 09.	70
4.1: Spectral and electrochemical characteristics of radical cations and dications.....	82
7.1: FMBDAA36:PC ₇₁ BM ratio optimization and OPV device performance results.	124
9.1: Abbreviations for solvents and reagents used in this chapter.	157

LIST OF FIGURES

Figure	Page
1.1: Solar flux as a function of wavelength (bottom axis) and energy in electron volts (top axis).....	2
1.2: Left, generic bilayer p-n heterojunction solar cell diagram showing the main photovoltaic processes. A, light absorption to create an exciton. B, exciton migration to the p-n junction. C, exciton dissociation at the p/n junction into a hole/electron pair in the p- and n-type materials, and charge migration to the anode and cathode, respectively. D, charge collection at the electrodes, current generated. Right, the same process depicted using an energy level diagram.	4
1.3: Bicontinuous p/n bulk heterojunction with interspersed p- and n-type materials and hole/electron percolation pathways.....	5
1.4: NREL record solar cell efficiency evolution up to 2/25/2014. “Emerging PV” (red) are mostly organic-based solar cells, most notably including dye-sensitized solar cells (DSSCs), perovskite cells, and organic bilayer and bulk heterojunction cells. At present, this chart is periodically updated at www.nrel.gov/ncpv/images/efficiency_chart.jpg	7
1.5: Energy level alignment requirements for a typical BHJ solar cell using PC ₇₁ BM as the n-type material with an indium tin oxide (ITO) anode and an aluminum cathode.....	8
1.6: Perturbation theory model for the modular construction of push-pull system (D-A) frontier molecular orbitals, using generic acceptor modules A, A ₁ , and A ₂ with different donor modules D, D ₁ , and D ₂	9
1.7: Energy level splitting with increasing π -conjugation length, starting at n π -bonds. ΔE decreases with concomitant absorption red-shift, but $\Delta E = 0$ is never reached.....	11
1.8: (1) Potential energy wells depicting the aromatic stabilization energy of the phenyl system versus the quinonal system shown in (2). (3) Polythiophene versus polyacetylene, the latter shown in a topologically-locked conformation for comparison.....	12
1.9: Some fused/linked conjugated systems.	13

2.1: Syntheses of FOCz, FODPA, and FODAA: (a) (<i>p</i> -MeOPh) ₂ NH, 0.02 eq Pd ₂ dba ₃ , P(<i>t</i> -Bu) ₃ , <i>t</i> -BuONa, Δ 2 days for FODAA (70%); (b) Ph ₂ NH, 0.02 eq Pd ₂ dba ₃ , P(<i>t</i> -Bu) ₃ , <i>t</i> -BuONa, Δ 1 h for FODPA (66%); (c) carbazole, 0.02 eq Pd ₂ dba ₃ , P(<i>t</i> -Bu) ₃ , <i>t</i> -BuONa, Δ 1 h for FOCz (51%); (d) I ₂ /KIO ₃ /H ₂ SO ₄ /HOAc, 90 °C, 2 h for 2-bromo-7-iodofluorene (68%); (e) 2.5 eq CrO ₃ , Ac ₂ O, 16 h for 2-bromo-7-iodofluorenone (97%); (f) 3,4,5-tri-MeOPh-CH=CH ₂ , 0.07 eq Pd(OAc) ₂ , 0.2 eq P(<i>o</i> -tolyl) ₃ , DMF, Δ 3 days for 7-BrFOS (44%); (g) (<i>p</i> -MeOPh) ₂ NH, 0.02 eq Pd ₂ dba ₃ , P(<i>t</i> -Bu) ₃ , <i>t</i> -BuONa, Δ 5 h for FODAAS (33%); (h) (<i>p</i> -MeOPh) ₂ NH, 0.02 eq Pd ₂ dba ₃ , P(<i>t</i> -Bu) ₃ , NaO- <i>t</i> -Bu, Δ for FOBDAAS (50%); (i) <i>N</i> -(3,4,5-trimethoxy-Ph)- <i>N</i> -(<i>p</i> -MeOPh)NH, 0.02 eq Pd ₂ dba ₃ , P(<i>t</i> -Bu) ₃ , <i>t</i> -BuONa, Δ 17 h for FOBTMPMPA (21%). (j) 3,4,5-tri-MeOPh-CH=CH ₂ , 0.92 eq <i>p</i> -bromobenzaldehyde, 0.07 eq Pd(OAc) ₂ , 0.2 eq P(<i>o</i> -tolyl) ₃ , DMF, Δ 3 days for SPhCHO (61%); (k) SPhCHO, 1.3 eq PPh ₃ CH ₃ Br, 1.5 eq <i>n</i> -BuLi, THF, 0-26 °C, overnight for SPV (66%). (l) SPV, 0.07 eq Pd(OAc) ₂ , 0.2 eq P(<i>o</i> -tolyl) ₃ , DMF, Δ 3 days for FODPVS (24%).	22
2.2: Absorption spectra of FODAA (black), FODPA (red), FOCz (blue) in hexane (left charts) and in acetonitrile (right charts).	23
2.3: Normalized emission spectra of FODAA (black line, excited at 355 nm), FODPA (red line, excited at 475 nm), and FOCz (blue line, excited at 289 nm) in hexane; and FODPA (red dots, excited at 500 nm) and FOCz (blue dots, excited at 289 nm) in acetonitrile. FODAA does not emit detectably in acetonitrile.	27
2.4: Absorption spectra of FODAAS (black), FOBDAAS (red), and FOBTMPMPA (blue) in hexanes (upper chart) and acetonitrile (lower chart).	29
2.5: Normalized emission spectra of FODAAS (excited at 545 nm), FOBDAAS (excited at 590 nm), and FOBTMPMPA (excited at 550) in hexane.	29
2.6: FODS and FODPVS absorption spectra in acetonitrile and dichloromethane. Left, 275-600 nm absorption window. Right, focus on ICT band region.	31
2.7: Literature examples of fluorenone systems for comparison.	31
2.8: Normalized solid film absorption spectra for D-A compounds FOCz, FODPA, and FODAA (left chart), and D-A-D compounds FODAAS, FOBDAAS, and FOBTMPMPA (right chart).	34
2.9: Cyclic voltammograms for all D-A compounds and their constituent D and A modules, obtained in acetonitrile using the ferrocene/ferrocenium redox couple as an external standard.	36
2.10: HOMO and LUMO energy levels derived from equations (1)-(2) for push-pull compounds and modular building blocks. DAA = dianisylamine, DPA = diphenylamine, Cz = carbazole, FO = fluorenone. See above for details of energy level determinations.	40
2.11: Modular deconstruction of push-pull system (D-A) frontier molecular orbitals derivable from interaction of generic acceptor module A with different donor modules D ₁ and D ₂ , where D ₂ is the stronger donor.	40

2.12: HOMO (left) and LUMO (right) plots for FODAA, computed using the B3LYP/6-31G* level of theory and basis set in Gaussian09.	41
2.13: Fluorescent lifetime studies of FOBDA (BDAFO), FODAA (DAAFO), and FODAAS (DAAFOPV) in hexanes and FODS (OFOPV) in chloroform.	43
3.1: Fluorenone-based molecular design strategy and FMO energy tuning rationale.	51
3.2: Cyclic voltammograms for donor-acceptor molecules, obtained in acetonitrile as described in Chapter 9.	56
3.3: Absorption spectra of FOs (left) and FMs (right) with one donor substituent, in acetonitrile. Full spectra top, ICT bands bottom.	58
3.4: B3LYP/6-31+G(d,p) level frontier molecular orbital plots for FMDAA HOMO (a) and LUMO (b), and FMBDAA HOMO (c) and LUMO (d).	59
3.5: Comparison of lowest-energy absorption spectral regions for FODAA and FMDAA in diethyl ether (Et ₂ O) and acetonitrile (MeCN).	61
3.6: Absorption spectra of FOs (left) and FMs (right) with two donor substituents, in acetonitrile. Full spectra top, ICT bands bottom.	64
3.7: Modular deconstruction of push-pull system (D-A) frontier molecular orbitals derivable from interaction of generic acceptor module A with different donor modules D ₁ and D ₂	66
3.8: Frontier molecular orbital energies for donor-acceptor molecules compared with orbital energies of constituent donor and acceptor modules (data from Table 3.1 and Equations 1-2).	67
3.9: Lowest-energy absorption spectral regions in acetonitrile comparing FOBDA, FMBDAA, FOBDA36, and FMBDAA36 (left), and frontier molecular orbital energies for FOBDA, FMBDAA, FOBDA36, and FMBDAA36 compared to constituent modules' FMO energies (right).	71
4.1: Cyclic voltammograms showing the amine oxidation region. Potentials are referenced to the ferrocene/ferrocenium redox standard reaction in dry acetonitrile.	82
4.2: Room temperature CH ₂ Cl ₂ solution EPR spectra for: (a) FODAA/SbCl ₅ (9.6000 GHz); (b) FODPA/SbCl ₅ (9.6464 GHz); FODAAS/SbCl ₅ (9.6472 GHz); FOBDA/AgSbF ₆ (9.6146 Gz).	83
4.3: UV-vis-NIR oxidation spectra (left) and titration curves (right) for FODAA, FODPA, FODAAS, and FOCz.	85
4.4: Normalized UV-vis-NIR spectra from solution protocol oxidation of FODAA, FODPA, and FODAAS with SbCl ₅ . Red bars show UB3LYP/6-31G(d,p) TDDFT predicted band positions and relative transition moments.	86

4.5: UV-vis-NIR spectra for FOBDA in MeCN oxidized with AgSbF ₆ : 0 equiv. (A), 0.8 equiv. (B), 1.6 equiv. (C), and 4.0 equiv. (D). Long wavelength solvent absorbance artifacts were digitally subtracted. Bars show B3LYP/6-31G(d,p) TDDFT predicted band positions and transition moment intensities for FOBDA ⁺ (solid) and FOBDA ⁺⁺ (dashed).....	88
4.6: UV-vis-NIR oxidation spectra for FMDAA.....	91
5.1: Generic DSSC diagram showing the main photovoltaic processes. A, photon absorbed by dye molecule to form excited state. B, Excited state electron transferred to TiO ₂ n-type material, followed by electron injection into transparent electrode C. D, Electron transferred from counter electrode to I ₂ to form I ₃ ⁻ . E, I ₃ ⁻ transfers electron to oxidized dye molecule to regenerate its neutral ground state.....	97
5.2: Normalized absorption spectra of Z907 sensitizing dye and the triarylamine additive molecules.....	101
5.3: IPCE spectra for DSSCs with increasing amounts of FODAA (left) and FODAAS (right) in the redox couple solution.....	102
5.4: Current density versus voltage (J-V) curves for DSSCs incorporating (A) Acetonitrile (B) FODAAS (C) FODAA and (D) FOBDA. The arrows in plots display increasing acetonitrile (A) and D-A triarylamine additives (B-D).....	103
6.1: General molecular design strategy for the squaraine-based materials in this chapter, using a systematic modular synthetic approach for FMO energy tuning.....	107
6.2: Forrest's amino squaraines used throughout the literature.....	108
6.3 Molecular design of squaraine dyes with tunable bandgaps and HOMO energy levels. SQ-H is the control molecule for reference to Forrest's DPSQ. SQ-C6 and SQ-OH are squaraine dyes with increasing electron donor strength. SQ-F and SQ-CF3 are squaraine dyes with increasing electron withdrawing strength.....	109
6.4: Expected HOMO energy trend based on electron donating/withdrawing triarylamine substituents. The stronger the electron donor, the higher the E _{HOMO}	109
6.5 Representative example for SQ-OH synthesis. Other dyes were synthesized by Dr. Della Pelle and Youngju as reported in <i>J. Phys. Chem. C</i>	110
6.6: SQ-OH DCM solution (red) and neat thin film (black) UV-vis absorption spectra. Film absorption intensity normalized to DCM solution molar absorptivity.....	110
6.7: Left, Titration spectra for SQ-OH in 0-100% DMSO in CHCl ₃ , normalized to 100% CHCl ₃ . Right, titration curves compiled from the lower energy versus higher energy transition strengths using the normalized transition intensities from the titration spectra.....	111

6.8: FMO energies for SQ-compounds compared to PC ₇₁ BM. SQ-compound FMO energies obtained using cyclic voltammetric redox potentials. SQ-CF ₃ E _{HOMO} was calculated by subtracting the solution phase optical band gap from E _{LUMO}	112
6.9: Left, SQ-OH:PC ₇₁ BM device configuration, using ITO anode, PEDOT:PSS electron blocking layer, LiF hole blocking layer, and Al cathode. Right, energy level diagram for SQ-OH device components. Neat thin film SQ-OH and PC ₇₁ BM E _{HOMO} determined by Professor Volodymyr Duzhko using ultraviolet photoelectron spectroscopy (UPS).....	113
6.10: SQ-OH solution vs. neat thin film absorption spectra (left) and current density versus voltage curve for BHJ solar cells using 1:5 SQ-OH:PC ₇₁ BM and 0.5% diiodooctane additive.	115
7.1: FMO energies for FMBDAA36 and PC ₇₁ BM. LUMO-LUMO offset is 0.6 eV, and maximum theoretical device voltage is 1.0 V based on FMBDAA36 E _{HOMO} to PC ₇₁ BM E _{LUMO} difference of 1.0 eV. HOMO energies were determined by Professor Volodymyr Duzhko using UPS.	120
7.2: FMBDAA36 and PC ₇₁ BM UV-vis absorption spectra (left). UV-vis absorption spectra for thin film mixtures of FMBDAA36 and PC ₇₁ BM (right). Thin film UV-vis spectra obtained by Dr. Karak.....	121
7.3: Bis-cyanofulvalene analogues of FMBDAA36 used in OPV devices.....	122
7.4: Left, FMBDAA36:PC ₇₁ BM device configuration, using ITO anode, PEDOT:PSS electron blocking layer, LiF hole blocking layer, and Al cathode. Right, energy level diagram for FMBDAA36 device components. Neat thin film FMBDAA36 and PC ₇₁ BM E _{HOMO} determined by Professor Volodymyr Duzhko using ultraviolet photoelectron spectroscopy (UPS).....	122
7.5: Current density versus voltage curve for BHJ solar cells using 1:3 FMBDAA36:PC ₇₁ BM.....	123
8.1: π -Macrocycles synthesized by DV Group (left), Wan et al. (middle), and Zhang et al. (right).	128
8.2: DFT results exhibiting dithiafulvalenyl truxenes (a-c) interacting with C ₆₀ through π - π stacking. See Martín <i>et al</i> (permission license number 3342620583207).....	129
8.3: Truxenone and heterotriangulene π -macrocycle acceptor cores, and proposed π -macrocycle D-A compounds.....	130
8.4: Proposed D-A π -macrocycle compounds, condensed to their bis-cyanofulvenoid analogues.	131
8.5: (A) Indigo, with the 5,5'- and 6,6'-connectivity positions labeled. (B) "Nindigo", an aniline-condensate of indigo, with variable R groups for different electronic and molecular packing effects. (C) Isoindigo.....	138

8.6: (A) indigo and (B) nindigo intramolecular hydrogen bonding. (C) Indigo intra- and intermolecular hydrogen bonding and crystal packing scheme.	139
8.7: Proposed indigo-based materials for OPV and FET applications.....	140
8.8: Solar flux as a function of wavelength (bottom axis) and energy in electron volts (top axis).....	143
8.9: Panchromatic azulene-porphyrin (Jiang <i>et al.</i>) and heteroleptic organoruthenium complex (Grätzel <i>et al.</i>).	144
8.10: Perturbation theory model for two separate D-A compounds where they each have the same donor module but different acceptor modules with different electron affinity.....	145
8.11: Proposed examples of A-D-A' donor-acceptor materials for panchromatic visible spectrum absorption.	147

LIST OF SCHEMES

Scheme	Page
2.1: General molecular design strategy for the fluorenone-based materials described in this chapter. HOMO and LUMO energies (E_{HOMO} and E_{LUMO}) tuned by arylamine modules and fluorenone, respectively.....	20
3.1: General synthetic plan and FMO energy tuning strategy based on donor/acceptor strengths.....	50
3.2: General structural design units used in donor-acceptor fluoren-9-ylidne malononitrile (FM) and precursor fluorenone (FO) systems in this study.....	53
3.3: Donor-Acceptor systems compared in this study.....	54
3.4: Neckers' push-pull FO and FM-based systems with phenylethynylene-linked donors.....	69
4.1: Chemical oxidation process, and fluorenone-based triarylamine compounds studied.....	79
4.2: Oxidation sequence for FOBDA.....	87
4.3: Triarylamine system from the literature for comparison to the fluorenone-based compounds in Scheme 4.1.....	89
5.1: Electron transport processes in control and additive-modified DSSCs, and the additives' molecular structures. Green, dye regeneration via energy cascade through additive's HOMO. Blue, dye regeneration by direct electron transfer from I^-/I_3^-	100
8.1: Synthesis of 4,9,14-tribromotru xenone, adapted from the literature.....	131
8.2: Attempted synthesis of truxenone-cored D-A compounds TrOS and TrODAA.....	132
8.3: Synthesis of triiodoheterotriangulene, adapted from the literature.....	132
8.4: Soluble D-A π -macrocycle proposal, using a wide variety of soluble components for structural and physical chemical engineering.....	134
8.5: Modular engineering of E_{HOMO} levels and intermolecular interactions using primary amines with various electronic and side chain interaction properties.....	135
8.6: Modular engineering of E_{LUMO} levels using electron withdrawing groups with various electronic properties.....	135
8.7: Covalent organic framework possibilities for π -macrocycles, using proposed π -macrocycle 3 and primary-amine-containing condensation partners.....	137
8.8: Nindigo synthesis from indigo and aniline derivatives, following the procedure used by Hicks and coworkers.....	141

9.1: Typical chemical vapor deposition crystal growth process. Reproduced from Bao and coworkers (permission license number 3360900411130). 159

CHAPTER 1

GENERAL BACKGROUND AND MOLECULAR DESIGN STRATEGIES

1.1 Introduction

The amount of solar energy that the sun provides Earth over the course of an hour is the same amount of electrical energy that humankind consumes throughout an entire year: over 130,000 terawatts.^{1,2} Due to this large availability of solar energy, photovoltaic devices have been growing in popularity as a source of CO₂-free energy. Since Bell Labs' first silicon-based solar cell in 1954,³ solar cell efficiencies have increased from about 6% up to 24% for typical laboratory crystalline silicon-based solar cells.⁴ Unfortunately, silicon-based solar cells are not always economically viable^{5,6} due to the expensive manufacturing process required to make necessarily pure material. In addition to financial drawbacks, silicon-based solar cells are heavy, fragile, and bulky, which limits their application to areas where robust structures can support them. Manufacturing requirements also limit their size, so many solar cell modules must be connected in series for large-area devices. Finally, silicon has a low light absorption coefficient; so silicon-based solar cells must be very thick, a major reason that they are so heavy and costly.

Organic photovoltaic (OPV) devices are emerging as a potential alternatives to inorganic solar cells due to prospects that they can be made quickly, cheaply, and under mild manufacturing conditions.^{4,7,8} Because organic materials can have very large molar absorptivities, the active layer in an OPV can be as thin as 100 nm, and be placed on light-weight flexible substrates. This wastes less active layer material, and allows the devices to be less fragile and highly amenable to thin film roll-to-roll manufacturing techniques such as those already used in the photography and inkjet printing industries. Organic molecules are also synthetically tunable, so it is possible to engineer the material's properties using a bottom-up molecular design approach.

Unfortunately, OPVs have not reached widespread commercial viability due to their so far comparably low efficiencies and short device lifetimes. To solve these problems, it is important to engineer new organic materials starting on a fundamental physical chemical and

molecular/structural level, keeping in mind the structure-property relationships at the heart of the molecular design process for light-harvesting photoconverting materials, as well as practical requirements for producing efficient devices.

Specifically, effective photoconverting materials must be photochemically stable, and absorb strongly and broadly throughout the visible and near-infrared (NIR) spectrum. Materials that absorb light where the solar flux is highest (between 400-900 nm or 3.1-1.4 eV) are particularly desirable (Figure 1.1). Because these materials must also be able to transport charges and excitons, a π -conjugated molecular architecture is appropriate to allow inter- and intramolecular electron mobility. This π -architecture requirement also imparts optoelectronic, electrochemical, and bulk electronic tunability into the materials. In particular, the materials should form smooth, continuous films in which individual molecules can self-assemble to enhance electron mobility through inter- and intra-material interactions (e.g. via π -stacking). Finally, these materials should also be solution- or vacuum-processable to allow practical device fabrication.

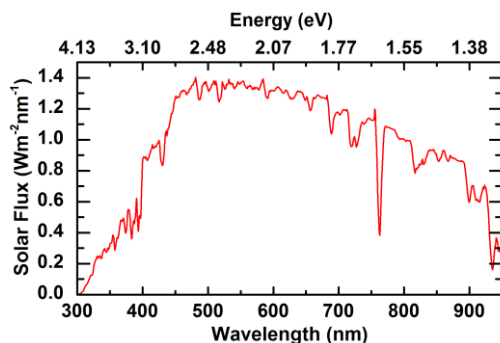


Figure 1.1: Solar flux as a function of wavelength (bottom axis) and energy in electron volts (top axis).

Ideally molecular design strategies for photoconverting compounds should also be modular, allowing many structural variations based on common molecular frameworks. Using a modular molecular design approach provides a high degree of structural and physical chemical tunability, allowing one to assess and integrate a broad array of structure-property choices.

Ultimately, this strategy should not only produce a robust library of electronic materials, but also provide fundamental insight into the design of whole classes of new organic electronic materials.

Toward these ends, new molecular frameworks were synthesized and their optoelectronic, electrochemical, and in some cases photoconversion properties characterized. They were derived from carefully selected examples in a wide range of organic electronics literature, to ensure that each of the above fundamental objectives was addressed in each new material.

As general background for this work, some fundamental physical chemical concepts will be discussed in relation to bottom-up molecular design. General OPV operating principles will be discussed in the context of desired properties, followed by strategies for chromophore design with focus on π -conjugation and “push-pull” or “donor-acceptor” (D-A) effects using a theoretical molecular orbital mixing or perturbation theory approach. Finally, the molecular design strategies used in this work will be introduced briefly, focusing on small molecule development using relatively simple yet highly versatile structural components/modules.

1.2 General OPV Operating Principles and Historical Context

OPVs all operate by the same general processes (Figure 1.2).^{4,7,9} First, a photon is absorbed by the active layer material (A) promoting an electron from the highest occupied molecular orbital (HOMO) to the lowest unoccupied molecular orbital (LUMO), and creating an excited state or *exciton* (B). An exciton is a charge-polarized electronic perturbation that can travel within the bulk p- or n-type material in which it was formed. In this example, if an exciton is formed in the p-type material and migrates to a p/n junction, it can dissociate (C) into (+) and (–) free charges that can move separately in the p- and n-type phases (respectively). This has been found to work so long as the LUMO energy of the p-type material is at least 0.3 eV higher than the LUMO energy of the n-type material. This energy offset provides the electrochemical gradient required to dissociate the coulombically-bound electron and hole components of the exciton. Once formed in their respective layers, the free (+) and (–) charges will migrate to anode

and cathode (respectively, D) according to the intrinsic potential of the device, thereby producing an electric current.

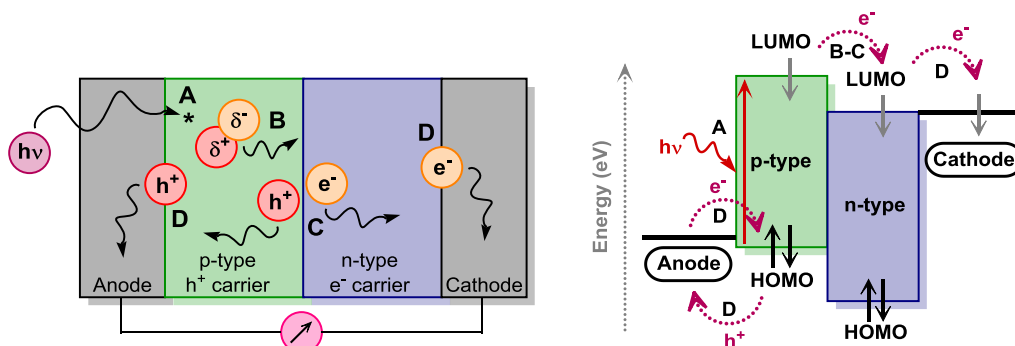


Figure 1.2: Left, generic bilayer p-n heterojunction solar cell diagram showing the main photovoltaic processes. A, light absorption to create an exciton. B, exciton migration to the p-n junction. C, exciton dissociation at the p/n junction into an hole/electron pair in the p- and n-type materials, and charge migration to the anode and cathode, respectively. D, charge collection at the electrodes, current generated. Right, the same process depicted using an energy level diagram.

This is, of course, an oversimplified description of real solar cell operation processes.^{5,9-11} It depicts a simple, p/n bilayer heterojunction solar cell. Bilayer OPV devices are not as efficient for organic semiconductor materials as bulk heterojunction (BHJ) devices, due to the fact that (1) they have relatively low p/n interfacial surface area, and (2) most of the excitons formed in each organic phase radiatively or vibrationally decay before migrating to a p/n junction or electrode for charge transfer. The typical distance an organic material exciton can travel before decaying is 10-20 nm,¹¹ so it is important for the p- and n-type domains to be no more than 20-40 nm across. Because typical organic active layers are often 100-200 nm thick, their component p- and n-type materials should form an interspersed p/n nanomorphology that maximizes the p/n junction surface area, while providing percolation pathways for the separated charges to reach their respective electrodes. With careful material design and device fabrication conditions, it is possible to obtain such complex bicontinuous nanomorphology (Figure 1.3).

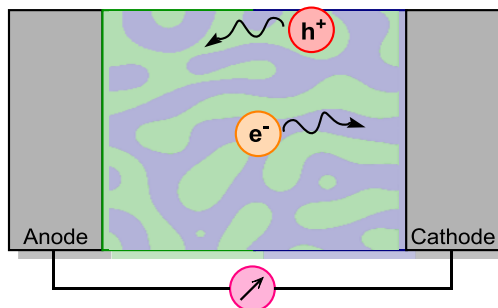


Figure 1.3: Bicontinuous p/n bulk heterojunction with interspersed p- and n-type materials and hole/electron percolation pathways.

Unfortunately, it is difficult to predict and engineer nanoscale assembly based on individual molecular design; so it is important to design materials with inherent synthetic tunability so that intermolecular interactions can be varied with little synthetic difficulty. For example, installation of different types or lengths of alkyl chain is desirable. Even in the few situations where morphology can be controlled, it is still important to enhance exciton transport distance based on intrinsic molecular properties (versus emergent properties, like unpredictable intermolecular interactions). One way to enhance exciton transport distance is to increase exciton lifetime. From a molecular design perspective, this can be accomplished, in part, by ensuring that a molecule's excited state is stabilized by either steric (twisting) or electronic effects. This can be done by designing compounds that undergo twisted intramolecular charge transfer (TICT)¹²⁻¹⁶ upon photoexcitation, or by delocalizing electron density in the excited state by using molecular components that withdraw electron density via π -resonance effects.¹⁷⁻²⁴ The latter can be accomplished using a push-pull or donor-acceptor (D-A) architecture,^{20,25-29} which will be discussed in more detail later.

With careful device engineering, organic BHJ devices reached 12% power conversion efficiency (PCE, Figure 1.4) in January 2013 at Heliatek, a German company that specializes in small molecule organic solar cells.^{30,31} PCEs for small molecule solar cells were no better than 0.03%²⁵ in 2005 and stayed consistently low for several years after that.^{26-28,32} In 2009 and 2011 Zhang³³ et al. and Shang³⁴ et al. described small molecule solar cell efficiencies of 2.36% and

4.3%, respectively. Just a short time later in 2012, Chen³⁵ et al. made a small molecule device with PCE = 6.6%, followed quickly by Bazan et al., who achieved 6.7%. In 2013, Yang³⁶ and coworkers at UCLA obtained 8.02% PCE with a small molecule OPV device. For further information, the reader is referred to several good review articles that describe the history and molecular design of small molecule OPV materials.^{11,26–28,32}

Polymer-based solar cells, on the other hand, have historically performed much better than small molecules until recently. Although polymer-based OPVs are outside the scope of this dissertation, many of the photoconverting polymer design principles apply to small molecule development; so their historical and molecular design context is important. Polymer-based solar cells initially outperformed small molecules due to their superior film-forming and morphology control properties. Now that small molecule design has improved, they will likely continue to outperform polymers for a variety of reasons.

First, small molecule materials have a well-defined molecular weight and structure. They can be made in high purity, with no polydispersity or batch-to-batch variation. They are also frequently soluble in a large variety of solvents. These properties provide superior device performance reproducibility, since small variations in molecular structure (e.g. polydispersity) can have drastic impacts on device active layer fabrication and overall performance. Secondly, small molecules can be synthetically optimized in a very controlled manner, and the fundamental properties of individual structural components tested. Finally, small molecules are comparatively simple to characterize, which makes molecular, bulk material, and device characterization testing more straightforward.

Nonetheless, conjugated polymers research laid much of the fundamental groundwork for organic photovoltaic materials design. The first polymer-based OPV consisted of a methoxy-ethylhexyloxy-poly(phenylenevinylene) (MEH-PPV) p-type material in 1992-1993 with a PCE of 0.04%.^{37–39} Subsequently, for many years poly(3-hexylthiophene) (P3HT) based solar cells performed the best, with PCEs maximizing at just over 5% in 2006 – but only by using the

highest quality material and extensive device engineering.³⁹⁻⁴¹ Since then, the D-A architecture became popular for conjugated polymer design, giving rise to many new materials with strong, broad spectral coverage and PCEs exceeding 8.6% in 2012.^{39,42,43} The reader is referred to numerous excellent review articles about conjugated polymer design for OPVs and organic electronic devices in general.^{9,10,20,29,39,42,44,45}

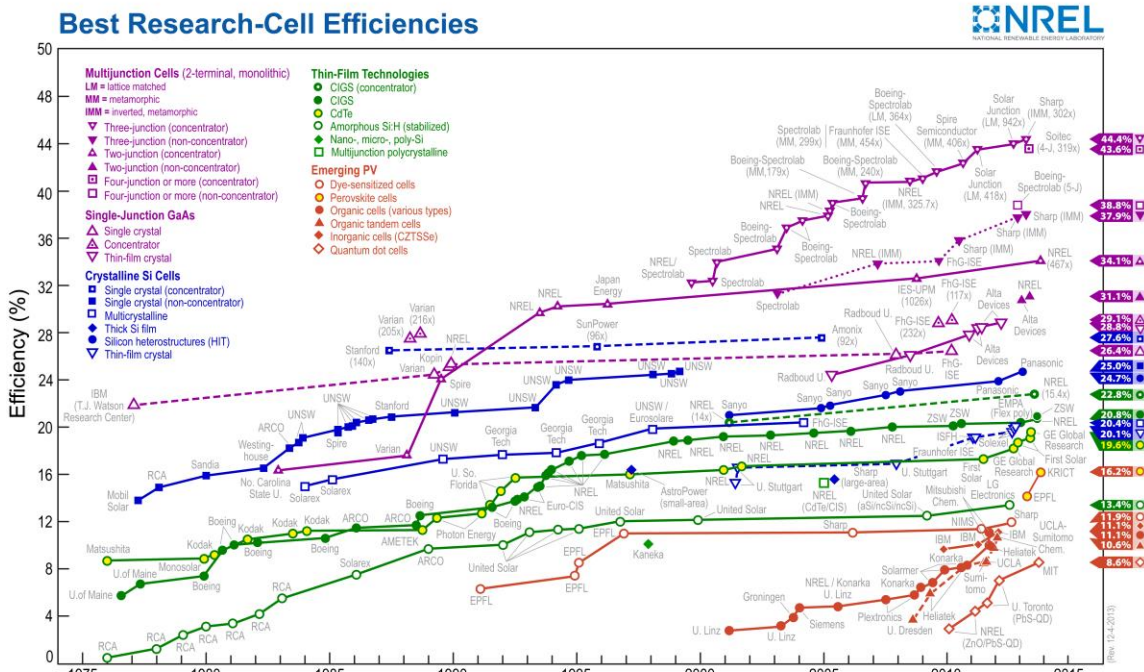


Figure 1.4: NREL record solar cell efficiency evolution up to 2/25/2014.³⁰ “Emerging PV” (red) are mostly organic-based solar cells, most notably including dye-sensitized solar cells (DSSCs), perovskite cells, and organic bilayer and bulk heterojunction cells. At present, this chart is periodically updated at www.nrel.gov/ncpv/images/efficiency_chart.jpg

1.3 Molecular Design Requirements and Donor-Acceptor Architecture

Organic electronic materials intended for p-type active layer use in photovoltaic devices require specific electrochemical and photophysical properties in order to produce photocurrent efficiently. First, they must absorb strongly and broadly throughout as much of the visible spectrum as possible. This requires a low band gap, or low HOMO/LUMO energy gap (E_g), of

$\leq 1.4\text{-}1.5$ eV (Figure 1.1). Since *strong* absorption is also important, materials should also have high molar absorptivity $\geq 10^4 \text{ M}^{-1}\text{cm}^{-1}$.

The second requirement is that a material's HOMO/LUMO energy levels be favorably aligned with those of other electronic device components, in order to maximize power output. This is shown in Figure 1.5, where the optimal HOMO/LUMO energies are -5.4 and -3.9 eV, respectively, assuming that a typical BHJ device energy level design is used: indium-tin oxide anode, p-type active material, n-type C_{71} fullerene-derivative material, and aluminum cathode (or other metal with similar work function). The p-type material's LUMO energy (E_{LUMO}) is particularly important, and typically desired to be ~ 0.3 eV above the n-type material's LUMO to provide a strong enough electrochemical gradient to separate the p-material's exciton into separate electron and hole components, allowing current to flow. This E_{LUMO} requirement necessitates that the p-material's HOMO energy (E_{HOMO}) be about -5.4 eV for optimal power output. As a result, it is advantageous to design materials whose electrochemical properties can be adjusted in a selective and straightforward way. For this purpose, "push-pull" or "donor-acceptor" (D-A) molecules consisting of an electron rich "donor" (D) and an electron-poor "acceptor" (A) are often used to tune a D-A compound's properties by the mechanism described below.

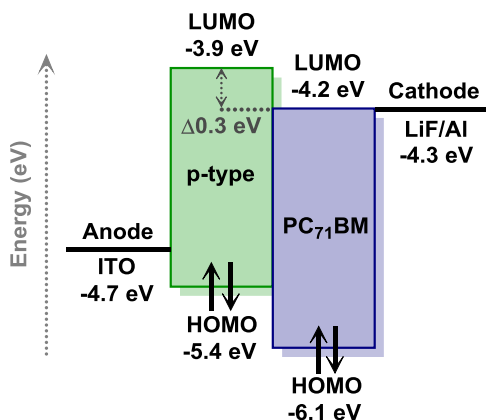


Figure 1.5: Energy level alignment requirements for a typical BHJ solar cell using PC_{71}BM as the n-type material with an indium tin oxide (ITO) anode and an aluminum cathode.

D-A molecules undergo intramolecular charge transfer (ICT) upon photoexcitation, with an electron transferred from an electron-rich “donor” component to an electron-poor “acceptor” component. From a molecular orbital perspective, the HOMO of a strongly push-pull molecule is located primarily on the donor module while the LUMO is located on the acceptor module. So, photoexcitation typically reverses the polarity of the molecule, forming a charge-separated excited state with a partial positive charge on the donor and a partial negative on the acceptor. This process makes push-pull chromophores particularly advantageous for organic solar cell applications because the exciton formed upon photoexcitation is charge-separated. Such inherent molecular charge separation can therefore potentially lead to better charge transfer between the p- and n-type materials.

D-A molecular design is well-described by MO perturbation theory (Figure 1.6). Specifically, using a D-module with a high-lying E_{HOMO} relative to that of the A-module should give a D-A molecule whose HOMO character and energy is determined by the D-module. Similarly, the A-module’s low-lying E_{LUMO} should dominate the D-A molecule’s LUMO character. Using this modular D-A design strategy, a D-A material’s E_g and energy levels can (in principle) be engineered in a systematic, synthetically rational way.

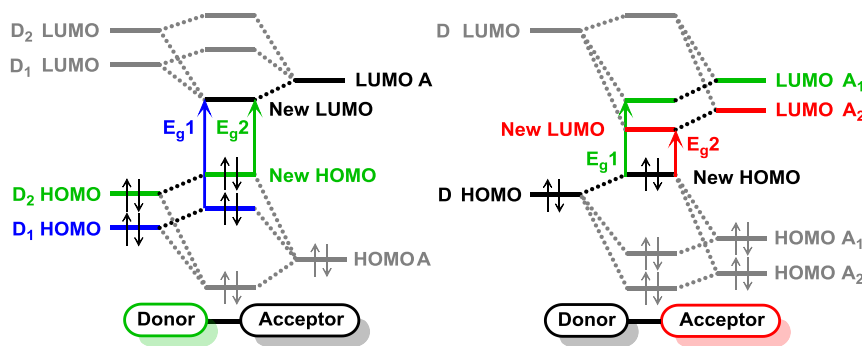


Figure 1.6: Perturbation theory model for the modular construction of push-pull system (D-A) frontier molecular orbitals, using generic acceptor modules A, A₁, and A₂ with different donor modules D, D₁, and D₂.

A third p-type material requirement is that it must have a long enough excited state lifetime for its excitons to be mobile over a substantial distance (≥ 10 nm). D-A molecules

typically have a charge-separated excited state that lengthens exciton lifetime. The materials described in this dissertation were designed with this in mind, specifically using primarily di- and triarylamine donor modules to form the D-A molecules, since triarylaminines are well known to be good hole-transporting materials.⁴⁶

1.4 π -Conjugation

Conjugated molecules have an uninterrupted, coplanar network of p-orbitals through which electrons can be delocalized. π -Conjugated materials are critical targets for OPVs and other organic electronic devices because their π -conjugation allows for electronic interactions within molecules, and assists interactions between the molecules in a bulk material. Extended π -conjugation also decreases absorption band gaps and increases absorption cross sections, which can allow a material to absorb very strongly well into the visible and NIR spectral region. As a result, π -conjugated polymers and π -extended small molecules and oligomers are popular target materials for OPVs.

The basic mechanism by which conjugation extension decreases the band gap can be considered in multiple ways, including the “particle in a one-dimensional box” model,⁴⁷ Bloch functions and band structure,⁴⁸ and Hückel molecular orbital (HMO) theory.⁴⁷ The former two models follow a physics-based perspective, while HMO theory is the most visually intuitive model from an organic chemist’s design perspective.

Using HMO theory as a model, linearly extending a π -conjugated network results in the convergence of HOMO and LUMO energies, by HOMO destabilization with simultaneous LUMO stabilization. Using oligoacetylene as a model system, this occurs by splitting of energy levels with each successive ethylene extension such that E_{HOMO} and E_{LUMO} approach each other (Figure 1.7). But, with each extension the energy difference between the newly-split energy levels decreases. As a result, E_{HOMO} and E_{LUMO} eventually reach a specific, nonzero difference (in most cases), loosely called the bandgap in borrowing from solid state terminology.

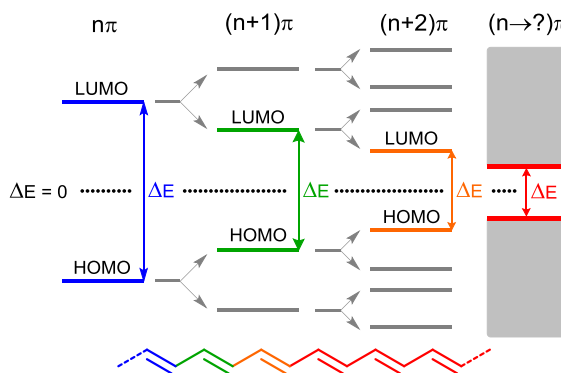


Figure 1.7: Energy level splitting with increasing π -conjugation length, starting at n π -bonds. ΔE decreases with concomitant absorption red-shift, but $\Delta E = 0$ is never reached.

The bandgap limit is a result of Peierls distortion which, from a molecular orbital theory perspective, is due to the mixing of bonding and antibonding interactions between component orbitals within the occupied and unoccupied bands. More simply, in most cases electron-electron repulsion and electron spin-pairing assure a tendency to bond alternation in conjugated systems, which overmatches any tendency for full electron delocalization and degenerate HOMO/LUMO energies. But, even decreasing the band gap by conjugation extension in small organic molecules, oligomers, and polymers is effective for designing materials that absorb strongly throughout a readily attainable range of 3.1-1.4 eV.

π -Extended compounds are also able to interact electronically in the solid state, to enable exciton and charge transport over distances much larger than the size of an individual molecule. Intermolecular interactions, such as π -stacking, are crucial to allow organic materials to perform an electronic function in devices such as solar cells, light emitting diodes, electrochromic devices, transistors, etc. This feature is presently the hardest to control in designing solid state materials.

So, one molecular design strategy is to extend conjugation linearly by vinylic or aryl extension. For example, oxidatively-doped polyacetylene is an excellent organic semiconductor, having almost metallic-like conductivity.^{21,49} Unfortunately polyacetylene is not thermally or photochemically stable enough to incorporate into a practical organic electronic device. Also, long-chain polyacetylene can adopt numerous distinct conformations giving rise to variable

optoelectronic properties and non-ideal intermolecular interactions. Finally, polyacetylene is poorly soluble, which makes device fabrication impractical outside of a purely academic environment.

One solution to these problems is to extend conjugation through cyclic π -systems, aromatics being the most robust. Unfortunately, these can also pose problems. Polyphenylene, for example, is not planar due to *ortho-ortho* dihedral strain and thus does not provide true conjugation throughout the polymer. Also, phenylene units do not easily break aromaticity, which creates a large energetic barrier to electronic and geometric changes required in photoexcitation and effective charge conduction.⁵⁰ With polyphenylene-based materials, there is a competition between π -electron confinement within the aromatic π -system and electron delocalization along the conjugated chain (Figure 1.8).

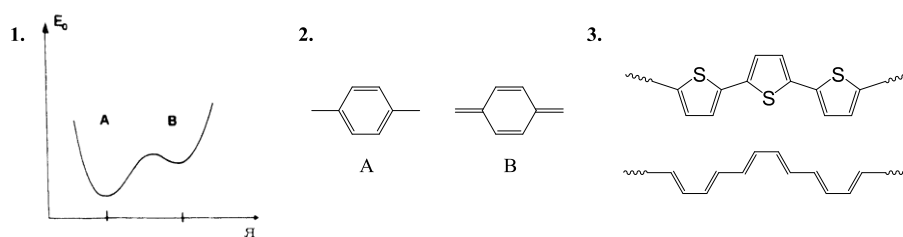


Figure 1.8:^{21,49,50} (1) Potential energy wells depicting the aromatic stabilization energy of the phenyl system versus the quinonal system shown in (2). (3) Polythiophene versus polyacetylene, the latter shown in a topologically-locked conformation for comparison.

Fortunately, a practical compromise can be achieved by using heteroaromatics such as thiophenes, pyrroles, and furans. These systems act to some extent like topologically-locked conjugated dienes which can be polymerized or oligomerized to various extents (Figure 1.8₃).²¹ Their π -electron confinement is drastically lower than that of phenyl systems, making them good π -extension components despite their pseudoaromaticity. They are also more stable than their polyene counterparts while still possessing similar semiconducting properties. Thus one can engineer a new material's optoelectronic properties by tuning heteroaromatic π -system length.

Despite these possibilities, there are fundamental limits to how extended a system's conjugation can be. Extended aromatic chains eventually start to kink, or deviate from planarity, with growing chain length. Their "effective conjugation length" is the maximum length of oligomer or polymer which does not give further bandgap decreases with additional lengthening. This limit is due in part to electronic reasons such as Peierls distortion, and geometric reasons such as twisting.^{51,52} Two ways to limit this issue are to (1) design fused, planarized conjugated systems such as fluorenones, fluorenylidene-malononitriles, and triangulenes (Figure 1.9), and (2) implement a "push-pull" or "donor-acceptor" molecular architecture for more direct (and thus more selective and predictable) frontier molecular orbital (FMO) and band gap control, as described above.

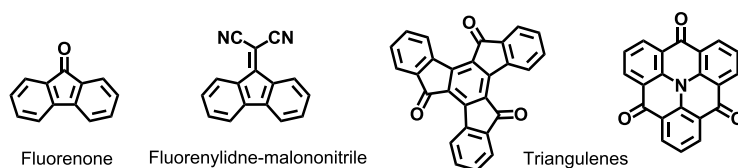


Figure 1.9: Some fused/linked conjugated systems.

1.5 Molecular Design Strategy

To utilize the D-A molecular architecture strategy in designing new low band gap p-type organic electronic materials, fluorenone (FO), fluorenylidene malononitrile (FM), and squaric acid (SQ) were utilized as electron acceptor modules in D-A molecules. Using one of these modules as a molecular core, electron donor module strength was varied using a styrene-based and several di- and triarylamine-based electron-rich donor components.



The background described above is applied in various parts of the following chapters, which describe the actual work done to pursue the main goal of designing, synthesizing, and characterizing conjugated organic molecules for potential use in OPV devices. Some of the

synthesized compounds have been tested in OPVs, with results that are described in each appropriate section.

1.6 References

- (1) Morton, O. Solar Energy: A New Day Dawning? Silicon Valley Sunrise. *Nature* **2006**, *443*, 19–22.
- (2) Lewis, N. S. Toward Cost-Effective Solar Energy Use. *Science* **2007**, *315*, 798–801.
- (3) Chapin, D. M.; Fuller, C. S.; Pearson, G. L. A New Silicon P-N Junction Photocell for Converting Solar Radiation into Electrical Power. *J. Appl. Phys.* **1954**, *25*, 676.
- (4) Spanggaard, H.; Krebs, F. C. A Brief History of the Development of Organic and Polymeric Photovoltaics. *Sol. Energy Mater. Sol. Cells* **2004**, *83*, 125–146.
- (5) Kippelen, B.; Brédas, J.-L. Organic Photovoltaics. *Energy Environ. Sci.* **2009**, *2*, 251.
- (6) Keppner, H.; Meier, J.; Torres, P.; Fischer, D.; Shah, A. Microcrystalline Silicon and Micromorph Tandem Solar Cells. *Appl. Phys. A Mater. Sci. Process.* **1999**, *69*, 169–177.
- (7) Helgesen, M.; Søndergaard, R.; Krebs, F. C. Advanced Materials and Processes for Polymer Solar Cell Devices. *J. Mater. Chem.* **2010**, *20*, 36.
- (8) Kippelen, B.; Bredas, J.-L. Organic Photovoltaics. *Energy Environ. Sci.* **2009**, *2*, 251–261.
- (9) Thompson, B. C.; Fréchet, J. M. J. Polymer-Fullerene Composite Solar Cells. *Angew. Chem. Int. Ed. Engl.* **2008**, *47*, 58–77.
- (10) Beaujuge, P. M.; Fréchet, J. M. J. Molecular Design and Ordering Effects in Π -Functional Materials for Transistor and Solar Cell Applications. *J. Am. Chem. Soc.* **2011**, *133*, 20009–20029.
- (11) Roncali, J. Molecular Bulk Heterojunctions: An Emerging Approach to Organic Solar Cells. *Acc. Chem. Res.* **2009**, *42*, 1719–1730.
- (12) Tanaka, H.; Shizu, K.; Nakanotani, H.; Adachi, C. Twisted Intramolecular Charge Transfer State for Long-Wavelength Thermally Activated Delayed Fluorescence. *Chem. Mater.* **2013**, *25*, 3766–3771.
- (13) Wang, E.; Lam, J. W. Y.; Hu, R.; Zhang, C.; Zhao, Y. S.; Tang, B. Z. Twisted Intramolecular Charge Transfer{,} Aggregation-Induced Emission{,} Supramolecular Self-Assembly and the Optical Waveguide of Barbituric Acid-Functionalized Tetraphenylethene. *J. Mater. Chem. C* **2014**, *2*, 1801–1807.
- (14) Chudomel, J. M.; Yang, B.; Barnes, M. D.; Achermann, M.; Mague, J. T.; Lahti, P. M. Highly Twisted Triarylamines for Photoinduced Intramolecular Charge Transfer. *J. Phys. Chem. A* **2011**, *115*, 8361–8368.
- (15) Rettig, W. Charge Separation in Excited States of Decoupled Systems—TICT Compounds and Implications Regarding the Development of New Laser Dyes and the Primary Process of Vision and Photosynthesis. *Angew. Chemie Int. Ed. English* **1986**, *25*, 971–988.

- (16) Grabowski, Z. R.; Rotkiewicz, K.; Rettig, W. Structural Changes Accompanying Intramolecular Electron Transfer: Focus on Twisted Intramolecular Charge-Transfer States and Structures. *Chem. Rev.* **2003**, *103*, 3899–4032.
- (17) Raimundo, J.; Blanchard, P.; Gallego-Planas, N.; Mercier, N.; Ledoux-Rak, I.; Hierle, R.; Roncali, J. Design and Synthesis of Push–Pull Chromophores for Second-Order Nonlinear Optics Derived from Rigidified Thiophene-Based Π -Conjugating Spacers. *J. Org. Chem.* **2002**, *67*, 205–218.
- (18) Leriche, P.; Frère, P.; Cravino, A.; Alévêque, O.; Roncali, J. Molecular Engineering of the Internal Charge Transfer in Thiophene-Triphenylamine Hybrid Π -Conjugated Systems. *J. Org. Chem.* **2007**, *72*, 8332–8336.
- (19) Roquet, S.; Cravino, A.; Leriche, P.; Alévêque, O.; Frère, P.; Roncali, J. Triphenylamine-Thienylenevinylene Hybrid Systems with Internal Charge Transfer as Donor Materials for Heterojunction Solar Cells. *J. Am. Chem. Soc.* **2006**, *128*, 3459–3466.
- (20) Zhang, Z.; Wang, J. Structures and Properties of Conjugated Donor–Acceptor Copolymers for Solar Cell Applications. *J. Mater. Chem.* **2012**, *22*, 4178–4187.
- (21) Roncali, J. Synthetic Principles for Bandgap Control in Linear Π -Conjugated Systems. *Chem. Rev.* **1997**, *97*, 173–206.
- (22) Bundgaard, E.; Krebs, F. Low Band Gap Polymers for Organic Photovoltaics. *Sol. Energy Mater. Sol. Cells* **2007**, *91*, 954–985.
- (23) Oliva, M. M.; Casado, J.; Navarrete, J. T. L.; Berridge, R.; Skabara, P. J.; Kanibolotsky, A. L.; Perepichka, I. F. Electronic and Molecular Structures of Trigonal Truxene-Core Systems Conjugated to Peripheral Fluorene Branches. Spectroscopic and Theoretical Study. *J. Phys. Chem. B* **2007**, *111*, 4026–4035.
- (24) Wang, J.; Xiao, Q.; Pei, J. Benzothiadiazole-Based D- Π -A- Π -D Organic Dyes with Tunable Band Gap: Synthesis and Photophysical Properties. *Org. Lett.* **2010**, *12*, 4164–4167.
- (25) Sun, X.; Liu, Y.; Xu, X.; Yang, C.; Yu, G.; Chen, S.; Zhao, Z.; Qiu, W.; Li, Y.; Zhu, D. Novel Electroactive and Photoactive Molecular Materials Based on Conjugated Donor–Acceptor Structures for Optoelectronic Device Applications. *J. Phys. Chem. B* **2005**, *109*, 10786–10792.
- (26) Walker, B.; Kim, C.; Nguyen, T.-Q. Small Molecule Solution-Processed Bulk Heterojunction Solar Cells †. *Chem. Mater.* **2011**, *23*, 470–482.
- (27) Riede, M.; Mueller, T.; Tress, W.; Schueppel, R.; Leo, K. Small-Molecule Solar Cells-Status and Perspectives. *Nanotechnology* **2008**, *19*, 424001.
- (28) Lloyd, M. T.; Anthony, J. E.; Malliaras, G. G. Photovoltaics from Soluble Small Molecules. *Mater. Today* **2007**, *10*, 34–41.

- (29) Cheng, Y.-J.; Yang, S.-H.; Hsu, C.-S. Synthesis of Conjugated Polymers for Organic Solar Cell Applications. *Chem. Rev.* **2009**, *109*, 5868–5923.
- (30) National Center for Photovoltaics Home Page <http://www.nrel.gov/ncpv> (accessed Mar 13, 2014).
- (31) Heliatek Newscenter http://www.heliatek.com/newscenter/latest_news/neuer-weltrekord-fur-organische-solarzellen-heliatek-behauptet-sich-mit-12-zelleffizienz-als-technologiefuhrer/?lang=en (accessed Mar 13, 2014).
- (32) Mishra, A.; Bäuerle, P. Small Molecule Organic Semiconductors on the Move: Promises for Future Solar Energy Technology. *Angew. Chem. Int. Ed. Engl.* **2012**, *51*, 2020–2067.
- (33) Zhang, J.; Yang, Y.; He, C.; He, Y.; Zhao, G.; Li, Y. Solution-Processable Star-Shaped Photovoltaic Organic Molecule with Triphenylamine Core and Benzothiadiazole–Thiophene Arms. *Macromolecules* **2009**, *42*, 7619–7622.
- (34) Shang, H.; Fan, H.; Liu, Y.; Hu, W.; Li, Y.; Zhan, X. A Solution-Processable Star-Shaped Molecule for High-Performance Organic Solar Cells. *Adv. Mater.* **2011**, *23*, 1554–1557.
- (35) Chen, Y.-H.; Lin, L.-Y.; Lu, C.-W.; Lin, F.; Huang, Z.-Y.; Lin, H.-W.; Wang, P.-H.; Liu, Y.-H.; Wong, K.-T.; Wen, J.; *et al.* Vacuum-Deposited Small-Molecule Organic Solar Cells with High Power Conversion Efficiencies by Judicious Molecular Design and Device Optimization. *J. Am. Chem. Soc.* **2012**, *134*, 13616–13623.
- (36) Liu, Y.; Chen, C.-C.; Hong, Z.; Gao, J.; Michael Yang, Y.; Zhou, H.; Dou, L.; Li, G.; Yang, Y. Solution-Processed Small-Molecule Solar Cells: Breaking the 10% Power Conversion Efficiency. *Sci. Rep.* **2013**, *3*, 3356.
- (37) Sariciftci, N. S.; Smilowitz, L.; Heeger, A. J.; Wudl, F. Photoinduced Electron Transfer from a Conducting Polymer to Buckminsterfullerene. *Science (80-.)*. **1992**, *258*, 1474–1476.
- (38) Sariciftci, N. S.; Braun, D.; Zhang, C.; Srdanov, V. I.; Heeger, A. J.; Stucky, G.; Wudl, F. Semiconducting Polymer-buckminsterfullerene Heterojunctions: Diodes, Photodiodes, and Photovoltaic Cells. *Appl. Phys. Lett.* **1993**, *62*.
- (39) Zhou, H.; Yang, L.; You, W. Rational Design of High Performance Conjugated Polymers for Organic Solar Cells. *Macromolecules* **2012**, *45*, 607–632.
- (40) Dennler, G.; Scharber, M. C.; Brabec, C. J. Polymer-Fullerene Bulk-Heterojunction Solar Cells. *Adv. Mater.* **2009**, *21*, 1323–1338.
- (41) Kim, Y.; Cook, S.; Tuladhar, S. M.; Choulis, S. A.; Nelson, J.; Durrant, J. R.; Bradley, D. D. C.; Giles, M.; McCulloch, I.; Ha, C.-S.; *et al.* A Strong Regioregularity Effect in Self-Organizing Conjugated Polymer Films and High-Efficiency Polythiophene:fullerene Solar Cells. *Nat. Mater.* **2006**, *5*, 197–203.
- (42) Li, G.; Zhu, R.; Yang, Y. Polymer Solar Cells. *Nat. Photonics* **2012**, *6*, 153–161.

- (43) Guo, X.; Zhou, N.; Lou, S. J.; Smith, J.; Tice, D. B.; Hennek, J. W.; Ortiz, R. P.; Navarrete, J. T. L.; Li, S.; Strzalka, J.; *et al.* Polymer Solar Cells with Enhanced Fill Factors. *Nat. Photonics* **2013**, *7*, 825–833.
- (44) Stalder, R.; Mei, J.; Reynolds, J. R. Isoindigo-Based Donor–Acceptor Conjugated Polymers. *Macromolecules* **2010**, *43*, 8348–8352.
- (45) Bian, L.; Zhu, E.; Tang, J.; Tang, W.; Zhang, F. Recent Progress in the Design of Narrow Bandgap Conjugated Polymers for High-Efficiency Organic Solar Cells. *Prog. Polym. Sci.* **2012**, *37*, 1292–1331.
- (46) Thelakkat, M. Star-Shaped, Dendrimeric and Polymeric Triarylaminines as Photoconductors and Hole Transport Materials for Electro-Optical Applications. *Macromol. Mater. Eng.* **2002**, *287*, 442.
- (47) Anslyn, E. V.; Dougherty, D. A. *Modern Physical Organic Chemistry*; University Science Books: Sausalito, CA, 2006.
- (48) Hoffmann, R. How Chemistry and Physics Meet in the Solid State. *Angew. Chemie Int. Ed. English* **1987**, *26*, 846–878.
- (49) Morley, J. Calculated Hyperpolarisabilities of Polythiophenes, Polyfurans and Polypyrroles. *J. Chem. Soc., Faraday Trans.* **1991**, *87*, 3009–3013.
- (50) Hernandez, V.; Castiglioni, C.; Del Zoppo, M.; Zerbi, G. Confinement Potential and Π -Electron Delocalization in Polyconjugated Organic Materials. *Phys. Rev. B* **1994**, *50*, 9815–9823.
- (51) Meier, H.; Stalmach, U.; Kolshorn, H. Effective Conjugation Length and UV/vis Spectra of Oligomers. *Acta Polym.* **1997**, *48*, 379–384.
- (52) Meier, H. Conjugated Oligomers with Terminal Donor-Acceptor Substitution. *Angew. Chem. Int. Ed. Engl.* **2005**, *44*, 2482–2506.

CHAPTER 2

DIARYLAMINOFLUORENONE PUSH-PULL MOLECULES

Adapted from Homnick, P. J.; Lahti, P. M. Modular Electron Donor Group Tuning of Frontier Energy Levels in Diarylamino-fluorenone Push-Pull Molecules. *Phys. Chem. Chem. Phys.* **2012**, 11961–11968.¹ Reproduced by permission of the PCCP Owner Societies
<http://pubs.rsc.org/en/content/articlelanding/2012/cp/c2cp41813d#!divAbstract>

[Some changes were made for adapted use in this dissertation.]

2.1 Introduction

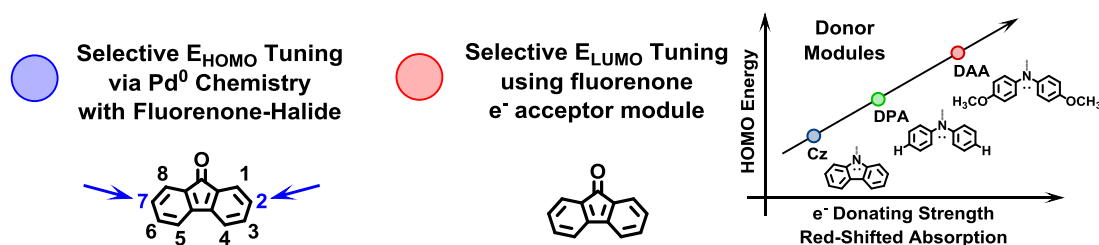
There has recently been a surge in the use of push-pull donor-acceptor (D-A) small molecules and polymers for organic electronic applications. The D-A architecture has been exploited due to the large amount of synthetic control over HOMO/LUMO energy levels when using a modular synthetic approach.¹⁻⁸ Since energy level and band gap engineering are critical components of organic electronic molecular design, especially for photovoltaic applications, further developing this modular D-A design strategy is crucial to designing new high performance materials.

I developed a set of fluorenone-based materials using this modular approach, for the purpose of selectively tuning the HOMO/LUMO energy levels. Fluorenone (acceptor module) and the four arylamine donor modules chosen are relatively simple synthons, and the final D-A molecules are synthetically straightforward to access. Using these D and A modules, I synthesized six D-A materials with a wide range of visible spectrum absorption coverage and highly tuned HOMO/LUMO energies that correlate well with their component D and A modules.

Push-pull molecules with both electron donor and electron acceptor groups (D and A, respectively) have long drawn interest for their second harmonic generation nonlinear optical behavior.⁹⁻¹⁴ More recently, there has been much interest targeted at making molecules with decreased band gaps and tunable highest occupied and lowest unoccupied molecular orbital (HOMO, LUMO) energy levels, for potential use as electronic and light-harvesting materials,

especially in solar cells.^{4,6,15-17} This is an important and increasingly used strategy in designing new materials for organic electronic applications.

Fluorenone (*9H*-fluorenone) has not drawn major attention in synthesis of push-pull systems, even though it provides a planarized biphenyl chromophore for conjugation and a cyclopentadienone central ring for electron acceptor capability.¹⁸⁻²⁰ Its derivatives frequently show excimer photophysics,²¹⁻²⁴ and as an impurity it has been implicated in undesirable green emission from fluorene based organic blue light emitting diodes (OLEDs).²⁵⁻²⁸ But, fluorenone should be a good electron acceptor module for assembly of push-pull molecules due to its low cost and high amenability to synthetic functionalization. As such, more extensive testing of electronic materials based on fluorenone-containing molecules is desirable.



Scheme 2.1: General molecular design strategy for the fluorenone-based materials described in this chapter. HOMO and LUMO energies (E_{HOMO} and E_{LUMO}) tuned by arylamine modules and fluorenone, respectively.

Thus, highly synthetically-tunable systems are important target materials. For this purpose a group of six fluorenone-derived D-A small molecules were designed, synthesized, and characterized. These materials were specifically designed using relatively inexpensive DAA starting materials which are highly amenable to synthetic functionalization. This chapter describes the synthetic strategy, physical chemical analysis, and rationale regarding energy level engineering principles using these fluorenone-based materials. The general molecular design strategy is summarized in Scheme 2.1.

In this chapter, the electronic spectroscopy and electrochemistry are compared for a set of through-conjugated, push-pull molecules having fluorenone as the common electron acceptor (A)

module and diarylamines as electron donor (D) modules. The primary goal of this study was to demonstrate systematic band gap and frontier molecular orbital (FMO) energy tuning, as well as to promote intramolecular charge transfer (ICT) character in the photoexcited state. Because a charge separated excited state in ICT systems tends to be longer lived, the D-A architecture were hoped to provide longer-lived excitons for farther exciton transport in a device in addition to systematic FMO energy and band gap control.

As will be shown below, direct C-N attachment of diarylamine onto fluorenone promotes strong ICT character in the resulting molecules by comparison to structures where conjugated hydrocarbon units intervene. In addition, the electronic behaviors of these materials are well described by a modular deconstruction analysis of HOMO and LUMO energy level tuning by comparison to the individual donor (D) and acceptor (A) structural units. Finally, some preliminary fluorescence lifetime results will be discussed briefly, in the optimistic context of potentially increased device exciton lifetime.

2.2 Experimental Methods

The basic design strategy for this study was to attach diarylamine units to the 2- or 2,7-positions of fluorenone. This connectivity permits conjugation of the amine lone pairs through both benzene rings. Both simpler D-A push-pull systems and D-A-D systems with a centrally placed acceptor fluorenone were tested.

Figure 2.1 shows the syntheses of D-A type systems FOCz, FODPA, and FODAA, and of D-A-D systems FODAAS, FOBDA, and FOBTMPMPA. The D-A systems test the behaviors of directly coupling carbazole (Cz), diphenylamine (DPA), and dianisylamine (DAA) to the fluorenone 2-position. As described later, dianisylamine showed the strongest donor effect, due to the alkoxy donor substituents on its aryl ring *para*-positions. Using this evaluation, additional donor groups were attached at the 7-position: a trimethoxystyrene unit in FODAAS, an additional dianisylamine in FOBDA, and a diarylamine with extra electron donating alkoxy groups on two of the aminophenyl rings in FOBTMPMPA. Intermediates 2-bromofluorenone, 2,7-

dibromofluorenone, and 2-bromo-7-iodofluorenone were made by oxidizing corresponding fluorenes;²⁸⁻³⁰ dianisylamine was made by a literature³¹ procedure. Intermediate 7-BrFOS was made via Heck coupling with one equivalent of 3,4,5-trimethoxystyrene²⁸ and 2-bromo-7-iodofluorenone at the iodine-functionalized site (confirmed by ¹H-NMR and mass spectrometry). The last step in each synthesis was a Pd-catalyzed Buchwald-Hartwig³²⁻³⁴ type amination. Details of synthetic procedures and characterization are given in the experimental procedures chapter. New compounds were characterized and identified using ¹H-NMR, high resolution mass spectrometry, FT-IR spectroscopy, and electronic absorption and emission spectroscopy; their purities were established by HPLC.

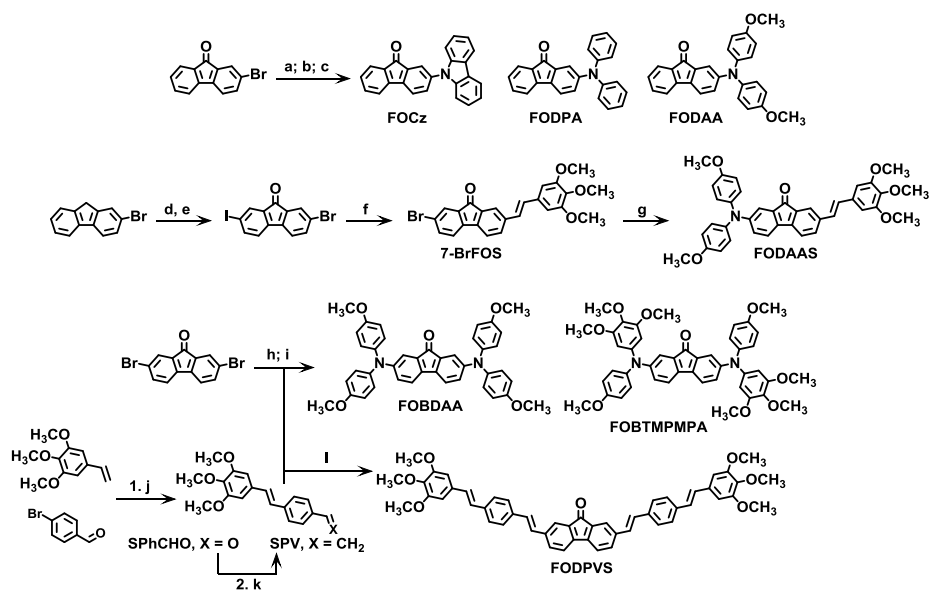


Figure 2.1: Syntheses of FOCz, FODPA, and FODAA: (a) (*p*-MeOPh)₂NH, 0.02 eq Pd₂dba₃, P(*t*-Bu)₃, *t*-BuONa, Δ 2 days for FODAA (70%); (b) Ph₂NH, 0.02 eq Pd₂dba₃, P(*t*-Bu)₃, *t*-BuONa, Δ 1 h for FODPA (66%); (c) carbazole, 0.02 eq Pd₂dba₃, P(*t*-Bu)₃, *t*-BuONa, Δ 1 h for FOCz (51%); (d) I₂/KIO₃/H₂SO₄/HOAc, 90 °C, 2 h for 2-bromo-7-iodofluorene (68%); (e) 2.5 eq CrO₃, Ac₂O, 16 h for 2-bromo-7-iodofluorenone (97%); (f) 3,4,5-tri-MeOPh-CH=CH₂, 0.07 eq Pd(OAc)₂, 0.2 eq P(*o*-tolyl)₃, DMF, Δ 3 days for 7-BrFOS (44%); (g) (*p*-MeOPh)₂NH, 0.02 eq Pd₂dba₃, P(*t*-Bu)₃, *t*-BuONa, Δ 5 h for FODAAS (33%); (h) (*p*-MeOPh)₂NH, 0.02 eq Pd₂dba₃, P(*t*-Bu)₃, NaO-*t*-Bu, Δ for FOBDAA (50%); (i) *N*-(3,4,5-trimethoxy-Ph)-*N*-(*p*-MeOPh)NH, 0.02 eq Pd₂dba₃, P(*t*-Bu)₃, *t*-BuONa, Δ 17 h for FOBTMPMPA (21%). (j) 3,4,5-tri-MeOPh-CH=CH₂, 0.92 eq *p*-bromobenzaldehyde, 0.07 eq Pd(OAc)₂, 0.2 eq P(*o*-tolyl)₃, DMF, Δ 3 days for SPhCHO (61%); (k) SPhCHO, 1.3 eq PPh₃CH₃Br, 1.5 eq *n*-BuLi, THF, 0-26 °C, overnight for SPV (66%). (l) SPV, 0.07 eq Pd(OAc)₂, 0.2 eq P(*o*-tolyl)₃, DMF, Δ 3 days for FODPVS (24%).

2.3 Results and Discussion

2.3.1 Solution Electronic Spectroscopy for D-A Systems

The solution absorption spectroscopy of the push-pull molecules provides insight about their excited state behavior, especially intramolecular charge transfer (ICT) character and its variation as a function of the donor strengths of the different diarylamine modules while the acceptor fluorenone module is held constant. The absorption spectra for asymmetric D-A systems FODAA, FODPA, and FOCz in hexane and acetonitrile are compared in Figure 2.2.

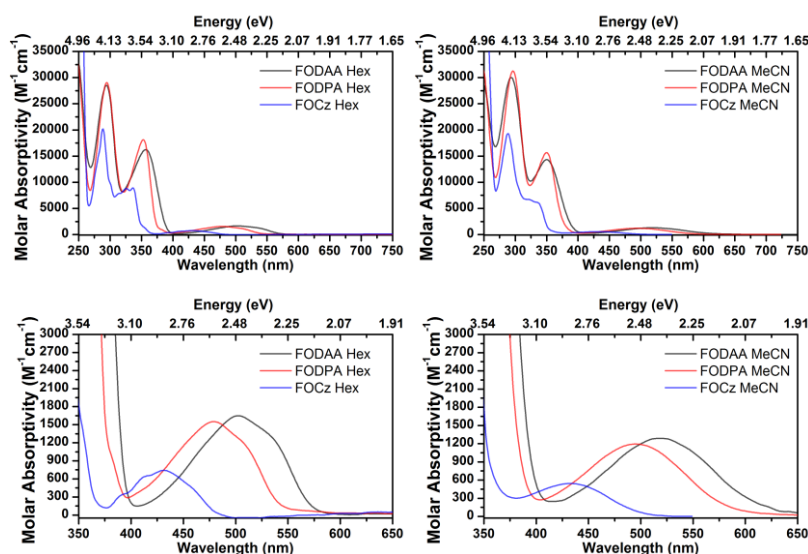


Figure 2.2: Absorption spectra of FODAA (black), FODPA (red), FOCz (blue) in hexane (left charts) and in acetonitrile (right charts).

Fluorenone itself has solvent-dependent absorption bands associated with excited states whose $\pi \rightarrow \pi^*$ or $n \rightarrow \pi^*$ character is solvent dependent.³⁵⁻³⁸ By comparison, dianisylamine substituted system FODAA has its lowest energy absorption at $\lambda_{\max} = 518$ nm, 790 meV red shifted *versus* fluorenone. The analogous band for diphenylamine substituted FODPA is at $\lambda_{\max} = 494$ nm, a 116 meV blue shift *versus* FODAA due to lesser electron donation from the donor module. Carbazole substituted FOCz is quite blue shifted by 500 meV *versus* FODAA with $\lambda_{\max} = 430$ nm. Systems FODAA and FODPA show 10-15 nm (75-80 meV) solvatochromic red shifts of their long wavelength absorption peaks in polar acetonitrile *versus* nonpolar hexane, consistent

with ICT nature for these transitions. The high energy, lower molar absorptivity, and minimal solvatochromism (2 nm) of the longest wavelength band in FOCz presumably occur because its carbazole donor unit loses central ring pseudo-aromaticity if it donates its nitrogen lone pair; so its electron donating strength is less than those of dianisylamine or diphenylamine. As the electron donating strength decreases in FODAA, FODPA, and FOCz the blue shift in the long wavelength absorption is even evident by inspection, since acetonitrile solutions of these are purple, red, and yellowish-orange, respectively. No qualitative changes in absorption spectra occur at higher concentrations to indicate aggregation in hexane, dichloromethane, or acetonitrile. Table 2.1 summarizes the absorption spectral results with comparisons to results from other measurements described below.

Table 2.1: Optical and oxidation properties of fluorenone-diarylamine D-A molecules.

Compound	Absorption λ_{\max}/nm ($\epsilon = L [\text{mol cm}^{-1}]^{-1}$) Hexane	Absorption λ_{\max}/nm ($\epsilon = L [\text{mol cm}^{-1}]^{-1}$) Acetonitrile	Absorption λ_{\max}/nm (onset/nm) Neat Film	Emission λ_{\max}/nm Hexane	Emission λ_{\max}/nm Acetonitrile	Oxidation Onset/mV *	Reduction Onset/mV *
FODAA	249 (33 700)	250 (29 400)	531 (650)	585	Negligible	232, 816	-1980
	295 (28 400)	294 (30 000)					
	357 (16 200)	350 (14 300)					
	502(1650)	518 (1280)					
FODPA	247 (34 400)	248 (32 900)	512 (600)	552	670 (weak)	320, 824	-1370
	295 (29 400)	296 (31 400)					
	354 (18 200)	350 (15 700)					
	479 (1550)	494 (1190)					
FOCz	255 (22 200)	253 (51 600)	445 (540)	521	600 (weak)	715	-1490
	290 (22 000)	290 (20 200)					
	430 (740)	432 (540)					
FOBDAAS	298 (35 700)	306 (41 700)	592 (710)	608	Negligible	178, 667, 1040	-1590
	386 (40 000)	384 (44 000)					
	524 (3310)	543 (2700)					
FOBDA	298 (36 800)	298 (53 000)	600 (700)	650 (very weak)	Negligible	155, 355, 949	-1410
	382 (29 000)	376 (38 200)					
	554 (1780)	586 (1740)					
FOBTMPMPA	298 (43 000)	298 (46 600)	588 (698)	640	Negligible	200, 414, 734	-1640
	382 (33 900)	376 (33 600)					
	554 (2080)	585 (1530)					

* Onset potentials in millivolts in acetonitrile *versus* ferrocene/ferrocenium oxidation.

FODAA, FODPA, and FOCz all show luminescence emission in hexane (Figure 2.3), with peak maxima at progressively longer wavelengths following the trend of increasingly

electronic π -donor ability: DAA > DPA > Cz. In more polar acetonitrile, FODPA and FOCz show greatly weakened, strongly red shifted emission, while DAA substituted FODPA shows virtually no emission. The strong emission solvatochromism and polar solvent quenching supports ICT type charge separation in the excited state, with the strongest electron donating substituent DAA giving the strongest ICT effects. The stronger solvatochromism in emission versus absorption is reasonable, since there is time for solvent molecules to adjust position around the molecule during the lifetime of an excited state with significant charge separation.³⁹ These data are summarized in Table 2.2.

Table 2.2: Absorption solvatochromism from hexanes to acetonitrile, emission Stokes shifts and solvatochromism from hexanes to acetonitrile, in meV.

Compound	Absorption	Stokes Shift		Emission
	Solvatochromism from Hex to MeCN (meV)	Hex (meV)	MeCN (meV)	Solvatochromism from Hex to MeCN (meV)
FODAA	76	350	N/A	Quenched
FODPA	79	342	649	396
FOCz	20	504	797	313
FODAAS	83	327	N/A	Quenched
FOBDAA	122	331	N/A	Quenched
FOBTMPMPA	119	301	N/A	Quenched

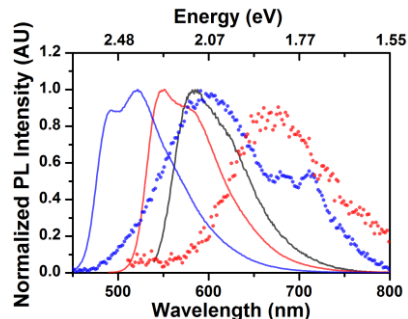
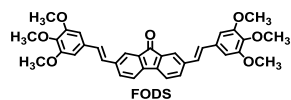


Figure 2.3: Normalized emission spectra of FODAA (black line, excited at 355 nm), FODPA (red line, excited at 475 nm), and FOCz (blue line, excited at 289 nm) in hexane; and FODPA (red dots, excited at 500 nm) and FOCz (blue dots, excited at 289 nm) in acetonitrile. FODAA does not emit detectably in acetonitrile.

2.3.2 Solution Electronic Spectroscopy for D-A-D Systems

The results for the D-A systems showed that the dianisylamine donor gives the strongest ICT type behavior. The D-A-D systems having variable strength donors attached to a 2-dianisylamofluorenone system were therefore tested: FODAAS with a moderately electron donating trimethoxystyrene module added, FOBDAA with two dianisylamine donors, and FOBTMPMPA with diarylamine substituents bearing extra electron donating alkoxy substituents.

The D-A-D' system FODAAS has competition between trimethoxystyrene and dianisylamine donors connected in direct resonance through the 2,7-fluorenone module. FODS, a fluorenone bearing two trimethoxystyrene units in analogous positions to the compounds of this study, is a convenient comparison system to FODAAS and shows excimer formation^{23,28} at higher concentrations, like fluorenone²¹⁻²⁴ itself. The intent was to see whether FODAAS would give spectral behavior more like FODS, or more like the D-A system FODAA.



The absorption spectrum of FODAAS shows two major $\pi \rightarrow \pi^*$ transitions in the 280-400 nm region, significantly red shifted by extended conjugation from the trimethoxystyrene versus the analogous bands in FODAA (Figure 2.4). The lower energy, strong

$\pi \rightarrow \pi^*$ transition is slightly red shifted in acetonitrile versus hexane, similar in behavior to FOCz, FODAAS, and FOBDA. The broad, featureless, ICT transition at 524 nm in hexane red shifts to 543 nm in acetonitrile, a solvatochromic shift of 85 meV. FODAAS has a 608 nm emission peak in hexane (Figure 2.5) that is completely quenched in acetonitrile, again supporting the excited state ICT character. The hexane emission peak does not change shape with concentration in the 10-100 micromolar range and shows no indication of excimer band formation analogous to the behavior of FODS. Thus, the strong dianisylamine π -donation to the fluorenone acceptor changes the fluorenone behavior by comparison to a trimethoxystyrene substituent. But, use of a trimethoxystyrene unit conjugated through fluorenone to a dianisylamine gives stronger ICT character in FODAAS than occurs in the D-A system FODAA, judging by the lower ICT band energy in FODAAS, a 22-25 nm red shift (about 100 meV) relative to FODAA. Absorption and emission solvatochromism and Stokes shift data are summarized in Table 2.2 above.

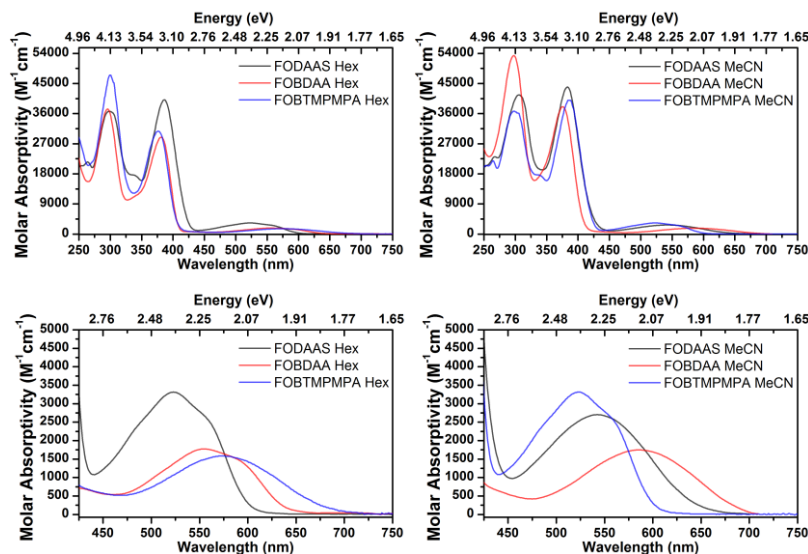


Figure 2.4: Absorption spectra of FODAAS (black), FOBDAAs (red), and FOBTMPMPAs (blue) in hexanes (upper chart) and acetonitrile (lower chart).

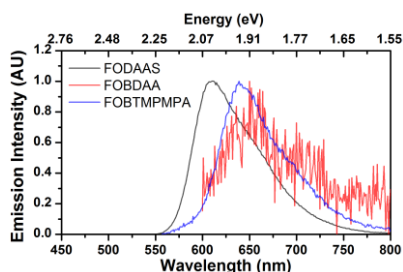


Figure 2.5: Normalized emission spectra of FODAAS (excited at 545 nm), FOBDAAs (excited at 590 nm), and FOBTMPMPAs (excited at 550 nm) in hexane.

The two bis(diarylamine) D-A-D systems FOBDAAs and FOBTMPMPAs show the strongest solvatochromic absorption spectral characteristics in this study. The relatively intense $\pi \rightarrow \pi^*$ absorptions are at similar positions to those in FODAAS (Figure 2.4) and at longer wavelengths than in the D-A systems FODAA, FODPA, and FOCz. Connecting the two diarylamine groups in FOBDAAs and FOBTMPMPAs in direct resonance through the 2,7-positions thus gives an effective conjugation extension effect on the $\pi \rightarrow \pi^*$ transitions by comparison to FODAA.

The ICT bands in FOBDAAs and FOBTMPMPAs appear at 554 nm, which is at lower energy by 128 meV versus FODAAS. They strongly red-shift in acetonitrile to 585-586 nm with

tailing absorption to ~700 nm. This is a ~140 meV change relative to hexane, a significantly larger solvatochromic shift than in the D-A systems or in the D-A-D' system FODAAS with only one dianisylamine module. Figure 2.5 compares the emission spectra of FODAAS, FOBDA, and FOBTMPMPA in hexane. The emission for FOBDA in hexane is barely detectable at roughly 650 nm, and (as with FODAAS) is nil in acetonitrile. FOBTMPMPA shows modest emission at 636 nm in hexane, with very weak, broad emission at about 650 nm in acetonitrile. The behaviors for all of FODAAS, FOBDA, and FOBTMPMPA are consistent with ICT type fluorescence quenching that is enabled by the strongly electron donating nature of their diarylamine substituents. It was somewhat surprising that FOBTMPMPA with extra alkoxy groups on its diarylamine modules showed stronger emission than FOBDA, indicating less effective ICT in FOBTMPMPA. Perhaps the extra alkoxy groups in proximity to one another cause twisting of the groups out of the phenyl ring plane, limiting resonance delocalization of the oxygen lone pairs; but this is speculative.

Extending the conjugation length of the FODS compound by an extra phenylene-vinylene unit on each donor module was also tested, to give FODPVS. It was expected that extending the donor group conjugation length would increase the HOMO energy (and decrease the band gap) and increase the molar absorptivity. Surprisingly, the band gap did not change, but the ICT band molar absorptivity nearly doubled for FODPVS versus FODS (Figure 2.6). However, the π - π^* band around 375 nm for FODS red-shifted to about 400 nm for FODPVS, and the absorption onsets red-shifted from ~400 to ~450 nm, respectively. So, while the band gap for FODPVS did not decrease using this strategy, its molar absorptivity and visible spectral coverage increased considerably.

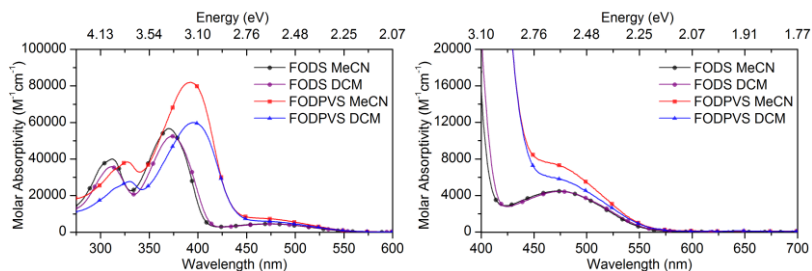


Figure 2.6: FODS and FODPVS absorption spectra in acetonitrile and dichloromethane. Left, 275-600 nm absorption window. Right, focus on ICT band region.

2.3.3 Comparative Amino Substituent Effects on Fluorenone Acceptors

In work that has bearing on the present study, Inoue and coworkers²⁹ carried out an extensive study of absorption and emission spectral behavior in multiple solvents for twelve D-A fluorenone systems functionalized with NH_2 , $\text{NH}(\text{CH}_3)$, and $\text{N}(\text{CH}_3)_2$ at each of the 1- through 4-positions shown generically below as structure FO. They found absorption solvatochromic red-shifts of 130-175 meV in cyclohexane versus acetonitrile, and strong luminescence solvatochromic red shifts with quenching in polar media. Increasing amino group methylation gave larger ICT absorption band red shifts, due to increased amine electron donor strength. Comparatively, the results for FODAA, FODPA, and FOCz show that substituent electronic effects that are transmitted indirectly to an amino group through the π -electrons of a *para*-linked benzene ring are also strong enough to be readily observed.

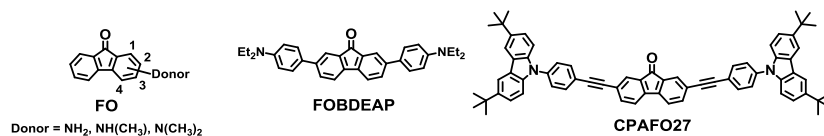


Figure 2.7: Literature examples of fluorenone systems for comparison.

From the same work,²⁹ 2-((*N,N*-dimethylamino)fluorenone (2DMAF, FO with $-\text{NMe}_2$ in the 2-position) exhibits ICT absorption maxima at 484 nm in cyclohexane and 510 nm in acetonitrile. It has emission maxima at 600 nm in cyclohexane, 644 nm in benzene, and full quenching in acetonitrile. Dianisylamino substituted FODAA in the present study – with the strongest donor substitution – has a lower energy ICT band maximum in hexane, but a higher

energy emission band maximum. The larger Stokes shift in 2DMAF *versus* FODAA indicates a greater geometric difference between ground and excited ICT states in 2DMAF. Inoue considered²⁹ twisted ICT (TICT) state formation in their systems from effects of increasing methyl substitution on the amino group, but concluded that only the sterically hindered 1-aminofluorenones had the possibility of TICT. Qualitative structural considerations and computational modeling indicate that all of the diarylamino substituted fluorenones except FOCz (with a planar carbazole) have a propeller shape about the amine nitrogen. The smaller Stokes shift for FODAA versus 2DMAF is consistent with a lesser geometric change from ground to ICT excited state, since FODAA is already nonplanar in the ground state.

The electronic spectral results for FODAA, FODPA, FOCz, FODAAS, FOBDA, and FOBTMPMPA can be compared to results from systems where an amino lone pair is not directly attached to fluorenone, but is resonance connected through conjugated hydrocarbon units. Konishi and coworkers³⁰ reported that FOBDEAP has two $\pi \rightarrow \pi^*$ absorption bands analogous to those in FODAAS, FOBDA, and FOBTMPMPA and an ICT band exhibiting a solvatochromic shift from 496 nm in hexane to 529 nm in acetonitrile (155 meV); the analogous solvatochromism for FOBDA and FOBTMPMPA in hexane versus acetonitrile is 122 meV. However, the luminescence behavior of FOBDEAP is much more complex than that in FODAA, FODPA, FOCz, FODAAS, FOBDA, and FOBTMPMPA, with localized emission at 409-417 nm, ICT emission at 436-450 nm, and excimer bands that shift from 619 nm in toluene to 644 nm in tetrahydrofuran. The competing behaviors in FOBDEAP are likely due to attenuation of the diethylamine electron donation by the intervening phenylene units and the torsional flexibility caused thereby, allowing other fluorescent processes to occur that would be quenched in systems with strong ICT from stronger, more direct electron donation.

Neckers and coworkers³¹ studied D-A-D system CPAFO27 (Figure 2.7) with carbazole donor modules linked through intervening but still resonance conjugating phenylethynyl units in a 2,7-fluorenone connectivity. System CPAFO27 has a $\pi \rightarrow \pi^*$ band at 350 nm, which is

significantly higher in energy (by ~ 300 meV) than the corresponding bands in FOBDA, and FOBTMPMPA. The ICT band of CPAFO27 at 440 nm in tetrahydrofuran is 580 meV to higher energy by comparison to the 554 nm bands for FOBDA, and FOBTMPMPA in hexane. The difference is attributable both to the attenuating effect of the phenylethynylene units intervening between fluorenone and the amino donor lone pair, and a lesser electron donor strength of carbazole. But, although FODAAS, FOBDA, and FOBTMPMPA – like 2DMAF and its analogues with less methyl substitution – shows lower energy ICT absorption bands than CPAFO27, the ICT band molar absorptivity for CPAFO27 is 5- to 6-fold stronger. Neckers described how a non-through-conjugated 3,6-isomer of CPAFO27 gives more intense ICT bands due to excited state dipole alignment of donor-acceptor interactions with the C=O group dipole in that connectivity. That design model offers increased ICT absorption intensity in push-pull substituted fluorenones, albeit at a cost of decreased through-bond resonance donor-acceptor interaction that can result in higher energy ICT absorption bands. Analogous 3,6-isomers were synthesized as a continuation of the studies described in this chapter, and will be discussed in Chapter 3.

2.3.4 Solid State Absorption Spectroscopy

The absorption spectral band maxima and onsets for drop-cast solid films of FODAA, FODPA, FOCz, FODAAS, FOBDA, and FOBTMPMPA are given in Table 2.1 and their changes compared in Table 2.3; normalized comparisons of the spectra are shown in Figure 2.8. FOCz shows the highest energy onset at 530 nm (2.34 eV), while FODAAS, FOBDA, and FOBTMPMPA absorb strongly through much of the visible spectrum with band onsets at 600-630 nm (2.08-1.97 eV). The samples appear magenta to aquamarine as thin films and dark magenta to black as crystals or as thicker films. None of the films exhibits fluorescence emission at room temperature. Interestingly, D-A-D' system FODAAS with only one dianisylamine unit exhibits a broadly absorbing film UV-vis spectrum at just slightly lower onset energy than FOBDA, and FOBTMPMPA. FODAAS also shows a large absorption maximum red-shift

from acetonitrile to neat film (190 meV), while FODPA, FODAA, and FOBTMPMPA show the smallest shift.

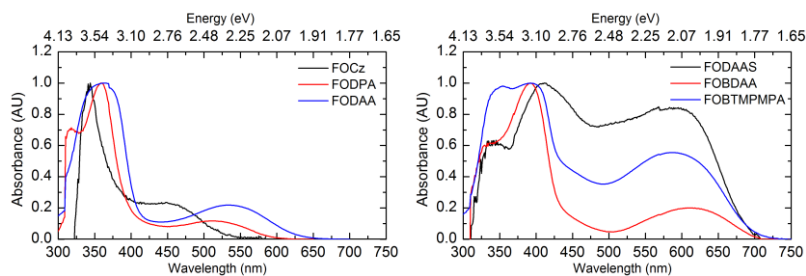


Figure 2.8: Normalized solid film absorption spectra for D-A compounds FOCz, FODPA, and FODAA (left chart), and D-A-D compounds FODAAS, FOBDAA, and FOBTMPMPA (right chart).

Table 2.3: Solution and neat film band gap onset comparisons.

Compound	Solution Band Gap Onset		Solid Band Gap Onset		Solution-Solid Band Gap Shift	
	Wavelength (nm)	Energy (eV)	Wavelength (nm)	Energy (eV)	Wavelength (nm)	Energy (eV)
FODAA	616	2.01	629	1.97	13	0.04
FODPA	587	2.11	596	2.08	9	0.03
FOCz	503	2.46	530	2.34	27	0.12
FODAAS	644	1.93	695	1.78	51	0.15
FOBDAA	710	1.74	702	1.77	-8	-0.03
FOBTMPMPA	683	1.82	698	1.78	15	0.04

The large shift in FODAAS – and smaller but still readily observable red shifts in FODAA, FODPA, FOCz, and FOBDAA – may be due to generalized dipole effects, although it is unlikely that the dielectric field of these materials is stronger than that of acetonitrile with a dielectric constant of 37.5 and a molecular dipole of 3.92 D. They may also be due to aggregation in the solid state, but there are no shoulders or other features in any of the film spectra that differ from the solution spectra to suggest appreciably well-organized aggregate π -stack formation. The small shift in FOBTMPMPA for solid versus solution absorption may occur because its asymmetric diarylamine substitution inhibits π -stacking in the films. By comparison, the relatively large shift in “hybrid” D-A-D’ compound FODAAS may be due to a slightly greater amount of π -stacking of its trimethoxyfluorene units in the solid state. However, this hypothesis

is speculative at present, and a search of the Cambridge Structure Database showed no diarylamino fluorenes or 2-styryl fluorenes for solid state packing comparisons.

Since π -stacking is an important feature in organic electronic devices, the permissive evidence that these materials may undergo some organization in the solid state suggests that they may be promising candidates for solid state organic electronic devices. Indeed, preliminary charge carrier mobility measurements conducted in a PMMA matrix using the time of flight (TOF) methodology (performed by Dr. Akshay Kokil at UMass Lowell) indicate that FODAA and FODAAS each transport holes on the order of $2 \times 10^{-5} \text{ cm}^2/\text{Vs}$, a modest mobility for organic electronic materials.

2.3.5 Electrochemistry

Cyclic voltammetry of the push-pull compounds in this study was evaluated in solution against the ferrocene/ferrocenium redox couple in acetonitrile (Figure 2.9). Table 2.1 gives redox onset voltages for all compounds, and half-wave potentials $E_{1/2}$ where observed. Not all of the compounds exhibit sufficiently reversible redox behavior for $E_{1/2}$ determination, as shown by the cyclic voltammograms below. Therefore, redox onsets were used for energy level determinations described below, following practices reported⁴⁴⁻⁴⁷ by other workers.

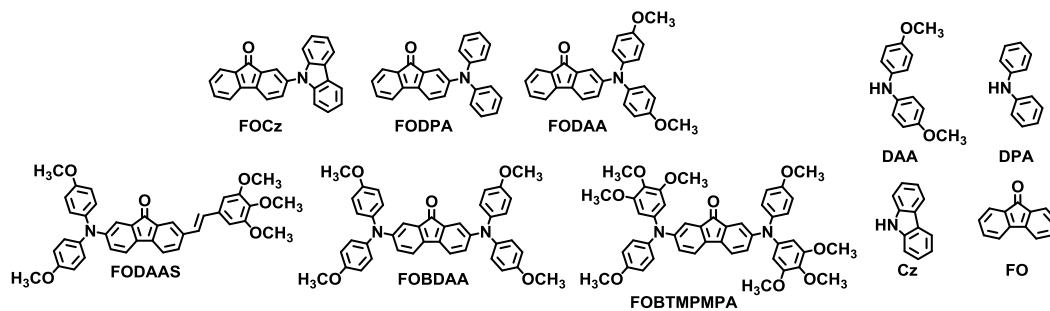
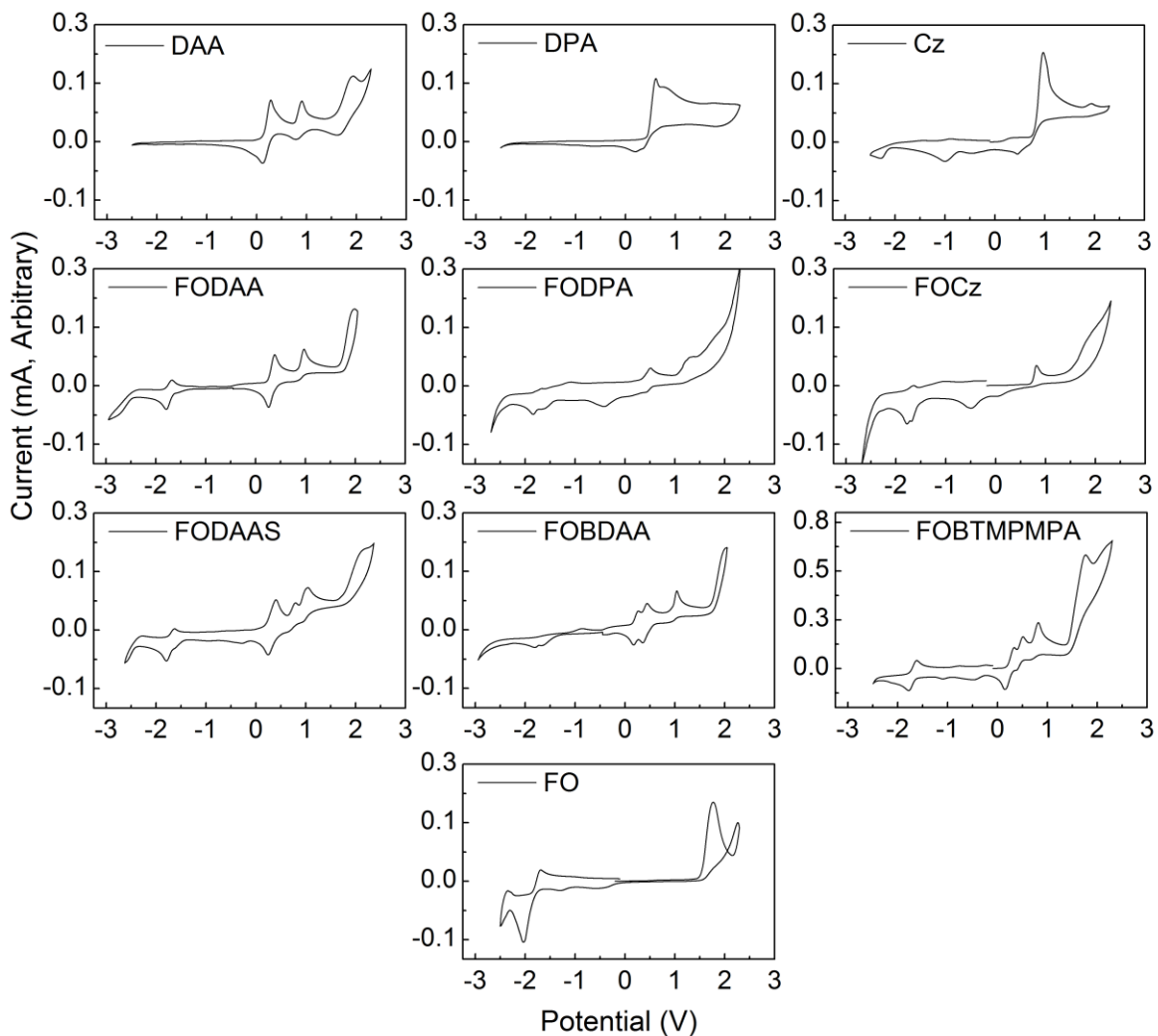


Figure 2.9: Cyclic voltammograms for all D-A compounds and their constituent D and A modules, obtained in acetonitrile using the ferrocene/ferrocenium redox couple as an external standard.

All of FODAA, FODPA, FOCz, FODAAS, FOBDA, and FOBTMPMPA show a reduction feature in the -1.4 to -1.7 V range that is attributable to the fluorenone module, although in some cases the feature is weak and clearly irreversible. These are all lower potentials than the quasireversible -1.9 V half-wave reduction potential observed for fluorenone itself, due to variations in LUMO energy from the attached functional groups, as is described later. The reduction potentials are similar to Neckers' electrochemical findings³¹ for CPAFO27 (Figure 2.7) and the related system without carbazole groups. The D-A systems FODAA, FODPA, and FOCz show increasing voltage oxidation features in order appropriate for their electron donor strengths; the +715 mV irreversible oxidation feature for FOCz is again consistent with Neckers' electrochemical findings³¹ for the carbazole group in CPAFO27, and is close to the +809 mV irreversible oxidation onset for carbazole itself. FODAA shows reversible onset oxidation at +232 mV, while FODPA – like FOCz – shows an irreversible oxidation feature, but at +320 mV. The poor definition of the amine oxidation features for FODPA and FOCz may be due to a lack of protecting or π -stabilizing substituents on their diarylamino groups, making oxidation less reversible. In addition to the lack of protecting groups in FOCz, loss of pseudoaromaticity upon oxidation also presents a strong driving force against easy oxidation and likely contributes to its oxidative irreversibility.

D-A-D' system FODAAS shows a reversible oxidation onset at +178 mV that presumably arises from its dianisylamine module, with decreased oxidation potential due to conjugation to the conjugating trimethoxystyrene unit; a barely resolved oxidation feature at about +670 mV may be associated with the trimethoxystyrene-fluorenone unit. By comparison, both FOBDA, and FOBTMPMPA show two reversible, overlapping oxidation peaks from monocation and dication products from their two diarylamino modules, at +155/+355 mV and +200/+414 mV, respectively. The higher oxidation potentials and second oxidation quasireversibility for FOBTMPMPA are in qualitative accord with the spectral evidence that the

N(PhOMe)(Ph[OMe]₃) groups in FOBTMPMPA are poorer electron donors than the simpler dianisylamine groups in FOBDAAs.

The electrochemistry of FODAA, FODPA, FOCz, FODAAS, FOBDAAs, and FOBTMPMPA provides useful electronic information, especially when combined and compared with the spectral data. These are used in the next section to analyze how donor group variation modulates the electronic energy levels (FMO energies) of the systems examined.

2.3.6 Modular Analysis of Donor Group Tuning of Push-Pull Molecule FMO Energies

Evaluation of organic molecules for potential use as electronic materials typically involves estimating the energies of their highest occupied and lowest unoccupied molecular orbitals ($E_{\text{HOMO}}/E_{\text{LUMO}}$) and their band gaps (E_g). It has been pointed out elsewhere³⁵ that various models have been used to estimate E_{HOMO} and E_{LUMO} from solution phase cyclic voltammetry plus absorption spectroscopy. This can give uncertainties in comparing nominally analogous properties evaluated in different studies. But, this type of evaluation allows reasonable comparison of varying electronic effects in structurally related molecules.

Stearman and coworkers recently reported³⁶ a detailed study of electrochemistry and optical spectroscopy to determine frontier orbital energetic and excited state natures for several fluorenones having simple electron donor or electron acceptor groups in 2- or 2,7-positions, including -NH₂. They correlated their molecular electronic findings with Hammett substituent σ_{para} constants to gauge the effect of relative electron donating and withdrawing effects. Further, they interpreted the HOMO and LUMO energy tuning in these systems in terms of substituent effects on band gap excitation of an $n \rightarrow \pi^*$ transition involving the carbonyl lone pair electrons; this was partly based on variation of vibrational carbonyl stretching mode energies. Bérces and coworkers similarly concluded³⁷ that singlet excited states in 2-substituted fluorenones were much influenced by changes in electron density at the carbonyl oxygen. Neckers' work that included³¹ studies of CPAFO27, on the other hand, interpreted the band gap transitions of that donor-substituted fluorenone as being more ICT than $n \rightarrow \pi^*$ in character. Of

course, structural differences in the molecules evaluated between the two studies allow for different mechanisms of behavior. In the discussion below, Neckers' interpretation was used to consider how changes to the diarylamine substituents modulate the electronic properties of the materials. An ICT interpretation of the band gap transitions in these systems seems most consistent with their DFT-computed HOMO and LUMO natures, and with the strong solvatochromic effects seen in the fluorescence spectroscopy. Spectral solvation effects in my and Neckers' systems seemed likely to be similar to one another – since all incorporate diarylamine substituents – than they would be to the simpler -NH₂ substituted systems in Stearman's and Bérces' studies.

In the following discussion, equation (1) was used³⁵ to convert the first oxidation onset voltages from Table 2.1 to HOMO energies in Figure 2.10, including values for the individual donor modules as determined from the synthetic building blocks DAA, DPA, Cz, S, and FO. Spectral band gaps E_g in eV from the low energy absorption peak onsets of the longest wavelength spectral peaks in acetonitrile were used to estimate E_{LUMO} using equation (2). This was done for consistency among all the systems having amine units, since some of these did not show voltammetric reduction features. Under the conditions used in these studies, fluorenone does not show a readily interpreted voltammetric oxidation feature, but does give a clear, reversible reduction wave yielding a LUMO energy of -2.98 eV directly from equation (1), in reasonable agreement with its reported³⁸ electron affinity of -3.1 eV.

$$E_{\text{HOMO/LUMO}} = -(E_{\text{ox/red}} + 4.8) \text{ eV} \quad 1)$$

$$E_{\text{LUMO}} = E_{\text{HOMO}} + E_{\text{g}} \quad 2)$$

Figure 2.10 compares the experimentally determined FMO energies for FODAA, FODPA, FOCz, FODAAS, FOBDA, and FOBTMPMPA and for the modular components used to construct them. The FMO energies can be understood using a modular, component analysis model. Figure 2.11 shows in a simplified manner how the component MOs can be considered to determine the MO energies for a general donor-acceptor π-system. In particular, using a typical

perturbation interaction approach, the low-lying LUMO of the acceptor and the HOMO of the donor(s) will dominate the donor-acceptor system's electronic behavior.

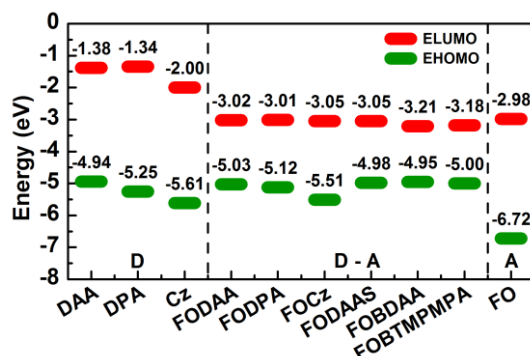


Figure 2.10: HOMO and LUMO energy levels derived from equations (1)-(2) for 2-7 and modular building blocks. DAA = dianisylamine, DPA = diphenylamine, Cz = carbazole, FO = fluorenone. See above for details of energy level determinations.

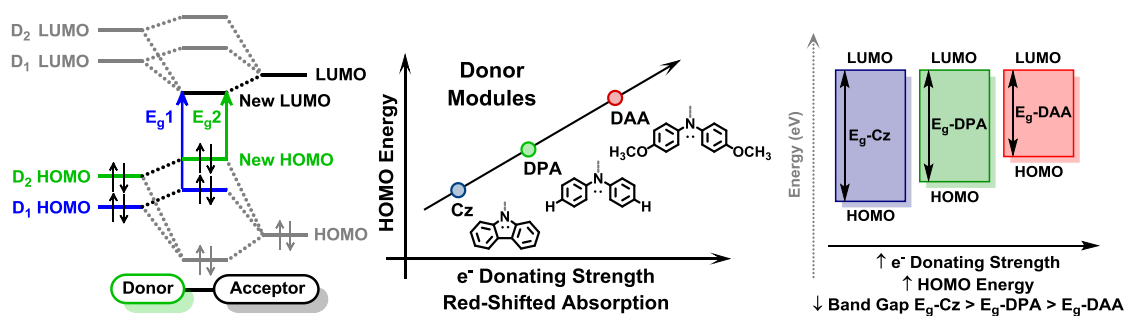


Figure 2.11: Modular deconstruction of push-pull system (D-A) frontier molecular orbitals derivable from interaction of generic acceptor module A with different donor modules D₁ and D₂, where D₂ is the stronger donor.

The nearly constant experimental LUMO energies for FODAA, FODPA, and FOCz in Figure 2.10 reflect the dominance of the common fluorenone acceptor component used in all of the D-A system LUMOs. Both B3LYP/6-31G(d)⁵¹⁻⁵³ and M06-2X/6-311G(d,p)^{42,43} hybrid density functional computations* further support this, showing the LUMO density to reside almost totally on fluorenone (Figure 2.12). Changing the donor HOMO levels alters the D-A system HOMO energies, because the D-A HOMO has a large contribution from the donor unit. Neckers'

* Computational modeling was carried out using Spartan 2010 for Linux from Wavefunction Inc., Irvine, CA, USA, Gaussian 09,⁴⁵ and the Gaussian NBO population routines.⁴⁸

analysis³¹ of the photophysical behavior of CPAFO27 as an ICT system (which he noted was applicable to other donor-substituted fluorenones) outlined a similar reasoning that donor substituents on a fluorenone aryl unit will push up the π -orbital energies selectively. Similar arguments have been used^{10,44} with other push-pull systems.

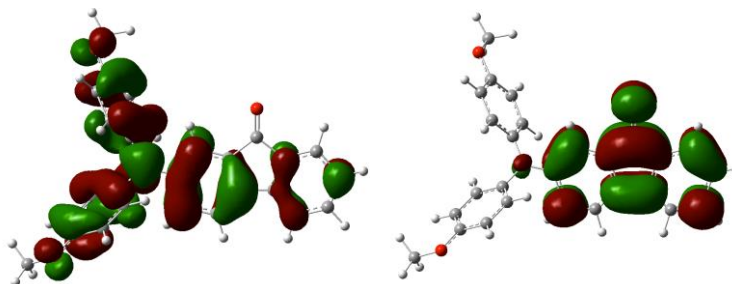


Figure 2.12: HOMO (left) and LUMO (right) plots for FODAA, computed using the B3LYP/6-31G* level of theory and basis set in Gaussian09.⁴⁵

Table 2.4: Computed ground state dipole moments.

Compound	Dipole Moment (B3LYP/6-31G*) ^a	Dipole Moment (M06-2X/6-311G[d,p]) ^b	Experimental E _{HOMO} (eV)	Computed E _{HOMO} (eV)
FODAA	3.27 D	3.08 D	-5.03	-4.74
FODPA	3.13 D	3.12 D	-5.12	-5.05
FOCz	3.76 D	3.69 D	-5.51	-5.41
FODAAS	5.27 D	5.70 D	-4.98	-4.66
FOBDA	3.04 D ^c	2.01 D ^c	-4.95	-4.44
FOBTMPMPA	--- ^d	--- ^d	-5.00	-4.51

Ground state dipole moments (in vacuum) were computed using geometries optimized at the same level of theory. ^aB3LYP/6-31G* dipole moments computed using Spartan 2012 for Linux (Wavefunction Inc., Irvine CA, USA). ^bM06-2X/6-311G(d,p) dipole moments computed using NBO routine in Gaussian 09⁴⁵ for molecules optimized at the same level of theory. ^cThe two computed conformers were different, partly due to symmetry constraints placed on the M06-2X computation; this contributes to the difference between dipole moments at the two levels of theory. ^dNot listed due to multiple different conformations.

In the present study, the experimental HOMO energies for the donor modules track the donor strengths: dianisylamine > diphenylamine > carbazole. The dianisylamine HOMO interaction with fluorenone – generically shown in Figure 2.11 – pushes the HOMO of FODAA to higher energy than the diphenylamine HOMO does for the HOMO of FODPA. Conversely, the lower energy HOMO of carbazole interacts less with fluorenone, so the HOMO

of FOCz is lower than the HOMO for either FODAA or FODPA. Thus, the experimental HOMO energies of dianisylamine, diphenylamine, and carbazole largely determine E_{HOMO} for the push-pull systems FODAA, FODPA, and FOCz, consistent with the Figure 2.11 model. The stable LUMO energies from the common fluorenone acceptor module in FODAA, FODPA, and FOCz, combined with the variation of HOMO energies by varying their donor modules, provide an effective “molecular engineering” strategy for systematically tuning frontier energy levels and band gaps in this set of push-pull chromophores. This trend is also supported by computational methodology, which further reinforces the predictive engineering nature of this synthetic design strategy (computed and experimental HOMO energies shown in Table 2.4).

The behaviors of the D-A-D systems FODAAS, FOBDA, and FOBTMPMPA are complicated by their having two donor modules per fluorenone (two different donors in the case of FODAAS). But, again, their fluorenone acceptor modules essentially determine the energy and nature of their LUMOs. System FODAAS with only one dianisylamine group has the same LUMO energy as seen in FODAA, FODPA, and FOCz, so adding the conjugating, electron donating trimethoxystyrene group in FODAAS does not much alter its frontier orbital energies relative to FODAA. The electronic similarity of the donor units for FOBDA and FOBTMPMPA results in these having similar HOMO energies. The LUMO energies in FOBDA and FOBTMPMPA are somewhat decreased relative to the LUMOs of FODAA, FODPA, and FOCz, because of the added interaction of a second donor LUMO with the acceptor LUMO (Figure 2.11). The change is not large, since the fluorenone acceptor nature still dominates the LUMO – as shown in the computed orbital pictures – but the decrease is consistent with the donor-acceptor modular interaction model.

2.3.7 Time Resolved Photoluminescence Spectroscopy for Selected Push-Pull Systems

Time resolved photoluminescence spectroscopy (TRPL) was done by Boqian Yang from Professor Michael Barnes’ group. Fluorescence lifetimes ranged from 1.1 – 4.3 ns, which is within the typical 1 – 20 ns lifetime range of solution phase poly(3-hexylthiophene) (P3HT),^{46,47} a

commonly used p-type OPV material. These results are given in Figure 2.13 and Table 2.5.

Although excited state lifetimes in neat films were not determined, it would be desirable if they are long enough to allow for moderately long-lived excitons. Because many solid state properties are difficult to predict from solution-phase behavior, it is not useful to conjecture about the possible exciton lifetime or maximum exciton diffusion length for thin films of these compounds.

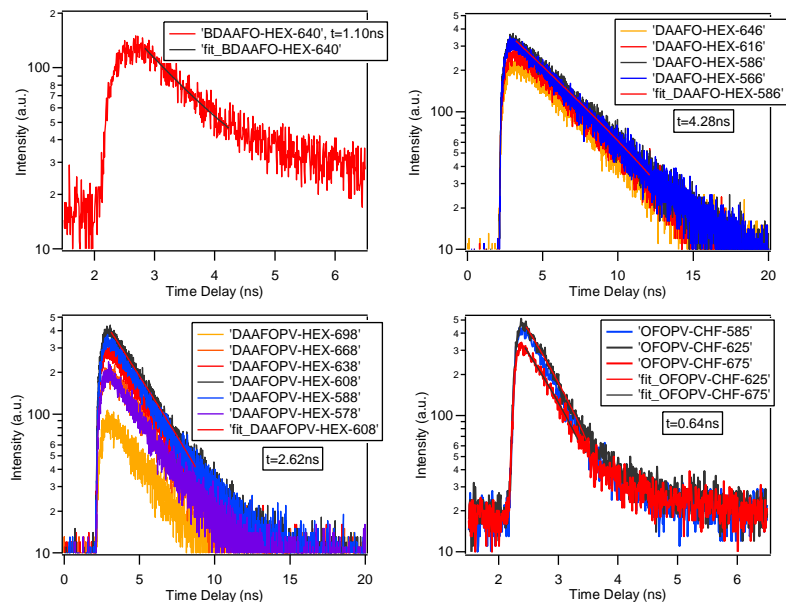


Figure 2.13: Fluorescent lifetime studies of FOBDAA (BDAAFO), FODAA (DAAFO), and FODAAS (DAAFOPV) in hexanes and FODS (OFOPV) in chloroform.

Table 2.5: Fluorescence lifetimes of BDAAFO, DAAFO, and DAAFOPV in hexanes, and OFOPV and NB in chloroform.

Compound	Fluorescence Lifetime (ns)
FOBDAA	1.10
FODAA	4.28
FODAAS	2.62
FODS	0.640

2.4 Conclusions

Fluorenone is a simple, readily available electron-accepting module for push-pull conjugated systems. Spectral and electrochemical properties were assessed for a set of 2-diarylamino fluorenone push-pull systems designed using a modular, electronic building block approach. Varying the diarylamino donor group strength gave tunable energy levels and band

gaps, with strongly quenched emission attributable to intramolecular charge transfer effects. A modular analysis of interactions between donor and acceptor modules by a combination of optical spectroscopy and electrochemistry works well to interpret and fine-tune molecule orbital energy levels for a set of structurally related, push-pull systems. This approach to tuning HOMO and LUMO levels and band gaps should be highly effective to optimize properties of such systems for electronic materials uses. For example, use of diarylamine donor groups will allow further synthetic elaboration at the donor aryl units, including potential incorporation into polymeric structures. An extension of this work using a fluorenylidene malononitrile acceptor core, and 3,6- versus 2,7-connectivity is discussed further in Chapter 3.

2.5 References

- (1) Homnick, P. J.; Lahti, P. M. Modular Electron Donor Group Tuning of Frontier Energy Levels in Diarylamino-fluorenone Push-Pull Molecules. *Phys. Chem. Chem. Phys.* **2012**, 11961–11968.
- (2) Prasad, P. N.; Williams, D. J. *Introduction to Nonlinear Optical Effects in Molecules & Polymers*; John Wiley & Sons: New York, 1991.
- (3) Meyers, F.; Bredas, J. L. Electronic Structure and Nonlinear Optical Properties of Push-Pull Conjugated Molecules. *Int. J. Quantum Chem.* **1992**, 42, 1595–1614.
- (4) Kirtman, B.; Champagne, B. Nonlinear Optical Properties of Quasilinear Conjugated Oligomers, Polymers and Organic Molecules. *Int. Rev. Phys. Chem.* **1997**, 16, 389–420.
- (5) Meier, H. Conjugated Oligomers with Terminal Donor-Acceptor Substitution. *Angew. Chem. Int. Ed. Engl.* **2005**, 44, 2482–2506.
- (6) Cho, M.; Choi, D.; Sullivan, P.; Akelaitis, a; Dalton, L. Recent Progress in Second-Order Nonlinear Optical Polymers and Dendrimers. *Prog. Polym. Sci.* **2008**, 33, 1013–1058.
- (7) Dalton, L. R.; Sullivan, P. a; Bale, D. H. Electric Field Poled Organic Electro-Optic Materials: State of the Art and Future Prospects. *Chem. Rev.* **2010**, 110, 25–55.
- (8) Beaujuge, P. M.; Fréchet, J. M. J. Molecular Design and Ordering Effects in Π -Functional Materials for Transistor and Solar Cell Applications. *J. Am. Chem. Soc.* **2011**, 133, 20009–20029.
- (9) Zhou, H.; Yang, L.; You, W. Rational Design of High Performance Conjugated Polymers for Organic Solar Cells. *Macromolecules* **2012**, 45, 607–632.
- (10) Zhang, Z.; Wang, J. Structures and Properties of Conjugated Donor–Acceptor Copolymers for Solar Cell Applications. *J. Mater. Chem.* **2012**, 22, 4178–4187.
- (11) Boudreault, P.-L. T.; Najari, A.; Leclerc, M. Processable Low-Bandgap Polymers for Photovoltaic Applications †. *Chem. Mater.* **2010**, 101012131424030.
- (12) Bundgaard, E.; Krebs, F. Low Band Gap Polymers for Organic Photovoltaics. *Sol. Energy Mater. Sol. Cells* **2007**, 91, 954–985.
- (13) Lincker, F.; Heinrich, B.; De Bettignies, R.; Rannou, P.; Pécaut, J.; Grévin, B.; Pron, A.; Donnio, B.; Demadrille, R. Fluorenone Core Donor–acceptor–donor Π -Conjugated Molecules End-Capped with Dendritic Oligo(thiophene)s: Synthesis, Liquid Crystalline Behaviour, and Photovoltaic Applications. *J. Mater. Chem.* **2011**, 21, 5238.
- (14) Lincker, F.; Delbosc, N.; Bailly, S.; De Bettignies, R.; Billon, M.; Pron, A.; Demadrille, R. Fluorenone-Based Molecules for Bulk-Heterojunction Solar Cells: Synthesis, Characterization, and Photovoltaic Properties. *Adv. Funct. Mater.* **2008**, 18, 3444–3453.

- (15) Demadrille, R.; Delbosc, N.; Kervella, Y.; Firon, M.; De Bettignies, R.; Billon, M.; Rannou, P.; Pron, A. Conjugated Alternating Copolymer of Dialkylquaterthiophene and Fluorenone: Synthesis, Characterisation and Photovoltaic Properties. *J. Mater. Chem.* **2007**, *17*, 4661.
- (16) Arathi Rani, S.; Sobhanadri, J.; Prasada Rao, T. . Determination of the Excited State Dipole Moment of Fluorenone Using the Method of Solvatochromism. *Spectrochim. Acta Part A Mol. Biomol. Spectrosc.* **1995**, *51*, 2473–2479.
- (17) Kamin, J.; Heldt, J. R.; Heldt, J.; Jo, M. Spectroscopic Studies of Fluorenone Derivatives. **2001**, *11*.
- (18) Scott, J. L.; Yamada, T.; Tanaka, K. Guest Specific Solid-State Fluorescence Rationalised by Reference to Solid-State Structures and Specific Intermolecular Interactions. *New J. Chem.* **2004**, *28*, 447.
- (19) Liu, Y.; Tao, X.; Wang, F.; Shi, J.; Sun, J.; Yu, W.; Ren, Y.; Zou, D.; Jiang, M. Intermolecular Hydrogen Bonds Induce Highly Emissive Excimers: Enhancement of Solid-State Luminescence. *J. Phys. Chem. C* **2007**, *111*, 6544–6549.
- (20) Ferenczi, T. a M.; Sims, M.; Bradley, D. D. C. On the Nature of the Fluorenone-Based Emission in Oxidized Poly(dialkyl-Fluorene)s. *J. Phys. Condens. Matter* **2008**, *20*, 045220.
- (21) Montilla, F.; Mallavia, R. On the Origin of Green Emission Bands in Fluorene-Based Conjugated Polymers. *Adv. Funct. Mater.* **2007**, *17*, 71–78.
- (22) Gong, X.; Iyer, P. K.; Moses, D.; Bazan, G. C.; Heeger, a. J.; Xiao, S. S. Stabilized Blue Emission from Polyfluorene-Based Light-Emitting Diodes: Elimination of Fluorenone Defects. *Adv. Funct. Mater.* **2003**, *13*, 325–330.
- (23) Rathnayake, H. P.; Cirpan, A.; Karasz, F. E.; Odoi, M. Y.; Hammer, N. I.; Barnes, M. D.; Lahti, P. M. Luminescence of Molecular and Block Copolymeric 2,7-Bis(phenylethynyl)-Fluorenes; Identifying Green-Band Emitter Sites in a Fluorene-Based Luminophore. *Chem. Mater.* **2007**, *19*, 3265–3270.
- (24) Kuboyama, A. Similarity between the π , π^* Absorption Spectra of Fluorenone and 9, 10-Phenanthrenequinone. *Chem. Phys. Lett.* **1976**, *41*, 544–546.
- (25) Józefowicz, M.; Heldt, J. R. Dipole Moments Studies of Fluorenone and 4-Hydroxyfluorenone. *Spectrochim. Acta. A. Mol. Biomol. Spectrosc.* **2007**, *67*, 316–320.
- (26) Andrews, L. J.; Deroulede, A.; Linschitz, H. Photophysical Processes in Fluorenone. *J. Phys. Chem.* **1978**, *82*, 2304–2309.
- (27) Kobayashi, T.; Nagakura, S. Picosecond Time-Resolved Spectroscopy and the Intersystem Crossing Rates of Anthrone and Fluorenone. *Chem. Phys. Lett.* **1976**, *43*, 429–434.

- (28) Rathnayake, H. P.; Cirpan, A.; Lahti, P. M.; Karasz, F. E. Optimizing LED Properties of 2,7-Bis(phenylethenyl)fluorenes. *Chem. Mater.* **2006**, *18*, 560–566.
- (29) Yatsushashi, T.; Nakajima, Y.; Shimada, T.; Inoue, H. Photophysical Properties of Intramolecular Charge-Transfer Excited Singlet State of Aminofluorenone Derivatives. *J. Phys. Chem. A* **1998**, *102*, 3018–3024.
- (30) Shigeta, M.; Morita, M.; Konishi, G.-I. Selective Formation of Twisted Intramolecular Charge Transfer and Excimer Emissions on 2,7-bis(4-Diethylaminophenyl)-Fluorenone by Choice of Solvent. *Molecules* **2012**, *17*, 4452–4459.
- (31) Estrada, L. A.; Yarnell, J. E.; Neckers, D. C. Revisiting Fluorenone Photophysics via Dipolar Fluorenone Derivatives. *J. Phys. Chem. A* **2011**, *115*, 6366–6375.
- (32) Pommerehne, J.; Vestweber, H.; Guss, W. Efficient Two Layer LEDs on a Polymer Blend Basis. *Adv. Mater.* **1995**, *7*, 551–554.
- (33) Johansson, T.; Mammo, W.; Svensson, M.; Andersson, M. R.; Inganas, O. Electrochemical Bandgaps of Substituted Polythiophenes. *J. Mater. Chem.* **2003**, *13*, 1316.
- (34) Sun, Q.; Wang, H.; Yang, C.; Li, Y. Synthesis and Electroluminescence of Novel Copolymers Containing Crown Ether Spacers. *J. Mater. Chem.* **2003**, *13*, 800–806.
- (35) Cardona, C. M.; Li, W.; Kaifer, A. E.; Stockdale, D.; Bazan, G. C. Electrochemical Considerations for Determining Absolute Frontier Orbital Energy Levels of Conjugated Polymers for Solar Cell Applications. *Adv. Mater.* **2011**, *23*, 2367–2371.
- (36) Eakins, G. L.; Alford, J. S.; Tiegs, B. J.; Breyfogle, B. E.; Stearman, C. J. Tuning HOMO-LUMO Levels: Trends Leading to the Design of 9-Fluorenone Scaffolds with Predictable Electronic and Optoelectronic Properties. *J. Phys. Org. Chem.* **2011**, *24*, 1119–1128.
- (37) Biczók, L.; Bérces, T.; Inoue, H. Effects of Molecular Structure and Hydrogen Bonding on the Radiationless Deactivation of Singlet Excited Fluorenone Derivatives †. *J. Phys. Chem. A* **1999**, *103*, 3837–3842.
- (38) Behrendt, A.; Screttas, C. G.; Bethell, D.; Schiemann, O.; Steele, B. R. Magnetic and Electrochemical Investigations on Anions Derived from Oligoketones Containing Fluorenone and Benzophenone Units. An Approach to the Design of Stable Multiradical Organic Materials. **1998**, 2039–2045.
- (39) Stephens, P. J.; Devlin, F. J.; Chabalowski, C. F.; Frisch, M. J. Ab Initio Calculation of Vibrational Absorption and Circular Dichroism Spectra Using Density Functional Force Fields. *J. Phys. Chem.* **1994**, *98*, 11623–11627.
- (40) Becke, A. D. Density-Functional Thermochemistry. III. The Role of Exact Exchange. *J. Chem. Phys.* **1993**, *98*, 5648.

- (41) Lee, C.; Yang, W.; Parr, R. G. Development of the Colle-Salvetti Correlation-Energy Formula into a Functional of the Electron Density. *Phys. Rev. B* **1988**, *37*, 785–789.
- (42) Zhao, Y.; Truhlar, D. G. The M06 Suite of Density Functionals for Main Group Thermochemistry, Thermochemical Kinetics, Noncovalent Interactions, Excited States, and Transition Elements: Two New Functionals and Systematic Testing of Four M06-Class Functionals and 12 Other Function. *Theor. Chem. Acc.* **2007**, *120*, 215–241.
- (43) Zhao, Y.; Truhlar, D. G. Density Functionals with Broad Applicability in Chemistry. *Acc. Chem. Res.* **2008**, *41*, 157–167.
- (44) Oliva, M. M.; Casado, J.; Navarrete, J. T. L.; Berridge, R.; Skabara, P. J.; Kanibolotsky, A. L.; Perepichka, I. F. Electronic and Molecular Structures of Trigonal Truxene-Core Systems Conjugated to Peripheral Fluorene Branches. Spectroscopic and Theoretical Study. *J. Phys. Chem. B* **2007**, *111*, 4026–4035.
- (45) Frisch, M. J.; Trucks, G. W.; Schlegel, H. B.; Scuseria, G. E.; Robb, M. A.; Cheeseman, J. R.; Scalmani, G.; Barone, V.; Mennucci, B.; Petersson, G. A.; Nakatsuji, H.; Caricato, M.; Li, X.; Hratchian, H. P.; Izmaylov, A. F.; Bloino, J.; Zheng, G.; Sonnenberg, J. L.; Hada, M.; Ehara, M.; Toyota, K.; Fukuda, R.; Hasegawa, J.; Ishida, M.; Nakajima, T.; Honda, Y.; Kitao, O.; Nakai, H.; Vreven, T.; Montgomery, J. A., Jr.; Peralta, J. E.; Ogliaro, F.; Bearpark, M.; Heyd, J. J.; Brothers, E.; Kudin, K. N.; Staroverov, V. N.; Kobayashi, R.; Normand, J.; Raghavachari, K.; Rendell, A.; Burant, J. C.; Iyengar, S. S.; Tomasi, J.; Cossi, M.; Rega, N.; Millam, N. J.; Klene, M.; Knox, J. E.; Cross, J. B.; Bakken, V.; Adamo, C.; Jaramillo, J.; Gomperts, R.; Stratmann, R. E.; Yazyev, O.; Austin, A. J.; Cammi, R.; Pomelli, C.; Ochterski, J. W.; Martin, R. L.; Morokuma, K.; Zakrzewski, V. G.; Voth, G. A.; Salvador, P.; Dannenberg, J. J.; Dapprich, S.; Daniels, A. D.; Farkas, Ö.; Foresman, J. B.; Ortiz, J. V.; Cioslowski, J.; Fox, D. J. Gaussian 09, Revision D.01, 2009.
- (46) Magnani, L.; Rumbles, G.; Samuel, I. D. W.; Murray, K.; Moratti, S. C.; Holmes, A. B.; Friend, R. H. Photoluminescence Studies of Chain Interactions in Electroluminescent Polymers. *Synth. Met.* **1997**, *84*, 899–900.
- (47) Rumbles, G.; Samuel, I. D. W.; Magnani, L.; Murray, K. A.; DeMello, A. J.; Crystall, B.; Moratti, S. C.; Stone, B. M.; Holmes, A. B.; Friend, R. H. Chromism and Luminescence in Regioregular poly(3-Dodecylthiophene). *Synth. Met.* **1996**, *76*, 47–51.
- (48) Reed, A. E.; Curtiss, L. a.; Weinhold, F. Intermolecular Interactions from a Natural Bond Orbital, Donor-Acceptor Viewpoint. *Chem. Rev.* **1988**, *88*, 899–926.

CHAPTER 3

ENGINEERING FRONTIER ENERGY LEVELS IN DONOR-ACCEPTOR FLUOREN-9-YLIDENE MALONONITRILES VERSUS FLUORENONES

Adapted with permission from Homnick, P. J.; Tinkham, J. S.; Devaughn, R.; Lahti, P. M. Engineering Frontier Energy Levels in Donor-Acceptor Fluoren-9-Ylidene Malononitriles versus Fluorenones. *J. Phys. Chem. A* **2014**, *118*, 475–486.¹ Copyright 2014 American Chemical Society.

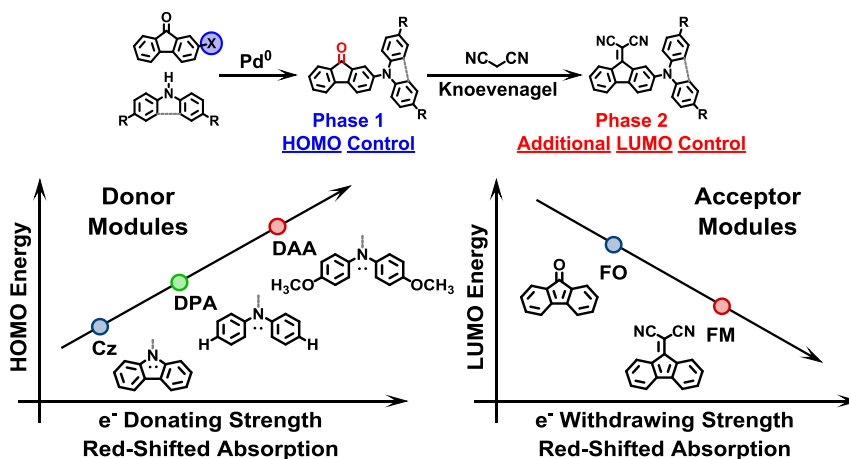
<http://pubs.acs.org/doi/abs/10.1021/jp407854r>

[Some changes were made for adapted use in this dissertation.]

3.1 Introduction

Push-pull donor-acceptor (D-A) small molecules and polymers have recently received considerable attention for use in organic electronic applications. The D-A architecture is of interest due to the large amount of synthetic control over HOMO/LUMO energy levels when using a modular synthetic approach.¹⁻⁸ Since energy level and band gap engineering are critical components of organic electronic molecular design, especially for photovoltaic applications, further developing this modular D-A design strategy is crucial to designing new high performance materials.

This chapter describes my expansion of the Chapter 2 set of fluorenone materials to include some extra donor-fluorenone combinations. This full set of molecules was then converted to the corresponding fluoren-9-ylidene malononitrile analogues for the purpose of selectively tuning *both* the HOMO/LUMO energy levels (Scheme 3.1) in the series. Fluorenone (acceptor module) and the five donor modules chosen are relatively simple synthons, and the final D-A molecules are synthetically straightforward to make. Most importantly, condensation at the C-9 position to obtain fluorenylidene malononitrile derivatives is a straightforward, moderate yield reaction with relatively simple purification. Frontier molecular orbital (FMO) energies are well-correlated to their structural components, suggesting this modular approach using fluorenone as a promising molecular design strategy.



Scheme 3.1: General synthetic plan and FMO energy tuning strategy based on donor/acceptor strengths.

Dipolar molecules incorporating fluorene-9-ylidene malononitrile acceptor units conjugated to trimethoxystyrene and/or diarylamine donor units were synthesized, and their electronic spectral properties and electrochemical behaviors evaluated by comparison to those of the analogous fluorenones. Frontier energy level and band gap trends are explained based on a quantitative, modular donor-acceptor interaction model. A connectivity effect on absorption transition moment strength is also described, comparing 2,7- versus 3,6-conjugated bis-dianisylamino-substituted fluorenone and fluorenylidene malononitrile systems.

3.2 Background

Dipolar molecules incorporating electron donor and acceptor (D and A, respectively) substitution – also called donor-acceptor or "push-pull" systems – have drawn much attention for potential use as electronic materials for nonlinear optical, energy harvesting and charge transport testing.^{10–12} Much work and molecular design strategy has aimed for specific band gaps as well as specific highest occupied and lowest unoccupied molecular orbital (HOMO, LUMO) energy levels in dipolar materials, because of their potential utility in electronic applications. Many donor and acceptor units have been tested, each with their own advantages and disadvantages. Because of the high promise of molecular electronic devices, considerable effort continues to

design new, synthetically simple dipolar and related conjugated organic species, and to improve means to predict their spectral and electronic behaviors.

The synthetically simple and readily functionalized fluorenone has been heavily studied for its electronic spectral behavior¹³⁻¹⁷, and for its role in green emission bands¹⁸⁻²⁰ from fluorene-based organic LEDs. There have also been a number of studies of substitution effects on fluorenone spectroscopy²¹⁻²⁸. The previous chapter described²⁹ how synthetically simple 2-fluorenyl and 2,7-fluorenediyl acceptor units can be linked in a modular fashion to diarylamine donor groups to give consistent LUMO levels from the fluorenone unit, and tunable HOMO levels from the donors. In the work described in this chapter, the initial design is extended to additional fluorenone systems and especially to the stronger electron acceptor fluorene-9-ylidene malononitrile (FM). FM-based systems have lower LUMO levels relative to their FO-based analogues, decreasing all band gaps because the donor-controlled HOMO levels remain the same, to a first approximation. The results described below show that the FM-based D-A and D-A-D dipolar compounds fit a modular "building block" strategy that is well suited to engineering *molecular* electronic properties that are critical for developing new organic electronic *materials*. This strategy is summarized schematically in Figure 3.1.

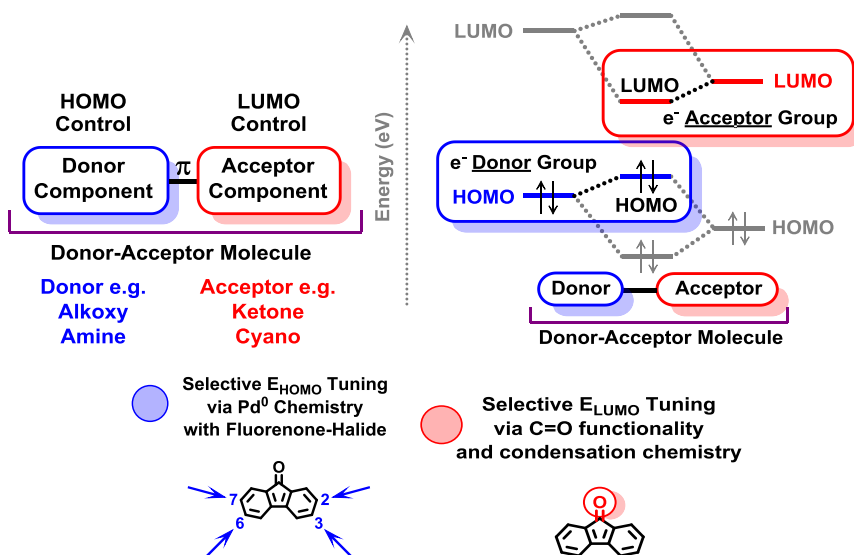


Figure 3.1: Fluorenone-based molecular design strategy and FMO energy tuning rationale.

3.3 Experimental Methods

Fluorenone (FO) derivatives used in this study were synthesized by variations of literature routes,^{20,29} then converted to fluoren-9-ylidene malononitriles (FMs) by Knoevenagel condensation. Full experimental details are given in Chapter 9.

For the molecules in this study, first oxidation onset voltages were used to estimate³⁰⁻³³ HOMO energy levels (E_{HOMO}) using equation (1). The spectral band gaps (E_{g}) in eV from the lowest energy absorption peak onsets in acetonitrile were then used to estimate E_{LUMO} using equation (2). For electron acceptor units FO and FM both E_{HOMO} and E_{LUMO} were obtained from voltammetric oxidation/reduction onsets with equation (1).

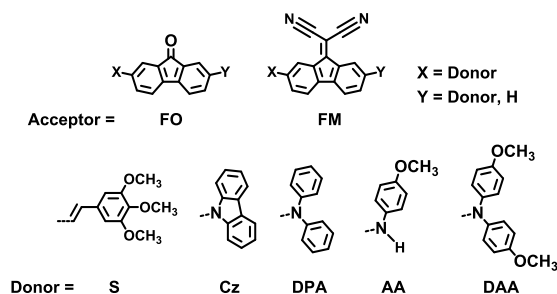
$$E_{\text{MO}} = -(E_{\text{redox}} + 4.8) \text{ eV} \quad (1)$$

$$E_{\text{LUMO}} = E_{\text{HOMO}} + E_{\text{g}} \quad (2)$$

All computations were carried out using Gaussian 09³⁴ Revision B.01 on a Linux computer running openSuSE. Molecular geometries were optimized at a B3LYP³⁵⁻³⁷/6-31G(d,p) level, and these geometries fixed to compute molecular properties at a B3LYP/6-31+G(d,p) level. Molecular orbital diagrams were generated from the final checkpoint files using GaussView³⁴ version 5.0.9 with default parameter settings unless otherwise stated.

3.4 Results and Discussion

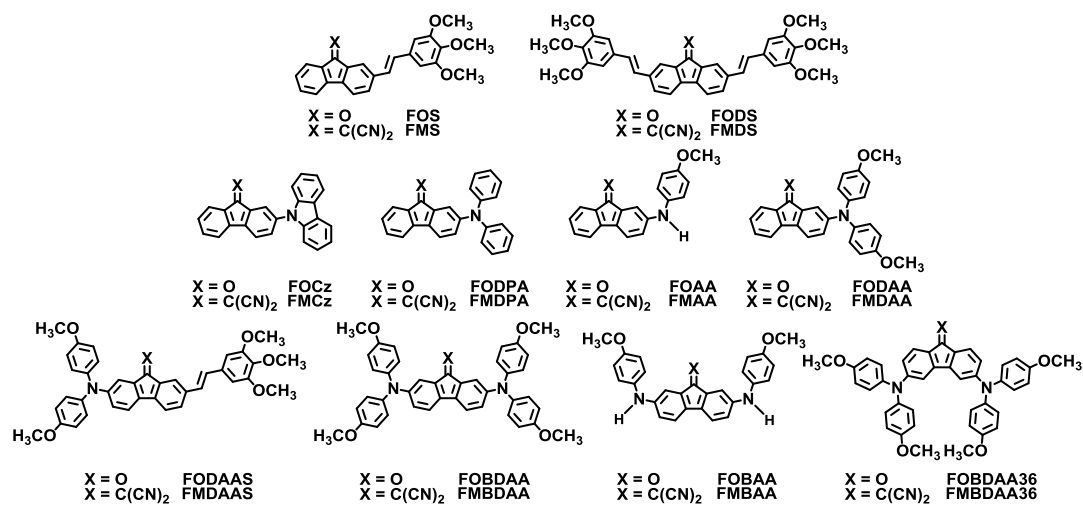
Subsequent discussions use the abbreviations shown in Scheme 3.2 for the structural modules used to make the dipolar molecules of Scheme 3.3. As mentioned earlier, for analogous structures having the same donor units, the LUMO level of an FO-based molecule will be lower in the analogous FM-based system. The results described below confirm that this approach works well to give a range of absorption profiles and electronic HOMO/LUMO levels.



Scheme 3.2: General structural design units used in donor-acceptor fluorene-9-ylidene malononitrile (FM) and precursor fluorenone (FO) systems in this study.

3.4.1 Energy levels of electronic donor and acceptor structural modules.

The spectroscopic behaviors of all of the dipolar systems in this study are interpreted below in terms of interactions between the donor (D) and acceptor (A) modules that comprise the overall D-A and D-A-D molecules. These interpretations are, in turn, related to HOMO and LUMO levels estimated from equations (1)-(2) from the experimental methods section. Therefore, each of the building block modules from Scheme 3.1 was electrochemically evaluated. The individual donor modules trimethoxystyrene (S), carbazole (Cz), diphenylamine (DPA), and anisylamine (AA) each show one irreversible oxidation feature (Table 3.1, Figure 3.2). Dianisylamine (DAA) shows well-differentiated oxidation onsets at 140, 783, and 1620 mV: the lowest potential oxidation is highly reversible and attributable to formation of the aminium radical cation, while the quasi-reversible second oxidation is attributable to diarylaminium oxidation. Neither of the acceptor modules FO or FM shows oxidation onset below 1500 mV, so oxidation features in the dipolar molecules at lower potentials can confidently be attributed to donor module electrochemistry. FO shows a quasi-reversible reduction onset at -1820 mV, and FM shows reversible first and second reduction onsets at -1010 mV and -1710 mV, respectively; the features in the stronger acceptor-substituent FM are well defined and reversible. Table 3.1 lists these "building block" electrochemical potentials for use in subsequent discussions, and the individual cyclic voltammograms are given in Figure 3.1.



Scheme 3.3: Donor-Acceptor systems compared in this study.

Table 3.1: Redox potentials and HOMO/LUMO energies of donor-acceptor molecules.

Compound	Oxidation onset(s) (mV) ^a	Reduction onset(s) (mV) ^a	HOMO Energy (eV) Expt. ^b [Computed ^c]	LUMO Energy (eV) Expt. ^b [Computed ^c]
FOS	594	Not Observed	-5.39 [-5.61]	-2.98 [-2.59]
FMS	591	-817, -1612	-5.39 [-5.72]	-3.49 [-3.46]
FODS	556	-1430	-5.36 [-5.40]	-3.12 [-2.61]
FMDS	642	-1090, -1720	-5.44 [-5.50]	-3.71 [-3.44]
FOCz	715	-1490	-5.51 [-5.73]	-3.05 [-2.80]
FMCz	484, 859	-1140	-5.28 [-5.83]	-3.35 [-3.66]
FODPA	320, 824	-1370	-5.12 [-5.37]	-3.01 [-2.54]
FMDPA	517, 1280	-966, -1700	-5.32 [-5.51]	-3.73 [-3.42]
FOAA	350, 838	-1660	-5.15 [-5.32]	-3.07 [-2.44]
FMAA	438, 984	-970, -1650	-5.24 [-5.53]	-3.72 [-3.38]
FODAA	232, 816	-1980	-5.03 [-5.05]	-3.02 [-2.41]
FMDAA	220, 835	-1290, -1490, -1820	-5.02 [-5.19]	-3.55 [-3.30]
FODAAS	178, 667, 893	-1590	-4.98 [-4.97]	-3.05 [-2.40]
FMDAAS	229, 688, 962	-959, -1670	-5.03 [-5.31 ^e]	-3.63 [-3.51 ^e]
FOBDA	155, 355, 949	-1410	-4.95 [-4.72]	-3.21 [-2.28]
FMBDAA	176, 401, 943	-1170, -1760	-4.98 [-4.83]	-3.77 [-3.14]
FOBAA	157, 412	-1660	-4.96 [-4.91]	-3.13 [-2.33]
FMBAA	243, 543, 1160	-952, -1610	-5.04 [-5.06]	-3.78 [-3.24]
FOBDA36	290 (424, 533) ζ	-959, (-1127) ^d	-5.09 [-4.99]	-2.86 [-2.01]
FMBDAA36	279 (437, 572) ζ	-1060, -1730 (-1230, -1850) ^d	-5.08 [-5.24]	-3.32 [-2.79]
S	637	Not Observed	-5.44 [-5.87]	-1.51 [-1.11]
Cz	810	Not Observed	-5.61 [-5.78]	-2.00 [-1.09]
DPA	440	Not Observed	-5.25 [-5.42]	-1.34 [-0.63]
AA	190	Not Observed	-4.99 [-5.31]	-1.29 [-0.34]
DAA	140, 793, 1620	Not Observed	-4.94 [-4.92]	-1.38 [-0.48]
FO	1550	-1820	-6.35 [-6.56]	-2.98 [-2.63]
FM	1500	-1010, -1710	-6.36 [-6.87]	-3.79 [-3.55]

^a Onset potentials in millivolts. All results obtained in acetonitrile and referenced against ferrocene/ferrocenium external standard in acetonitrile. ^b Calculated using equations 1-2. ^c Computed at the P3LYP/6-31+G(d,p)//B3LYP/6-31G(d,p) level of theory unless otherwise stated. ^d Potential of peak maximum in millivolts. ^e Computed at the B3LYP/6-31G(d,p)//B3LYP/6-31G(d) level.

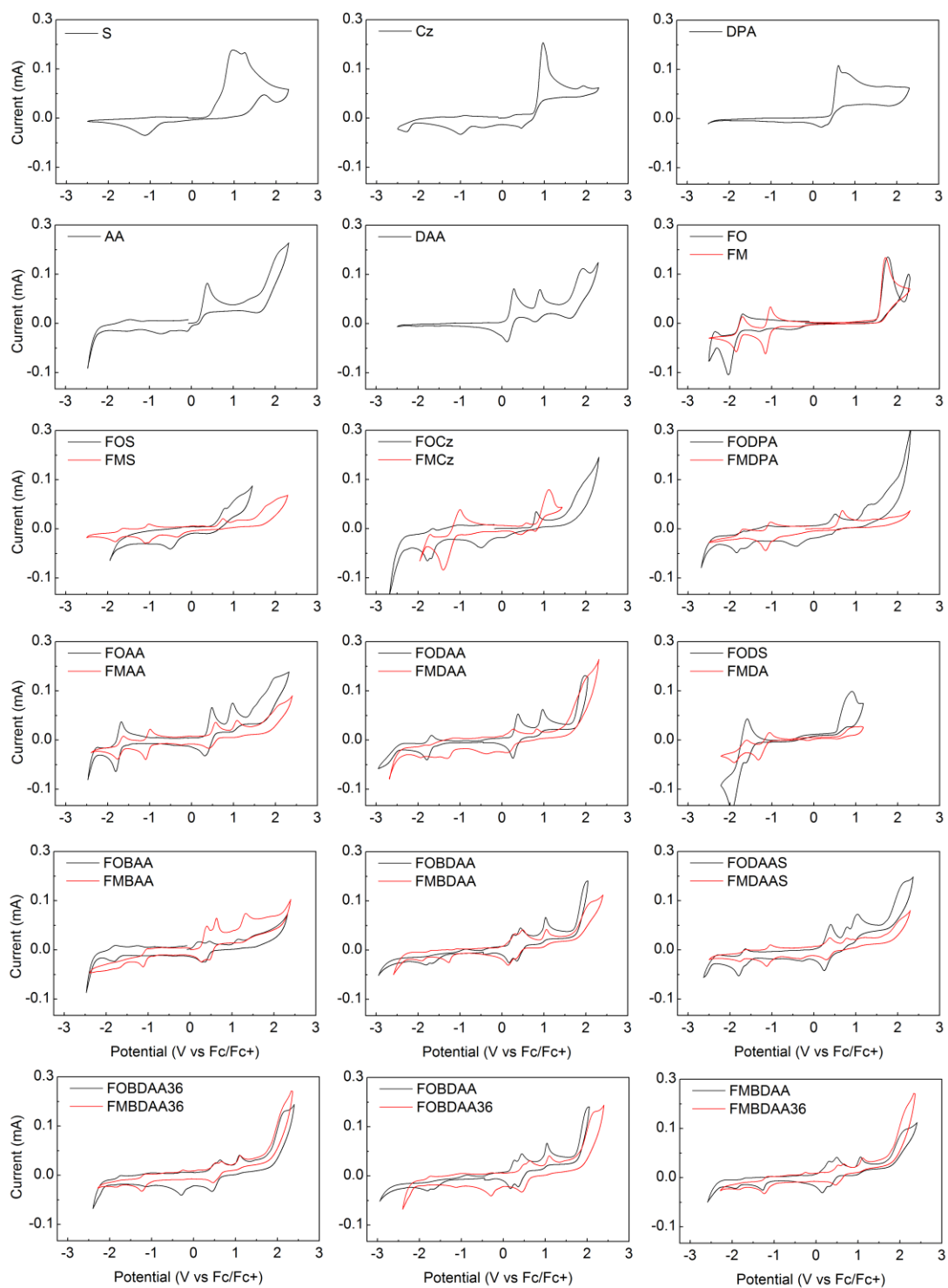


Figure 3.2: Cyclic voltammograms for donor-acceptor molecules, obtained in acetonitrile as described in Chapter 9.

Table 3.2: Absorption spectra maxima of donor-acceptor molecules in low versus high polarity solvents.

Compound	Absorption λ_{\max}/nm ^a ($\epsilon = \log\{\text{M}^{-1}\text{cm}^{-1}\}$) Low Polarity ^b	Absorption λ_{\max}/nm ^a ($\epsilon = \log\{\text{M}^{-1}\text{cm}^{-1}\}$) High Polarity ^c
FOS	302(4.45), 348(4.45) 433(3.27)	307(4.49), 347(4.49), 441(3.26)
FMS	331(4.64) 547 (2.93) ^d	330(4.77), 539(2.84)
FODS	306(4.50), 360(4.55), 454(3.63)	312(4.60), 370(4.75), 474(3.65)
FMDS	345(4.86), 373(4.77), 608(3.24) ^d	340(4.86), 366(4.81), 589(3.21)
FOCz	255(4.35), 290 (4.34) 430(2.87)	253(4.71), 290(4.31), 432(2.73)
FMCz	317(4.33), 340(4.28), 537(2.61) ^e	310(4.52), 338(4.44), 520(2.62)
FODPA	295(4.47), 354(4.26), 479(3.19)	296(4.50), 350(4.20), 496(3.08)
FMDPA	289(4.02), 325(4.20), 627(2.63)	324(4.35), 635(2.76)
FOAA	288(4.51), 344(4.20), 498(3.05) ^e	289(4.48), 344(4.13), 505(2.96)
FMAA	(insoluble in multiple solvents)	314(4.61), 342(4.35,sh), 649(2.73)
FODAA	295(4.45), 357(4.21), 502(3.22)	294(4.48), 350(4.16), 518(3.11)
FMDAA	212(4.72), 323(4.44), 677(2.96)	323(4.37), 672(2.90)
FODAAS	298 (4.55) 386 (4.50) 524 (3.52)	306(4.62), 384(4.64), 543(3.43)
FMDAAS	342(4.58), 397(4.39), 730(2.94) ^d	370(4.50), 389(4.51), 710(2.98)
FOBDA	298(4.57), 382(4.46), 554(3.25)	298(4.72), 376(4.58), 586(3.24)
FMBDAA	388(4.36), 522(2.05), 788(2.74) ^e	373(4.33), 531(2.46), 785(2.73)
FOBAA	295(4.64), 360(4.52), 559(3.11)	296(4.68), 359(4.53), 571(3.07)
FMBAA	(insoluble in multiple solvents)	354(4.38,sh), 450(2.41,sh), 762(2.68)
FOBDA36	334(4.28), 388(4.17), 463(4.07) ^e	327(4.28), 380(4.15), 474(4.02)
FMBDA36	359(3.84), 488(4.03), 585(3.70) ^e	347(3.80), 483(3.97), 597(3.64)

^a Up to three lowest energy maxima above 250 nm. ^b Hexane solvent used unless otherwise stated. ^c Acetonitrile used unless otherwise stated. ^d Spectrum obtained in dichloromethane due to hexane insolubility. ^e Spectrum obtained in diethyl ether due to hexane insolubility.

3.4.2 Monosubstituted D-A type dipolar systems

Figure 3.3 summarizes major solution UV-vis-NIR spectral features for the monosubstituted, donor-acceptor (D-A) dipolar FOs and FMs whose structures are given in Scheme 3.3. As shown in Table 3.2 and in Figure 3.3, all of the FO-based compounds have multiple strong transitions between 250-380 nm with molar absorptivities ranging from about 9,000-60,000 $\text{M}^{-1}\text{cm}^{-1}$, but mostly about 30,000 $\text{M}^{-1}\text{cm}^{-1}$. The FM-based systems exhibit overlapping bands at 300-380 nm with more variable molar absorptivities of about 18,000-60,000 $\text{M}^{-1}\text{cm}^{-1}$. With minor variations in position, and somewhat greater variations in intensity, these

stronger bands are seen in the absorption spectra of all of the Scheme 3.2 compounds, except for the FM systems with 3,6-connectivity. This will be subsequently discussed below.

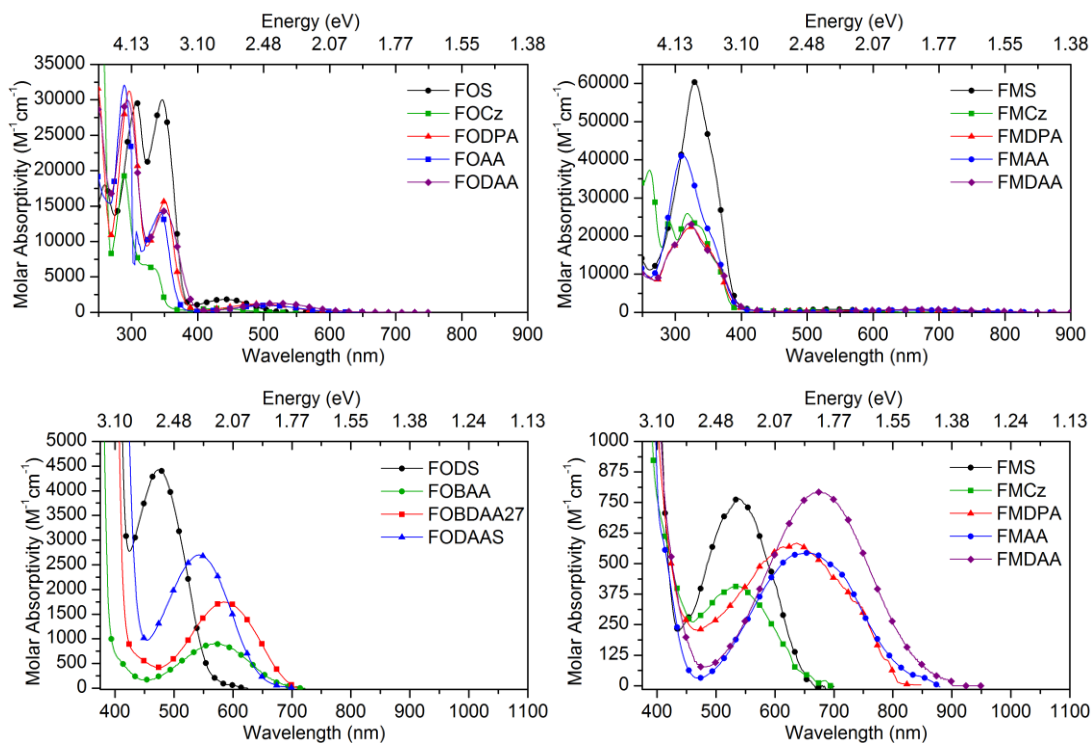


Figure 3.3: Absorption spectra of FOs (left) and FMs (right) with one donor substituent, in acetonitrile. Full spectra top, ICT bands bottom.

Figure 3.3 shows the lowest energy absorption band regions of the monosubstituted systems. The FO-based systems show absorption onset at 500-650 nm, with molar absorptivities of about 500-1800 $M^{-1} cm^{-1}$. The FM-based systems are red-shifted by comparison to their FO-based structural analogues, with absorption onset at about 650-900 nm, and molar absorptivities of about 400-800 $M^{-1} cm^{-1}$. Despite their modest molar absorptivities by comparison to the main transitions below 400 nm, these long wavelength bands impart strong colors to the neat solids and in sufficiently concentrated solutions, ranging from red to blue-black.

The FO- and FM-based systems functionalized with trimethoxystyrene – FOS and FMS – exhibit the highest energy absorption onsets, along with the *N*-carbazolyl (Cz) functionalized systems. The longer π -system conjugation in FOS and FMS gives larger molar absorptivities compared to the systems monosubstituted by amines, but the relatively high-energy absorption

onsets show the styrene unit to be less effective as an electron donor than the non-carbazolyl amines tested in this study.

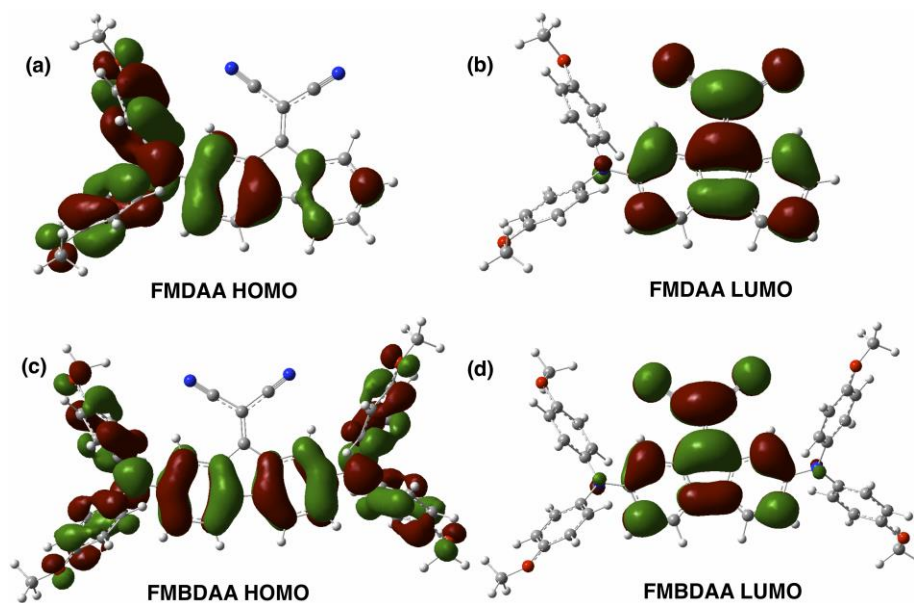


Figure 3.4: B3LYP/6-31+G(d,p) level frontier molecular orbital plots for FMDAA HOMO (a) and LUMO (b), and FMBDAA HOMO (c) and LUMO (d).

The FOS long wavelength absorption band red shifts in polar solvents, a trend typically attributed to $\pi \rightarrow \pi^*$ transitions. Interestingly, the FMS long wavelength band exhibits a blue shift in acetonitrile versus less polar solvents, as do most of the Scheme 3.3 FM-based derivatives described subsequently. Such behavior is often attributed to $n \rightarrow \pi^*$ transitions, but this generalization has not proven straightforward to apply to fluorenones, since the lowest energy transition nature can be solvent dependent¹³⁻¹⁷. Computational modeling indicates that the long wavelength transitions in both FO- and FM-based systems here are $\pi \rightarrow \pi^*$ type, from a π -HOMO that is delocalized throughout the full π -system to a LUMO that is largely localized on the FO or FM unit. The computed MO plots show the frontier and subjacent orbitals of the Scheme 3.3 compounds to be π -orbitals, without interspersed n-type orbitals. Examples are given in Figure 3.4 for both D-A and D-A-D dipolar systems; all of the frontier MOs can be found in the supporting information of the published paper arising from work described in this chapter.¹ Conformational differences in the AA donor-substituted systems show only small differences in

computed MO energy levels (≤ 0.1 eV). Therefore, the low energy bands for FOS and FMS, as in the amine-substituted systems described subsequently, appear to be $\pi \rightarrow \pi^*$ transitions with significant intramolecular charge transfer (ICT) character.

To evaluate ICT character in FOS and FMS, the electrochemistry of these and the related amine-substituted D-A compounds needs to be considered. Cyclic voltammetry shows a much higher oxidation potential for trimethoxystyrene than for any of the amines except Cz, showing trimethoxystyrene to be a reluctant electron donor, despite extending conjugation at the 2-position of FO or FM. FOS and FMS show only poorly resolved oxidation features with onsets similar to but somewhat lower in voltage from trimethoxystyrene, probably due to conjugation into the biphenyl-type π -system of FO and FM. FOS also shows no clear reduction feature, but the more strongly electron acceptor substituted FMS shows quasi-reversible reduction features similar to (though weaker than) those for the FM group. Converting the FO to the FM group is so electron withdrawing that oxidation of the trimethoxystyrene unit becomes ineffective.

For the D-A systems bearing only one arylamine substituent, voltammetric features can be readily identified from reduction of the FO and FM units in each series of molecules (Figure 3.2). FODAA shows reversible first oxidation and second oxidation features (232 and 816 mV) that can be associated with the electron rich DAA group; FOAA also shows reversible first and second oxidation features (350 and 838 mV) that can be attributed to the electron rich AA group, indicating that even one anisyl group is sufficient to stabilize oxidation to the FOAA aminium species. Similarly FODPA and FOCz show quasi-reversible oxidation features that are analogous to features in DPA and Cz. Strong electron withdrawing substitution on the FM-based systems stabilizes the reduction electrochemistry by comparison, giving clear and reversible FM-associated reduction features in FMCz, FMDPA, and FMAA, and somewhat less so but still readily identified reduction in FMDAA. But, no FMCz, FMDPA, or FMDAA oxidation features are strong or clearly reversible (FMAA oxidation is quasi-reversible); the poor reversibility is consistent with destabilization of oxidation by the strongly electron-withdrawing FM module.

Experimentally, the FO systems all show solvatochromic red shifts of the lowest energy transition in more polar solvents, consistent with $\pi \rightarrow \pi^*$ and ICT character for these transitions.^{38–43} The solvatochromic trends for the FM systems favor small blue shifts in more polar solvents, as with the FMS versus FOS. Figure 3.5 shows the long wavelength regions of the spectra for FODAA and FMDAA in diethyl ether and acetonitrile. Tabular results for all solvatochromic experiments are given in Table 3.3. As mentioned above, the blue shifts in some of the FM systems are attributable⁴⁴ to specific solvent-solute interactions in acetonitrile.

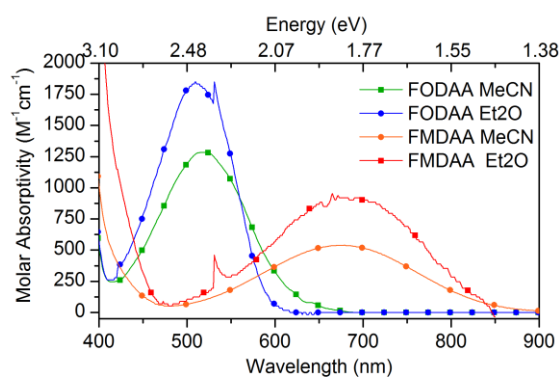


Figure 3.5: Comparison of lowest-energy absorption spectral regions for FODAA and FMDAA in diethyl ether (Et₂O) and acetonitrile (MeCN).

Table 3.3: Solvatochromism data for donor-acceptor molecules, taken in hexane, diethyl ether, and acetonitrile. Solvatochromic shifts reported in meV.

Compound	Absorption Onset (nm)			Absorption Onset (eV)			Solvatochromic Shift from Hex to MeCN (meV)	Solvatochromic Shift from Et ₂ O to MeCN (meV)
	Hexanes	Et ₂ O	MeCN	Hexanes	Et ₂ O	MeCN		
FOS	433	439	441	2.86	2.82	2.81	52	13
FODS	454	468	474	2.73	2.65	2.62	115	34
FOCz	430	428	432	2.88	2.90	2.87	13	27
FODPA	479	485	496	2.59	2.56	2.50	89	57
FOAA	N/A	489	505	N/A	2.54	2.46	N/A	80
FODAA	502	510	518	2.47	2.43	2.39	76	38
FODAAS	524	534	543	2.37	2.32	2.28	83	38
FOBAA	N/A	559	568	N/A	2.22	2.18	N/A	35
FOBDAA	554	564	586	2.24	2.20	2.12	122	83
FMS	N/A	544	539	N/A	2.28	2.30	N/A	-21
FMDS	N/A	586	589	N/A	2.12	2.11	N/A	11
FMCz	N/A	537	520	N/A	2.31	2.38	N/A	-75
FMDPA	627	634	635	1.98	1.96	1.95	25	3
FMAA	N/A	N/A	665	N/A	N/A	1.86	N/A	N/A
FMDAA	677	684	672	1.83	1.81	1.85	-14	-32
FMDAAS	N/A	722	710	N/A	1.72	1.75	N/A	-29
FMBAAS	N/A	N/A	759	N/A	N/A	1.63	N/A	N/A
FMBDAA	N/A	788	785	N/A	1.57	1.58	N/A	-6

Interestingly, the band onsets for the Cz-functionalized D-A systems are nearly the same as those for the trimethoxystyrene-functionalized systems. The pyrrole ring of Cz is less able to donate an aromatic π -electron, than the other amine donors are to donate a non-aromatic lone pair electron. This makes Cz a relatively poor donor for an ICT transition, resulting in a relatively higher band gap. Interestingly, the relatively lower oxidation potential and higher computed HOMO energy of trimethoxystyrene (Table 3.1) make it a superior electron donor to Cz. For the stronger donor amines, the absorption onsets in Figure 1 move to increasingly lower energy in the series FOCz > FODPA > FOAA > FODAA. The decreasing band gap correlates with increasing E_{HOMO} of Cz < DPA < AA < DAA, while E_{LUMO} in the FO-series remains fixed at about -3.0 eV, as shown experimentally by both electrochemical measurements and computational modeling. The same trend is seen for the FM-functionalized analogues, but in each case the FM-analogue

absorption is lower in energy by about 0.50 eV. The reduced band gaps in the FM-series occur because their HOMO levels are essentially defined by the same donor HOMO levels as in their FO analogues, but the FM-analogues all have lower E_{LUMO} energies in the range of -3.4 to -3.7 eV (Table 3.1). The computations for all of the amine-functionalized D-A systems show even stronger ICT character than in FOS or FMS, with the π -HOMO in each case favoring the side of the FO or FM ring that holds the amine, and the π^* -LUMO being localized on the FO or FM module.

3.4.3 Disubstituted D-A-D dipolar systems

The through-conjugated 2,7-FO and 2,7-FM systems show quite similar higher energy absorption spectral features to those of the monosubstituted 2-FO and 2-FM analogues, with strong features at higher energy around 400 nm that overlap more thoroughly in the FM systems than FO systems. The low energy bands > 400 nm are shown in Figure 3.6. The molar absorptivities for these disubstituted systems are higher than for the monosubstituted analogues, as expected. Solvatochromic effects parallel the behavior of the monosubstituted analogues for both FO- and FM-series disubstituted molecules (Table 3.3).

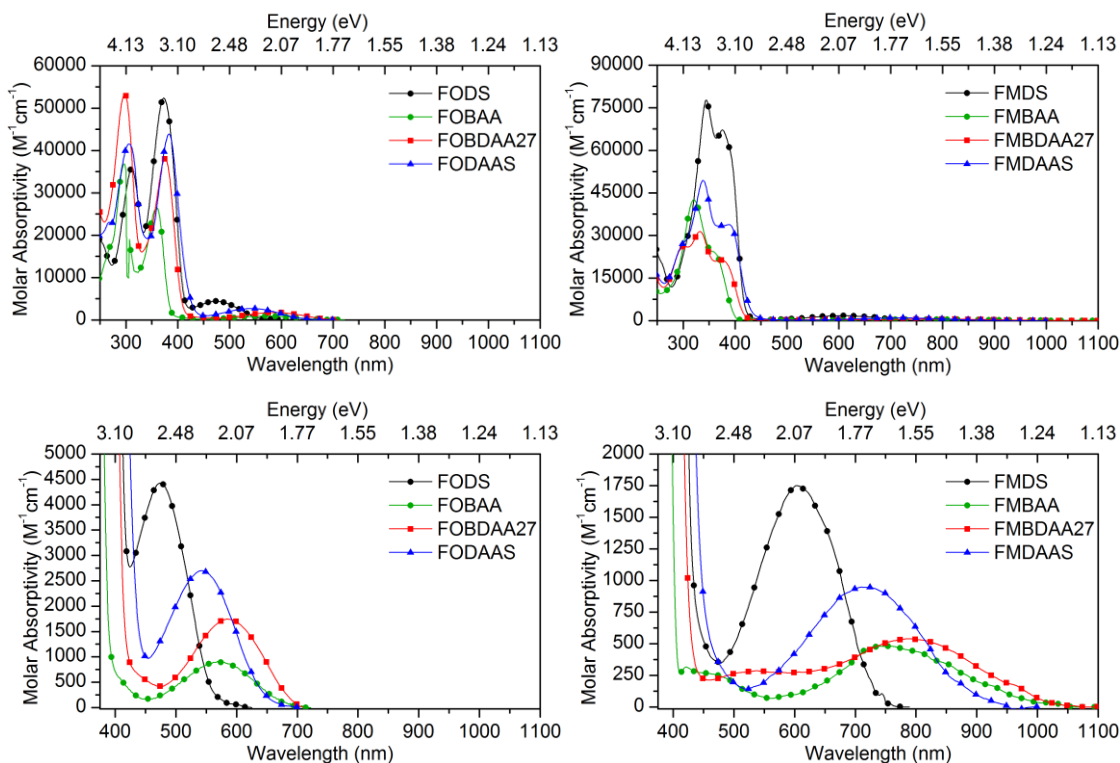


Figure 3.6: Absorption spectra of FOs (left) and FMs (right) with two donor substituents, in acetonitrile. Full spectra top, ICT bands bottom.

The increased effective conjugation achieved by placing two donor substituents in the 2,7-positions – with resonance connectivity between them – is most strongly seen in red-shifted low energy bands by comparison to the monosubstituted systems, plus reduced oxidation potentials with more oxidation features in the voltammograms (Figure 3.2). Although FODS and FMDS have the longest extended C=C type π -systems, the amine-substituted D-A-D systems give the largest band gap decrease relative to monosubstituted systems. The band onset for FMBDAA is at about 1000 nm (1.2 eV), in the NIR region: the neat solids appear black to the naked eye.

Comparing the monosubstituted to disubstituted systems allows some relative comparisons of substituent effects on the spectroscopy. FODAAS has an absorbance maximum at 0.34 eV lower energy than in FODS: the higher HOMO energy for the DAA group (Table 3.1) gives this lower bandgap, since the LUMO levels are very similar for FODS and FODAAS.

Similarly, FMDAAS has an absorbance maximum 0.36 eV lower than FMDS. Although FMDAAS has only one amine donor group, the combination of the DAA donor with the C=C conjugation extension of the trimethoxystyrene unit gives a low energy band onset in acetonitrile of ~900 nm (1.4 eV).

The D-A-D systems with the strongest donor substitution, FOBDAA and FMBDAA, show the electrochemical voltammetric features of both their constituent donor (DAA) *and* acceptor modules. FOBDAA shows reduction consistent with FO at -1410 mV, and FMBDAA at -1170 and -1760 mV consistent with FM. Both show a closely spaced pair of oxidation features attributable to the two DAA groups in each. From the Figure 3.2 and Table 3.1 data, the two lowest oxidation onset potentials are split by 200 mV and 225 mV for FOBDAA and FMBDAA; the analogous splittings for FOBA and FMBAA are 255 mV and 300 mV. The splittings in both sets of diamines are larger in the FM systems than the FO systems, indicating stronger interaction and better 2,7-through-conjugation in the FM system. The larger splittings in the bis-AA versus the bis-DAA systems may be due to greater planarity and better through-conjugation in the sterically less hindered bis-AA systems. Finally, FODAAS with two different donor groups exhibits two oxidation features attributable to the DAA group (178 mV and 893 mV), plus an onset feature at 667 mV from the trimethoxystyrene unit. FMDAAS shows three oxidation features analogous to those in FODAAS.

3.4.4 Modular electronic analysis of the dipolar molecules

The electrochemical findings, in particular, support two critical needs for a modular scheme for understanding the electronic behavior of the dipolar molecules in this study. First, the molecules exhibit reduction electrochemistry in very reasonable accord with voltammetry measured for the FO and FM acceptor modules, with only minor variations with different attached donor groups (Figure 3.2). (The reduction half wave potentials also compare well to the FM reduction potential -1.01 V given by Neckers and coworkers).²² Second, the oxidation potentials of donor components are well retained in both FO- and FM-based systems. These

trends encourage the notion that the donor and acceptor components can be considered interchangeable modules that can be used to design and understand the electronic properties of the overall D-A molecules. From a molecular engineering perspective, this is very desirable for designing new electronic materials. In addition, as Table 3.1 shows, the HOMO energy levels computed by hybrid density functional theory for the Scheme 3.3 dipolar molecules are remarkably close to the experimentally estimated HOMO levels, on average about 0.1 ± 0.2 eV lower (uncertainty is standard deviation); the computed LUMO energy levels are 0.4 ± 0.3 eV higher than those obtained from voltammetry experiments.

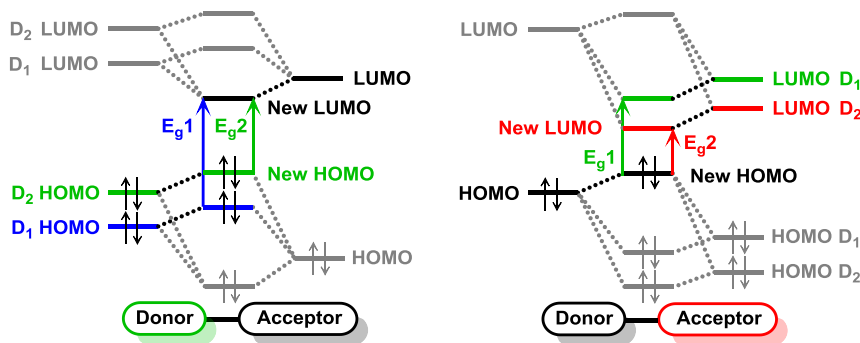


Figure 3.7: Modular deconstruction of push-pull system (D-A) frontier molecular orbitals derivable from interaction of generic acceptor module A with different donor modules D₁ and D₂.

One can rationalize the behavior of a set of dipolar molecules composed of donor and acceptor modular units (like those in Scheme 3.2) by using computational and/or experimental frontier energy levels for the modular units. Figure 3.7 shows how qualitative interactions between the frontier orbitals of donor and acceptor units decreases the band gap of a dipolar system, where donor strength $D_2 > D_1$ and/e acceptor strength $A_2 > A_1$. In the present study, the FO and FM acceptor unit HOMO energies are low enough not to interact strongly with the donor units. Similarly, the donor unit LUMOs are so high in energy relative to the acceptor LUMOs, that the dipolar system LUMOs are determined by the FO or FM units. Figure 3.8 shows quantitatively how the experimental dipolar system frontier energy levels track with the energies

of their modular components. The B3LYP computational modeling reproduces these trends with similar orbital energies.

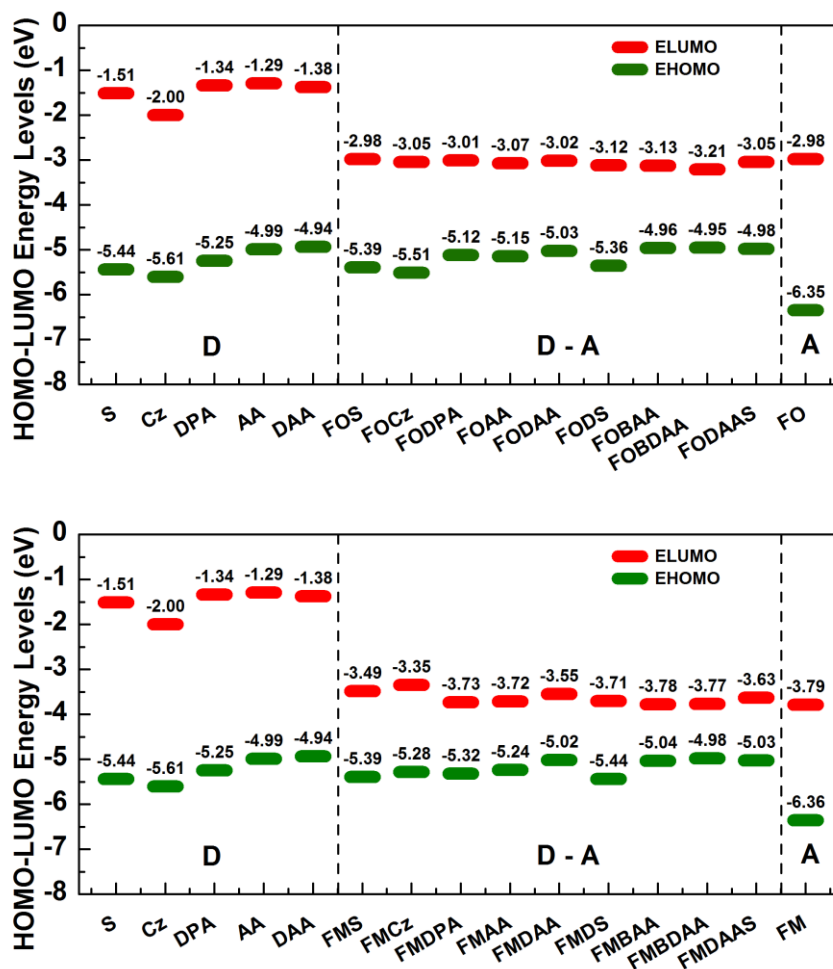


Figure 3.8: Frontier molecular orbital energies for donor-acceptor molecules compared with orbital energies of constituent donor and acceptor modules (data from Table 3.1 and Equations 1-2).

Experimentally, the LUMO energy levels in the FM systems are lower by an average of 0.6 ± 0.1 eV in comparison to their FO-based analogues (uncertainty is standard deviation considering only the dipolar systems, not the modular units). This correlates with the 0.8 eV LUMO energy decrease from FO to FM, and with the absorption spectroscopic band gap decreases (Table 1) in FM derivatives compared to FO derivatives. As shown in Table 3.4 and Table 3.5, the HOMO energies of the FO- and FM-based systems are within 0.016 ± 0.095 eV and

-0.022±0.15 eV of their constituent donor modules' HOMO energies, respectively. Similarly, the LUMO energies of the FO- and FM-based systems are on average within -0.091±0.067 eV and 0.15±0.13 eV of the individual FO and FM modules, respectively. Therefore, the modular FMO approach of Figure 3.7 is quite self-consistent in describing the electronic behaviors of the Scheme 3.3 dipolar molecules.

Table 3.4: Frontier molecular orbital energy variations for donor-acceptor molecules.

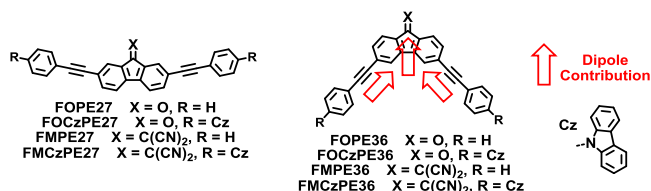
Compound	ΔE_{HOMO} vs. Donor (eV)	ΔE_{LUMO} vs. Acceptor (eV)
FOS	0.05	0.00
FOCz	0.10	-0.07
FODPA	0.13	-0.03
FOAA	-0.16	-0.09
FODAA	-0.09	-0.04
FODS	0.13	-0.14
FOBAA	0.03	-0.15
FOBDAAS	-0.01	-0.23
FODAAS	-0.04	-0.07
FMS	0.05	0.30
FMCz	0.33	0.40
FMDPA	-0.07	0.06
FMAA	-0.25	0.07
FMDAA	-0.08	0.24
FMDS	0.00	0.08
FMBAA	-0.05	0.01
FMBDAAS	-0.04	0.02
FMDAAS	-0.09	0.16

Table 3.5: Average FMO energy for FO- and FM-based compounds versus their component donor and acceptor modules' FMO energies, obtained by averaging ΔE_{HOMO} and ΔE_{LUMO} values for each FO- or FM-set from Table 3.4. FMO energy variations are the standard deviations of these sets.

Compound Series' Acceptor Module	Average E_{HOMO} Change (eV)	E_{HOMO} Variation (eV)	Average E_{LUMO} Change (eV)	E_{LUMO} Variation (eV)
FO	0.016	0.095	-0.091	0.067
FM	-0.022	0.15	0.15	0.13

3.4.5 Strengthening absorption by a connectivity change

The success of the Figure 3.7 modular donor-acceptor design strategy is somewhat offset (in terms of use for applied purposes) by the decreased molar absorptivities of the desirably low band gap absorptions in both FO and FM series. For photovoltaic and photoconversion applications, strong absorption bands are desirable to allow use of thinner layers of electroactive material.



Scheme 3.4: Neckers' push-pull FO and FM-based systems with phenylethynylene-linked donors.

To get stronger absorptivity, the strategy of Figure 3.8 was extended to consider work by Neckers and coworkers²¹⁻²³ that tested the effect of connectivity in the FO- and FM-based push-pull molecules shown in Scheme 3.4. They found that the absorption spectral blue shift from de-conjugating the donor substituents in the 3,6-FO/FM systems (FOPE36, etc.) by comparison to the through-conjugated 2,7-FO/FM systems (FOPE27, etc.) was accompanied by a substantially *increased* molar absorptivity. In the 2,7-connectivity systems, excited state dipole shift effects through the phenylethynyl groups cannot interact directly with the C=O or C=C(CN)₂ dipoles. In the 3,6-connectivity systems, the donor substituents are no longer through-conjugated with one another, but they *are* linked to the C=O or C=C(CN)₂ units. This gives a larger band gap, but

reinforces excited state dipole moment changes for the donor Cz groups interacting with the C=O or C=C(CN)₂ dipoles.

An analogous dipole enhancement was designed using the modules from Scheme 3.2. Jonathan Tinkham carried out computational modeling of FOBDA and FMBDA with time-dependent density functional (TDDFT⁴⁵) methods at the B3LYP/6-31G(d,p) level, and found long wavelength bands at 625 nm and 1042 nm, with oscillator strengths of 0.09 and 0.03, respectively (Table 3.6). The predicted band positions are good matches to the observed band onsets (Table 3.1), and the computed decrease in oscillator strength from the FO to the FM based system agrees with experiment. By comparison, the isomeric FOBDA36 and FMBDA36 were predicted to have long wavelength bands at 490 nm and 616 nm, with much stronger oscillator strengths of 0.23 and 0.24, respectively. Save for different orbital energies due to different connectivities, the 2,7- and 3,6-systems both have similar, push-pull separation in HOMO versus LUMO, indicating ICT type transitions to be expected in both. These computations supported the use of Neckers' connectivity change strategy to increase absorptivity, and indicated that FMBDA36 would absorb well into the visible spectrum despite deconjugation of the donor groups from one another.

Table 3.6: TDDFT B3LYP 6-31G(d,p) predicted band positions and oscillator strengths for FO- and FMBDA 2,7- and 3,6-derivatives using Gaussian 09³⁴.

Compound	Predicted Band Position (eV)	Predicted Oscillator Strength Scaling Factor f
FOBDA	1.98	0.090
FMBDA	1.19	0.035
FOBDA36	2.53	0.228
FMBDA36	2.01	0.224

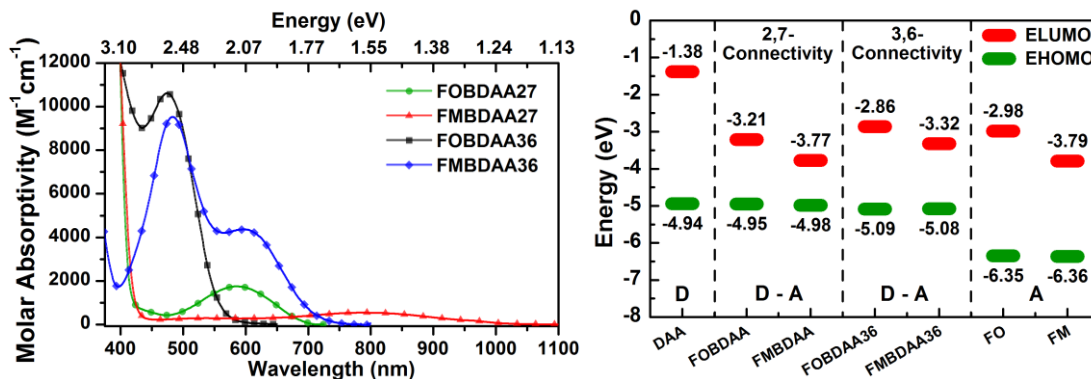


Figure 3.9: Lowest-energy absorption spectral regions in acetonitrile comparing FOBDAA, FMBDAA, FOBDAA36, and FMBDAA36 (left), and frontier molecular orbital energies for FOBDAA, FMBDAA, FOBDAA36, and FMBDAA36 compared to constituent modules' FMO energies (right).

Accordingly, FOBDAA36 and FMBDAA36 were made by methods similar to those used for the other systems in this study. Their absorption spectra in acetonitrile are shown in Figure 3.9, and their cyclic voltammetric redox potentials given in Table 3.1: the full voltammograms are given in Figure 3.2. Although feature onsets are given in Table 3.1 for consistent use with equations 1-2, oxidation potential *maxima* are compared here because they are more precisely resolved in the voltammograms. The oxidation potential maxima were 424 / 553 mV for FOBDAA36 and 437 / 572 mV for FMBDAA36, compared to 268 / 444 mV for FOBDAA and 314 / 494 mV for FMBDAA. Not only are the oxidation potentials – and therefore the HOMO energies (Table 3.1) – raised significantly in the 3,6-isomers, but the splitting *between* oxidation features is decreased: 129 and 135 mV in the FO and FM systems, by comparison to 176 and 180 mV, in the 2,7-connectivity systems. Smaller splitting indicates a smaller interaction between amine units⁴⁶ in the 3,6-connectivity, as expected because there is no mutual oxidative stabilization by amine to amine resonance through direct 2,7-conjugation.

Figure 3.9 shows that the absorption band energies increase in the 3,6- versus the 2,7-connectivity systems, as expected. The observed absorption onsets in acetonitrile are 0.3 ± 0.1 eV (standard deviation) higher energy than the TDDFT modeling predictions, but the predicted and observed spectra both show the desired strong increases in molar absorptivity for both the FO-

and FM-based systems for the 3,6-connectivity. Overall, the combination of LUMO lowering by use of the FM unit, plus increased dipole coupling by use of the 3,6-connectivity, makes FMBDAA36 absorb 8-fold more strongly (molar absorptivity $4500 \text{ M}^{-1} \text{ cm}^{-1}$) than any of the 2,7-connectivity systems, with an absorption profile that still absorbs strongly over much of the visible spectrum, 400-700 nm. Figure 3.9 shows how the component frontier molecular orbitals compare to those of both the 2,7- and 3,6-connectivity systems. Notably, by this analysis the LUMO levels in the 3,6-systems are raised somewhat (relative to those on the 2,7-connectivity system) by direct resonance interaction with the DAA donor groups, giving the observed band gap increase.

3.5 Conclusions

The absorption spectroscopy and electrochemistry of strong electron acceptor fluorenylidene malononitriles (FMs) bearing common 2- or 2,7- electron donor substituents were compared to the results for less electron withdrawing fluorenone (FO) analogues. The FM and FO units are structurally simple and synthetically accessible acceptor (A) units that interact with donor (D) substituents to give dipolar donor-acceptor electronic behavior, including longer wavelength absorption band gaps associated with intramolecular charge transfer (ICT) behavior.

This modular electronic engineering approach provides a rational path for tuning E_{HOMO} , E_{LUMO} , band gap, and absorptivity strength. Starting from FO-based systems bearing moderate donors such as trimethoxystyrene connected in a 2,7-fashion to maximize conjugation, stronger donor diarylamine substituents were used to raise HOMO levels, increasing ICT character and lowering the overall band gap. Changing to a 3,6-connectivity enhanced molar absorptivity considerably, at a cost of increasing the band gap by about 0.50 eV. But, FMBDAA36 derived by the above sequence of structure-property manipulations absorbs well in the 400-700 nm region. This absorption range is important for organic photoconversion and photoconductivity. For example, Chi and coworkers recently showed⁴⁷ that a close variant of FMBDAA36 (with methyl instead of methoxy groups) gives promising solid state photocurrent transport and

photoconversion efficiencies, with their best single-junction photovoltaic device (using C₇₀ as an electron acceptor material) having power conversion efficiency of 4.04%, with open-circuit voltage of 0.99 V, short circuit current of 7.64 mA/cm², and fill factor of 0.53. Other uses of FO or FM derivatives also show promise for hole-transport or dipolar charge transport.⁴⁸⁻⁵¹

It is important to keep in mind that organic molecules become effective electronic materials only through morphological manipulation (intermolecular control⁵²⁻⁵⁶) *as well as* intramolecular electronic control. Because molecular level electronic control is a necessary but insufficient criterion to produce desirable bulk electronic behavior, there is a continuing need to test many derivatives of electronically similar compounds, to find the best molecular-morphological electronic property combinations. The present study exemplifies a strategy for rational testing of whole families of related molecules for potential electronic materials use, starting from electrochemical, spectroscopic, and computational evaluation of donor and acceptor components, and using readily available molecular building blocks assembled in a few synthetic steps. Evaluation of these new materials for organic-based electronics is presently underway.

3.7 References

- (1) Homnick, P. J.; Tinkham, J. S.; Devaughn, R.; Lahti, P. M. Engineering Frontier Energy Levels in Donor-Acceptor Fluoren-9-Ylidene Malononitriles versus Fluorenones. *J. Phys. Chem. A* **2014**, *118*, 475–486.
- (2) Raimundo, J.; Blanchard, P.; Gallego-Planas, N.; Mercier, N.; Ledoux-Rak, I.; Hierle, R.; Roncali, J. Design and Synthesis of Push–Pull Chromophores for Second-Order Nonlinear Optics Derived from Rigidified Thiophene-Based Π -Conjugating Spacers. *J. Org. Chem.* **2002**, *67*, 205–218.
- (3) Leriche, P.; Frère, P.; Cravino, A.; Alévêque, O.; Roncali, J. Molecular Engineering of the Internal Charge Transfer in Thiophene-Triphenylamine Hybrid Π -Conjugated Systems. *J. Org. Chem.* **2007**, *72*, 8332–8336.
- (4) Roquet, S.; Cravino, A.; Leriche, P.; Alévêque, O.; Frère, P.; Roncali, J. Triphenylamine-Thienylenevinylene Hybrid Systems with Internal Charge Transfer as Donor Materials for Heterojunction Solar Cells. *J. Am. Chem. Soc.* **2006**, *128*, 3459–3466.
- (5) Zhang, Z.; Wang, J. Structures and Properties of Conjugated Donor–Acceptor Copolymers for Solar Cell Applications. *J. Mater. Chem.* **2012**, *22*, 4178–4187.
- (6) Roncali, J. Synthetic Principles for Bandgap Control in Linear Π -Conjugated Systems. *Chem. Rev.* **1997**, *97*, 173–206.
- (7) Bundgaard, E.; Krebs, F. Low Band Gap Polymers for Organic Photovoltaics. *Sol. Energy Mater. Sol. Cells* **2007**, *91*, 954–985.
- (8) Oliva, M. M.; Casado, J.; Navarrete, J. T. L.; Berridge, R.; Skabara, P. J.; Kanibolotsky, A. L.; Perepichka, I. F. Electronic and Molecular Structures of Trigonal Truxene-Core Systems Conjugated to Peripheral Fluorene Branches. Spectroscopic and Theoretical Study. *J. Phys. Chem. B* **2007**, *111*, 4026–4035.
- (9) Wang, J.; Xiao, Q.; Pei, J. Benzothiadiazole-Based D- Π -A- Π -D Organic Dyes with Tunable Band Gap: Synthesis and Photophysical Properties. *Org. Lett.* **2010**, *12*, 4164–4167.
- (10) Prasad, P. N.; Williams, D. J. *Introduction to Nonlinear Optical Effects in Molecules & Polymers*; John Wiley & Sons: New York, 1991.
- (11) Zyss, J. *Molecular Nonlinear Optics: Materials, Physics, and Devices (Quantum Electronics - Principles and Applications)*; Kelley, P.; Liao, P. F., Eds.; Academic Press: Boston, 1993.
- (12) Hu, W.; Tao, Y.-T.; Sirringhaus, H. Organic Electronics-New Physical Chemistry Insight. *Phys. Chem. Chem. Phys.* **2012**, *14*, 14097–14098.
- (13) Kuboyama, A. Similarity between the Π , Π^* Absorption Spectra of Fluorenone and 9, 10-Phenanthrenequinone. *Chem. Phys. Lett.* **1976**, *41*, 544–546.

- (14) Kobayashi, T.; Nagakura, S. Picosecond Time-Resolved Spectroscopy and the Intersystem Crossing Rates of Anthrone and Fluorenone. *Chem. Phys. Lett.* **1976**, *43*, 429–434.
- (15) Andrews, L. J.; Derouledé, A.; Linschitz, H. Photophysical Processes in Fluorenone. *J. Phys. Chem.* **1978**, *82*, 2304–2309.
- (16) Yoshihara, K. Spectroscopic Properties of the Lower-Lying Excited States of Fluorenone. *J. Chem. Phys.* **1966**, *45*, 1991.
- (17) Arathi Rani, S.; Sobhanadri, J.; Prasada Rao, T. . Determination of the Excited State Dipole Moment of Fluorenone Using the Method of Solvatochromism. *Spectrochim. Acta Part A Mol. Biomol. Spectrosc.* **1995**, *51*, 2473–2479.
- (18) Ferenczi, T. a M.; Sims, M.; Bradley, D. D. C. On the Nature of the Fluorenone-Based Emission in Oxidized Poly(dialkyl-Fluorene)s. *J. Phys. Condens. Matter* **2008**, *20*, 045220.
- (19) Montilla, F.; Mallavia, R. On the Origin of Green Emission Bands in Fluorene-Based Conjugated Polymers. *Adv. Funct. Mater.* **2007**, *17*, 71–78.
- (20) Rathnayake, H. P.; Cirpan, A.; Karasz, F. E.; Odoi, M. Y.; Hammer, N. I.; Barnes, M. D.; Lahti, P. M. Luminescence of Molecular and Block Copolymeric 2,7-Bis(phenylethenyl)-Fluorenones; Identifying Green-Band Emitter Sites in a Fluorene-Based Luminophore. *Chem. Mater.* **2007**, *19*, 3265–3270.
- (21) Estrada, L. a; Yarnell, J. E.; Neckers, D. C. Revisiting Fluorenone Photophysics via Dipolar Fluorenone Derivatives. *J. Phys. Chem. A* **2011**, *115*, 6366–6375.
- (22) Estrada, L. a; Cai, X.; Neckers, D. C. Nonradiative Decay Mechanism of Fluorene-9-Ylidene Malonitrile Ambipolar Derivatives. *J. Phys. Chem. A* **2011**, *115*, 2184–2195.
- (23) Estrada, L. a; Neckers, D. C. Synthesis and Photophysics of Ambipolar Fluorene-9-Ylidene Malonitrile Derivatives. *J. Org. Chem.* **2009**, *74*, 8484–8487.
- (24) Eakins, G. L.; Alford, J. S.; Tiegs, B. J.; Breyfogle, B. E.; Stearman, C. J. Tuning HOMO-LUMO Levels: Trends Leading to the Design of 9-Fluorenone Scaffolds with Predictable Electronic and Optoelectronic Properties. *J. Phys. Org. Chem.* **2011**, *24*, 1119–1128.
- (25) Shigeta, M.; Morita, M.; Konishi, G.-I. Selective Formation of Twisted Intramolecular Charge Transfer and Excimer Emissions on 2,7-bis(4-Diethylaminophenyl)-Fluorenone by Choice of Solvent. *Molecules* **2012**, *17*, 4452–4459.
- (26) Józefowicz, M.; Heldt, J. R. Dipole Moments Studies of Fluorenone and 4-Hydroxyfluorenone. *Spectrochim. Acta. A. Mol. Biomol. Spectrosc.* **2007**, *67*, 316–320.
- (27) Biczók, L.; Bérces, T.; Inoue, H. Effects of Molecular Structure and Hydrogen Bonding on the Radiationless Deactivation of Singlet Excited Fluorenone Derivatives †. *J. Phys. Chem. A* **1999**, *103*, 3837–3842.

- (28) Yatsuhashi, T.; Nakajima, Y.; Shimada, T.; Inoue, H. Photophysical Properties of Intramolecular Charge-Transfer Excited Singlet State of Aminofluorenone Derivatives. *J. Phys. Chem. A* **1998**, *102*, 3018–3024.
- (29) Homnick, P. J.; Lahti, P. M. Modular Electron Donor Group Tuning of Frontier Energy Levels in Diarylamino-fluorenone Push-Pull Molecules. *Phys. Chem. Chem. Phys.* **2012**, *14*, 11961–11968.
- (30) Pommerehne, J.; Vestweber, H.; Guss, W. Efficient Two Layer LEDs on a Polymer Blend Basis. *Adv. Mater.* **1995**, *7*, 551–554.
- (31) Johansson, T.; Mammo, W.; Svensson, M.; Andersson, M. R.; Inganäs, O. Electrochemical Bandgaps of Substituted Polythiophenes. *J. Mater. Chem.* **2003**, *13*, 1316.
- (32) Sun, Q.; Wang, H.; Yang, C.; Li, Y. Synthesis and Electroluminescence of Novel Copolymers Containing Crown Ether Spacers. *J. Mater. Chem.* **2003**, *13*, 800–806.
- (33) Cardona, C. M.; Li, W.; Kaifer, A. E.; Stockdale, D.; Bazan, G. C. Electrochemical Considerations for Determining Absolute Frontier Orbital Energy Levels of Conjugated Polymers for Solar Cell Applications. *Adv. Mater.* **2011**, *23*, 2367–2371.
- (34) Frisch, M. J.; Trucks, G. W.; Schlegel, H. B.; Scuseria, G. E.; Robb, M. A.; Cheeseman, J. R.; Scalmani, G.; Barone, V.; Mennucci, B.; Petersson, G. A.; Nakatsuji, H.; Caricato, M.; Li, X.; Hratchian, H. P.; Izmaylov, A. F.; Bloino, J.; Zheng, G.; Sonnenberg, J. L.; Hada, M.; Ehara, M.; Toyota, K.; Fukuda, R.; Hasegawa, J.; Ishida, M.; Nakajima, T.; Honda, Y.; Kitao, O.; Nakai, H.; Vreven, T.; Montgomery, J. A., Jr.; Peralta, J. E.; Ogliaro, F.; Bearpark, M.; Heyd, J. J.; Brothers, E.; Kudin, K. N.; Staroverov, V. N.; Kobayashi, R.; Normand, J.; Raghavachari, K.; Rendell, A.; Burant, J. C.; Iyengar, S. S.; Tomasi, J.; Cossi, M.; Rega, N.; Millam, N. J.; Klene, M.; Knox, J. E.; Cross, J. B.; Bakken, V.; Adamo, C.; Jaramillo, J.; Gomperts, R.; Stratmann, R. E.; Yazyev, O.; Austin, A. J.; Cammi, R.; Pomelli, C.; Ochterski, J. W.; Martin, R. L.; Morokuma, K.; Zakrzewski, V. G.; Voth, G. A.; Salvador, P.; Dannenberg, J. J.; Dapprich, S.; Daniels, A. D.; Farkas, Ö.; Foresman, J. B.; Ortiz, J. V.; Cioslowski, J.; Fox, D. J. Gaussian 09, Revision D.01, 2009.
- (35) Lee, C.; Yang, W.; Parr, R. G. Development of the Colle-Salvetti Correlation-Energy Formula into a Functional of the Electron Density. *Phys. Rev. B* **1988**, *37*, 785–789.
- (36) Becke, A. D. Density-Functional Exchange-Energy Approximation with Correct Asymptotic Behavior. *Phys. Rev. A* **1988**, *38*, 3098–3100.
- (37) Stephens, P. J.; Devlin, F. J.; Chabalowski, C. F.; Frisch, M. J. Ab Initio Calculation of Vibrational Absorption and Circular Dichroism Spectra Using Density Functional Force Fields. *J. Phys. Chem.* **1994**, *98*, 11623–11627.
- (38) Grabowski, Z. R.; Rotkiewicz, K.; Rettig, W. Structural Changes Accompanying Intramolecular Electron Transfer: Focus on Twisted Intramolecular Charge-Transfer States and Structures. *Chem. Rev.* **2003**, *103*, 3899–4032.

- (39) Martinez-Martinez, V.; Lim, J.; Banuelos, J.; Lopez-Arbeloa, I.; Miljanic, O. S. Strong Intramolecular Charge Transfer Emission in Benzobisoxazole Cruciforms: Solvatochromic Dyes as Polarity Indicators. *Phys. Chem. Chem. Phys.* **2013**, *15*, 18023–18029.
- (40) Ooyama, Y.; Oda, Y.; Mizumo, T.; Ohshita, J. Specific Solvatochromism of D- π -A Type Pyridinium Dyes Bearing Various Counter Anions in Halogenated Solvents. *Tetrahedron* **2013**, *69*, 1755–1760.
- (41) Vasilev, A. A.; De Mey, K.; Asselberghs, I.; Clays, K.; Champagne, B.; Angelova, S. E.; Spassova, M. I.; Li, C.; Müllen, K. Enhanced Intramolecular Charge Transfer in New Type Donor–Acceptor Substituted Perylenes. *J. Phys. Chem. C* **2012**, *116*, 22711–22719.
- (42) Hu, R.; Lager, E.; Aguilar-Aguilar, A.; Liu, J.; Lam, J. W. Y.; Sung, H. H. Y.; Williams, I. D.; Zhong, Y.; Wong, K. S.; Peña-Cabrera, E.; *et al.* Twisted Intramolecular Charge Transfer and Aggregation-Induced Emission of BODIPY Derivatives. *J. Phys. Chem. C* **2009**, *113*, 15845–15853.
- (43) Jenekhe, S. A.; Lu, L.; Alam, M. M. New Conjugated Polymers with Donor–Acceptor Architectures: Synthesis and Photophysics of Carbazole–Quinoline and Phenothiazine–Quinoline Copolymers and Oligomers Exhibiting Large Intramolecular Charge Transfer. *Macromolecules* **2001**, *34*, 7315–7324.
- (44) Aihara, J. Anomalous Solvatochromism of Charge-Transfer Absorption Bands. *Bull. Chem. Soc. Jpn.* **1981**, *54*, 1561–1562.
- (45) Scalmani, G.; Frisch, M. J.; Mennucci, B.; Tomasi, J.; Cammi, R.; Barone, V. Geometries and Properties of Excited States in the Gas Phase and in Solution: Theory and Application of a Time-Dependent Density Functional Theory Polarizable Continuum Model. *J. Chem. Phys.* **2006**, *124*, 94107.
- (46) Lambert, C.; Nöll, G. The Class II/III Transition in Triarylamine Redox Systems. *J. Am. Chem. Soc.* **1999**, *121*, 8434–8442.
- (47) Wong, W.-Y.; Lu, G.-L.; Choi, K.-H.; Lin, Z. Functionalization of 9-(Dicyanomethylene)fluorene Derivatives with Substituted Acetylenes. *European J. Org. Chem.* **2003**, *2003*, 365–373.
- (48) Lincker, F.; Heinrich, B.; De Bettignies, R.; Rannou, P.; Pécaut, J.; Grévin, B.; Pron, A.; Donnio, B.; Demadrille, R. Fluorenone Core Donor–acceptor–donor Π -Conjugated Molecules End-Capped with Dendritic Oligo(thiophene)s: Synthesis, Liquid Crystalline Behaviour, and Photovoltaic Applications. *J. Mater. Chem.* **2011**, *21*, 5238.
- (49) Porzio, W.; Destri, S.; Pasini, M.; Giovanella, U.; Ragazzi, M.; Scavia, G.; Kotowski, D.; Zotti, G.; Vercelli, B. Synthesis and Characterisation of Fluorenone–thiophene-Based Donor–acceptor Oligomers: Role of Moiety Sequence upon Packing and Electronic Properties. *New J. Chem.* **2010**, *34*, 1961.
- (50) Vijayakumar, C.; Saeki, A.; Seki, S. Optoelectronic Properties of Dicyanofluorene-Based N-Type Polymers. *Chem. Asian J.* **2012**, *7*, 1845–1852.

- (51) Usta, H.; Risko, C.; Wang, Z.; Huang, H.; Deliomeroglu, M. K.; Zhukhovitskiy, A.; Facchetti, A.; Marks, T. J. Design, Synthesis, and Characterization of Ladder-Type Molecules and Polymers. Air-Stable, Solution-Processable N-Channel and Ambipolar Semiconductors for Thin-Film Transistors via Experiment and Theory. *J. Am. Chem. Soc.* **2009**, *131*, 5586–5608.
- (52) Graham, K. R.; Stalder, R.; Wieruszewski, P. M.; Patel, D. G. D.; Salazar, D. H.; Reynolds, J. R. Tailor-Made Additives for Morphology Control in Molecular Bulk-Heterojunction Photovoltaics. *ACS Appl. Mater. Interfaces* **2013**, *5*, 63–71.
- (53) Subbiah, J.; Amb, C. M.; Reynolds, J. R.; So, F. Effect of Vertical Morphology on the Performance of Silole-Containing Low-Bandgap Inverted Polymer Solar Cells. *Sol. Energy Mater. Sol. Cells* **2012**, *97*, 97–101.
- (54) Li, R.; Hu, W.; Liu, Y.; Zhu, D. Micro- and Nanocrystals of Organic Semiconductors. *Acc. Chem. Res.* **2010**, *43*, 529–540.
- (55) Anthony, J. E. The Larger Acenes: Versatile Organic Semiconductors. *Angew. Chem. Int. Ed. Engl.* **2008**, *47*, 452–483.
- (56) Würthner, F.; Schmidt, R. Electronic and Crystal Engineering of Acenes for Solution-Processible Self-Assembling Organic Semiconductors. *ChemPhysChem* **2006**, *7*, 793–797.

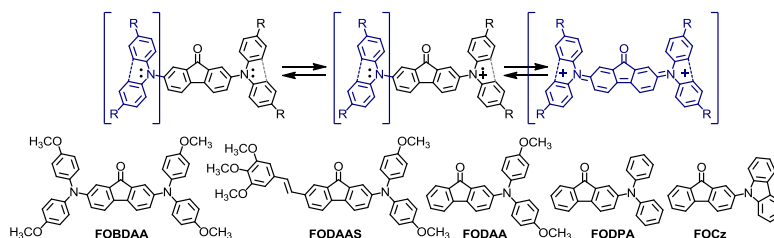
CHAPTER 4

RADICAL CATIONS FROM DIARYLAMINO-SUBSTITUTED FLUORENONES

Adapted with premission from Homnick, P. J.; Tinkham, J. S.; Lahti, P. M. Radical Cations from Diarylamino-Substituted Fluorenones. *Tetrahedron Lett.* **2013**, *54*, 35–39.¹ Copyright 2013 Elsevier Limited. License number 3342511465566
<http://www.sciencedirect.com/science/article/pii/S0040403912018175>

4.1 Introduction and Background

Conjugated aminium radical cations are of much interest as organic electronic materials. They can be spin-bearing building blocks in molecule based magnetic materials and polymers,² and as charge carriers in organic batteries³ and conducting polymers.^{4,5} They also play important roles in photovoltaic charge pair regeneration,⁶ typically as p-type materials. simpler model triarylaminium radical cations thus are useful models for the behavior of more complex electroactive materials.



Scheme 4.1: Chemical oxidation process, and fluorenone-based triarylamine compounds studied.

Triarylaminium cations tend to be very deeply colored, due in part to their strong conjugation. When structural connectivity allows direct π -resonance to the radical cation site, the resulting absorption bands can be energetically tuned. Adding triarylamine sites in direct π -resonance with a radical cation site can give intervalence charge transfer (IVCT) that pushes the band gap transition well into the near infrared (NIR) region.⁷ Comparison of the IVCT behavior gives insight about the ease of electron hopping through a π -conjugated linker or polymer, shows whether or not the radical cation and neutral triarylamine sites are strongly coupled, and shows how conjugative IVCT radical to amine coupling varies with linker types and lengths.^{7,8}

This chapter describes the absorption and electron paramagnetic resonance (EPR) spectra obtained from oxidation of the diarylamine substituted fluorenones FODAA, FODPA, FODAAS, and FOBDA (Scheme 4.1). The latter two systems were investigated to test the effects of extending through-conjugation across the fluorenone unit, with FOBDA providing linkage for intervalence transfer behavior in the radical cation. Although electronic properties have been investigated for fluorenes linked to diarylamines,^{9,10} to our knowledge this has not been done for electron deficient fluorenones attached to diarylamines. This study shows that fluorenones yield highly persistent triarylammonium cations, and are effective IVCT linkers.

4.2 Experimental Methods

The neutral amines used in this study were made and identified using the methods described in Chapter 2 of this dissertation, and published elsewhere.¹¹ Purities of the compounds were established by HPLC. Redox potentials were obtained by cyclic voltammetry using platinum auxiliary and working electrodes with an Ag/AgCl reference electrode (in acetonitrile). All measurements were done in dry acetonitrile with 0.1 M tetrabutylammonium hexafluorophosphate as a supporting electrolyte, using analyte concentrations of about 10 mM. Ferrocene oxidation under these conditions was used as an external voltage standard.

The neutral amines were oxidized by two procedures. For the precipitation protocol, roughly 30 μM of amine was dissolved in toluene and treated with SbCl_5 to give a very dark, powdery precipitate that could be isolated by filtration, and stored under ambient conditions for months. Re-dissolution of these precipitates in dichloromethane readily yielded the characteristic colors of the aminium cation species. For a solution oxidation protocol, the amine was dissolved in dry dichloromethane and directly treated with oxidants such as SbCl_5 , AgSbF_6 , $\text{Pb}(\text{OAc})_4$, or dissolved in acetonitrile for oxidation with CuClO_4 .

UV-vis spectra were obtained using a solution oxidation protocol or by re-dissolving the solid phase aminium cation salts obtained from a precipitation oxidation protocol; both are

described in the experimental procedures chapter. Molar absorptivities given for the oxidized species assume 100 % conversion of neutral triarylamine precursors, and so are minimum values.

EPR spectra were obtained at room temperature by the solution oxidation protocol, or by re-dissolving products from the precipitation oxidation protocol. Hyperfine coupling constants were obtained by spectral simulation, and *g*-values obtained for spectra were calibrated using a frequency counter and an E-036TM teslameter on a Bruker Elexsys E-500 spectrometer.

4.3 Results and Discussion

4.3.1 Mono(diarylamino)fluorenone oxidations

FODAA and FODAAS have lower oxidation potentials than FODPA (Figure 4.1, Table 4.1), consistent with the decreased donor strength for diphenylamine versus dianisylamine. Added conjugation in FODAAS vs. FODAA does not much change the oxidation potential. All of the monoamines show reversible to quasi-reversible behavior, indicating good stability of the radical cations, especially when *para*-donor substituents that block dimerization are present (FODAA, FODAAS). Hybrid density functional theory (DFT) B3LYP/6-31+G(d,p)//B3LYP/6-31G(d) computations^{*12-14} for the neutral amines give good agreement of computed HOMO energy levels with the observed first oxidation potentials converted^{11,15-17} into HOMO energies (despite taking no computational account of solvent or counterion effects). Many of these computations were carried out by Jonathan Tinkham as part of collaborative work investigating the experimental results that I obtained as described below.

* Computational modeling was carried out using Spartan 2010 for Linux from Wavefunction Inc., Irvine, CA, USA, and Gaussian 09.³¹

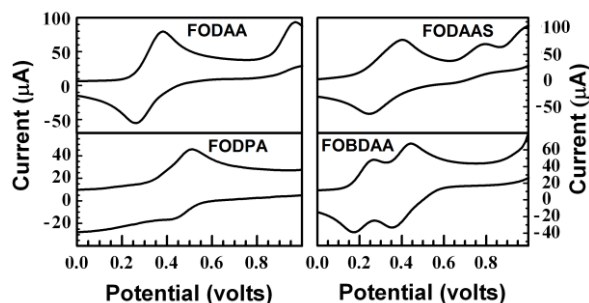


Figure 4.1: Cyclic voltammograms showing the amine oxidation region. Potentials are referenced to the ferrocene/ferrocenium redox standard reaction in dry acetonitrile.

Table 4.1: Spectral and electrochemical characteristics of radical cations and dications.

Compound	Oxidized absorption, nm [eV] ($\log_{10} \epsilon$) ^a	Computed Transition, ([eV], (oscillator strength)) ^b	Oxidation $E_{1/2}$ (mV) to Cation ^c	HOMO Energy (eV) Observed (Computed) ^d	Oxidized EPR spectrum Hyperfine (g-value) ^e
FODAA	777 [1.60] (4.41)	[1.57] (f = 0.24) [1.77] (f = 0.22)	320	-5.03 (-5.03)	8.6 gauss [1 N] (2.0033)
FODPA	823 [1.51] (4.86)	[1.54] (f = 0.26) [1.66] (f = 0.03)	460	-5.12 (-5.35)	5.8 gauss [1 N], (2.0028) ^f
FODAAS	1036 [1.20] (4.02) 747 [1.66] (4.32)	[0.77] (f = 0.65) [1.52] (f = 0.02)	326	-4.98 (-4.95)	≤ 8 gauss [1 N] (2.0033)
FOBDAA	1670 [0.74] (4.44) ^g 873 [1.42] (4.88) ^h 699 [1.77] (4.46) ^h	[0.83] (f = 0.59) [1.21] (f = 1.38) ^h [1.79] (f = 0.16) ^h [1.80] (f = 0.25) ^h	220 400	-4.95 (-4.73)	4.7 gauss [2 N] (2.0032)

^a Band maximum; $\epsilon = \text{M}^{-1} \text{cm}^{-1}$. ^b B3LYP/6-31G(d,p) computed transition energy, oscillator strength for radical cations, and FOBDAA singlet dication. ^c Cyclic voltammetric half-wave potential vs. ferrocene/ferrocenium standard (acetonitrile). ^d E_{HOMO} from Homnick and Lahti¹¹ using onset of first oxidation feature; computed E_{HOMO} from B3LYP/6-31+G(d,p)//B3LYP/6-31G(d) calculations in this work. ^e Solution X-band spectrum (~ 9.6 GHz) in dichloromethane. ^f Large linewidth spectrum (unresolved hfc?). ^g Monocation. ^h Dication.

Solution EPR spectroscopy obtained from solution oxidation of the neutral monoamines or from dissolving solid radical cation salts from the precipitation oxidation protocol gives deeply-colored solutions showing 1:1:1 triplet hyperfine coupling from one nitrogen (Figure 4.2, Table 4.1). The spectra and associated colored solutions are persistent for hours. The FODPA oxidation EPR spectrum is quite broadened relative to others (probably in part from unresolved

hyperfine coupling), but has a similar overall spectral width to others. FODPA oxidation does not give the five-line spectrum from dimeric benzidine type products that form rapidly from triphenylamine¹⁸⁻²⁰ oxidation. FODPA oxidation also shows no evidence of an IVCT band at >800 nm analogous to that from triphenylamine dimerization.²⁰ The fluorenone unit apparently provides at least kinetic stabilization for FODPA radical cation compared to the ready dimerization seen in triphenylamine radical cation. Indeed, the solid aminium salt products from the precipitation oxidation protocol can be stored for months under ambient conditions, and readily yield the characteristic radical cation EPR spectra and colors upon re-dissolution.

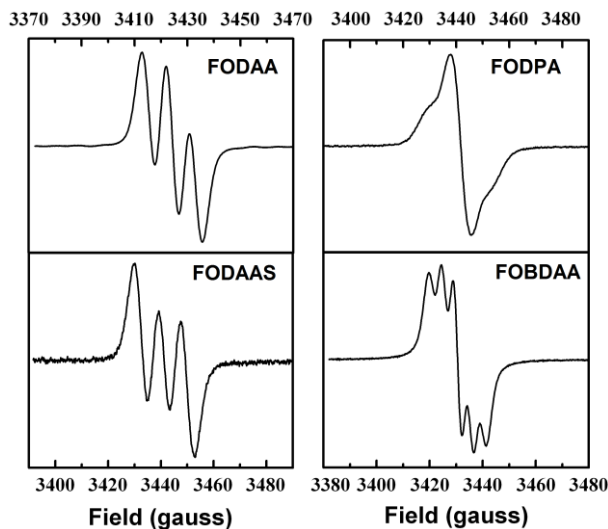


Figure 4.2: Room temperature CH_2Cl_2 solution EPR spectra for: (a) FODAA/ SbCl_5 (9.6000 GHz); (b) FODPA/ SbCl_5 (9.6464 GHz); FODAAS/ SbCl_5 (9.6472 GHz); FOBDAA/ AgSbF_6 (9.6146 Gz).

The UV-vis-NIR spectra of oxidized FODAA and FODPA (Figure 4.4, Table 4.1) exhibit intense long wavelength maxima at 777 and 823 nm, respectively, characteristic of triarylamine radical cations. The spectra from oxidation products are readily distinguished from those of the neutral¹¹ reactants (Figure 4.3). The FODAA⁺ bands for FODAA resemble those of the radical cations from *p*-(dianisylamino)benzoic acid (785 nm) and 5-(dianisylamino)isophthalic acid (777 nm),²¹ which also consist of an electron poor arene attached to a dianisylamine unit. FODAAS shows two bands at 747 and 1036 nm that increase proportionally together with

titration of the oxidant, consistent with both arising from the same species. Titration curves representing the appearance or depletion of selected peaks with increasing oxidant are also shown in Figure 4.3 to help with assigning peaks from the same oxidation product.

FOCz did not oxidize cleanly like the other triarylamines. Solutions would turn from light yellow to darker greenish brown upon oxidant addition, then quickly lose the new color. FOCz required a large excess of oxidant (measured in drops of *stock* oxidant solution) to give changes in the UV-vis-NIR spectrum. This behavior was attributed to side reactions occurring on the unprotected carbazole unit, but this assumption is speculative. No precipitate formed that might indicate polymerization or aggregation, and EPR spectra of FOCz do not indicate formation of conjugated diamine interactions that would be expected from carbazole-carbazole C-C dimerization (these should give more complex hyperfine patterns from interaction of the unpaired electron with multiple nitrogen atoms).

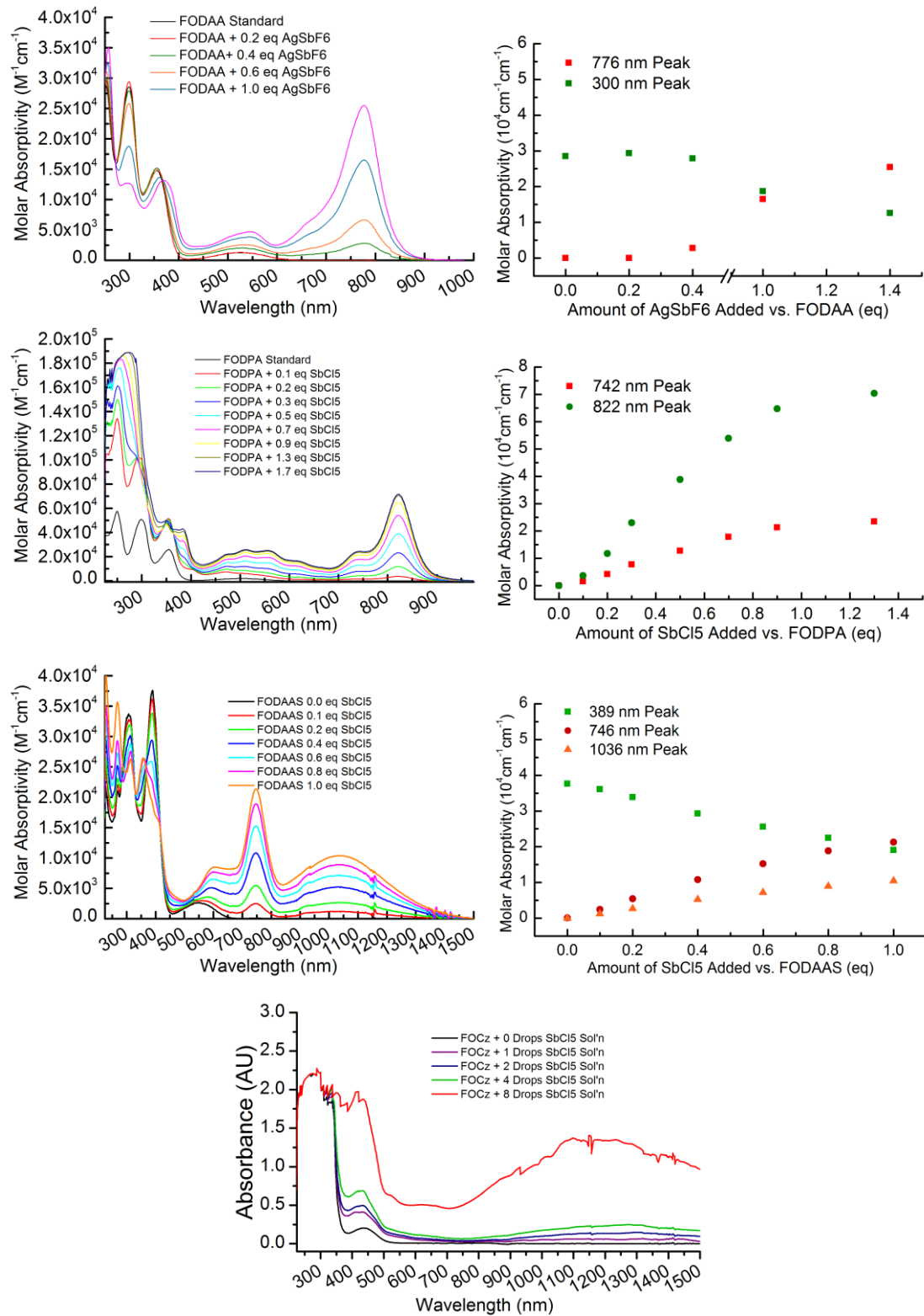


Figure 4.3: UV-vis-NIR oxidation spectra (left) and titration curves (right) for FODAA, FODPA, FODAAS, and FOCz.

UB3LYP¹²⁻¹⁴ and 10/6-31G(d,p) time-dependent DFT (TDDFT)²² computations show the longest wavelength bands in the FODAA, FODPA, and FODAAS cations to have some singly occupied molecular orbital (MO) to lowest unoccupied π -MO (α -SOMO \rightarrow α -LUMO) intramolecular charge transfer (ICT) character, but much stronger (β - π -HOMO \rightarrow β - π^* -LUMO) character. The computed band positions are in relatively good agreement with the experimental bands, even though the computations did not include counterion or solvent dielectric effects. The presence of two major bands in FODAAS is also supported by TDDFT, although the band gap energy and higher energy band oscillator strength are underestimated. Computed band positions and relative strengths are shown in Figure 4.4.

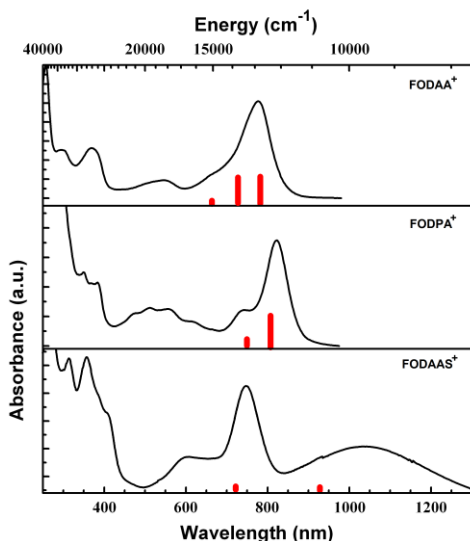


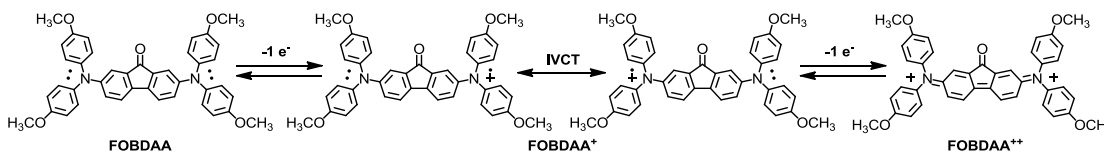
Figure 4.4: Normalized UV-vis-NIR spectra from solution protocol oxidation of FODAA, FODPA, and FODAAS with SbCl_5 . Red bars show UB3LYP/6-31G(d,p) TDDFT predicted band positions and relative transition moments.

Since FODAA showed the lowest voltage oxidation with good radical cation stability, the dianisylamine unit was used to make the FOBDAA system with two amine nitrogens connected in direct conjugation through the 2,7-fluorenediyl unit.

4.3.2 Multiple oxidation steps in FOBDAA

As shown in Figure 4.1, FOBDAA has overlapping reversible cyclic voltammetric oxidation peaks at about 220 and 400 mV, from mono- and di-oxidation, respectively. Solution

oxidations with either SbCl_5 or AgSbF_6 give similar pentet EPR spectra Figure 4.2, Table 4.1 indicating hyperfine coupling from two equivalent nitrogen atoms. Redissolved solid product isolated from the precipitation oxidation protocol from FOBDAA gives nearly the same spectrum. The spectra do not change significantly when cooled to $-70\text{ }^\circ\text{C}$. Thus FOBDA^+ is a single, static, delocalized structure, or undergoes equilibrating intervalence charge transfer faster than the EPR time scale (Scheme 4.2).



Scheme 4.2: Oxidation sequence for FOBDAA.

Addition of more than 1 equivalent of oxidant to FOBDAA solutions gave somewhat decreased EPR spin counts. Frozen solution EPR spectra for samples oxidized with 4 equivalents of SbCl_5 showed no dipolar interaction peaks or half-field transition from a possible triplet biradical dication state of FOBDA^{++} . FTIR spectroscopy comparing neutral FOBDAA to precipitates from oxidation with limited and excess oxidant gave three different spectra, with the $\text{C}=\text{O}$ stretch not observed in the putative FOBDA^+ sample, and the carbonyl region being different between the neutral and the putative FOBDA^{++} . The UB3LYP/6-31G(d,p) optimized computational geometries for FOBDA^+ and FOBDA^{++} (no counter ions) showed greater quinoidal bond alternation in the dication as shown in Scheme 4.2), but only by about 0.01 \AA . The MeOPh groups are twisted out of the fluorenone plane, which reduces the tendency to form a highly semiquinoidal/quinoidal cation/dication structure.

Titration of FOBDAA with multiple oxidants in each case clearly shows initial growth of a NIR band at 1670 nm (Figure 4.4, Table 4.1), which grows to a maximum and thereafter decreases as new, visible region bands grow at 699 and 873 nm . The NIR band is attributable to an IVCT transition of monocationic FOBDA^+ , and the visible bands to dicationic FOBDA^{++} . A small NIR absorption remains even at high oxidant concentrations, so Scheme 4.1 shows an

equilibration of monocation and dication forms. The reaction with AgSbF_6 shows a good isosbestic point at about 1100 nm, indicating no side reactions or decomposition over a few hours during the experiment. The band positions attributed to monocation and dication are completely consistent^{7,8} with assignments of similar bands in oxidation of other through-conjugated diamines.

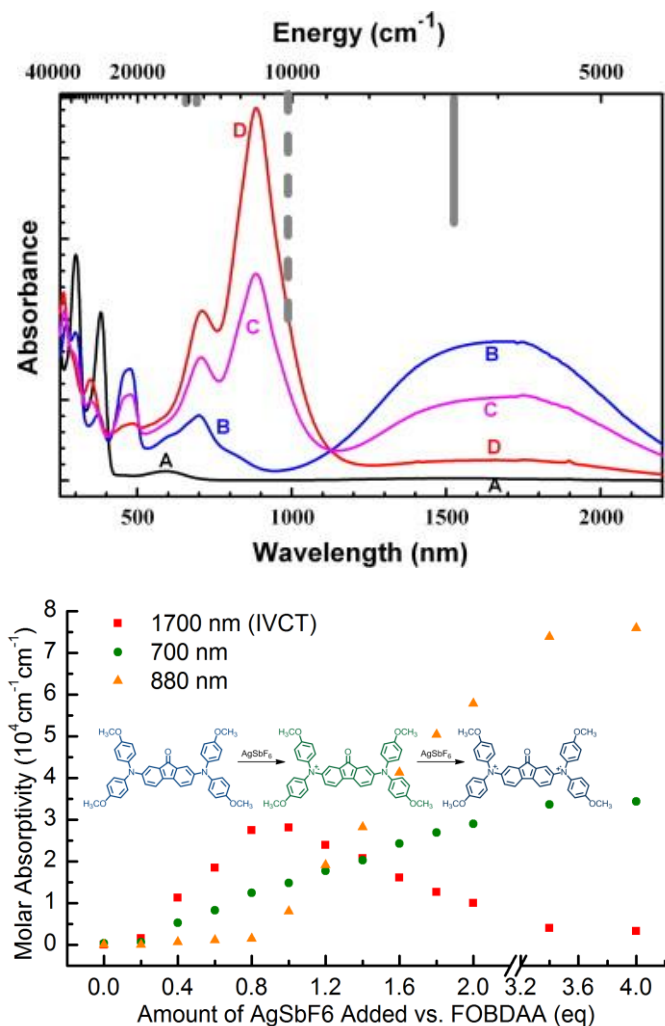
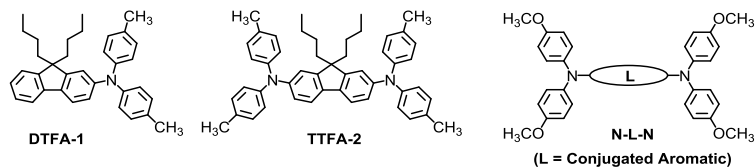


Figure 4.5: UV-vis-NIR spectra for FOBDAA in MeCN oxidized with AgSbF_6 : 0 equiv. (A), 0.8 equiv. (B), 1.6 equiv. (C), and 4.0 equiv. (D). Long wavelength solvent absorbance artifacts were digitally subtracted. Bars show B3LYP/6-31G(d,p) TDDFT predicted band positions and transition moment intensities for FOBDAA+(solid) and FOBDAA++ (dashed).

4.3.3 Comparisons to other conjugated aminium cation systems

Chang, Yueh, and Chen reported⁹ the oxidation behavior of DTFA-1 and TTFA-2 (Scheme 4.3), which are connectivity analogues to FODAA and FOBDAA. Solution EPR and UV-vis-NIR spectra from Cu⁺⁺ oxidation of the neutral amines showed triarylaminium cation formation with good persistence and minimal side reactions. For DTFA-1 and TTFA-2, the monocation absorptions are at 827 (1.5 eV) and 1305 nm (0.95 eV), respectively⁹; the dication band for the latter is at 739 nm (1.68 eV). Although the dianisylamine groups in FOBDAA are stronger electron donors than the ditolylamine groups in TTFA-2, the oxidation potentials for FOBDAA are somewhat higher at 220 and 400 mV than the 140 and 360 mV values for TTFA-2 in acetonitrile. The central fluorenone linker unit in FOBDAA is electron withdrawing, not electron rich like the dialkylfluorene in TTFA-2, which likely explains the electrochemical trend. The cation/dication cyclic voltammetric splitting in TTFA-2 is larger than in FOBDAA and its long wavelength IVCT band at higher energy than FOBDAA.



Scheme 4.3: Triarylamine system from the literature for comparison to the fluorenone-based compounds in Scheme 4.1.

The systems with ditolylamino groups cannot be directly compared to systems with dianisylamine groups, but the electrochemical comparison roughly indicates that 2,7-fluorenonediyl couples the amino groups somewhat less strongly than 9,9-dialkylfluorenone-2,7-diyl. The cation/dication voltammetric splitting in FOBDAA is also smaller than the 220 mV splitting that Lambert and Nöll⁸ observed in N-L-N with L = 4,4'-biphenylene, a π -connectivity analogue of fluorene, but larger than in aryleneethynylene or arylenediethynylene linked analogues. They noted that the splitting in related compounds could be used to compare electronic coupling, with stronger coupling giving a larger cation/dication potential difference.

Thus, the electrochemistry of FOBDAA suggests somewhat reduced coupling by fluorenone relative to 4,4-biphenylene.

The EPR and UV-vis-NIR behaviors of FOBDAA⁺ indicate that it acts as a Robin-Day²³ Class III IVCT system. Its EPR hyperfine splitting at room temperature gives an excellent fit for 2 equivalent ¹⁴N nuclei with much smaller hyperfine than in FODAA, FODPA, and FODAAS (Table 4.1 even below room temperature. This requires²⁴ that IVCT electron transfer is faster than $k_{ET} > 10^{10} \text{ s}^{-1}$ or that the monocation radical is a single static resonance hybrid between the FOBDAA⁺ structures as shown in Scheme 4.1. Its NIR IVCT band half-height bandwidth, simulated by fitting a single gaussian function to the higher energy side of the peak, is $(\nu_{1/2})^{IVCT} \sim 3365 \text{ cm}^{-1}$, significantly lower than the high temperature theoretical half-height bandwidth of 3710 cm^{-1} given by $(\nu_{1/2})^{HTL} = 47.94(\nu_{max})^{1/2}$, where ν_{max} is the band maximum position in wavenumbers. The condition $(\nu_{1/2})^{IVCT} < (\nu_{1/2})^{HTL}$ has been used as an indicator²⁴ of Class III resonance hybrid delocalization as in Scheme 4.2.

Alternatively, Hush's classical model^{8,25-27} can be used to estimate the IVCT transfer integral V between amine sites in FOBDAA⁺. Details are given below, based on a description⁸ by Lambert and Nöll for Gaussian-shaped transitions. Using a N-N distance of 9.7 Å from computational modeling, plus an IVCT band position of 6000 cm^{-1} and molar absorptivity $\epsilon = 27500 \text{ cm}^{-1} \text{ L}^{-1}$, the intervalence transfer energy $V = 1400\text{-}1600 \text{ cm}^{-1}$ for FOBDAA⁺. This is similar to the estimate⁸ published for N-L-N where $L = 4,4'$ -biphenylene, $V = 1550 \text{ cm}^{-1}$, indicating fluorenone to be similar to 4,4'-biphenyl in IVCT coupling strength. This is reasonable, since both have connectivity with the same number and types of bonds between amine centers. It is interesting that the planar fluorenone is not a better linker than the more freely rotating biphenyl; perhaps an electron-withdrawing effect of the C=O in fluorenone offsets the better conjugation of a constrained planar geometry.

$$V = (0.0206/r)\sqrt{(\epsilon \nu_{max} \nu_{1/2})}$$

V = Hush transfer integral in cm^{-1}

r = distance between amino nitrogen atoms in angstroms

ν_{max} = energy of IVCT band in cm^{-1}

$\nu_{1/2}$ = width at half-height of IVCT band in cm^{-1}

ϵ = molar absorptivity of the IVCT band in $\text{M}^{-1}\text{cm}^{-1}$

4.4 A Radical Cation from an Amine-Substituted Fluorenylidene Malononitrile

The UV-vis-NIR spectrum of oxidized FMDAA (Figure 4.6), the fluorenylidene malononitrile (FM) analogue of FODAA, exhibits intense long wavelength maxima at 780 nm and 640 nm, similarly to FODAA. The spectra from oxidation products are readily distinguished from the neutral²⁸ reactant spectrum even though the new oxidation peaks grow over the same region as the intramolecular charge transfer (ICT) peak for neutral FMDAA.

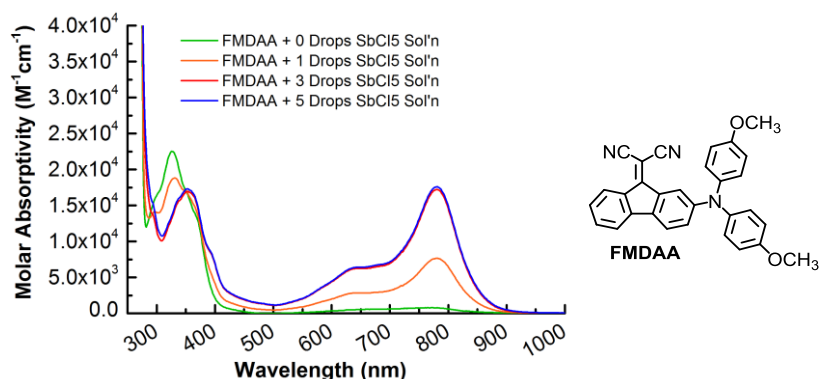


Figure 4.6: UV-vis-NIR oxidation spectra for FMDAA.

The solution color is qualitatively much darker upon oxidation and the color is persistent for several days, similarly to the fluorenone-based (FO-based) systems discussed above. No further study was pursued of this compound or any of the other Chapter 3 FM-based compounds; but it appears that the radical cations for the FM analogues are about as stable as those of the FO-based systems. Further study of the Chapter 3 compounds would be interesting due to their persistence and their significantly more electron withdrawing FM component. So far only qualitative oxidations of some of the Chapter 3 FM compounds was performed, giving persistent

and deeply colored solutions. No UV-vis-NIR absorption or EPR spectra were obtained.

Comparison of the 2,7- versus 3,6-bis-dianisylamino substituted FO and FM- based systems would be particularly interesting due to the break in amine-amine through-conjugation in the 3,6- versus 2,7-diamine systems. Because the amine sites in 3,6-FOBDAA and 3,6-FMBDAA are pseudo-meta to each other, the amines may interact ferromagnetically^{29,30} in the doubly oxidized species, which may be especially useful for spin-based applications.

4.5 Conclusions

A test set of conjugated amines having one fluorenone substituent yields highly persistent aminium radical cations upon solution oxidation. Solid powder samples of the radical cations are very stable. UV-vis-NIR transitions for the radical cations are in reasonably good agreement with hybrid functional TDDFT computational modeling. The through-conjugated diamine, FOBDAA, exhibits an intervalence charge transfer NIR band and EPR spectroscopy consistent with swift electron transfer, or one static delocalized structure. Preliminary results suggest that the FM-based analogues of these compounds are also quite persistent, so future studies on the Chapter 3 FM-based materials might be worth pursuing. The stabilities of these radical cation species are promising for potential use as electronic materials.

4.6 Acknowledgements

This work was supported as part of Polymer-Based Materials for Harvesting Solar Energy (PHaSE), an Energy Frontier Research Center funded by the U.S. Department of Energy, Office of Basic Energy Sciences under Award Number DE-SC0001087.

4.7 References

- (1) Homnick, P. J.; Tinkham, J. S.; Lahti, P. M. Radical Cations from Diarylamino-Substituted Fluorenones. *Tetrahedron Lett.* **2013**, *54*, 35–39.
- (2) Murata, H.; Takahashi, M.; Namba, K.; Takahashi, N.; Nishide, H. A High-Spin and Durable Polyradical: poly(4-Diphenylaminium-1,2-Phenylenevinylene). *J. Org. Chem.* **2004**, *69*, 631–638.
- (3) Kurata, T.; Koshika, K.; Kato, F.; Kido, J.; Nishide, H. An Unpaired Electron-Based Hole-Transporting Molecule: Triarylamine-Combined Nitroxide Radicals. *Chem. Commun.* **2007**, *1*, 2986–2988.
- (4) MacDiarmid, A. G. “Synthetic Metals”: A Novel Role for Organic Polymers (Nobel Lecture). *Angew. Chemie Int. Ed.* **2001**, *40*, 2581–2590.
- (5) Negi, Y. S.; Adhyapak, P. V. Development in Polyaniline Conducting Polymers. *J. Macromol. Sci. Part C Polym. Rev.* **2002**, *42*, 35–53.
- (6) Ning, Z.; Tian, H. Triarylamine: A Promising Core Unit for Efficient Photovoltaic Materials. *Chem. Commun.* **2009**, 5483–5495.
- (7) Heckmann, A.; Lambert, C. Neutral Organic Mixed-Valence Compounds: Synthesis and All-Optical Evaluation of Electron-Transfer Parameters. *J. Am. Chem. Soc.* **2007**, *129*, 5515–5527.
- (8) Lambert, C.; Nöll, G. The Class II/III Transition in Triarylamine Redox Systems. *J. Am. Chem. Soc.* **1999**, *121*, 8434–8442.
- (9) Chang, C.-C.; Yueh, H.; Chen, C.-T. Generation and Spectroscopic Profiles of Stable Multiarylaminium Radical Cations Bridged by Fluorenes. *Org. Lett.* **2011**, *13*, 2702–2705.
- (10) C. Ego, A.C. Grimsdale, F. Uckert, G. Yu, G. Srdanov, K. M. Triphenylamine-Substituted Polyfluorene—A Stable Blue-Emitter with Improved Charge Injection for Light-Emitting Diodes. *Adv. Mater.* **2002**, *14*, 809–811.
- (11) Homnick, P. J.; Lahti, P. M. Modular Electron Donor Group Tuning of Frontier Energy Levels in Diarylamino-fluorenone Push-Pull Molecules. *Phys. Chem. Chem. Phys.* **2012**, 11961–11968.
- (12) Lee, C.; Yang, W.; Parr, R. G. Development of the Colle-Salvetti Correlation-Energy Formula into a Functional of the Electron Density. *Phys. Rev. B* **1988**, *37*, 785–789.
- (13) Becke, A. D. Density-Functional Thermochemistry. III. The Role of Exact Exchange. *J. Chem. Phys.* **1993**, *98*, 5648.
- (14) Stephens, P. J.; Devlin, F. J.; Chabalowski, C. F.; Frisch, M. J. Ab Initio Calculation of Vibrational Absorption and Circular Dichroism Spectra Using Density Functional Force Fields. *J. Phys. Chem.* **1994**, *98*, 11623–11627.

- (15) Cardona, C. M.; Li, W.; Kaifer, A. E.; Stockdale, D.; Bazan, G. C. Electrochemical Considerations for Determining Absolute Frontier Orbital Energy Levels of Conjugated Polymers for Solar Cell Applications. *Adv. Mater.* **2011**, *23*, 2367–2371.
- (16) Johansson, T.; Mammo, W.; Svensson, M.; Andersson, M. R.; Inganas, O. Electrochemical Bandgaps of Substituted Polythiophenes. *J. Mater. Chem.* **2003**, *13*, 1316.
- (17) Pommerehne, J.; Vestweber, H.; Guss, W. Efficient Two Layer LEDs on a Polymer Blend Basis. *Adv. Mater.* **1995**, *7*, 551–554.
- (18) Dollish, F. R.; Hall, W. K. On the Interaction of Triphenylamine with Iodine and with Silica—Alumina Catalysts. *J. Phys. Chem.* **1965**, *69*, 2127–2129.
- (19) Stamires, D. N.; Turkevich, J. Electron Paramagnetic Resonance in Some Molecular Charge Transfer Complexes. *J. Am. Chem. Soc.* **1963**, *85*, 2557–2561.
- (20) Sreenath, K.; Suneesh, C. V.; Kumar, V. K. R.; Gopidas, K. R. Cu(II)-Mediated Generation of Triarylamine Radical Cations and Their Dimerization. an Easy Route to Tetraarylbendazines. *J. Org. Chem.* **2008**, *73*, 3245–3251.
- (21) Murata, H.; Lahti, P. M. Synthesis and Oxidation of Triarylamine Derivatives Bearing Hydrogen-Bonding Groups. *J. Org. Chem.* **2007**, *72*, 4974–4977.
- (22) Scalmani, G.; Frisch, M. J.; Mennucci, B.; Tomasi, J.; Cammi, R.; Barone, V. Geometries and Properties of Excited States in the Gas Phase and in Solution: Theory and Application of a Time-Dependent Density Functional Theory Polarizable Continuum Model. *J. Chem. Phys.* **2006**, *124*, 94107.
- (23) Robin, M. B.; Day, P. Mixed Valence Chemistry-A Survey and Classification. *Adv. Inorg. Chem. Radiochem.* **1968**, *10*, 247–422.
- (24) Lancaster, K.; Odom, S. a; Jones, S. C.; Thayumanavan, S.; Marder, S. R.; Brédas, J.-L.; Coropceanu, V.; Barlow, S. Intramolecular Electron-Transfer Rates in Mixed-Valence Triarylaminines: Measurement by Variable-Temperature ESR Spectroscopy and Comparison with Optical Data. *J. Am. Chem. Soc.* **2009**, *131*, 1717–1723.
- (25) Crutchley, R. J. Intervalence Charge Transfer and Electron Exchange Studies of Dinuclear Ruthenium Complexes. *Advances in Inorganic Chemistry*, 1994, *41*, 273–325.
- (26) Creutz, C. Mixed Valence Complexes of d5-d6 Metal Centers. In *Progress in Inorganic Chemistry*; John Wiley & Sons, Inc., 2007; pp. 1–73.
- (27) Hush, N. S. Intervalence-Transfer Absorption. Part 2. Theoretical Considerations and Spectroscopic Data. In *Progress in Inorganic Chemistry*; John Wiley & Sons, Inc., 2007; pp. 391–444.

- (28) Homnick, P. J.; Tinkham, J. S.; Devaughn, R.; Lahti, P. M. Engineering Frontier Energy Levels in Donor-Acceptor Fluoren-9-Ylidene Malononitriles versus Fluorenones. *J. Phys. Chem. A* **2014**, *118*, 475–486.
- (29) J. Bushby, R.; R. McGill, D.; M. Ng, K.; Taylor, N. Disjoint and Coextensive Diradical Dions. *J. Chem. Soc., Perkin Trans. 2* **1997**, 1405–1414.
- (30) Ratera, I.; Veciana, J. Playing with Organic Radicals as Building Blocks for Functional Molecular Materials. *Chem. Soc. Rev.* **2012**, *41*, 303–349.
- (31) Frisch, M. J.; Trucks, G. W.; Schlegel, H. B.; Scuseria, G. E.; Robb, M. A.; Cheeseman, J. R.; Scalmani, G.; Barone, V.; Mennucci, B.; Petersson, G. A.; Nakatsuji, H.; Caricato, M.; Li, X.; Hratchian, H. P.; Izmaylov, A. F.; Bloino, J.; Zheng, G.; Sonnenberg, J. L.; Hada, M.; Ehara, M.; Toyota, K.; Fukuda, R.; Hasegawa, J.; Ishida, M.; Nakajima, T.; Honda, Y.; Kitao, O.; Nakai, H.; Vreven, T.; Montgomery, J. A., Jr.; Peralta, J. E.; Ogliaro, F.; Bearpark, M.; Heyd, J. J.; Brothers, E.; Kudin, K. N.; Staroverov, V. N.; Kobayashi, R.; Normand, J.; Raghavachari, K.; Rendell, A.; Burant, J. C.; Iyengar, S. S.; Tomasi, J.; Cossi, M.; Rega, N.; Millam, N. J.; Klene, M.; Knox, J. E.; Cross, J. B.; Bakken, V.; Adamo, C.; Jaramillo, J.; Gomperts, R.; Stratmann, R. E.; Yazyev, O.; Austin, A. J.; Cammi, R.; Pomelli, C.; Ochterski, J. W.; Martin, R. L.; Morokuma, K.; Zakrzewski, V. G.; Voth, G. A.; Salvador, P.; Dannenberg, J. J.; Dapprich, S.; Daniels, A. D.; Farkas, Ö.; Foresman, J. B.; Ortiz, J. V.; Cioslowski, J.; Fox, D. J. Gaussian 09, Revision D.01, 2009.

CHAPTER 5

FLUORENONE-BASED DONOR-ACCEPTOR MOLECULES THAT ENHANCE DYE SENSITIZED SOLAR CELL PERFORMANCE

Adapted with permission from Kokil, A.; Chudomel, J. M.; Homnick, P. J.; Lahti, P. M.; Kumar, J. Push-pull Triarylamine Additives That Enhance Dye Sensitized Solar Cell Performance. *RSC Adv.* **2013**, *3*, 15626.¹ Reproduced by permission of The Royal Society of Chemistry. <http://pubs.rsc.org/en/content/articlelanding/2013/RA/c3ra40986d#!divAbstract>

[This section is based on the publication described above; some portions are used verbatim per copyright permission as given above.]

5.1 Introduction

This chapter describes a new strategy for improving basic dye-sensitized solar cell (DSSC) performance, which was developed using three of the D-A and D-A-D fluorenone (FO)-based compounds described in Chapter 2. The work was published in *RSC Advances*¹ ([DOI 10.1039/C3RA40986D](https://doi.org/10.1039/C3RA40986D)) in collaboration with Dr. Akshay Kokil and Professor Jayant Kumar from UMass Lowell, and Dr. John Matthew Chudomel from UMass Amherst. Work at UMass Lowell showed device relative power conversion efficiency (PCE) improvements of up to 33 % versus control device PCEs that did not use the fluorenone-based additives. Although not initially one of the goals of the Chapters 2 and 3 projects, this work is promising and suggests wider uses for fluorenone-based triarylamine due to their highly tuned highest occupied molecular orbital (HOMO) energies^{2,3} and their remarkable oxidative stability.⁴

DSSCs are of notable interest due to reported power conversion efficiencies (PCEs) up to 15%.^{5,6} But, before this record-breaking PCE, DSSC efficiency improvement has been very slow over the past two decades, rising from a PCE of 10% in 1997.⁷ This chapter describes a strategy for enhancing DSSC performance by adding a small amount of FO-based triarylamine to the iodide/triiodide (I^-/I_3^-) redox electrolyte solution that is used in many DSSCs for regenerating the active layer dye after charge transfer to an n-type substrate. This redox couple additive strategy is attractive, because the additives are not attached to the n-type electrode material and thus require no extra solid state processing steps. Secondly, the additive design strategy is versatile for testing

a wide variety of compounds or combinations of compounds in the future, such as those described in Chapters 2 and 3. Finally, the electronically tunable molecular structures of the FO-based additives,^{2,3} in addition to their stability in the oxidized state,⁴ allow for fine-tuning their electrochemical potentials to fit, in principle, a wide array of specific DSSC electrical configurations.

5.2 Background

In contrast to bulk heterojunction (BHJ) thin film organic solar cells, DSSCs (or Grätzel cells) are frequently constructed from TiO₂ nanoparticles (n-type material), an organic or inorganic/organic dye (p-type material), and a redox electrolyte system such as I⁻/I₃⁻. Grätzel DSSCs require a redox system which regenerates the dye molecule to its neutral state after it donates an electron to the TiO₂ layer post-photoexcitation. Figure 5.1 shows a simplified description of this process. First, light is absorbed by a dye molecule (p-type material) that is adsorbed onto an n-type metal oxide nanoparticle, typically anatase TiO₂ (A). The excited state electron is transferred (B) to the TiO₂ (LUMO energy is -3.9 eV). The electron is then injected into a transparent electrode material (C), which is in circuit with a counter electrode. At the counter electrode an electron is transferred to form I₃⁻ (D), which then transfers an electron back to the oxidized dye molecule (E), returning it to its neutral ground state. Once the dye is regenerated in this manner, the process can continue.

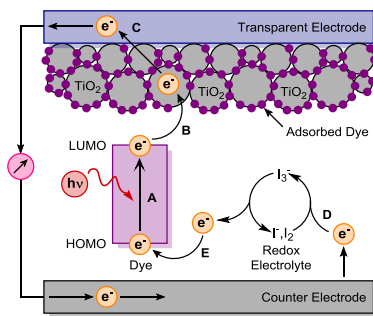


Figure 5.1: Generic DSSC diagram showing the main photovoltaic processes. A, photon absorbed by dye molecule to form excited state. B, Excited state electron transferred to TiO₂ n-type material, followed by electron injection into transparent electrode C. D, Electron transferred from counter electrode to I₂, I⁻ to form I₃⁻. E, I₃⁻ transfers electron to oxidized dye molecule to regenerate its neutral ground state.

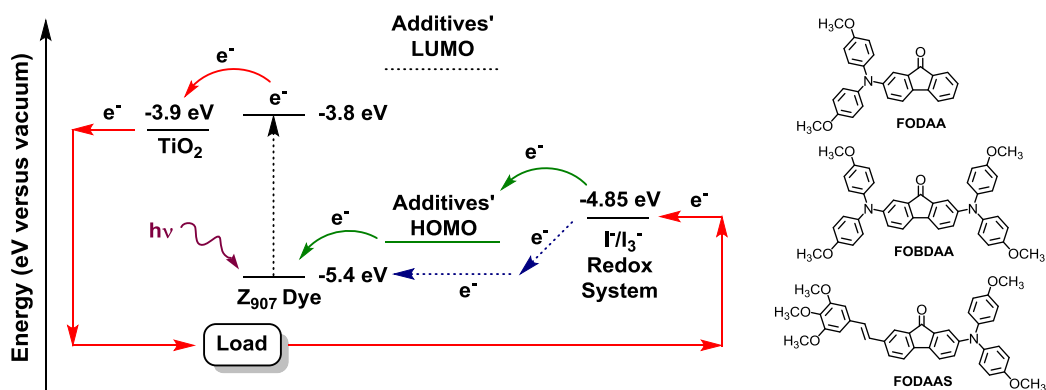
While DSSCs are physically much different than BHJ solar cells, the physical processes and molecular design principles are very similar, save for a few, notable differences. In particular, the photoactive dye performance is not dictated by intermolecular packing/crystallinity, as it is in BHJ solar cell photoactive layers. The hole transport process is performed by the redox electrolyte solution, so the dye material does not have to transport charges over a long distance. This makes one fewer complicated molecular design parameter to engineer. Still, DSSC dyes are typically asymmetrical so that one end has a TiO₂ binding group such as a carboxylate. Because this group needs to reside at the dye's TiO₂ attachment site, the dye must have a donor-acceptor structure that drives electron density towards the attachment interface. This requires some extra consideration during the molecular design and synthesis processes, which can sometimes make dye development more complicated. Another difference is that DSSCs usually use a *liquid* phase electrolyte redox system. Not only does this need for liquid make commercialization more challenging, the use of iodide/triiodide can quickly cause device components to corrode, decreasing device lifetime. Solid state hole transporting materials that replace the iodide/triiodide redox solution are a promising alternative, but they so far have had much lower PCEs.

Despite all of the molecular design efforts and device architecture improvements aimed at making better DSSC dyes, metal oxides, and redox electrolytes (solution or solid state),^{8,9} DSSC PCEs have not increased greatly over the last 10 years.⁷ To enhance the energy gathering and charge-pair generation process, numerous organometallic ruthenium complexes and organic dyes have been used as sensitizers.⁸ Unfortunately, ruthenium is too expensive to incorporate in commercially-viable devices, and organic sensitizers have historically fallen short of the best ruthenium-based PCEs. To further improve DSSC PCEs, some groups have utilized sensitizing dye pairs that collectively absorb over the whole visible spectrum, with the higher energy absorbing dye relaying its energy to the lower energy absorbing dye by Förster resonance energy transfer (FRET).¹⁰⁻¹³ Although relative PCE improvements of 26-28 % have been obtained using

sets of energy relay dyes, these FRET-based strategies are limited by the number of dye pairs that can effectively be utilized.

Alternative PCE improvement methods include altering the DSSCs' electrochemical processes. For example, improving the device's open circuit voltage (V_{OC}) is desirable, since it is an important measure of the cell's power-generating potential. V_{OC} arises from the energy difference between the electron quasi-Fermi level (E_F) of the TiO_2 n-type material and the equilibrium redox potential (E_{Redox}) of the redox electrolyte system.¹⁴ So, increasing E_F or E_{Redox} should increase V_{OC} . Recently, *N*-heterocyclic organic electrolyte additives, such as 4-*tert*-butylpyridine, have been reported to increase V_{OC} .¹⁵ PCE improvements were attributed to increased E_F with surface passivation of the nanoporous TiO_2 electrode to suppress undesirable electron-hole recombination at the inorganic/organic interface.¹⁶ The short circuit currents (J_{SC}) of these devices were reportedly unaffected, so their overall PCEs increased due to increased V_{OC} . Other V_{OC} improvement methods include the use of redox electrolyte systems other than iodide/triiodide that have a higher oxidation potential and/or do not require bimolecular redox chemistry at the anode, such as the ferrocene/ferrocenium¹⁷ redox couple.

In the work carried out at UMass Lowell using the fluorenone push-pull molecules, the goal was to improve basic DSSC performance by improving the redox electrolyte system for dye regeneration. Toward this goal, three of the Chapter 2-3 compounds (FODAA, FOBDA, and FODAAS) were used as redox electrolyte solution additives in only $\sim 10^{-5}$ M concentration. These compounds were used because their HOMO energies reside between the HOMO of a typical DSSC dye (Z907) used in the study, and the I/I_3^- electrolyte system E_{Redox} . PCE improvements that were observed are described below, and are attributed to an electron flow improvement between the electrolyte system and the oxidized dye by way of the additives' intermediately arranged redox energies (Scheme 5.1).



Scheme 5.1: Electron transport processes in control and additive-modified DSSCs, and the additives' molecular structures. Green, dye regeneration via energy cascade through additive's HOMO. Blue, dye regeneration by direct electron transfer from I^-/I_3^- .

This redox couple additive strategy is attractive for further development because it is versatile for testing a wide variety of compounds or combinations of compounds (like those described in Chapters 2 and 3), and it does not add any additional processing steps.

5.3 Results and Discussion

A fairly common DSSC configuration was used for all experiments in this study, that has Z907 ((*cis*-bis(isothiocyanato)(2,2'-bipyridyl-4,4'-dicarboxylato)(4,4'-di-nonyl-2'-bipyridyl)-ruthenium(II)) adsorbed as the sensitizing dye onto a 10 μm thick nanoporous anatase TiO_2 electrode.¹⁸ Electrolyte solutions consisted of 0.8 M 1-propyl-3-methylimidazolium iodide and 0.15 M I_2 in 3-methoxypropionitrile, plus push-pull additives tested as described below. DSSC test devices were fabricated by Dr. Akshay Kokil at UMass Lowell according to literature protocols, using a platinized fluorine doped SnO_2 glass counter electrode.¹⁹

The absorption spectra of the additives are compared to that of Z907 in Figure 5.2 (9-DAAA and 9,10-BAA were synthesized by Dr. J. Matthew Chudomel and used¹ as electrolyte solution additives, but are outside the scope of this discussion). The molar absorptivity of Z907 is about $1.25 \times 10^4 \text{ M}^{-1} \text{ cm}^{-1}$, much higher than that of the additives. HOMO energies (E_{HOMO}) for all compounds were established from cyclic voltammetry half-wave potentials using the equation

$E_{\text{HOMO}} = - (4.8 + [\text{oxidation potential in volts}]) \text{ eV}$,^{20,21} and LUMO energies (E_{LUMO}) were determined by adding the optical band gap (low energy onset in eV) to E_{HOMO} .

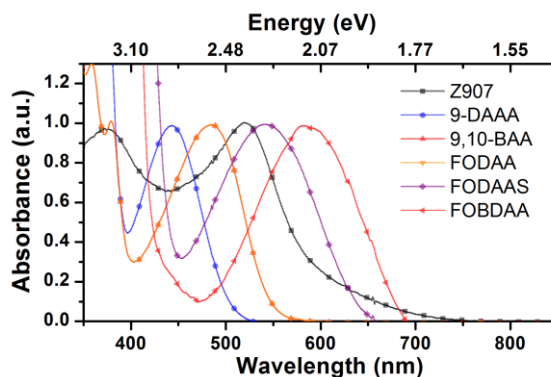


Figure 5.2: Normalized absorption spectra of Z907 sensitizing dye and the triarylamine additive molecules.

To compare the effects of each triarylamine additive on DSSC performance, the device characteristics for a standard control cell were first measured, then aliquots of the additive in acetonitrile were added to the electrolyte and the measurements repeated. The incident photon-to-current conversion efficiency (IPCE) spectra for the devices are similar to the absorption spectrum of Z907 and do not appear to change upon addition of the additives. Representative IPCE traces for DSSCs using FODAA and FODAAS as additives are shown in Figure 5.3. These results indicate that the current in the device is primarily generated from Z907 photoexcitation and *not* from sensitization by the additive molecules. IPCE yields increased substantially upon triarylamine additive addition, even though the additive concentrations are significantly lower than the *N*-heterocycle concentrations used in other²² DSSCs.

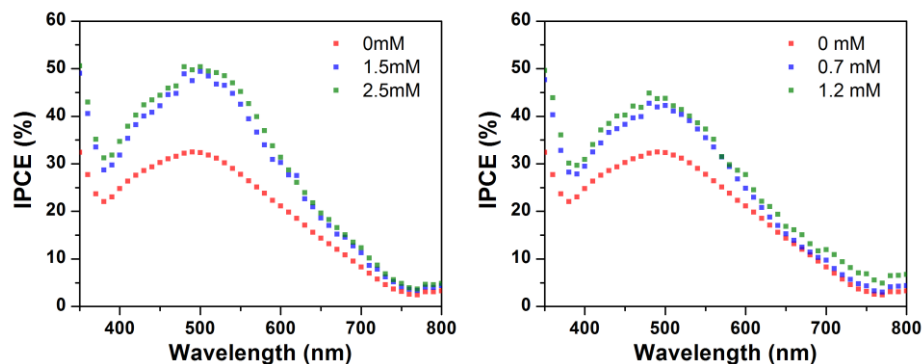


Figure 5.3: IPCE spectra for DSSCs with increasing amounts of FODAA (left) and FODAAS (right) in the redox couple solution.

Current density versus voltage plots for DSSCs with the triarylamine additives FODAA, FODAAS, and FOBDAA are displayed in Figure 5.4. In a control experiment, neat acetonitrile (without additive) was added to the DSSC electrolyte solution, decreasing PCE, fill factor (FF), and J_{SC} (Figure 5.4A) as expected, due to dilution of the iodide/triiodide electrolyte. By comparison, all of the D-A compounds gave improved DSSC performance up to a maximum additive concentration of 1-3 mM. No further improvement was observed past 3 mM.

The power curves for DSSCs with addition of FODAA, FODAAS, and FOBDAA into the iodide/triiodide electrolyte are displayed in Figure 5.4B-D, showing significant improvements in J_{SC} with little to no change in V_{OC} . In contrast, previously studied *N*-heterocycles used for DSSC enhancement increase the V_{OC} with no increase in the J_{SC} .²² FODAA and FODAAS improved J_{SC} by as much as 30% and 26% respectively versus control devices, and the devices' current outputs correlate with improved IPCE spectra. These J_{SC} improvements correspond to overall PCE improvements of 33% for FODAA and 30% for FODAAS. FOBDAA behaved similarly, improving relative PCE by 24% versus control devices.

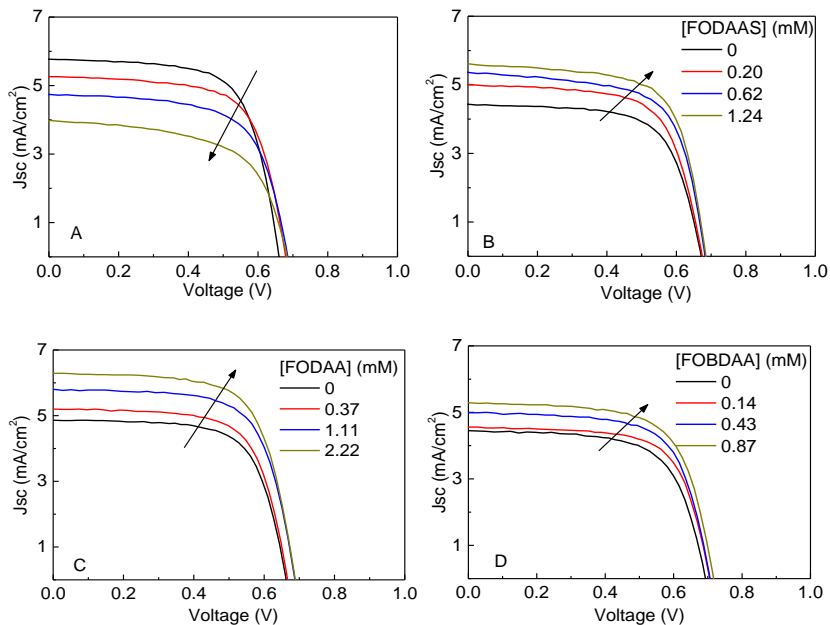


Figure 5.4: Current density versus voltage (J-V) curves for DSSCs incorporating (A) Acetonitrile (B) FODAAS (C) FODAA and (D) FOBDAA. The arrows in plots display increasing acetonitrile (A) and D-A triarylamine additives (B-D).

It is unlikely that the additive-enhanced PCEs are due to improved spectral energy harvesting by absorption and/or FRET for several reasons. The additives are present in very low concentration, their absorption energy is similar to that of Z907, and their molar absorptivities are much lower than Z907. Their fluorescence strength in polar solvent is also very weak (see Chapter 2) and mostly not in Z907's absorption region, which rules out a FRET-based mechanism. Given the fact that the IPCE spectra track well with the Z907 absorption spectral profile, it is reasonable to conclude that the additives do not enhance DSSC performance by increasing light harvesting or charge pair generation.

Thus, the PCE improvements must be a result of some other process. Because the additives' E_{HOMO} values lie between Z907 E_{HOMO} (-5.40 eV) and iodide/triiodide E_{Redox} (-4.85 eV) as shown in Scheme 5.1, the additives could provide an additional or alternate pathway for hole transport to regenerate Z907 either in cooperation with or instead of the iodide/triiodide redox couple. E_{HOMO} for FODAA, FODAAS, and FOBDAA are -5.12 eV, -5.13 eV, and -5.02 eV respectively, obtained from cyclic voltammetric halfwave potentials. So, this explanation is

consistent with the improved IPCE and J_{SC} data. Experiments using these additives *without* iodide/triiodide give severely decreased device performance, so they turn out *not* to be effective hole transport materials on their own in the DSSC.

Due to the fact that the additive HOMO energies lie between the $E_{HOMO/Redox}$ of Z907 and iodide/triiodide, the additives can assist in electron shuttling between Z907 and the redox couple (Scheme 5.1). Because the iodide/triiodide electron shuttling process is so important for DSSC performance,⁸ increasing the effectiveness of this process should result in increased IPCE and J_{SC} values as we observed. As such, it is reasonable to conclude that the additives are enhancing this electron shuttling process, although lack of PCE improvement past a certain concentration suggests a saturation of kinetics among multiple electron shuttling reactions. Unfortunately there is no obvious trend with respect to the additives' capacity to improve J_{SC} , so more work is needed to establish the mechanism of their effect on DSSC performance. But, these initial results are promising; and the structural versatility of fluorenone-based materials provides the opportunity for further study of structure-property-based mechanics involved in this work.

5.4 Conclusions

FODAA, FODAAS, and FOBDA significantly improved DSSC performance as iodide/triiodide redox couple additives, in concentrations of less than 3 mM. The intermediately placed HOMO energies of these additives appear to assist multiple iodide/triiodide electron shuttling processes, improving the regeneration of Z907, although they are alone not effective replacements for iodide/triiodide. Unfortunately, the relationship between photoinduced charge generation and electrochemistry in DSSCs is complicated and requires *simultaneous* optimization of many variables. Consequently these additives may not necessarily improve DSSC performance with a different sensitizing dye or in other configurations. Despite these uncertainties, this work demonstrates a potentially useful new strategy for improving DSSC performance using structurally versatile yet simple fluorenone-based D-A compounds.

5.5 References

- (1) Kokil, A.; Chudomel, J. M.; Homnick, P. J.; Lahti, P. M.; Kumar, J. Push-pull Triarylamine Additives That Enhance Dye Sensitized Solar Cell Performance. *RSC Adv.* **2013**, *3*, 15626.
- (2) Homnick, P. J.; Lahti, P. M. Modular Electron Donor Group Tuning of Frontier Energy Levels in Diarylamino-fluorenone Push-Pull Molecules. *Phys. Chem. Chem. Phys.* **2012**, 11961–11968.
- (3) Homnick, P. J.; Tinkham, J. S.; Devaughn, R.; Lahti, P. M. Engineering Frontier Energy Levels in Donor-Acceptor Fluorene-9-Ylidene Malononitriles versus Fluorenones. *J. Phys. Chem. A* **2014**, *118*, 475–486.
- (4) Homnick, P. J.; Tinkham, J. S.; Lahti, P. M. Radical Cations from Diarylamino-Substituted Fluorenones. *Tetrahedron Lett.* **2013**, *54*, 35–39.
- (5) dye-sensitized-solar-cells.com <http://dye-sensitized-solar-cells.com/new-record-efficiency-for-dye-sensitized-solar-cells/#more-619> (accessed Jul 3, 2014).
- (6) Grätzel, M. Recent Advances in Sensitized Mesoscopic Solar Cells. *Acc. Chem. Res.* **2009**, *42*, 1788–1798.
- (7) National Center for Photovoltaics Home Page <http://www.nrel.gov/ncpv> (accessed Mar 13, 2014).
- (8) Hagfeldt, A.; Boschloo, G.; Sun, L.; Kloo, L.; Pettersson, H. Dye-Sensitized Solar Cells. *Chem. Rev.* **2010**, *110*, 6595–6663.
- (9) Hardin, B. E.; Snaith, H. J.; McGehee, M. D. The Renaissance of Dye-Sensitized Solar Cells. *Nat. Photonics* **2012**, *6*, 162–169.
- (10) Hardin, B. E.; Hoke, E. T.; Armstrong, P. B.; Yum, J.-H.; Comte, P.; Torres, T.; Fréchet, J. M. J.; Nazeeruddin, M. K.; Grätzel, M.; McGehee, M. D. Increased Light Harvesting in Dye-Sensitized Solar Cells with Energy Relay Dyes. *Nat. Photonics* **2009**, *3*, 406–411.
- (11) Yum, J.-H.; Hardin, B. E.; Moon, S.-J.; Baranoff, E.; Nüesch, F.; McGehee, M. D.; Grätzel, M.; Nazeeruddin, M. K. Panchromatic Response in Solid-State Dye-Sensitized Solar Cells Containing Phosphorescent Energy Relay Dyes. *Angew. Chemie Int. Ed.* **2009**, *48*, 9277–9280.
- (12) Shankar, K.; Feng, X.; Grimes, C. A. Enhanced Harvesting of Red Photons in Nanowire Solar Cells: Evidence of Resonance Energy Transfer. *ACS Nano* **2009**, *3*, 788–794.
- (13) Etgar, L.; Park, J.; Barolo, C.; Lesnyak, V.; Panda, S. K.; Quagliotto, P.; Hickey, S. G.; Nazeeruddin, M. K.; Eychmüller, A.; Viscardi, G.; *et al.* Enhancing the Efficiency of a Dye Sensitized Solar Cell due to the Energy Transfer between CdSe Quantum Dots and a Designed Squaraine Dye. *RSC Adv.* **2012**, *2*, 2748–2752.

- (14) Snaith, H. J. Estimating the Maximum Attainable Efficiency in Dye-Sensitized Solar Cells. *Adv. Funct. Mater.* **2010**, *20*, 13–19.
- (15) Boschloo, G.; Häggman, L.; Hagfeldt, A. Quantification of the Effect of 4-Tert-Butylpyridine Addition to I⁻/I₃⁻ Redox Electrolytes in Dye-Sensitized Nanostructured TiO₂ Solar Cells. *J. Phys. Chem. B* **2006**, *110*, 13144–13150.
- (16) Nazeeruddin, M. K.; Kay, A.; Rodicio, I.; Humphry-Baker, R.; Mueller, E.; Liska, P.; Vlachopoulos, N.; Graetzel, M. Conversion of Light to Electricity by Cis-X₂bis(2,2'-Bipyridyl-4,4'-dicarboxylate)ruthenium(II) Charge-Transfer Sensitizers (X = Cl⁻, Br⁻, I⁻, CN⁻, and SCN⁻) on Nanocrystalline Titanium Dioxide Electrodes. *J. Am. Chem. Soc.* **1993**, *115*, 6382–6390.
- (17) Daeneke, T.; Kwon, T.-H.; Holmes, A. B.; Duffy, N. W.; Bach, U.; Spiccia, L. High-Efficiency Dye-Sensitized Solar Cells with Ferrocene-Based Electrolytes. *Nat. Chem.* **2011**, *3*, 211–215.
- (18) Wang, P.; Zakeeruddin, S. M.; Moser, J. E.; Nazeeruddin, M. K.; Sekiguchi, T.; Grätzel, M. A Stable Quasi-Solid-State Dye-Sensitized Solar Cell with an Amphiphilic Ruthenium Sensitizer and Polymer Gel Electrolyte. *Nat. Mater.* **2003**, *2*, 402–407.
- (19) Kim, Y.-G.; Walker, J.; Samuelson, L. a.; Kumar, J. Efficient Light Harvesting Polymers for Nanocrystalline TiO₂ Photovoltaic Cells †. *Nano Lett.* **2003**, *3*, 523–525.
- (20) Cardona, C. M.; Li, W.; Kaifer, A. E.; Stockdale, D.; Bazan, G. C. Electrochemical Considerations for Determining Absolute Frontier Orbital Energy Levels of Conjugated Polymers for Solar Cell Applications. *Adv. Mater.* **2011**, *23*, 2367–2371.
- (21) Johansson, T.; Mammo, W.; Svensson, M.; Andersson, M. R.; Inganas, O. Electrochemical Bandgaps of Substituted Polythiophenes. *J. Mater. Chem.* **2003**, *13*, 1316.
- (22) Wang, M.; Chamberland, N.; Breau, L.; Moser, J.-E.; Humphry-Baker, R.; Marsan, B.; Zakeeruddin, S. M.; Grätzel, M. An Organic Redox Electrolyte to Rival Triiodide/iodide in Dye-Sensitized Solar Cells. *Nat. Chem.* **2010**, *2*, 385–389.

CHAPTER 6

MOLECULAR ENGINEERING OF SQUARINE-BASED DONOR-ACCEPTOR COMPOUNDS FOR ORGANIC PHOTOVOLTAIC DEVICES

Adapted with permission from Della Pelle, A. M.; Homnick, P. J.; Bae, Y.; Lahti, P. M.; Thayumanavan, S. Effect of Substituents on Optical Properties and Charge-Carrier Polarity of Squaraine Dyes. *J. Phys. Chem. C*. **2014**, *118*, 1793-1799.¹ Copyright 2014 American Chemical Society. <http://pubs.acs.org/doi/abs/10.1021/jp410362d>

6.1 Introduction

This chapter summarizes my part of a collaborative project with Dr. Andrea Della Pelle and Youngju Bae from Professor Sankaran Thayumanavan's group, and Dr. Supravat Karak as part of the Energy Frontier Research Center at UMass. In collaboration with the Thayumanavan group, I synthesized one of a series of five squaraine triarylamine dyes with a range of electron donating (-OH, -C₆H₁₃), electron "neutral" (-H), and electron withdrawing (-F, -CF₃) groups on the amine's peripheral aryl groups. Due to the donor-acceptor (D-A) nature of these dyes, their absorption spectra track varying electron donating character of the triarylamine donor module.²⁻⁵ All dyes in the series exhibited an intramolecular charge transfer (ICT) absorption band with high molar absorptivity around $\epsilon = 10^4 - 10^5 \text{ M}^{-1}\text{cm}^{-1}$ at low energy with $\lambda_{\text{max}} = 660 - 690 \text{ nm}$ (1.88 - 1.80 eV). Due to the central intramolecular hydrogen bonding architecture, absorption spectra are also dependent on solvent polarity and hydrogen bonding potential, giving insight into the importance of π -coplanarity in these materials. The general structure and molecular design rationale for these materials is exemplified in Figure 6.1.

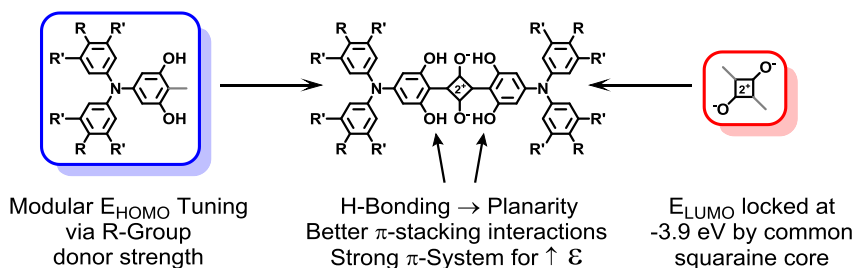


Figure 6.1: General molecular design strategy for the squaraine-based materials in this chapter, using a systematic modular synthetic approach for FMO energy tuning.

My synthetic contribution was the OH-functionalized dye (SQ-OH, R = OH, R' = H), which has the lowest band gap dye in the series due to the strong electron donor OH substitution compared to the other dyes. Solution and neat solid absorption spectra onsets for SQ-OH occurred at 799 nm (1.55 eV) and 866 nm (1.43 eV) respectively, and the neat films absorb broadly throughout the visible spectrum from 540 – 866 nm (2.30 – 1.43 eV). The SQ-OH LUMO energy (E_{LUMO}) was -3.9 eV based on electrochemical placement of the HOMO energy plus the optical band onset energy. This is considered an ideal E_{LUMO} for the typical organic photovoltaic device (OPV) configuration using PC₇₁BM as the n-type material (as discussed in Chapter 1).

In addition to these encouraging results, all dyes in the series exhibited modest solid state charge carrier mobilities in a thin film field effect transistor (FET) configuration, as described in *J. Phys. Chem. C*.¹ Dr. Della Pelle performed most of the FET mobility testing.

6.2 Background

Triarylamine and alkylamine squaraine-based compounds have recently become popular as p-type OPV active layer materials due to their typical low band gaps, high molar absorptivities, convenient synthetic accessibility, and low-lying HOMO and LUMO energies.⁶⁻¹⁶ These characteristics are ideal for OPVs, and reported PCEs are typically good: from around 4-5%^{6,7,9,15-18} to just over 6%.¹⁴ But, PCEs can also be quite low for squaraine-based materials (below 2%^{13,19-23}) and many of the higher-performance solar cells required considerable optimization efforts. As a result, there is much molecular engineering work being done on these promising materials.

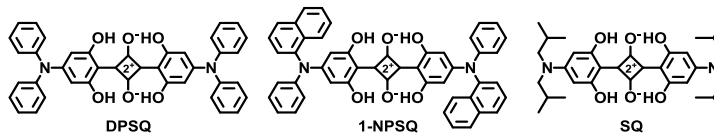


Figure 6.2: Forrest's amino squaraines used throughout the literature.^{7,15,16}

Due to the importance of intermolecular interactions and frontier molecular orbital (FMO) energy tuning in OPV materials, a synthetic strategy similar to that in Chapters 2 and 3 was used^{4,5} for systematically tuning the squaraine dye E_{HOMO} using a triarylamine-based model structure described by Forrest and coworkers (Figure 6.2, DPSQ).^{7,15,16} The UMass molecular development approach was specifically designed to allow a broad range of optoelectronic and electrochemical tunability.

6.3 Results and Discussion

6.3.1 Molecular Design and Synthetic Procedure

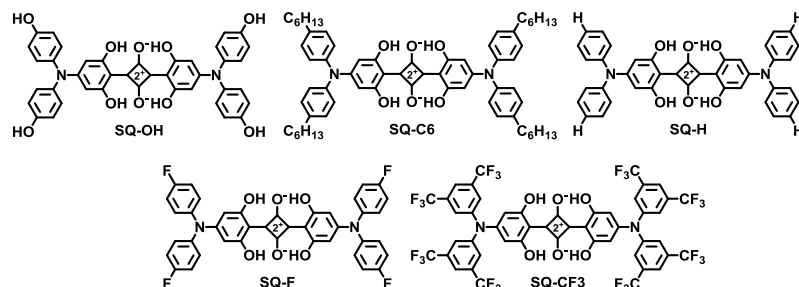


Figure 6.3 Molecular design of squaraine dyes with tunable bandgaps and HOMO energy levels. SQ-H is the control molecule for reference to Forrest's DPSQ. SQ-C6 and SQ-OH are squaraine dyes with increasing electron donor strength. SQ-F and SQ-CF3 are squaraine dyes with increasing electron withdrawing strength.

Using SQ-H as the control compound for literature comparison, a series of five squaraine dyes was synthesized as shown in Figure 6.3. In a manner analogous to the discussions in Chapters 2-3, Figure 6.4 depicts the expected E_{HOMO} trend for the substituted bis(triarylamino)squaraines.

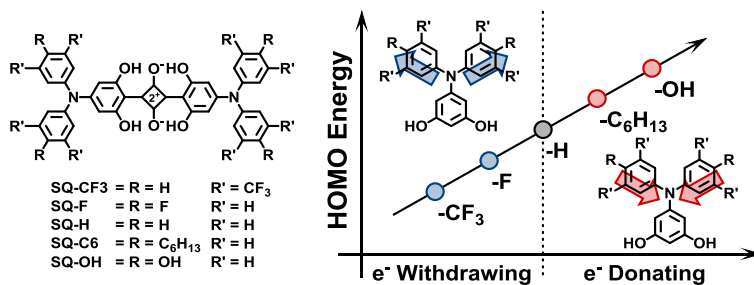


Figure 6.4: Expected HOMO energy trend based on electron donating/withdrawing triarylamine substituents. The stronger the electron donor, the higher the E_{HOMO} .

Synthesis of SQ-OH was relatively straightforward (Figure 6.5), starting with triarylamine donor module synthesis using Buchwald-Hartwig or Ullmann amination conditions in modest to good yield. The methoxy groups were then deprotected with boron tribromide in quantitative yield, and then condensed with squaric acid in modest to good yield to form the final squaraine dyes. This final step is simple, and the final compound typically precipitates from the reaction mixture as a pure and very darkly colored solid with no subsequent purification steps necessary (aside from washing away high boiling solvent with low boiling solvent). The synthetic procedures for all of the squaraines, including those synthesized by Dr. Della Pelle and Youngju Bae, are reported in *J. Phys. Chem. C*.¹

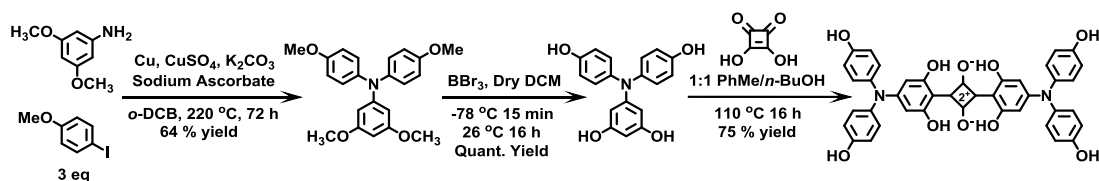


Figure 6.5 Representative example for SQ-OH synthesis. Other dyes were synthesized by Dr. Della Pelle and Youngju Bae as reported in *J. Phys. Chem. C*.¹

6.3.2 Optoelectronic Properties

SQ-OH, like the other squaraine dyes in this study, absorbs *broadly* throughout the orange-NIR region of the spectrum, at 540 – 866 nm, or 2.30 – 1.43 eV (Figure 6.6). Because the typical n-type BHJ material PC₇₁BM absorbs throughout the UV-mid-visible region, these materials are *spectroscopically* a good complementary match.

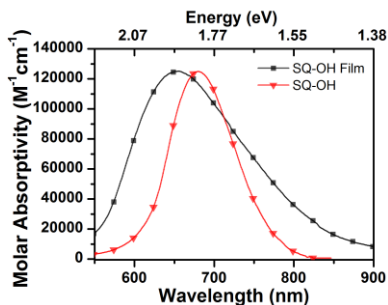


Figure 6.6: SQ-OH DCM solution (red) and neat thin film (black) UV-vis absorption spectra. Film absorption intensity normalized to DCM solution molar absorptivity.

The central hydroxyl groups on the triarylamine donor modules play an essential role, since they are hydrogen bonded with the squarylium oxygens, resulting in the planarization of the molecules' cores. To test the importance of this hydrogen bonding, the compounds were dissolved in chloroform (CHCl_3) and titrated with increasing amounts of dimethylsulfoxide (DMSO), a highly polar, hydrogen bond-accepting solvent. In neat DMSO, the compounds' low band gap ICT bands were very strongly diminished or completely quenched with concomitant emergence of a higher energy absorption band more reminiscent of a non- or weaker-push-pull triarylamine (Figure 6.7). This is presumably due to squarylium-triarylamine out-of-plane twisting, which interrupts the D-A-D π -conjugation and thereby increases the excitation energy gap.¹

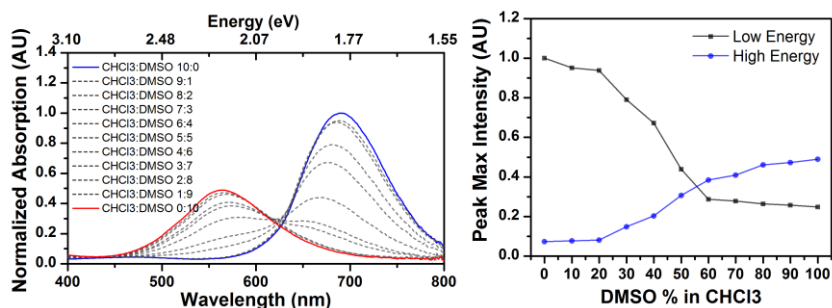


Figure 6.7: Left, Titration spectra for SQ-OH in 0-100% DMSO in CHCl_3 , normalized to 100% CHCl_3 . Right, titration curves compiled from the lower energy versus higher energy transition strengths using the normalized transition intensities from the titration spectra.

6.3.3 Electrochemical Properties

Figure 6.8 depicts compares the SQ-OH FMO energy along with those of the other squaraine dyes and the typical BHJ n-type material PC_{71}BM . FMO energies were calculated from the cyclic voltammetric redox potentials (performed by Dr. Della Pelle), except for SQ-CF₃ whose E_{HOMO} was determined by subtracting the optical band gap energy from E_{LUMO} . In good accord with the initial hypothesis, LUMO energies were essentially locked in by the squarylium core around -3.9 eV while the HOMO energies increased with the triarylamine substituents' increasing electron donor strengths. These electrochemical results agree with the absorption spectra red shifts observed when going from strongly electron withdrawing to strongly electron

donating triarylamine substituents. Most importantly, these data in combination with the optoelectronic properties show that the squaraine-triarylamine molecular design approach with tunable triarylamine is a useful molecular development model for varying the compounds' redox properties.

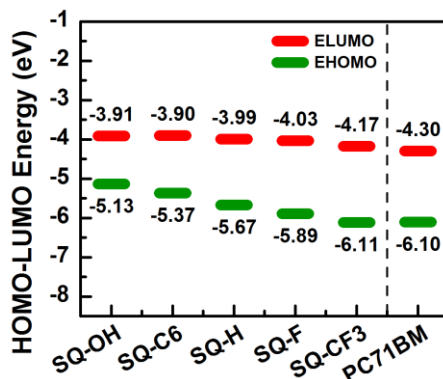


Figure 6.8: FMO energies for SQ-compounds compared to PC₇₁BM. SQ-compound FMO energies obtained using cyclic voltammetric redox potentials. SQ-CF₃ E_{HOMO} was calculated by subtracting the solution phase optical band gap from E_{LUMO}.

6.4 Summary of Squaraine Dye Physical Chemistry

The D-A-D squaraine dyes – including the SQ-OH system primarily described in this chapter – were specifically designed to have low band gaps, low-lying LUMO energies, strong molar absorptivities, and straightforward synthetic accessibility. All of the dyes absorbed well into the red-NIR region of the solar spectrum with high molar absorptivities on the order of 10^4 – 10^5 M⁻¹cm⁻¹. Neat thin film absorption spectra are broad, covering the low energy region of the visible-NIR spectrum from 540 – 866 nm (2.30 – 1.43 eV). LUMO energies were locked at about 3.9 eV while HOMO energies were systematically tunable in good accord with triarylamine donor strength.

These physical chemical properties are very promising for OPV device testing, and serve as a useful proof-of-principle molecular design model for future materials. Due to its lowest band gap out of the five compounds in the series, SQ-OH was tested as the p-type active layer in solution processed BHJ solar cells by Dr. Supravat Karak, as part of the UMass Energy Frontier

Research Center's materials design and device optimization research efforts. The PCEs for SQ-OH-based devices were as high as 4.8%,²⁴ a competitive value for squaraine-based OPVs,⁶⁻¹⁶ suggesting that this design strategy is quite promising. These results are described in the next section.

6.5 SQ-OH:PC₇₁BM BHJ Solar Cell Results

Due to the fact that SQ-OH has the most ideal band gap throughout the SQ series, it was the first to be tested as a p-type OPV active layer. Dr. Karak fabricated the devices using a typical configuration: transparent indium tin oxide (ITO) anode on glass, poly(ethylenedioxythiophene):poly(styrenesulfonate) (PEDOT:PSS) electron blocking layer, SQ-OH:PC₇₁BM active layer, lithium fluoride (LiF) hole blocking layer, and aluminum (Al) cathode (Figure 6.9). At the time of this writing, these results are being prepared for submission.²⁴

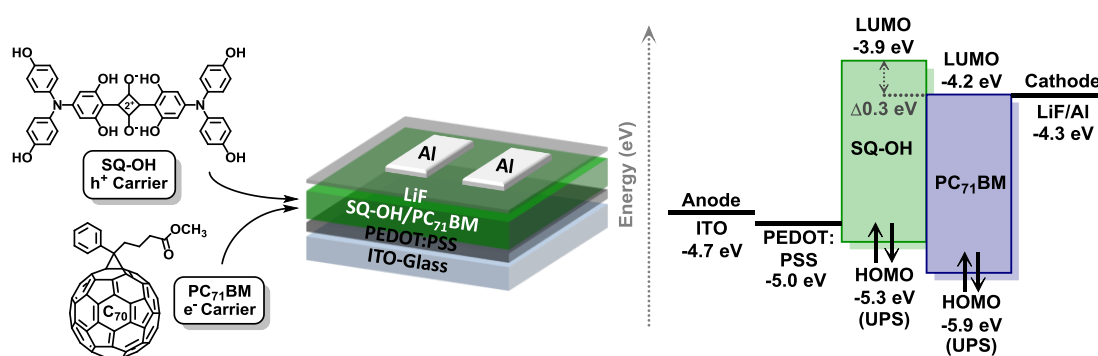


Figure 6.9: Left, SQ-OH:PC₇₁BM device configuration, using ITO anode, PEDOT:PSS electron blocking layer, LiF hole blocking layer, and Al cathode. Right, energy level diagram for SQ-OH device components. Neat thin film SQ-OH and PC₇₁BM E_{HOMO} determined by Professor Volodymyr Duzhko using ultraviolet photoelectron spectroscopy (UPS).

Although a detailed discussion of the device engineering and characterization processes are outside the scope of this chapter, it is useful to discuss them briefly because they provide insight into some of the *bulk material* properties of this new squaraine *compound*. First, because these devices were solution-processed via spin-coating, both SQ-OH and PC₇₁BM had to be soluble in the processing medium. A typical solvent for PC₇₁BM is chlorobenzene (CB), but SQ-

OH is poorly soluble in this medium. While a better solvent for SQ-OH is the more polar solvent tetrahydrofuran (THF), PC₇₁BM is poorly soluble in THF. To avoid wasteful and time consuming testing of a broad range of solvents to find one compatible with both materials, Dr. Karak utilized a THF/CB mixture that fortunately dissolved both components sufficiently for spin-coating. The optimized THF:CB ratio used for all subsequent SQ-OH-based OPV devices was 3:7 THF:CB.

Squaraine materials in the literature tend to have a relatively short exciton diffusion length, as low as 4.5 nm, in contrast to PC₆₀BM's exciton diffusion length of approximately 23 nm.¹⁸ One way to increase the exciton diffusion length is by thermal or solvent vapor annealing, which works well to improve squaraine-based OPV PCE.^{6,7,10,15,16} Even with better nanophase crystallinity, the exciton diffusion length is still shorter than fullerene-based n-type materials, so devices using a squaraine-fullerene blend require a low squaraine:fullerene weight ratio.

^{6,7,10,15,16,18} Dr. Karak's device optimization process is consistent with these observations, requiring a 1:5 SQ-OH:PC₇₁BM weight ratio to obtain 0.63% PCE, the best out of the other ratios tested (0.21%, 0.43%, and 0.32% PCE using 1:1, 1:3, and 1:7 weight ratios, respectively). This 0.63% PCE was obtained using neat THF as the processing solvent, but using the optimized 3:7 THF/CB solvent blend increased PCE considerably to 2.44%.

Before doing any additional annealing techniques or using any special solvent additives, 2.44% PCE is already better than many of the optimized squaraine-based devices in the literature.^{13,19-23} Due to the fact that crystallinity and nanoscale morphology are so important for exciton and charge transport in bulk organic materials, thermal and/or solvent vapor annealing are useful techniques for improving nanodomain size and crystallinity. Similar to solvent annealing, using a high-boiling solvent additive that selectively dissolves one of the p- or n-type active layer materials is a useful method of manipulating the crystallinity and nanodomain size scales of just one of the p/n components.

A typical additive for this purpose is 1,8-diiodo-*n*-octane (DIO), which tends to selectively dissolve PC₇₁BM versus most p-type materials. Thus, using DIO as a processing solvent additive typically has the effect of increasing fullerene domain crystallinity and allowing for better control over the n-type material phase and overall device nanomorphology. Dr. Karak tested DIO as a solution processing solvent additive, which increased device PCE to 3.74% from 2.44% using just 0.5% DIO by volume in 3:7 THF/CB. Subsequent thermal annealing at 130 °C for 10 minutes further increased PCE to 4.44% on average, and to 4.8% for the single best device (Figure 6.10).

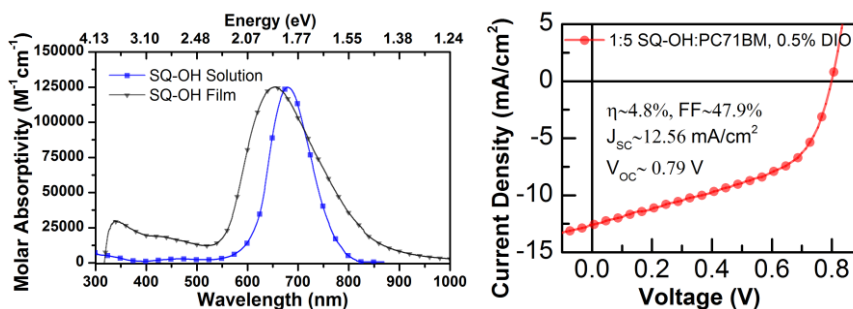


Figure 6.10: SQ-OH solution vs. neat thin film absorption spectra (left) and current density versus voltage curve for BHJ solar cells using 1:5 SQ-OH:PC₇₁BM and 0.5% diiodooctane additive.

Electronic properties for optimized SQ-OH:PC₇₁BM OPVs are shown in Figure 6.10. Using a device configuration consisting of ITO/PEDOT:PSS/SQ-OH:PC₇₁BM/LiF/Al, a maximum PCE of 4.8% was obtained with V_{oc} = 0.84 – 0.86 V, J_{sc} = 10 mA/cm², and FF = 0.53. This final PCE is well within the upper echelon of squaraine-based OPV devices in the literature.^{6,7,9,15–18} Although outside the scope of this discussion, much additional device characterization was performed by Dr. Feng Liu from Professor Thomas Russell’s research group. These results consist of some detailed morphological studies using several advanced light source x-ray diffraction techniques, and are reported in detail in the manuscript submitted for publication.

6.6 Conclusions

SQ-OH is a promising variant of the low band gap, high molar absorptivity family of squaraine-based p-type OPV materials. Solution-processed BHJ type solar cells using SQ-OH and PC₇₁BM spin-cast from a 3:7 mixed tetrahydrofuran/chlorobenzene solvent system containing 0.5% diiodooctane exhibited a reproducible average efficiency of 4.4% with a top PCE of 4.8%. This is a competitive value among the squaraine-based OPV materials in the literature, especially since device engineering strategies and material preparation/purification efforts were not as intensive as those reported elsewhere.^{6,7,9,14-18} Final optimized device PCEs are sevenfold higher than for devices fabricated using the initial testing conditions using just THF as the processing solvent with no active layer p/n ratio optimization, annealing, or solvent additives. These latter device engineering techniques are cheap, simple to use, and are scalable to an industrial production setting. So, even though much more work needs to be done in this area, these SQ-OH-based devices can serve as promising model systems for the continuing advancement of OPV device technology. Most importantly, this work represents the synergistic power of collaborative efforts among synthetic and physical organic chemists, device fabrication engineers, and device characterization physicists. The organic photovoltaics field is progressing forward in great strides, and collaborative interdisciplinary relationships are a major part of this advancement. Because new materials design is at the foundation of this technology, and these materials may serve as useful molecular design models for future materials. Chapter 8 discusses some of the future directions this work may lead, from a molecular engineering perspective.

6.7 References

- (1) Della Pelle, A. M.; Homnick, P. J.; Bae, Y.; Lahti, P. M.; Thayumanavan, S. Effect of Substituents on Optical Properties and Charge-Carrier Polarity of Squaraine Dyes. *J. Phys. Chem. C* **2014**, *118*, 1793–1799.
- (2) Zhang, Z.; Wang, J. Structures and Properties of Conjugated Donor–Acceptor Copolymers for Solar Cell Applications. *J. Mater. Chem.* **2012**, *22*, 4178–4187.
- (3) Cheng, Y.-J.; Yang, S.-H.; Hsu, C.-S. Synthesis of Conjugated Polymers for Organic Solar Cell Applications. *Chem. Rev.* **2009**, *109*, 5868–5923.
- (4) Homnick, P. J.; Lahti, P. M. Modular Electron Donor Group Tuning of Frontier Energy Levels in Diarylamino-fluorenone Push-Pull Molecules. *Phys. Chem. Chem. Phys.* **2012**, *14*, 11961–11968.
- (5) Homnick, P. J.; Tinkham, J. S.; Devaughn, R.; Lahti, P. M. Engineering Frontier Energy Levels in Donor-Acceptor Fluorene-9-Ylidene Malononitriles versus Fluorenones. *J. Phys. Chem. A* **2014**, *118*, 475–486.
- (6) Wei, G.; Lunt, R. R.; Sun, K.; Wang, S.; Thompson, M. E.; Forrest, S. R. Efficient, Ordered Bulk Heterojunction Nanocrystalline Solar Cells by Annealing of Ultrathin Squaraine Thin Films. *Nano Lett.* **2010**, *10*, 3555–3559.
- (7) Wei, G.; Xiao, X.; Wang, S.; Zimmerman, J. D.; Sun, K.; Diev, V. V.; Thompson, M. E.; Forrest, S. R. Arylamine-Based Squaraine Donors for Use in Organic Solar Cells. *Nano Lett.* **2011**, *11*, 4261–4264.
- (8) Wang, S.; Hall, L.; Diev, V. V.; Haiges, R.; Wei, G.; Xiao, X.; Djurovich, P. I.; Forrest, S. R.; Thompson, M. E. N,N-Diarylanilinosquaraines and Their Application to Organic Photovoltaics. *Chem. Mater.* **2011**, *23*, 4789–4798.
- (9) Zimmerman, J. D.; Lassiter, B. E.; Xiao, X.; Sun, K.; Dolocan, A.; Gearba, R.; Vanden Bout, D. A.; Stevenson, K. J.; Wickramasinghe, P.; Thompson, M. E.; *et al.* Control of Interface Order by Inverse Quasi-Epitaxial Growth of Squaraine/Fullerene Thin Film Photovoltaics. *ACS Nano* **2013**, *7*, 9268–9275.
- (10) Guan, Z.; Yu, J.; Huang, J.; Zhang, L. Power Efficiency Enhancement of Solution-Processed Small-Molecule Solar Cells Based on Squaraine via Thermal Annealing and Solvent Additive Methods. *Sol. Energy Mater. Sol. Cells* **2013**, *109*, 262–269.
- (11) Cho, Y. J.; Lee, J. Y.; Chin, B. D.; Forrest, S. R. Polymer Bulk Heterojunction Photovoltaics Employing a Squaraine Donor Additive. *Org. Electron.* **2013**, *14*, 1081–1085.
- (12) Silvestri, F.; Irwin, M. D.; Beverina, L.; Facchetti, A.; Pagani, G. A.; Marks, T. J. Efficient Squaraine-Based Solution Processable Bulk-Heterojunction Solar Cells. *J. Am. Chem. Soc.* **2008**, *130*, 17640–17641.

- (13) Völker, S. F.; Uemura, S.; Limpinsel, M.; Mingebach, M.; Deibel, C.; Dyakonov, V.; Lambert, C. Polymeric Squaraine Dyes as Electron Donors in Bulk Heterojunction Solar Cells. *Macromol. Chem. Phys.* **2010**, *211*, 1098–1108.
- (14) Chen, G.; Sasabe, H.; Wang, Z.; Wang, X.-F.; Hong, Z.; Yang, Y.; Kido, J. Co-Evaporated Bulk Heterojunction Solar Cells with >6.0% Efficiency. *Adv. Mater.* **2012**, *24*, 2768–2773.
- (15) Wei, G.; Xiao, X.; Wang, S.; Sun, K.; Bergemann, K. J.; Thompson, M. E.; Forrest, S. R. Functionalized Squaraine Donors for Nanocrystalline Organic Photovoltaics. *ACS Nano* **2012**, *6*, 972–978.
- (16) Xiao, X.; Wei, G.; Wang, S.; Zimmerman, J. D.; Renshaw, C. K.; Thompson, M. E.; Forrest, S. R. Small-Molecule Photovoltaics Based on Functionalized Squaraine Donor Blends. *Adv. Mater.* **2012**, *24*, 1956–1960.
- (17) Wei, G.; Wang, S.; Sun, K.; Thompson, M. E.; Forrest, S. R. Solvent-Annealed Crystalline Squaraine: PC70BM (1:6) Solar Cells. *Adv. Energy Mater.* **2011**, *1*, 184–187.
- (18) Chen, G.; Yokoyama, D.; Sasabe, H.; Hong, Z.; Yang, Y.; Kido, J. Optical and Electrical Properties of a Squaraine Dye in Photovoltaic Cells. *Appl. Phys. Lett.* **2012**, *101*, -.
- (19) Ananda Rao, B.; Yesudas, K.; Siva Kumar, G.; Bhanuprakash, K.; Jayathirtha Rao, V.; Sharma, G. D.; Singh, S. P. Application of Solution Processable Squaraine Dyes as Electron Donors for Organic Bulk-Heterojunction Solar Cells. *Photochem. Photobiol. Sci.* **2013**, *12*, 1688–1699.
- (20) Yang, D.; Guan, Z.; Yang, L.; Huang, Y.; Wei, Q.; Lu, Z.; Yu, J. Novel High-Performance Photovoltaic D–A Conjugated Polymers Bearing 1,2-Squaraine Moieties as Electron-Deficient Units. *Sol. Energy Mater. Sol. Cells* **2012**, *105*, 220–228.
- (21) Maeda, T.; Tsukamoto, T.; Seto, A.; Yagi, S.; Nakazumi, H. Synthesis and Characterization of Squaraine-Based Conjugated Polymers With Phenylene Linkers for Bulk Heterojunction Solar Cells. *Macromol. Chem. Phys.* **2012**, *213*, 2590–2597.
- (22) Kylberg, W.; Zhang, Y.; Aebersold, A.; de Castro, F. A.; Geiger, T.; Heier, J.; Kuster, S.; Ma, C.-Q.; Bäuerle, P.; Nüesch, F.; *et al.* Oligothiophene Dendron-Decorated Squaraine Dyes: Synthesis, Thin Film Formation, and Performance in Organic Solar Cells. *Org. Electron.* **2012**, *13*, 1204–1212.
- (23) So, S.; Choi, H.; Ko, H. M.; Kim, C.; Paek, S.; Cho, N.; Song, K.; Lee, J. K.; Ko, J. Novel Unsymmetrical Push–pull Squaraine Chromophores for Solution Processed Small Molecule Bulk Heterojunction Solar Cells. *Sol. Energy Mater. Sol. Cells* **2012**, *98*, 224–232.

- (24) Karak, S.; Homnick, P. J.; Della Pelle, A. M.; Bae, Y.; Duzhko, V.; Liu, F.; Russell, T. P.; Lahti, P. M.; Thayumanavan, S. Morphological Size Scale Correlations with Performance in Solvent-Processed Solar Cells with a Triarylamine Substituted Squaraine. *Manuscr. Prep.* **2014.**

CHAPTER 7

ORGANIC PHOTOVOLTAIC DEVICES USING FMBDAA36 AS A MOLECULAR LOW BAND GAP HOLE TRANSPORTING MATERIAL

7.1 Introduction

This chapter summarizes organic photovoltaic (OPV) device results obtained by Dr. Supravat Karak as part of the Energy Frontier Research Center (EFRC) at UMass, using the low band gap small molecule FMBDAA36 described in Chapter 3¹ (Figure 7.1). FMBDAA36 was tested as an OPV device p-type material due to its promising optoelectronic and electrochemical properties. FMBDAA36's optical band gap in the solid state is approximately 1.6 eV, with $E_{\text{HOMO}} = -5.2$ eV (determined by Professor Volodymyr Duzhko using ultraviolet photoelectron spectroscopy, UPS) and $E_{\text{LUMO}} = -3.6$ eV = $E_{\text{HOMO}} +$ (optical band gap). These FMO energies are close to the ideal values (-5.4 eV and -3.9 eV, respectively) desired for organic photovoltaics when using PC₇₁BM as the n-type active layer component. With this configuration, OPV devices would have a good maximum theoretical voltage of 1.0 V.

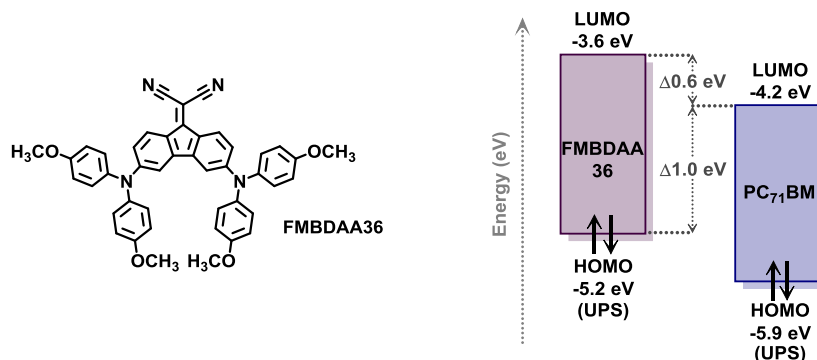


Figure 7.1: FMO energies for FMBDAA36 and PC₇₁BM. LUMO-LUMO offset is 0.6 eV, and maximum theoretical device voltage is 1.0 V based on FMBDAA36 E_{HOMO} to PC₇₁BM E_{LUMO} difference of 1.0 eV. HOMO energies were determined by Professor Volodymyr Duzhko using UPS.

FMBDAA36's optoelectronic properties are also quite promising. FMBDAA36 absorbs strongly throughout much of the visible spectrum, from approximately 400 – 700 nm (3.1 – 1.8 eV) with two λ_{max} at approximately 475 nm (2.61 eV, $\epsilon = 10,000$ M⁻¹cm⁻¹) and 600 nm (2.07 eV, ϵ

= 5,010 M⁻¹cm⁻¹) in acetonitrile (Figure 7.2, left). As a neat thin film, FMBDAA36 absorbs over 400 – 750 nm (3.1 – 1.6 eV) with λ_{max} at approximately 500 nm (2.48 eV) and 625 nm (1.99 eV). Due to this broad absorption profile and strong molar absorptivity, FMBDAA36 looks very dark purple, almost black, to the naked eye as a neat film. PC₇₁BM also absorbs strongly in this region of the visible spectrum, most importantly where FMBDAA36's absorption is weaker at approximately 400 nm and 575 nm). When FMBDAA36 and PC₇₁BM are blended as thin films, their collective absorption is nearly panchromatic over 400 – 750 nm (Figure 7.2, right).

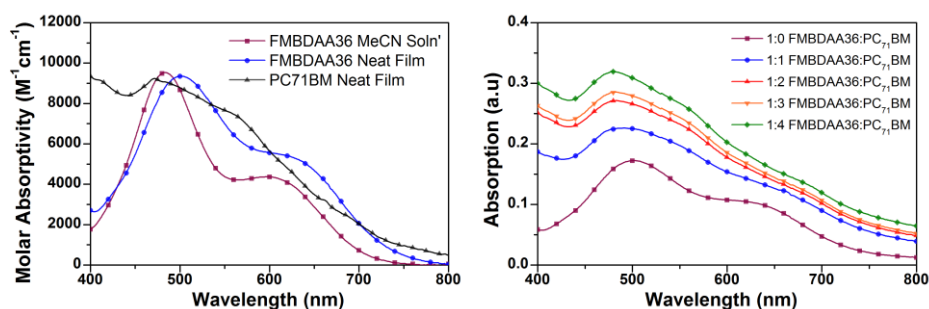


Figure 7.2: FMBDAA36 and PC₇₁BM UV-vis absorption spectra (left). UV-vis absorption spectra for thin film mixtures of FMBDAA36 and PC₇₁BM (right). Thin film UV-vis spectra obtained by Dr. Karak.

Recently, Chi and coworkers² showed that a close variant of FMBDAA36 (with methyl instead of methoxy groups, Figure 7.3) gives promising solid state photocurrent transport and photoconversion efficiencies, with their best single-junction OPV device (using C₇₀ as an electron acceptor material) having a PCE of 4.04% with V_{OC} (open-circuit voltage) = 0.99 V, J_{SC} (short circuit current) = 7.64 mA/cm², and FF (fill factor) = 0.53. Also recently, Andrew and Bulovic³ synthesized some dicyanofulvalenes (e.g. DCF1 Figure 7.3) for use as a PC₆₁BM supplement for poly(3-hexylthiophene)- (P3HT)-based OPV devices. Bulovic's compounds are interesting because they are constructed from a cyclopentadienyliidene core like the fluorenone- and fluorenyliidene malononitrile-based compounds discussed in Chapters 2-3. DCF1 was able to replace up to 50% of the PC₆₁BM in 1:1 P3HT:PC₆₁BM devices, increasing PCE by approximately 55% from 2.9% in P3HT:PC₆₁BM control devices to 4.5% in

P3HT:DCF1/PC₆₁BM devices. These results further encouraged us to test FMBDAA36 as a p-type active layer material with PC₇₁BM.

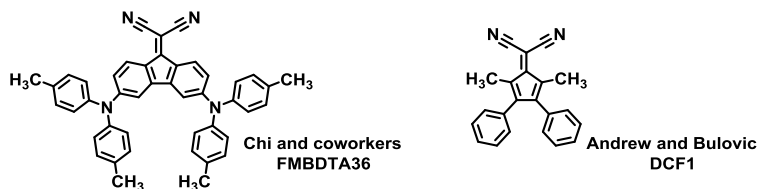


Figure 7.3: Bis-cyanofulvalene analogues of FMBDAA36 used in OPV devices.^{2,3}

7.2 Results and Discussion – FMBDAA36:PC₇₁BM BHJ Solar Cells

Although a detailed discussion of Dr. Karak's solution-processed BHJ device engineering and characterization processes using FMBDAA36 are outside the scope of this chapter, a basic description of the device fabrication is given here. Dr. Karak fabricated FMBDAA36:PC₇₁BM OPV devices by spin-coating from chlorobenzene (CB) onto glass substrates treated with indium tin oxide (ITO) and coated with a poly(ethylenedioxythiophene):poly(styrenesulfonate) (PEDOT:PSS) electron blocking layer. Lithium fluoride (LiF) was then applied as a hole blocking layer, followed by thermal deposition of aluminum (Al) cathodes. The device configuration and energy levels are shown in Figure 7.4.

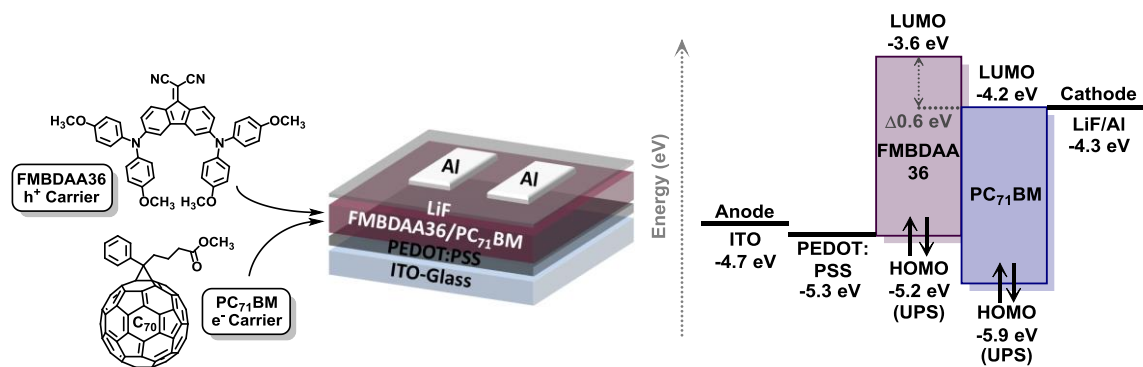


Figure 7.4: Left, FMBDAA36:PC₇₁BM device configuration, using ITO anode, PEDOT:PSS electron blocking layer, LiF hole blocking layer, and Al cathode. Right, energy level diagram for FMBDAA36 device components. Neat thin film FMBDAA36 and PC₇₁BM E_{HOMO} determined by Professor Volodymyr Duzhko using ultraviolet photoelectron spectroscopy (UPS).

After optimizing the FMBDAA36:PC₇₁BM material ratio, Dr. Karak obtained a maximum PCE of 4.1% using 1:3 (w/w) FMBDAA36:PC₇₁BM. Optimized devices gave $J_{SC} = 10.35 \text{ mA/cm}^2$, $V_{OC} = 0.89 \text{ V}$, and $FF = 0.448$ (Figure 7.5 and Table 7.1). This PCE is essentially the same as reported for Chi and coworkers² single junction device PCE of 4.04% with $V_{OC} = 0.99 \text{ V}$, $J_{SC} = 7.64 \text{ mA/cm}^2$, and $FF = 0.53$ using their FMBDTA36 material. Our higher J_{SC} compared to Chi's can be attributed (at least in part) to the fact that FMBDAA36's thin film absorption onset is 1.60 eV while Chi's FMBDTA36's onset is at 1.77 eV. This broader absorption profile may allow the device to collect more photons for photoconversion – in principle, more photoconversion results in higher current. Our V_{OC} is lower than Chi's, despite the similar HOMO energies of the materials (FMBDAA36 is -5.2 eV, FMBDTA36 is -5.25 eV as also determined by photoelectron spectroscopy), although different device fabrication procedures can also effect V_{OC} . Our FF is somewhat lower, but Chi's devices were vacuum-processed while ours were solution-processed so it is difficult to compare this sensitive parameter.

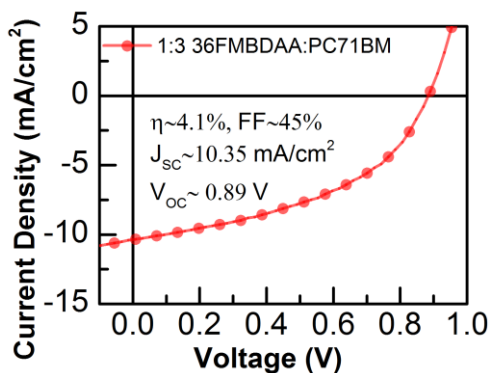


Figure 7.5: Current density versus voltage curve for BHJ solar cells using 1:3 FMBDAA36:PC₇₁BM.

Table 7.1: FMBDAA36:PC₇₁BM ratio optimization and OPV device performance results.

Weight ratio (FMBDAA36:PC ₇₁ BM)	J _{sc} (mA/cm ²)	V _{oc} (V)	FF (%)	η (%)
1:1	7.14	0.86	34.1	2.1
1:2	9.09	0.87	34.2	2.7
1:3	10.35	0.89	44.8	4.1
1:4	4.18	0.90	34.3	1.3

7.3 Conclusions

FMBDAA36 was specifically designed to have a low band gap, low-lying LUMO energy, strong molar absorptivity, and straightforward synthetic accessibility. FMBDAA absorbs broadly throughout the visible spectrum with modest molar absorptivity, and has favorable FMO energies. Due to these promising optoelectronic and electrochemical properties, FMBDAA36 was tested as the p-type active layer in solution processed BHJ solar cells by Dr. Supravat Karak. The PCEs for FMBDAA36-based devices were as high as 4.1%, a good value for a simple molecular material,² suggesting that this design strategy is quite promising. Indeed, FMBDAA36 is a particularly simple molecule in comparison to many small molecule materials being tested for photovoltaics in the literature,⁴ so 4.1% PCE is an encouraging accomplishment. Most importantly, these results show the value of employing the molecular engineering strategies discussed in Chapters 2-3. FMBDAA36 was specifically engineered using a bottom-up physical chemical approach, using simple, synthetically accessible molecular components. Since new materials design is at the foundation of OPV device technology, this material may serve as useful molecular design model for future materials.

7.4 References

- (1) Homnick, P. J.; Tinkham, J. S.; Devaughn, R.; Lahti, P. M. Engineering Frontier Energy Levels in Donor-Acceptor Fluoren-9-Ylidene Malononitriles versus Fluorenones. *J. Phys. Chem. A* **2014**, *118*, 475–486.
- (2) Chi, L.-C.; Chen, H.-F.; Hung, W.-Y.; Hsu, Y.-H.; Feng, P.-C.; Chou, S.-H.; Liu, Y.-H.; Wong, K.-T. Donor-Acceptor Small Molecule with Coplanar and Rigid Π -Bridge for Efficient Organic Solar Cells. *Sol. Energy Mater. Sol. Cells* **2013**, *109*, 33–39.
- (3) Andrew, T. L.; Bulović, V. Bulk Heterojunction Solar Cells Containing 6,6-Dicyanofulvenes as N-Type Additives. *ACS Nano* **2012**, *6*, 4671–4677.
- (4) Sun, Y.; Welch, G. C.; Leong, W. L.; Takacs, C. J.; Bazan, G. C.; Heeger, A. J. Solution-Processed Small-Molecule Solar Cells with 6.7% Efficiency. *Nat. Mater.* **2011**, *11*, 44–48.

CHAPTER 8

FUTURE WORK: π -MACROCYCLES, INDIGO-BASED MATERIALS, AND PANCHROMATIC A-D-A' CHROMOPHORE ENGINEERING

8.1 Introduction

Bottom-up control of molecular electronic properties with simultaneous control over photovoltaic device nanoarchitecture has long been a "grail" of interest in materials chemistry due to its inherent challenge and large application payout.¹ Dramatic improvements in organic bulk heterojunction solar cell efficiency can be realized by enhancing visible spectrum absorption strength and coverage and improving frontier molecular orbital energy alignment, exciton/charge mobility, and p/n-type domain nanoarchitecture.²⁻⁶ Designing new materials that address all of these molecular optimization criteria presents a considerable synthetic challenge; but there are some fundamental molecular design principles that can provide rational synthetic direction.

Absorption characteristics and energy level alignment can be controlled through selective highest occupied and lowest unoccupied molecular orbital energy (E_{HOMO} and E_{LUMO}) engineering as described in Chapters 1-3.²⁻⁵ Absorption strength can be enhanced through direct conjugation effects⁷⁻⁹ as well as by increasing π -conjugation length or optical cross section with large aromatic π -extended chromophores.^{5,10-13} Large aromatic π -systems and hydrogen bonding capability can also impart strong intermolecular interactions like π -stacking and extended hydrogen bonded networks, which can aid in exciton/charge transport throughout the material, and can also assist p-n nanoarchitecture engineering.¹⁴⁻²¹

In addition to enhancing transport and nanoarchitecture properties, strongly self-assembling materials can also increase absorption breadth in the solid state, further enhancing spectral activity. Interdigitated nanoscale domains with good interfacial contact enable efficient exciton dissociation and charge transport to the electrodes in an organic photovoltaic device, and conjugated materials containing triarylamine modules often have modest hole mobility characteristics as p-type materials.^{2-4,6} Given these structure-property design tools, it should be

possible to engineer new high-performance materials using a bottom-up molecular design approach that allows each property to be systematically adjusted in a modular, synthetically efficient way.

This chapter describes three research proposals that integrate the design principles and molecular design strategies discussed in previous chapters. The first proposal describes some preliminary and proposed work on the design and synthesis of large π -macrocycle chromophores. These materials are intended to have FMO energies and self-assembly properties that are tunable over a broad range by manipulating their molecular structure. The second proposal involves the synthesis and hydrogen bond-directed self-assembly of indigo-based compounds. These compounds were specifically designed to be straightforward to synthesize, and to possess a broad range of tunability for testing substituent and connectivity effects on their optoelectronic, electrochemical, charge carrier mobility, and self-assembly properties. Finally, the third proposal describes the design and synthesis of potentially panchromatically absorbing squaraine-based materials using the molecular design principles from Chapters 2, 3, and 6.

8.2 Preliminary and Proposed Development of Fused Aromatic π -Macrocycles as Self-Assembling Push-Pull Chromophores

π -Macrocycle materials are promising targets for OPVs and general organic electronics applications due to their potential supramolecular assembly properties.^{14–19} They can have excellent absorption strength and spectral coverage due to their large π -conjugation system.^{5,10–13} Also, large aromatic systems can impart strong intermolecular π -stacking properties, which can aid in exciton/charge transport throughout the material and assist p-n nanoarchitecture engineering.^{14–19} In addition to these transport and nanoarchitecture properties, strongly self-assembling materials can also have increased absorption breadth and optical density in the solid state, further enhancing spectral activity.

Several new disk-shaped π -macrocycle-cored donor-acceptor molecules were designed that should provide synthetic access to all of these properties, most notably columnar π -stacking

self-assembly and considerable electronic and morphological tunability at each synthetic step. The proposed synthetic route should also provide the opportunity to develop a new set of 2D polymeric covalent organic framework (COF) electronic materials using strategies recently reported in the literature.²²⁻³¹

The ultimate goal of this project is to prepare new high-performance photovoltaic materials by using a modular synthetic approach that integrates each design requirement into individual modular components for systematic molecular property engineering.

8.2.1 Background Information for Truxene- and Heterotriangulene-Based π -Macrocycles

Truxene and truxenone derivatives have seen some use in OLEDs³² and NLO materials.^{33,34} The work done in both fields indicates that these structures are promising candidates for organic electronic materials due to their propensity to form π -stacked networks. Truxenones are particularly interesting due to their large molar extinction coefficients ($\sim 35,000$ - $95,000 \text{ M}^{-1}\text{cm}^{-1}$), multiple reversible redox states, and strong self-assembly properties.³²⁻³⁵ Another module of interest is the heterotriangulene synthesized by Professor Dhandapani Venkataraman's group³⁶ at UMass Amherst, and utilized by Wan³⁷ and Zhang³⁸ as a triangular acceptor component that could serve as another electron-withdrawing core for the proposed systems (Figure 8.1).

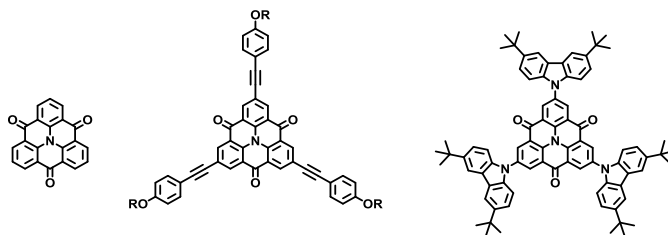
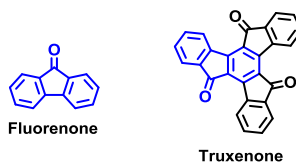


Figure 8.1: π -Macrocycles synthesized by DV Group (left), Wan et al. (middle), and Zhang et al. (right).

The truxenone system is related to the FO- and FM-based chromophores discussed in Chapters 2-3. Truxenone is structurally comprised of three fused fluorenones sharing one central benzene ring. Thus, reactive similarities to fluorenones should follow in such a way that the

triangulene chromophores proposed should be attainable using similar procedures to those used for the fluorenone systems already made. The proposed systems should behave similarly to those already characterized, with the added benefit of much larger molar absorptivities and better intermolecular assembly properties.



In addition to these optoelectronic and intramolecular assembly properties, bridge-carbon-substituted truxenes are especially promising targets due to the fact that many of them have been found to adopt bowl-shape geometries.^{34,35,39} The benefits of these geometric properties arise because such bowl-shaped molecules have been shown computationally to interface well with PCBM (Figure 8.2).³⁹⁻⁴² As discussed, increasing donor-acceptor interactions through an inherent molecular drive for intra- and inter-material self-assembly is one of the keys to engineering efficient materials.

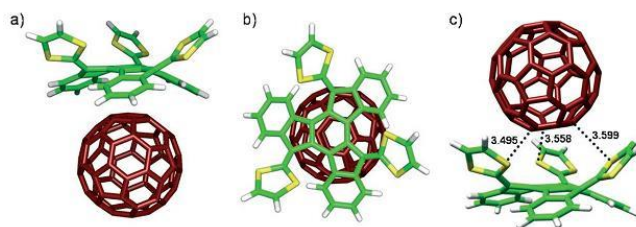


Figure 8.2:³⁹ DFT results exhibiting dithiafulvalenyl truxenes (a-c) interacting with C60 through π - π stacking. See Martín *et al* (permission license number 3342620583207).³⁹

8.2.2 Molecular Design and Preliminary Work

I prepared the electron-poor “acceptor” π -macrocycles tribromotruxenone and tris-iodoheterotriangulene shown in Figure 8.3, and attempted to couple **1** to styrene or diarylamine derivative donor modules. Synthetic procedures for truxenone and heterotriangulene-based compounds are shown in Scheme 8.1-Scheme 8.3. This architecture was designed to allow for E_{HOMO} tuning based on the electron donating strength of the donor module, *and* provide a means

to control packing/self-assembly characteristics by the nature of the donor functionalities chosen.

The π -macrocycle cores serve as the LUMO-tuning acceptor modules, and they should form

columnar π -stacks.^{36–38,43}

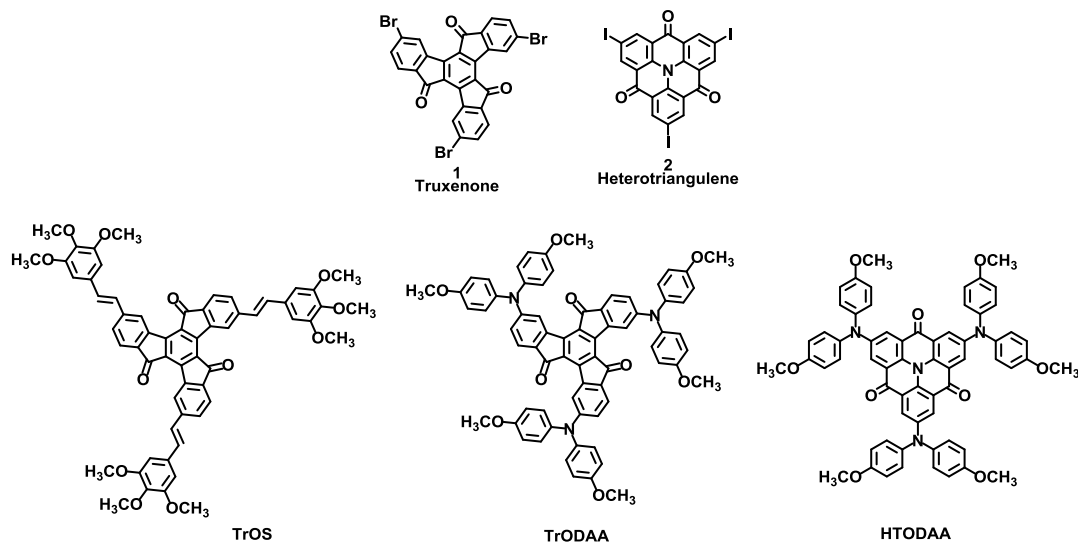


Figure 8.3: Truxenone and heterotriangulene π -macrocycle acceptor cores, and proposed π -macrocycle D-A compounds.

The π -macrocycle core modules chosen for this work also provide the opportunity for subsequent LUMO energy (E_{LUMO}) tuning via Knoevenagel condensation at the ketone groups, as described previously in Chapter 3 and shown in Figure 8.4. Core functionalization should also impart interesting self-assembly properties, since installing dicyanomethylene groups in place of the ketones is predicted^{39–42} by DFT to impart a bowl-shaped molecular deformation which may provide better interfacial contact with adjacent fullerene-type materials (Figure 8.2). This molecular design plan thus serves to address multiple issues important for photovoltaic materials design: band gap and FMO energy control, self-assembly properties, good interfacial interactions with fullerene-based n-type materials, and favorable π -overlap for exciton and charge transport.

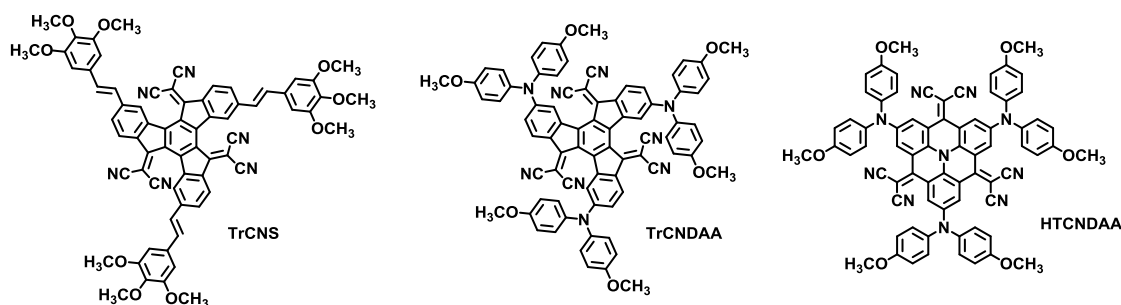
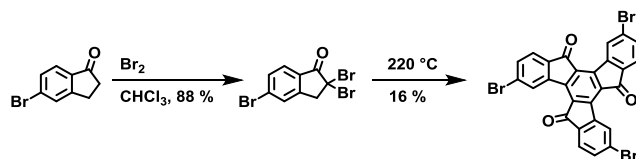
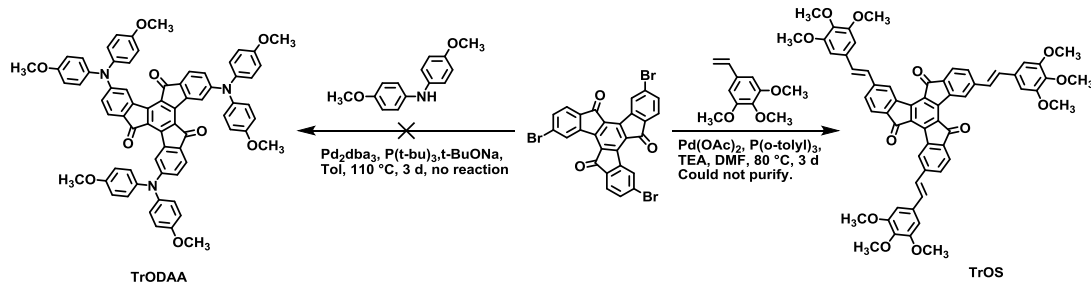


Figure 8.4: Proposed D-A π -macrocyclic compounds, condensed to their bis-cyanofulvenoid analogues.

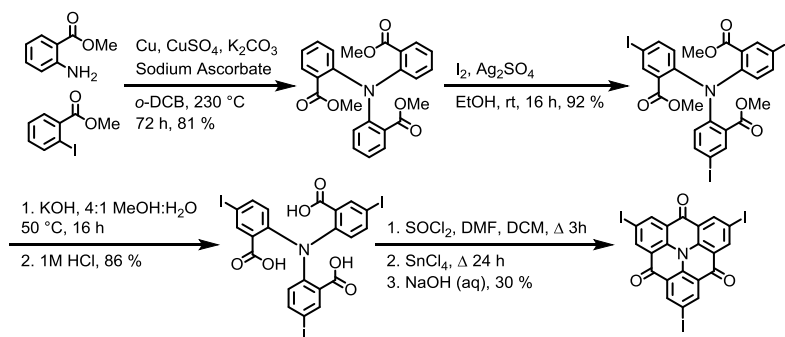
Unfortunately, this sub-project did not yield any of the pure final compounds proposed. Tribromotruxenone and triiodoheterotriangulene are poorly soluble in most organic solvents useful for Heck or Buchwald-Hartwig coupling reactions, so the only compound produced in even a crude, impure state was tris(trimethoxystyryl)truxenone (TrOS). This crude material is a reddish-brown solid which looks much like its fluorenone analogue FODS when dissolved in CHCl_3 .^{44,45} LR-MS (FAB⁺) indicates the presence of the desired molecular ion peak along with various fragmentation peaks. Molecular ion peaks corresponding to mono- and dicoupled products are absent, suggesting reaction completion. However, HPLC, TLC, ¹H-NMR, and MP all indicate that the product is impure. All attempts to purify TrOS were unsuccessful, although its deep red color and positive FAB-MS results are promising.



Scheme 8.1: Synthesis of 4,9,14-tribromotruxenone, adapted from the literature.³³



Scheme 8.2: Attempted synthesis of truxenone-cored D-A compounds TrOS and TrODAA.



Scheme 8.3: Synthesis of triiodoheterotriangulene, adapted from the literature.^{36,38,46}

Lambert⁴⁷ and coworkers recently synthesized the proposed TrODAA compound, which exhibited a molar absorptivity of around $30,000 \text{ M}^{-1}\text{cm}^{-1}$ at about 500 nm, with strong spectral coverage between 300-600 nm. In my hands, it was too difficult to obtain these materials – likely due to the difficulty in obtaining pure tribromotruxenone, and its poor solubility. But, Lambert's results lend promise to this molecular design although their materials' electronic and electrochemical properties have not been reported at the time of this writing.

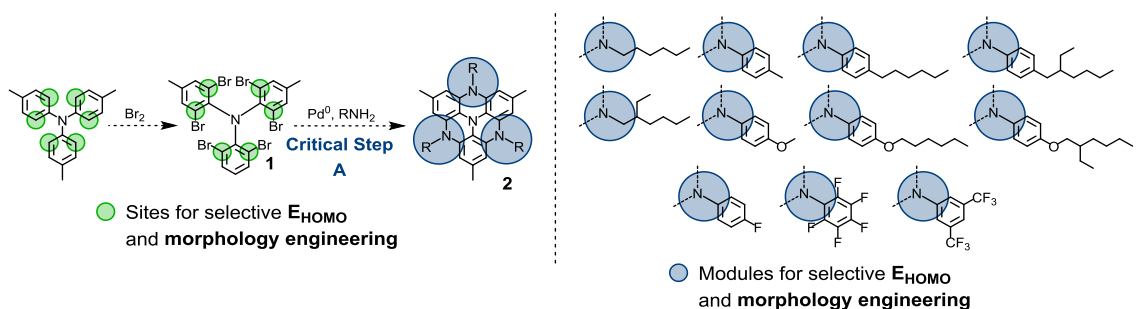
Should it be possible to obtain pure tribromotruxenone more easily, the proposed truxenone materials in Figure 8.3 and Figure 8.4 might be worth pursuing in light of these preliminary results and Lambert's findings. In particular, condensation of Lambert's TrODAA with malononitrile to form the proposed TrCNDAA may decrease the band gap from 600 nm (2.06 eV) to around 790 nm (1.56 eV) if the 0.5 eV band gap decrease trend described in Chapter 3 would translate to these systems. In addition, since the D-A connectivity is pseudo-*para* in these systems, the bis-cyanofulvenoid TrCNDAA analogue may behave panchromatically like its

fluorenylidene analogue FMBDAA36. Lastly, computational evidence³⁹⁻⁴² indicates that sterically-hindered truxene compounds tend to be bowl-shaped, which may provide improved interfacial interactions between TrCNDAA or TrCNS and a fullerene derivative (Figure 8.2).

For photovoltaic purposes, further pursuit of the proposed heterotriangulene materials HTODAA (Figure 8.3) and HTCNDAA (Figure 8.4) is not recommended. Although their molecular architecture lends itself to the optoelectronic tunability strategies discussed here and in earlier chapters, their D-A connectivity is pseudo-*meta* and thus not likely to give large ICT molar absorptivities. Indeed, carbazole- and anisyl-ethynylene-functionalized heterotriangulene derivatives studied by Zhang³⁸ and Wan³⁷, respectively, exhibit molar absorptivities that are somewhat low ($\sim 12,000 \text{ M}^{-1}\text{cm}^{-1}$) for their large π -cross section. While the proposed heterotriangulene systems are interesting, it was decided to discontinue pursuing them.

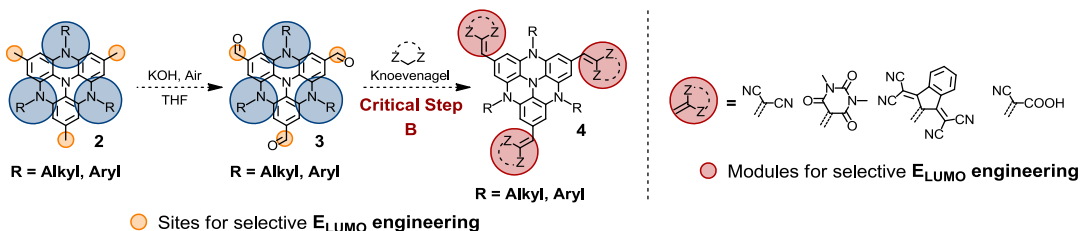
8.2.3 Highly Structurally Tunable π -Macrocycles via Soluble Synthetic Intermediates

Despite the above difficulties, π -macrocycle chromophores are still philosophically and practically worth pursuing as long as they can be obtained by route of soluble precursors and intermediates. One such possibility is proposed below (Scheme 8.4), which integrates a soluble π -macrocycle core obtained from soluble precursors that can serve as an electron-rich donor module as well as a self-assembly platform. This synthetic route should provide a high degree of HOMO tunability based on the wide range of primary amine starting materials that can be chosen (critical step A). With a soluble π -macrocycle in hand, installation of aldehyde components should provide a wide range of LUMO tunability based on the many electron-poor condensation partners that could be chosen (critical step B).



Scheme 8.5: Modular engineering of E_{HOMO} levels and intermolecular interactions using primary amines with various electronic and side chain interaction properties.

In addition to providing substantial E_{HOMO} engineering capability, this strategy would provide a means to control self-assembly and exciton/charge mobility characteristics by the nature of the alkyl/arylamine chosen. The triarylamine core should provide modest exciton/hole mobility due to its large conjugation, and the fact that triarylamines typically impart good hole transport characteristics. Due to the wide range of molecular properties engineered into these new core materials, they should possess a range of photophysical and electronic transport properties. Since much more work needs to be done to thoroughly understand mobility characteristics in organic electronic materials, this proposal should provide important insight in this area.^{49,50} Specifically, the individual tuning of morphology and electronic properties by use of amines with different side chains and electron donating characteristics should provide the means to study mobility as *independent* functions of morphology and electronic properties: set morphology with side chain properties and then tune the electronics, or set the electronics and then tune the morphology properties by side chain interchange (Scheme 8.5).



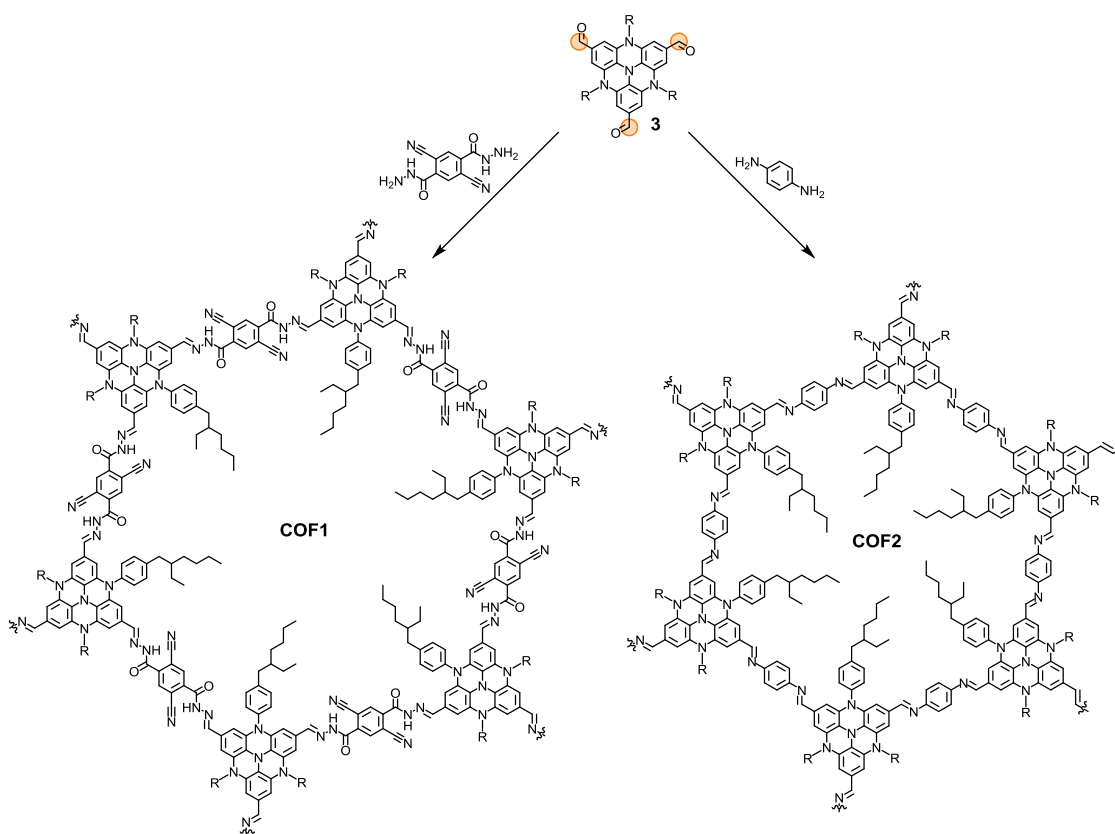
Scheme 8.6: Modular engineering of E_{LUMO} levels using electron withdrawing groups with various electronic properties.

Phase 2 of development will involve the synthesis of materials **4** via straightforward condensation chemistry with electron-withdrawing acceptor modules for E_{LUMO} engineering (Scheme 8.6). This second series of synthetic modifications introduces E_{LUMO} control through straightforward condensation chemistry with various electron accepting modules. π -Macrocyclic core **2** and its R-substituted variants will be oxidized to the trialdehyde under mild conditions, for subsequent Knoevenagel condensation with the chosen acceptor modules. These modules are either commercially available or straightforward to synthesize, thereby increasing the synthetic efficiency of producing these new materials. Due to the different electron withdrawing strengths of the modules chosen, the E_{LUMO} should be tunable as a function of module choice. It should also be possible to tune E_{LUMO} separately from E_{HOMO} due to the distinct separation donor-acceptor portions of the structures.^{12,13}

Following the preparation of this large library of new materials, their optoelectronic and electrochemical properties would be thoroughly characterized using UV-vis-NIR absorption and fluorescence spectroscopy, and cyclic voltammetry. These data would provide crucial information about the new materials' FMO energies, band gaps, and electrochemical characteristics. These materials are also expected to exhibit some different molecular assembly properties compared to their non-functionalized precursors, due to their peripheral π -conjugated acceptor modules. Specifically, these peripheral π -systems should impart useful intermolecular interactions in addition to their optoelectronic and electrochemical properties. As with the materials obtained in Phase 1, it should also be possible to relate the photophysical and electronic transport properties of these Phase 2 materials back to the molecular design components. Since molecular property engineering is the primary objective of this work, these resulting structure-property correlations should augment fundamental design principles for future work.

Finally, π -macrocycles like this should also be amenable to 2-dimensional covalent organic framework (COF) integration, shown in Scheme 8.7. 2-D COFs have become quite popular recently,²²⁻³¹ and this synthetic materials technology may be useful for photovoltaic or

other organic electronic applications. With the proposed π -macrocycles in hand, especially intermediate **3**, it should be possible to synthesis a wide variety of COFs using commercially-available or easily synthesized coupling partners. **COF1** for example, would be a push-pull COF, which may be useful for photovoltaic applications, while **COF2** may be more applicable to p-type field effect transistors (due to its lack of LUMO control character). These proposals are just two examples to illustrate the richness of this research approach.



Scheme 8.7: Covalent organic framework possibilities for π -macrocycles, using proposed π -macrocycle **3 and primary-amine-containing condensation partners.**

8.3 Proposed Development of Indigo-Based Organic Electronic Materials

Indigo-based materials have recently become popular p-type materials for organic photovoltaic (OPV) devices⁵¹ and p-/n-type and ambipolar materials for field effect transistors (FETs) due to their modest molar absorptivities,^{20,52–54} self-assembly properties,²¹ and modest to excellent charge carrier mobilities.^{20,55–58} Indigo dyes are straightforward to synthesize from 2-

nitrobenzaldehydes and acetone in water/NaOH solution,^{59,60} and there are many commercially available starting materials. Although this section will not focus on isoindigo-based materials, there are some excellent review articles describing their molecular design for organic electronic applications.^{61–65} The work proposed in this section describes a relatively simple, straightforward approach to obtain a wide variety of functionalized indigos using relatively inexpensive, commercially available starting materials. The basic molecular structures of the proposed indigo-based materials are shown in Figure 8.5.

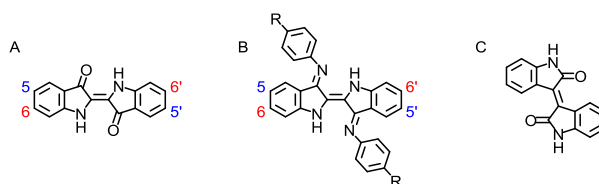


Figure 8.5: (A) Indigo, with the 5,5'- and 6,6'-connectivity positions labeled. (B) “Nindigo”,^{52–54} an aniline-condensate of indigo, with variable R groups for different electronic and molecular packing effects. (C) Isoindigo.

Unfortunately most indigo-based OPV devices are on the lower end of the PCE scale in tests to date; but, they often exhibit good charge carrier mobility properties in FET devices, which is attributed to strong hydrogen-bonding networks in the solid state (Figure 8.6). For example, indigo and Tyrian purple (5,5'-dibromoindigo) exhibit quite good hole and electron thin film FET mobilities²⁰ at 0.01-0.2 cm²/V·s. Although most of these indigo derivatives will likely be sparingly soluble in most organic solvents relevant to device fabrication, similar compounds have been vacuum deposited onto substrates for OPV and FET testing.^{20,21,56,57} No testing seems to have been done on single crystals grown from solution or by chemical vapor deposition (CVD) techniques. Single crystal and vacuum-deposited thin film device fabrication techniques are well established^{66–68} for highly crystalline materials, so this may be considered a relatively available area for fast advances.

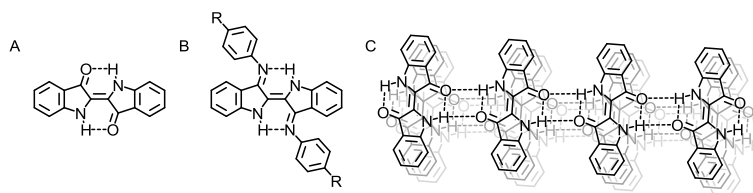


Figure 8.6: (A) indigo and (B) nindigo intramolecular hydrogen bonding. (C) Indigo intra- and intermolecular hydrogen bonding and crystal packing scheme.²⁰

Synthetically, this work could be done by an undergraduate^{59,60} or a young graduate student due to its simplicity; so the work is technically *and* logically straightforward. But, this work also spans a broad landscape of indigo-based material derivatives, so substituent and π -connectivity effects can be studied on a physical chemical, single crystal (when available), and device level (5,5'- vs. 6,6'-connectivity, Figure 8.5). This broad functionalization landscape should provide fundamental insight into the systematic design and synthesis of structurally simple small molecule organic electronic materials. Systematic structure-property engineering is important for organic electronics, so this has the potential to be a rich area of study.

Finally, this work should have a strong educational impact on the research student since a wide range of functional compounds can be synthesized and tested relatively quickly and with limited initial technical expertise. Educational development during this project would follow a natural progression of technical difficulty, starting with straightforward one-step synthesis and subsequent development of crystallization/sublimation purification techniques. CVD and solution crystallization techniques^{66,68-71} and rudimentary thin film and single crystal device testing techniques should take no more than six months of dedicated practice to develop (with some initial mentoring). This work would also expose the student to a broad range of other important organic electronics skills, including optoelectronic and electrochemical testing via UV-vis-NIR absorption and fluorescence spectroscopy and cyclic voltammetry, computational chemistry, x-ray crystallography (XRD), physical organic molecular design, and invaluable collaborative soft skills while learning these techniques and teaching them to others.

The ultimate goal of this project is to provide fundamental insight into the development of small molecule OPV and OFET materials by exploring a wide structure-property landscape using few synthetic steps. The specific synthetic plan is summarized in Figure 8.7. Tyrian purple and indigo are known ambipolar charge transport materials in the FET configuration,^{20,55–58} but compounds 3-7 have not been reported at the time of this writing. These proposed materials span a wide range of functionality, including aryl fluorides and alkoxy/amine donor groups in different connectivities.

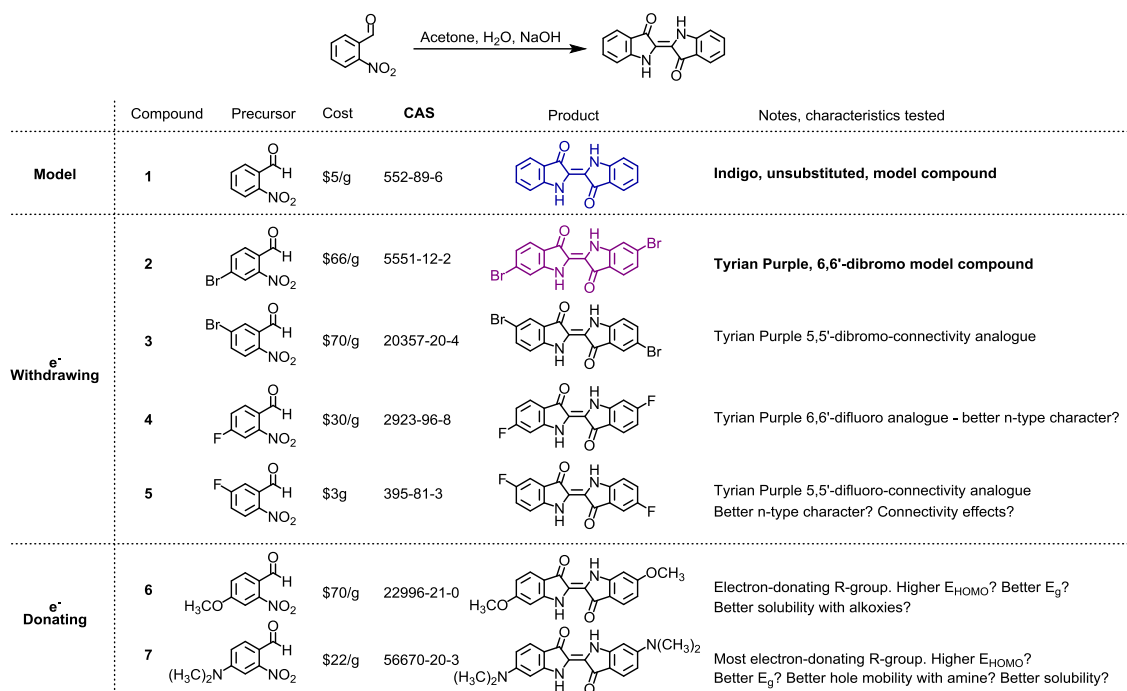


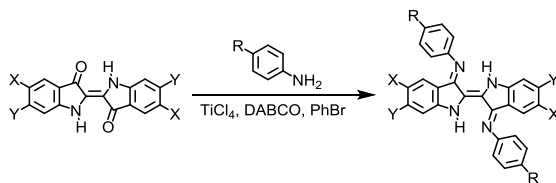
Figure 8.7: Proposed indigo-based materials for OPV and FET applications.

8.3.1 Experimental Plan and Expectations for Indigo-Based Materials

Bottom-up molecular control over charge carrier mobility and optical band gap in organic electronic materials has long been a topic of interest in synthetic organic chemistry. This is especially true for air-stable organic n-type materials,^{72–75} which are difficult to design due to LUMO limitations (cannot be below -3.8 eV)⁶⁸ and intermolecular packing requirements,⁷⁴ and due to the fact that still little is known about why and how they work.⁷⁶ Incorporation of halogens (usually fluoro)^{74,77,78} or cyano^{74,79} groups tends to help, but mobility trends are more difficult to

establish with n-type materials. As a result, designing new materials while establishing fundamental molecular design principles presents a considerable synthetic challenge. But, due to our understanding of the limited but effective pool of excellent charge carrying organic materials, there are some fundamental molecular design principles that can provide rational synthetic direction.

This proposal focuses on frontier molecular orbital (FMO) energy tuning in two different ways: by substituent type *and* connectivity around the indigo π -system, in addition to indigo-to-nindigo conversion (Scheme 8.8) using aniline derivatives with different electronic properties (electron donating versus withdrawing substituents). Part of this molecular design strategy involves intermolecular interaction engineering, which is driven by indigo's inherent inter- and intramolecular hydrogen bonding capabilities (Figure 8.6). The intermolecular interaction landscape will be tested by varying the type *and* connectivity of peripheral π -system substituents, in addition to indigo-to-nindigo conversion with aniline derivatives. The latter should provide similar intramolecular hydrogen bonding capability, while providing a π -system (aniline derivative) that is out of plane relative to the indigo core. Like rubrene, this may provide extra modes of contact between adjacent molecules, and alternative electron/hole percolation directionality within the crystal lattice. In addition, this extra functionality may impart better solubility to the nindigo materials due to the wide range of solubilizing anilines that can be used (e.g. R=alkoxy).



Scheme 8.8: Nindigo synthesis from indigo and aniline derivatives, following the procedure used by Hicks⁵² and coworkers.

As discussed in previous chapters, inherent synthetic tunability is crucial for the development of a wide variety of materials for fundamental structure/property analysis. Robust

synthetic methods are important, so that a broad structural landscape can be surveyed with minimal synthetic effort. This is expected to be the case with these proposed indigo-based materials, since they can be assembled in just one synthetic step from commercially-available starting materials using fast, high-yield, low-difficulty synthetic methodology. Since energy level modulation is an important part of electronic materials development, this proposal makes use of several different functional groups, from electron withdrawing (e.g. fluoro, bromo) to electron donating (e.g. alkoxy, amino), for the purpose of *synthetically* tuning the frontier molecular orbital (FMO) energies. Substituent connectivity effects are also important, and can be easily studied using this synthetic approach.

Conversion of the indigo to derivatives to their nindigo analogues can be completed in just one step, and provides an even broader structure/property molecular design landscape. This structural change should allow for finer tuning of the FMO electronics, in addition to molecular packing and solubility. In all, this work should serve as a strong molecular engineering platform based on the structural simplicity and broad range of functionality inherently built into the proposed molecular architecture.

If the new indigo-based materials perform well as organic electronic materials, this work should provide a strategic stepping stone for future indigo-based materials development. Due to the synthetic simplicity of the materials proposed herein, it should be possible to quickly survey a broad functional landscape for the purpose of establishing reliable molecular design trends. Because indigo based compounds have already shown promise as hole and electron transport materials, this work should propel forward the optimization of this molecular architecture, and/or at the very least provide fundamental insight into the design and synthesis of new small molecule organic electronic materials.

8.4 Panchromatic Materials Design

This section briefly outlines a molecular engineering proposal built using the concepts discussed in Chapters 2, 3, and 6. Ideally, an organic photoconversion material would absorb

strongly *and* broadly throughout the visible spectrum, spanning the entire 400-900 nm or 3.1-1.4 eV region (Figure 1.1). While photoexcitation bands in π -conjugated organic materials can be quite broad, most organic materials do not absorb over the entire 1.7 eV width of the visible spectrum. In OPV devices, this issue is typically circumvented by blending p/n materials that *additively* cover the visible spectrum, with one compound being a mid-low band gap absorber (e.g. SQ-OH from Chapter 6) and the other being a mid-high band gap absorber (e.g. PC₇₁BM).

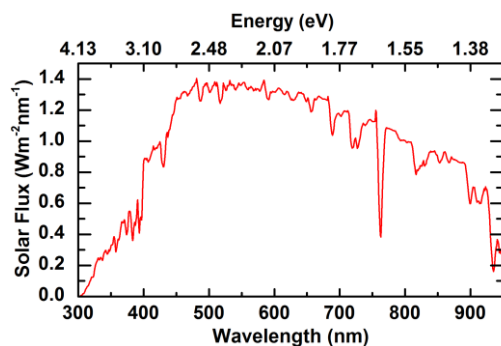


Figure 8.8: Solar flux as a function of wavelength (bottom axis) and energy in electron volts (top axis).

Unfortunately, this blending strategy limits the number of p/n material pairs that can be used together. If one p-type (or n-type) material could do all of the photoabsorption in the device, it would be possible to focus device engineering efforts on pairing electronically and morphologically compatible partner materials without the added frustration of spectral coverage pairing. For example, it might not be best to pair a p-type material with PC₇₁BM for morphological, economic, or other reasons; but if a p-type material only covers the low energy region of the solar spectrum, it might be necessary to sacrifice ideal morphology to collect more photons – a difficult balancing process between optimizing photon collection, charge pair generation, and exciton/charge transport.

There are few literature examples of molecular design attempts to *specifically engineer* panchromatic absorption behavior in organic electronic materials involving rational molecular design rules, although a couple are worth noting. Jiang and coworkers⁸⁰ performed a density

functional theory study on numerous azulene-porphyrins (Figure 8.9), where low molecular symmetry and low HOMO-LUMO/LUMO+1 gaps provide multiple strong transitions throughout the visible-NIR spectrum. Jiang's theoretical azulene-porphyrins possessed desirable panchromatic absorption based on their computations, but porphyrins can be difficult to synthesize and purify, and are often poorly soluble without peripheral solubilizing alkyl groups. So, while porphyrin dyes such as zinc phthalocyanines have worked well in OPV⁸¹ and DSSC⁸² devices, they are not necessarily ideal synthetic targets. Grätzel et al.^{83,84} and Meyer et al.⁸⁵ describe design rules for panchromatic ruthenium-based organometallic sensitizers for dye sensitized solar cells. Their organoruthenium systems are heteroleptic, with one set of ligands providing strong σ -donating character to destabilize the Ru t_{2g} orbital, and another set of ligands providing a low π^* orbital for lower energy metal to ligand charge transfer (MLCT). These organoruthenium structural/electronic properties provide multiple allowed optical transitions within the visible-NIR spectrum, giving dark black dyes that absorb well between 400 – 700 nm or 400 – 800 nm depending on the ligands used. Figure 8.9 shows an example of Grätzel's ruthenium dye.

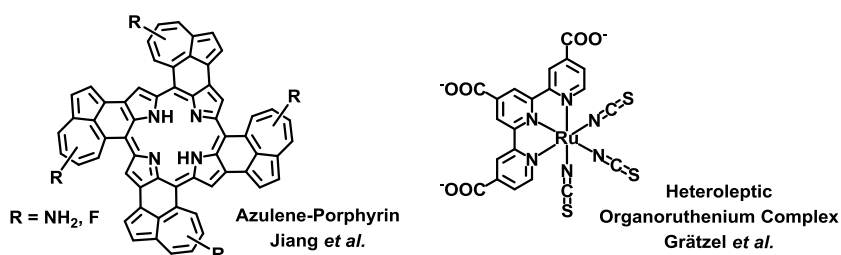


Figure 8.9: Panchromatic azulene-porphyrin (Jiang *et al.*)⁸⁰ and heteroleptic organoruthenium complex (Grätzel *et al.*),^{83,84}

This proposal aims to provide a physical chemical model for *organic* non-porphyrin molecular design, and some examples of molecular structures that may accomplish the goals dictated by the proposed model. The proposed materials were designed using some of the fluorenone and squaraine results and underlying physical chemistry discussed in Chapters 2, 3, and 6.

8.4.1 Proposed Physical Chemical Model for Panchromatic Absorption Behavior

This proposal takes advantage of some of the inherent properties of donor-acceptor molecules. In strong D-A molecules, the HOMO is located over the donor region of the structure while the LUMO is located over the acceptor region of the structure. Photoexcitation creates a charge-separated excited state, with the excited state electron residing over the acceptor component of the molecule, where the LUMO is largely separated from the HOMO region of the molecule.

It might be possible to take advantage of this inherent excited state charge separation, by connecting a donor module to two different acceptor modules with different electron affinities. An example of this would be using an A_1 -D- A_2 molecular architecture where A_2 is a stronger acceptor than A_1 . This would be, in principle, like having two donor-acceptor compounds within one structure, with the two acceptor modules separated by their common donor component. As separate molecules, A_1 -D and A_2 -D would have different band gaps defined by a common HOMO energy (driven by the common donor module) and different LUMO energies each driven by the different electron affinities of the acceptor modules. This is represented by the perturbation theory model in Figure 8.10. In this example, A_2 is a stronger acceptor (has a lower LUMO energy) than A_1 , and thus D- A_2 has a lower band gap than D- A_1 ($E_{g2} < E_{g1}$).

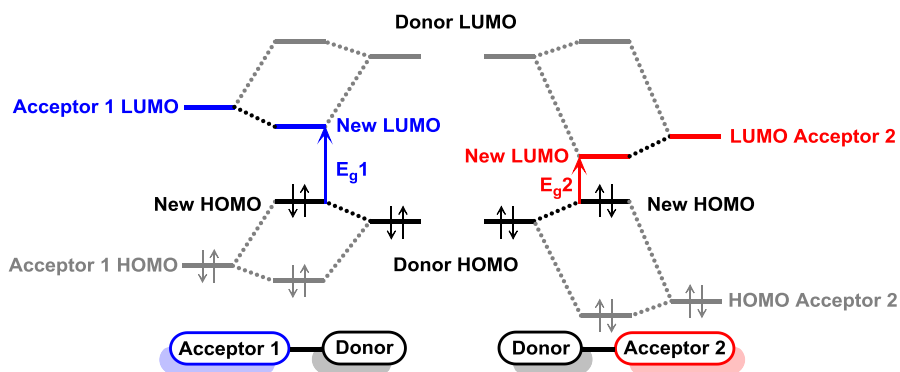


Figure 8.10: Perturbation theory model for two separate D-A compounds where they each have the same donor module but different acceptor modules with different electron affinity.

As an A_1 -D- A_2 triad, the acceptor modules are only conjugated together through their common donor module. But, since the LUMO of each D- A_1 and D- A_2 resides on the acceptor modules, the acceptor modules should not be able to interact in the A_1 -D- A_2 triad's excited state (no molecular orbital overlap, since the donor module intervenes). If the acceptor modules cannot interact due to spatial separation of their molecular orbitals, then the A_1 -D- A_2 triad may have *two* allowed photoexcitation processes: a low energy process exciting an electron from the donor to A_2 (HOMO-LUMO), and a higher energy process exciting an electron from the donor to A_1 (HOMO-LUMO+1). If the acceptor modules' electron affinities differ by 0.5 eV, and each D- A_1 and D- A_2 ICT band is approximately 0.5 eV wide at full width half max (FWHM), then this would give combined FWHM absorption coverage over 1.5 eV, which is most of the 1.7 eV width of the visible spectrum. Most of the compounds in this dissertation have ICT FWHM around 0.5 eV, so this is not an unreasonable expectation.

Extrapolating from Chapters 2, 3, and 6, the proposed compounds in Figure 8.11 integrate a squarylium core with diarylamine donor modules. These compounds are designed as A_1 -D- A_2 -D- A_1 chromophores, where the D- A_2 -D portion is a low band gap squaraine-diarylamine and the A_1 -D portion is mid-band gap with a weaker acceptor module. Because the squaraine-triarylamines in Figure 8.11 are so similar to those in Chapter 6, it is reasonable to expect them to impart a low E_{LUMO} , low band gap, and strong molar absorptivity. Benzothiadiazole- and fluorenone-based materials are also typically low band gap strong absorbers with fairly low LUMO energies, although not as low as the Chapter 6 squaraines. If the proposed physical chemical model holds, then this general molecular architecture may be able to combine all of these properties into one small molecule material that absorbs throughout most of the visible spectrum.

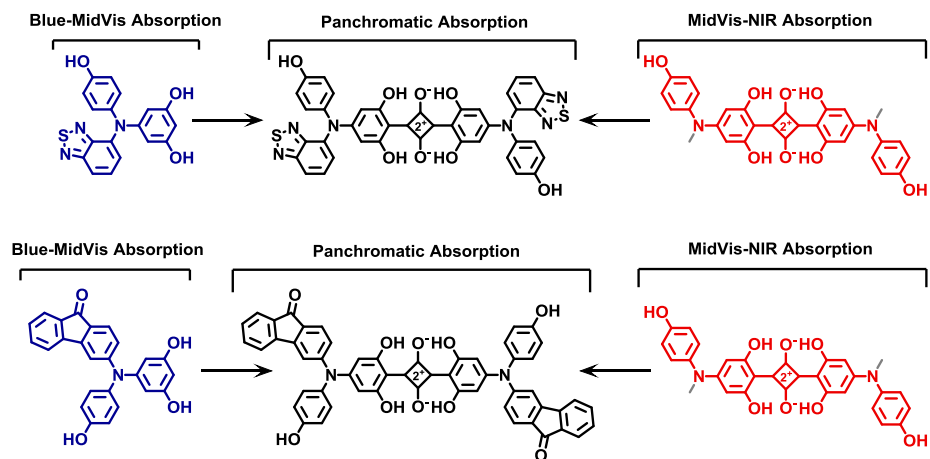


Figure 8.11: Proposed examples of A-D-A' donor-acceptor materials for panchromatic visible spectrum absorption.

8.5 Concluding Remarks

The π -macrocycles, indigos, and A-D-A' dual acceptor push-pull compounds should serve as a logical extension of the work described in this dissertation. The proposed materials were specifically designed to possess a high degree of synthetic tunability for a broad range of important organic electronic materials properties. This group of proposals is intended to provide specific physical chemical insight into charge carrier mobility engineering, FMO energy tuning, panchromatic absorption behavior, and self-assembly design. Should this work be successful, these materials should provide fundamental insight into a wide variety of organic electronic materials design, most notably photovoltaics and field effect transistors.

8.6 References

- (1) Peet, J.; Heeger, A. J.; Bazan, G. C. "Plastic" Solar Cells: Self-Assembly of Bulk Heterojunction Nanomaterials by Spontaneous Phase Separation. *Acc. Chem. Res.* **2009**, *42*, 1700–1708.
- (2) Zhou, H.; Yang, L.; You, W. Rational Design of High Performance Conjugated Polymers for Organic Solar Cells. *Macromolecules* **2012**, *45*, 607–632.
- (3) Zhang, Z.; Wang, J. Structures and Properties of Conjugated Donor–Acceptor Copolymers for Solar Cell Applications. *J. Mater. Chem.* **2012**, *22*, 4178–4187.
- (4) Cheng, Y.-J.; Yang, S.-H.; Hsu, C.-S. Synthesis of Conjugated Polymers for Organic Solar Cell Applications. *Chem. Rev.* **2009**, *109*, 5868–5923.
- (5) Roncali, J. Molecular Bulk Heterojunctions: An Emerging Approach to Organic Solar Cells. *Acc. Chem. Res.* **2009**, *42*, 1719–1730.
- (6) Aida, T.; Meijer, E. W.; Stupp, S. I. Functional Supramolecular Polymers. *Science (80-.)*. **2012**, *335*, 813–817.
- (7) Estrada, L. A.; Yarnell, J. E.; Neckers, D. C. Revisiting Fluorenone Photophysics via Dipolar Fluorenone Derivatives. *J. Phys. Chem. A* **2011**, *115*, 6366–6375.
- (8) Estrada, L. A.; Cai, X.; Neckers, D. C. Nonradiative Decay Mechanism of Fluoren-9-Ylidene Malonitrile Ambipolar Derivatives. *J. Phys. Chem. A* **2011**, *115*, 2184–2195.
- (9) Estrada, L. A.; Neckers, D. C. Synthesis and Photophysics of Ambipolar Fluoren-9-Ylidene Malonitrile Derivatives. *J. Org. Chem.* **2009**, *74*, 8484–8487.
- (10) Roncali, J. Synthetic Principles for Bandgap Control in Linear Pi-Conjugated Systems. *Chem. Rev.* **1997**, *97*, 173–206.
- (11) Raimundo, J.; Blanchard, P.; Gallego-Planas, N.; Mercier, N.; Ledoux-Rak, I.; Hierle, R.; Roncali, J. Design and Synthesis of Push–Pull Chromophores for Second-Order Nonlinear Optics Derived from Rigidified Thiophene-Based Pi-Conjugating Spacers. *J. Org. Chem.* **2002**, *67*, 205–218.
- (12) Leriche, P.; Frère, P.; Cravino, A.; Alévêque, O.; Roncali, J. Molecular Engineering of the Internal Charge Transfer in Thiophene-Triphenylamine Hybrid Pi-Conjugated Systems. *J. Org. Chem.* **2007**, *72*, 8332–8336.
- (13) Roquet, S.; Cravino, A.; Leriche, P.; Alévêque, O.; Frère, P.; Roncali, J. Triphenylamine-Thienylenevinylene Hybrid Systems with Internal Charge Transfer as Donor Materials for Heterojunction Solar Cells. *J. Am. Chem. Soc.* **2006**, *128*, 3459–3466.
- (14) Kanibolotsky, A. L.; Perepichka, I. F.; Skabara, P. J. Star-Shaped Pi-Conjugated Oligomers and Their Applications in Organic Electronics and Photonics. *Chem. Soc. Rev.* **2010**, *39*, 2695–2728.

- (15) Ito, S.; Wehmeier, M.; Brand, J. D.; Kubel, C.; Epsch, R.; Rabe, J. P.; Müllen, K. Synthesis and Self-Assembly of Functionalized Hexa-Peri-Hexabenzocoronenes. *Chem. - A Eur. J.* **2000**, *6*, 4327–4342.
- (16) Grimsdale, A. C.; Müllen, K. The Chemistry of Organic Nanomaterials. *Angew. Chem. Int. Ed. Engl.* **2005**, *44*, 5592–5629.
- (17) Watson, M. D.; Fechtenkötter, a; Müllen, K. Big Is Beautiful--“Aromaticity” Revisited from the Viewpoint of Macromolecular and Supramolecular Benzene Chemistry. *Chem. Rev.* **2001**, *101*, 1267–1300.
- (18) Charvet, R.; Yamamoto, Y.; Sasaki, T.; Kim, J.; Kato, K.; Takata, M.; Saeki, A.; Seki, S.; Aida, T. Segregated and Alternately Stacked Donor/acceptor Nanodomains in Tubular Morphology Tailored with Zinc Porphyrin-C60 Amphiphilic Dyads: Clear Geometrical Effects on Photoconduction. *J. Am. Chem. Soc.* **2012**, *134*, 2524–2527.
- (19) Miyajima, D.; Araoka, F.; Takezoe, H.; Kim, J.; Kato, K.; Takata, M.; Aida, T. Ferroelectric Columnar Liquid Crystal Featuring Confined Polar Groups within Core-Shell Architecture. *Science* **2012**, *336*, 209–213.
- (20) Glowacki, E. D.; Leonat, L.; Voss, G.; Bodea, M.; Bozkurt, Z.; Irimia-Vladu, M.; Bauer, S.; Sariciftci, N. S. Natural and Nature-Inspired Semiconductors for Organic Electronics. In *Organic Semiconductors in Sensors and Bioelectronics IV*; Shinar, R.; Kymissis, I., Eds.; San Diego, California, 2011; Vol. 8118, p. 81180M–81180M–10.
- (21) Głowacki, E. D.; Irimia-Vladu, M.; Bauer, S.; Sariciftci, N. S. Hydrogen-Bonds in Molecular Solids – from Biological Systems to Organic Electronics. *J. Mater. Chem. B* **2013**, *1*, 3742.
- (22) Ding, X.; Guo, J.; Feng, X.; Honsho, Y.; Guo, J.; Seki, S.; Maitrad, P.; Saeki, A.; Nagase, S.; Jiang, D. Synthesis of Metallophthalocyanine Covalent Organic Frameworks That Exhibit High Carrier Mobility and Photoconductivity. *Angew. Chem. Int. Ed. Engl.* **2011**, *50*, 1289–1293.
- (23) Wan, S.; Gándara, F.; Asano, A.; Furukawa, H.; Saeki, A.; Dey, S. K.; Liao, L.; Ambrogio, M. W.; Botros, Y. Y.; Duan, X.; *et al.* Covalent Organic Frameworks with High Charge Carrier Mobility. *Chem. Mater.* **2011**, *23*, 4094–4097.
- (24) Jin, S.; Ding, X.; Feng, X.; Supur, M.; Furukawa, K.; Takahashi, S.; Addicoat, M.; El-Khouly, M. E.; Nakamura, T.; Irle, S.; *et al.* Charge Dynamics in a Donor-Acceptor Covalent Organic Framework with Periodically Ordered Bicontinuous Heterojunctions. *Angew. Chem. Int. Ed. Engl.* **2013**, *52*, 2017–2021.
- (25) Dogru, M.; Handloser, M.; Auras, F.; Kunz, T.; Medina, D.; Hartschuh, A.; Knochel, P.; Bein, T. A Photoconductive Thienothiophene-Based Covalent Organic Framework Showing Charge Transfer towards Included Fullerene. *Angew. Chem. Int. Ed. Engl.* **2013**, *52*, 2920–2924.

- (26) Patwardhan, S.; Kocherzhenko, A. a.; Grozema, F. C.; Siebbeles, L. D. a. Delocalization and Mobility of Charge Carriers in Covalent Organic Frameworks. *J. Phys. Chem. C* **2011**, *115*, 11768–11772.
- (27) Spitler, E. L.; Colson, J. W.; Uribe-Romo, F. J.; Woll, A. R.; Giovino, M. R.; Saldivar, A.; Dichtel, W. R. Lattice Expansion of Highly Oriented 2D Phthalocyanine Covalent Organic Framework Films. *Angew. Chem. Int. Ed. Engl.* **2012**, *51*, 2623–2627.
- (28) Spitler, E. L.; Dichtel, W. R. Lewis Acid-Catalysed Formation of Two-Dimensional Phthalocyanine Covalent Organic Frameworks. *Nat. Chem.* **2010**, *2*, 672–677.
- (29) Feng, X.; Chen, L.; Honsho, Y.; Saengsawang, O.; Liu, L.; Wang, L.; Saeki, A.; Irle, S.; Seki, S.; Dong, Y.; *et al.* An Ambipolar Conducting Covalent Organic Framework with Self-Sorted and Periodic Electron Donor-Acceptor Ordering. *Adv. Mater.* **2012**, *24*, 3026–3031.
- (30) Feng, X.; Liu, L.; Honsho, Y.; Saeki, A.; Seki, S.; Irle, S.; Dong, Y.; Nagai, A.; Jiang, D. High-Rate Charge-Carrier Transport in Porphyrin Covalent Organic Frameworks: Switching from Hole to Electron to Ambipolar Conduction. *Angew. Chem. Int. Ed. Engl.* **2012**, *51*, 2618–2622.
- (31) Uribe-Romo, F. J.; Doonan, C. J.; Furukawa, H.; Oisaki, K.; Yaghi, O. M. Crystalline Covalent Organic Frameworks with Hydrazone Linkages. *J. Am. Chem. Soc.* **2011**, *133*, 11478–11481.
- (32) Yang, Z.; Xu, B.; He, J.; Xue, L.; Guo, Q.; Xia, H.; Tian, W. Solution-Processable and Thermal-Stable Triphenylamine-Based Dendrimers with Truxene Cores as Hole-Transporting Materials for Organic Light-Emitting Devices. *Org. Electron.* **2009**, *10*, 954–959.
- (33) Lambert, C.; Nöll, G.; Schmälzlin, E.; Meerholz, K.; Bräuchle, C. Synthesis, (Non)Linear Optical and Redox Properties of a Donor-Substituted Truxenone Derivative. *Chem. - A Eur. J.* **1998**, *4*, 2129–2135.
- (34) Sanguinet, L.; Williams, J. C.; Yang, Z.; Twieg, R. J.; Mao, G.; Singer, K. D.; Wiggers, G.; Petschek, R. G. Synthesis and Characterization of New Truxenones for Nonlinear Optical Applications. *Chem. Mater.* **2006**, *18*, 4259–4269.
- (35) Isoda, K.; Yasuda, T.; Kato, T. Truxene-Based Columnar Liquid Crystals: Self-Assembled Structures and Electro-Active Properties. *Chem. Asian J.* **2009**, *4*, 1619–1625.
- (36) Field, J. E.; Venkataraman, D. Heterotriangulenes - Structure and Properties. *Chem. Mater.* **2002**, *14*, 962–964.
- (37) Wan, X.; Zhang, H.; Li, Y.; Chen, Y. Self-Assembly Based on Heterotriangulene Derivatives: From Nanowires to Microrods. *New J. Chem.* **2010**, *34*, 661.

- (38) Zhang, H.; Wang, S.; Li, Y.; Zhang, B.; Du, C.; Wan, X.; Chen, Y. Synthesis, Characterization, and Electroluminescent Properties of Star Shaped Donor–acceptor Dendrimers with Carbazole Dendrons as Peripheral Branches and Heterotriangulene as Central Core. *Tetrahedron* **2009**, *65*, 4455–4463.
- (39) Pérez, E. M.; Sierra, M.; Sánchez, L.; Torres, M. R.; Viruela, R.; Viruela, P. M.; Ortí, E.; Martín, N. Concave Tetrathiafulvalene-Type Donors as Supramolecular Partners for Fullerenes. *Angew. Chem. Int. Ed. Engl.* **2007**, *46*, 1847–1851.
- (40) Pérez, E. M.; Illescas, B. M.; Herranz, M. Á.; Martín, N. Supramolecular Chemistry of Π -Extended Analogues of TTF and Carbon Nanostructures. *New J. Chem.* **2009**, *33*, 228.
- (41) Pérez, E. M.; Capodilupo, A. L.; Fernández, G.; Sánchez, L.; Viruela, P. M.; Viruela, R.; Ortí, E.; Bietti, M.; Martín, N. Weighting Non-Covalent Forces in the Molecular Recognition of C(60). Relevance of Concave-Convex Complementarity. *Chem. Commun. (Camb)*. **2008**, 4567–4569.
- (42) Pérez, E. M.; Martín, N. Curves Ahead: Molecular Receptors for Fullerenes Based on Concave-Convex Complementarity. *Chem. Soc. Rev.* **2008**, *37*, 1512–1519.
- (43) Zhao, K.-Q.; Chen, C.; Monobe, H.; Hu, P.; Wang, B.-Q.; Shimizu, Y. Three-Chain Truxene Discotic Liquid Crystal Showing High Charged Carrier Mobility. *Chem. Commun. (Camb)*. **2011**, *47*, 6290–6292.
- (44) Homnick, P. J.; Lahti, P. M. Modular Electron Donor Group Tuning of Frontier Energy Levels in Diarylamino-fluorenone Push-Pull Molecules. *Phys. Chem. Chem. Phys.* **2012**, *14*, 11961–11968.
- (45) Rathnayake, H. P.; Cirpan, A.; Karasz, F. E.; Odoi, M. Y.; Hammer, N. I.; Barnes, M. D.; Lahti, P. M. Luminescence of Molecular and Block Copolymeric 2,7-Bis(phenylethynyl)-Fluorenones; Identifying Green-Band Emitter Sites in a Fluorene-Based Luminophore. *Chem. Mater.* **2007**, *19*, 3265–3270.
- (46) Mahmood, K.; Liu, Z.-P.; Li, C.; Lu, Z.; Fang, T.; Liu, X.; Zhou, J.; Lei, T.; Pei, J.; Bo, Z. Novel Isoindigo-Based Conjugated Polymers for Solar Cells and Field Effect Transistors. *Polym. Chem.* **2013**, *4*, 3563.
- (47) Köhler, J.; Quast, T.; Buback, J.; Fischer, I.; Brixner, T.; Nuernberger, P.; Geiss, B.; Mager, J.; Lambert, C. Ultrafast Charge-Transfer Dynamics of Donor-Substituted Truxenones. *Phys. Chem. Chem. Phys.* **2012**, *14*, 11081–11089.
- (48) Wang, S.; Kivala, M.; Lieberwirth, I.; Kirchhoff, K.; Feng, X.; Pisula, W.; Müllen, K. Dip-Coating-Induced Fiber Growth of a Soluble Heterotriangulene. *Chemphyschem* **2011**, *12*, 1648–1651.
- (49) Brédas, J.-L.; Norton, J. E.; Cornil, J.; Coropceanu, V. Molecular Understanding of Organic Solar Cells: The Challenges. *Acc. Chem. Res.* **2009**, *42*, 1691–1699.

- (50) Maldonado, J.-L.; Bishop, M.; Fuentes-Hernandez, C.; Caron, P.; Domercq, B.; Zhang, Y.; Barlow, S.; Thayumanavan, S.; Malagoli, M.; Brédas, J.-L.; *et al.* Effect of Substitution on the Hole Mobility of Bis(diarylamino)biphenyl Derivatives Doped in Poly(Styrene). *Chem. Mater.* **2003**, *15*, 994–999.
- (51) Lu, Y.-M.; Wong, J.-S.; Hsu, L.-C. Characterization of Indigo-Doped poly(3-hexylthiophene):[6,6]-Phenyl C61-Butyric Acid Methyl Ester Bulk Heterojunction Solar Cells. *Thin Solid Films* **2013**, *529*, 58–61.
- (52) Nawn, G.; Oakley, S. R.; Majewski, M. B.; McDonald, R.; Patrick, B. O.; Hicks, R. G. Redox-Active, near-Infrared Dyes Based on “Nindigo” (indigo-N,N'-Diarylimine) Boron Chelate Complexes. *Chem. Sci.* **2013**, *4*, 612.
- (53) Oakley, S. R.; Nawn, G.; Waldie, K. M.; MacInnis, T. D.; Patrick, B. O.; Hicks, R. G. “Nindigo”: Synthesis, Coordination Chemistry, and Properties of Indigo Diimines as a New Class of Functional Bridging Ligands. *Chem. Commun.* **2010**, *46*, 6753–6755.
- (54) Nawn, G.; McDonald, R.; Hicks, R. G. Synthesis and Characterization of Heterobimetallic (Pd/B) Nindigo Complexes and Comparisons to Their Homobimetallic (Pd₂, B₂) Analogues. *Inorg. Chem.* **2013**, *52*, 10912–10919.
- (55) Głowacki, E. D.; Leonat, L.; Voss, G.; Bodea, M.-A.; Bozkurt, Z.; Ramil, A. M.; Irimia-Vladu, M.; Bauer, S.; Sariciftci, N. S. Ambipolar Organic Field Effect Transistors and Inverters with the Natural Material Tyrian Purple. *AIP Adv.* **2011**, *1*, 042132.
- (56) Głowacki, E. D.; Voss, G.; Leonat, L.; Irimia-Vladu, M.; Bauer, S.; Sariciftci, N. S. Indigo and Tyrian Purple - From Ancient Natural Dyes to Modern Organic Semiconductors. *Isr. J. Chem.* **2012**, *52*, 540–551.
- (57) Irimia-Vladu, M.; Głowacki, E. D.; Troshin, P. a; Schwabegger, G.; Leonat, L.; Susarova, D. K.; Krystal, O.; Ullah, M.; Kanbur, Y.; Bodea, M. a; *et al.* Indigo - A Natural Pigment for High Performance Ambipolar Organic Field Effect Transistors and Circuits. *Adv. Mater.* **2011**, 375–380.
- (58) Irimia-Vladu, M.; Troshin, P. a.; Reisinger, M.; Shmygleva, L.; Kanbur, Y.; Schwabegger, G.; Bodea, M.; Schwödiauer, R.; Mumyatov, A.; Fergus, J. W.; *et al.* Biocompatible and Biodegradable Materials for Organic Field-Effect Transistors. *Adv. Funct. Mater.* **2010**, *20*, 4069–4076.
- (59) The Microscale Synthesis of Indigo Dye. In *Microscale Chemistry*; Skinner, J., Ed.; Education Division, Royal Society of Chemistry, 1997; pp. 188–189.
- (60) McKee, J. R.; Zanger, M. A Microscale Synthesis of Indigo: Vat Dyeing. *J. Chem. Educ.* **1991**, *68*, A242.
- (61) Stalder, R.; Mei, J.; Graham, K. R.; Estrada, L. A.; Reynolds, J. R. Isoindigo, a Versatile Electron-Deficient Unit For High-Performance Organic Electronics. *Chem. Mater.* **2014**, *26*, 664–678.

- (62) Wang, E.; Mammo, W.; Andersson, M. R. 25th Anniversary Article: Isoindigo-Based Polymers and Small Molecules for Bulk Heterojunction Solar Cells and Field Effect Transistors. *Adv. Mater.* **2014**, n/a–n/a.
- (63) Deng, P.; Zhang, Q. Recent Developments on Isoindigo-Based Conjugated Polymers. *Polym. Chem.* **2014**.
- (64) Estrada, L. A.; Stalder, R.; Abboud, K. A.; Risko, C.; Brédas, J.-L.; Reynolds, J. R. Understanding the Electronic Structure of Isoindigo in Conjugated Systems: A Combined Theoretical and Experimental Approach. *Macromolecules* **2013**, *46*, 8832–8844.
- (65) Robb, M. J.; Ku, S.-Y.; Brunetti, F. G.; Hawker, C. J. A Renaissance of Color: New Structures and Building Blocks for Organic Electronics. *J. Polym. Sci. Part A Polym. Chem.* **2013**, *51*, 1263–1271.
- (66) Liu, S.; Wang, W. M.; Briseno, A. L.; Mannsfeld, S. C. B.; Bao, Z. Controlled Deposition of Crystalline Organic Semiconductors for Field-Effect-Transistor Applications. *Adv. Mater.* **2009**, *21*, 1217–1232.
- (67) De Boer, R. W. I.; Gershenson, M. E.; Morpurgo, A. F.; Podzorov, V. Organic Single-Crystal Field-Effect Transistors. *Phys. status solidi* **2004**, *201*, 1302–1331.
- (68) Mei, J.; Diao, Y.; Appleton, A. L.; Fang, L.; Bao, Z. Integrated Materials Design of Organic Semiconductors for Field-Effect Transistors. *J. Am. Chem. Soc.* **2013**, *135*, 6724–6746.
- (69) Briseno, A. L.; Tseng, R. J.; Ling, M.-M.; Falcao, E. H. L.; Yang, Y.; Wudl, F.; Bao, Z. High-Performance Organic Single-Crystal Transistors on Flexible Substrates. *Adv. Mater.* **2006**, *18*, 2320–2324.
- (70) Reese, C.; Bao, Z. Organic Single-Crystal Field-Effect Transistors. *Mater. Today* **2007**, *10*, 20–27.
- (71) Briseno, A. L.; Aizenberg, J.; Han, Y.-J.; Penkala, R. a; Moon, H.; Lovinger, A. J.; Kloc, C.; Bao, Z. Patterned Growth of Large Oriented Organic Semiconductor Single Crystals on Self-Assembled Monolayer Templates. *J. Am. Chem. Soc.* **2005**, *127*, 12164–12165.
- (72) Gao, X.; Hu, Y. Development of N-Type Organic Semiconductors for Thin Film Transistors: A Viewpoint of Molecular Design. *J. Mater. Chem. C* **2014**.
- (73) Anthony, J. E.; Facchetti, A.; Heeney, M.; Marder, S. R.; Zhan, X. N-Type Organic Semiconductors in Organic Electronics. *Adv. Mater.* **2010**, *22*, 3876–3892.
- (74) Usta, H.; Facchetti, A.; Marks, T. J. N-Channel Semiconductor Materials Design for Organic Complementary Circuits. *Acc. Chem. Res.* **2011**, *44*, 501–510.
- (75) Zhao, Y.; Guo, Y.; Liu, Y. 25th Anniversary Article: Recent Advances in N-Type and Ambipolar Organic Field-Effect Transistors. *Adv. Mater.* **2013**, *25*, 5372–5391.

- (76) Newman, C. R.; Frisbie, C. D.; da Silva Filho, D. A.; Brédas, J.-L.; Ewbank, P. C.; Mann, K. R. Introduction to Organic Thin Film Transistors and Design of N-Channel Organic Semiconductors. *Chem. Mater.* **2004**, *16*, 4436–4451.
- (77) Jones, B. A.; Ahrens, M. J.; Yoon, M.-H.; Facchetti, A.; Marks, T. J.; Wasielewski, M. R. High-Mobility Air-Stable N-Type Semiconductors with Processing Versatility: Dicyanoperylene-3,4:9,10-Bis(dicarboximides). *Angew. Chemie Int. Ed.* **2004**, *43*, 6363–6366.
- (78) Facchetti, A.; Yoon, M.-H.; Stern, C. L.; Katz, H. E.; Marks, T. J. Building Blocks for N-Type Organic Electronics: Regiochemically Modulated Inversion of Majority Carrier Sign in Perfluoroarene-Modified Polythiophene Semiconductors. *Angew. Chemie Int. Ed.* **2003**, *42*, 3900–3903.
- (79) Usta, H.; Risko, C.; Wang, Z.; Huang, H.; Deliomeroglu, M. K.; Zhukhovitskiy, A.; Facchetti, A.; Marks, T. J. Design, Synthesis, and Characterization of Ladder-Type Molecules and Polymers. Air-Stable, Solution-Processable N-Channel and Ambipolar Semiconductors for Thin-Film Transistors via Experiment and Theory. *J. Am. Chem. Soc.* **2009**, *131*, 5586–5608.
- (80) Qi, D.; Zhang, L.; Jiang, J. Toward Panchromatic Organic Functional Molecules: Density Functional Theory Study on the Nature of the Broad UV–Vis–NIR Spectra of Substituted Tetra(azulene)porphyrins. *J. Mol. Graph. Model.* **2012**, *38*, 304–313.
- (81) Meiss, J.; Merten, A.; Hein, M.; Schuenemann, C.; Schäfer, S.; Tietze, M.; Urich, C.; Pfeiffer, M.; Leo, K.; Riede, M. Fluorinated Zinc Phthalocyanine as Donor for Efficient Vacuum-Deposited Organic Solar Cells. *Adv. Funct. Mater.* **2012**, *22*, 405–414.
- (82) Ragoussi, M.-E.; Ince, M.; Torres, T. Recent Advances in Phthalocyanine-Based Sensitizers for Dye-Sensitized Solar Cells. *European J. Org. Chem.* **2013**, *2013*, 6475–6489.
- (83) Péchy, P.; Renouard, T.; Zakeeruddin, S. M.; Humphry-Baker, R.; Comte, P.; Liska, P.; Cevey, L.; Costa, E.; Shklover, V.; Spiccia, L.; *et al.* Engineering of Efficient Panchromatic Sensitizers for Nanocrystalline TiO₂-Based Solar Cells. *J. Am. Chem. Soc.* **2001**, *123*, 1613–1624.
- (84) K. Nazeeruddin, M.; Pechy, P.; Gratzel, M. Efficient Panchromatic Sensitization of Nanocrystalline TiO₂ Films by a Black Dye Based on a Trithiocyanato-Ruthenium Complex. *Chem. Commun.* **1997**, 1705–1706.
- (85) Anderson, P. A.; Strouse, G. F.; Treadway, J. A.; Keene, F. R.; Meyer, T. J. Black MLCT Absorbers. *Inorg. Chem.* **1994**, *33*, 3863–3864.

CHAPTER 9

EXPERIMENTAL AND SYNTHETIC PROCEDURES

9.1 Materials, Abbreviations, Instrumentation, Computational Methods

All reactions were carried out in sealed round bottom flasks under nitrogen atmosphere unless otherwise specified, and heated using sand baths. Tetrahydrofuran (THF) and toluene were freshly distilled from sodium/benzophenone before use, and dichloromethane (DCM) was freshly distilled from phosphorous pentoxide. All other solvents and commercial reagents were used as received unless otherwise stated. Abbreviations used for various solvents and reagents can be found on page 157.

All new compounds were identified by $^1\text{H-NMR}$ and high resolution mass spectrometry (FAB). $^1\text{H-NMR}$ and $^{13}\text{C-NMR}$ spectra were recorded on a Bruker Avance 400 MHz FT-NMR spectrometer, and the chemical shifts recorded in ppm downfield of tetramethylsilane. Mass spectral data were obtained at the University of Massachusetts Mass Spectrometry Facility, which is supported in part by the National Science Foundation. UV-vis-NIR, photoluminescence, and FT-IR spectra were obtained at room temperature using a Shimadzu UV-3600 UV-vis-NIR spectrophotometer, a Photon Technology International QuantaMaster 30 Phosphorescence/Fluorescence spectrophotometer, and a Bruker Alpha FT-IR spectrophotometer fitted with a Platinum ATR QuickSnap sampling module, respectively. Purities were established by HPLC obtained on a Buck Scientific BLC-10-11 instrument with a C18 reverse-phase column, using acetonitrile as solvent eluent at a rate of 0.25 mL/min where HPLC analysis is indicated below. Melting points are uncorrected. Cyclic voltammograms were obtained using a BASi Epsilon Electrochemical Workstation equipped with platinum auxiliary and working electrodes, and an Ag/AgCl reference electrode using 0.1 M tetrabutylammonium hexafluorophosphate as conducting electrolyte in acetonitrile and 0.01 M ferrocene in acetonitrile as an external standard. X-ray crystallography was either performed at UMass using a Bruker-Nonius Kappa-CCD diffractometer, or done where stated by Prof. Joel T. Mague at Tulane University or by Dr. John

A. Schleuter at Argonne National Lab. Field effect transistor (FET) charge carrier mobility measurements were carried out under inert atmosphere using an Agilent 4156C precision semiconductor parameter analyzer. All computations were carried out using Gaussian 09 Revision B.01 or Spartan10 on a Linux computer running openSuSE. Molecular geometries were optimized using the methodologies described for each system, and molecular orbital diagrams were generated from the final checkpoint files using GaussView version 5.0.9 or Spartan10 with default parameter settings, unless otherwise stated. The following abbreviations are used for various solvents and reagents:

Table 9.1: Abbreviations for solvents and reagents used in this chapter.

1,1'-Bis(diphenylphosphino)ferrocene	DPPF	<i>n</i> -butyllithium	<i>n</i> -BuLi
Antimony pentachloride	SbCl ₅	Nitric acid	HNO ₃
Boron tribromide	BBr ₃	<i>ortho</i> -dichlorobenzene	<i>o</i> -DCB
Bromine	Br ₂	Palladium (0) dibenzylideneacetone	Pd ₂ dba ₃
Cesium carbonate	Cs ₂ CO ₃	Palladium (II) acetate	Pd(OAc) ₂
Chloroform	CHCl ₃	Palladium on carbon	Pd/C
Chromium trioxide	CrO ₃	Palladium tetrakis	Pd(PPh ₃) ₄
Copper	Cu	Potassium carbonate	K ₂ CO ₃
Copper (I) iodide	CuI	Potassium fluoride	KF
Copper (II) sulfate	CuSO ₄	Potassium hydroxide	KOH
Copper perchlorate	CuClO ₄	Potassium permanganate	KMnO ₄
Deuteriochloroform	CDCl ₃	Silver hexafluoroantimonate	AgSbF ₆
Dichloromethane	DCM	Silver sulfate	AgSO ₄
Diethyl ether	Et ₂ O	Sodium carbonate	Na ₂ CO ₃
Dimethylsulfoxide	DMSO	Sodium hydroxide	NaOH
Ethanol	EtOH	Sodium tert-butoxide	<i>t</i> -BuONa
Ethyl acetate	EtOAc	Sulfuric acid	H ₂ SO ₄
Hexadeutero dimethylsulfoxide	DMSO- <i>d</i> ₆	Tetrahydrofuran	THF
Hydrochloric acid	HCl	Thin layer chromatography	TLC
Hydrogen bromide	HBr	Thionyl chloride	SOCl ₂
Iodine	I ₂	Tin tetrachloride	SnCl ₄
Lead tetraacetate	Pb(OAc) ₄	Toluene	Tol, PhMe
Magnesium sulfate	MgSO ₄	Tributyltin chloride	SnBu ₃ Cl
Methanol	MeOH	Trifluoroacetic acid	TFA
Methyltriphenylphosphonium bromide	CH ₃ PPh ₃ Br	Tri- <i>ortho</i> -tolyl phosphine	P(<i>o</i> -tolyl) ₃
<i>N,N'</i> -dimethylethylenediamine	DMEDA	Tri- <i>tert</i> -butyl phosphine	P(<i>t</i> -Bu) ₃
<i>N,N</i> -dimethylformamide	DMF	Water	H ₂ O

9.2 Triarylamine Oxidation Experiments¹

Neutral triarylamines were oxidized by two procedures. For the *precipitation protocol*, roughly 30 μM amine was dissolved in toluene and treated with SbCl_5 to give a very dark, powdery precipitate that could be isolated by filtration, and stored under ambient conditions for months. Re-dissolution of these precipitates in dichloromethane readily yielded the characteristic colors of the aminium cation species.

For the *solution oxidation protocol*, the triarylamine was dissolved in dry dichloromethane and directly treated with oxidants such as SbCl_5 , AgSbF_6 , $\text{Pb}(\text{OAc})_4$; alternatively, it was dissolved in acetonitrile for oxidation with CuClO_4 . A set of at least five 2 mL triarylamine stock solutions on the order of 10^{-5} M were treated by mixing with increasingly concentrated 2 mL oxidant solutions, from 0.2 eq up to 5 eq oxidant, and their UV-vis-NIR spectra were obtained immediately. Titration curves were plotted for absorption peak maximum values versus amounts of oxidant used, and molar absorptivities were calculated for the oxidized species by assuming 100 % conversion of the neutral triarylamine precursors.

EPR spectra were obtained at room temperature by the solution oxidation protocol, or by re-dissolving products from the precipitation oxidation protocol. Hyperfine coupling constants were obtained by spectral simulation, and g-values obtained for spectra were calibrated using a built-in frequency counter and an E-036TM teslameter on a Bruker Elexsys E-500 spectrometer.

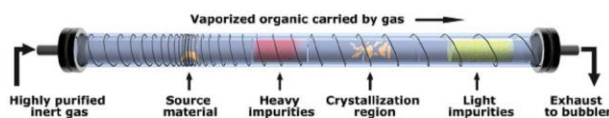
9.3 Field Effect Transistors (FET - Thin Film, Spin-Cast)

A given compound was dissolved in a good solvent typically at about 10 mg/mL concentration, and spin-coated at 1000 RPM onto a Fraunhofer OFET-G4 substrate circuit for one minute with a 3 second ramp-up time. The substrates were purchased from Fraunhofer IPMS (Dresden, Germany) as prefabricated wafers with sixteen device regions, four sets each of four different channel lengths, 2.5, 5.0, 10, and 20 μm . The device configuration was a bottom-contact, Si/SiO_2 (230 nm SiO_2) substrate with four sets of 30 nm thick gold contacts with 1.0 mm channel width. Spin-coated devices were analyzed under inert atmosphere using an Agilent

4156C precision semiconductor parameter analyzer. Two transistors of each channel length were tested as-spun, and the final two transistors in each channel length set were tested after annealing at approximately 60 °C for 30 min. Squaraine material FETs were analyzed by Dr. Andrea Della Pelle.

9.4 Chemical Vapor Deposition (CVD)

Crystallization by chemical vapor deposition was performed under nitrogen flow using either a homemade tube furnace or a Thermo Scientific Lindberg Blue M tube furnace. The general process is shown in Scheme 9.1 below, illustrated using a homemade furnace with temperature zones controlled by the spacing between heating wire wraps (black spiral). A quartz tube (about 1'' inner diameter) is fitted with several 3'' glass tubes arranged end-to-end along its entire length. A small spatula full of the sample material is placed in a small pile within the inner glass tube at the high-temperature zone, and the quartz tube is inserted in a larger tube with heating wire wrapped around it with variable spacing to control temperature. The quartz tube ends are fitted with gas inlet/outlet caps, and purified inert gas (typically nitrogen) is passed slowly through the CVD chamber.



Scheme 9.1: Typical chemical vapor deposition crystal growth process. Reproduced from Bao and coworkers (permission license number 3360900411130).²

Once the apparatus is assembled and the gas is flowing, the temperature at the hot zone is increased to approximately the melting point of the sample material. BUT, the effective hot zone temperature varies from sample to sample, since some materials require a higher or lower temperature than their recorded melting point to sublime an appreciable amount. As a result, trial and error with temperature control and gas flow rates is typically unavoidable. Under the proper operating conditions, chemical vapor is transported with the carrier gas from the source material down the tube toward increasingly cooler temperature zones, where the material may finally

crystallize or form a film. The intermediate zone between the crystallization and source zones may collect heavy impurities, while the cooler zones past the crystallization zone may collect lighter impurities. Purified material at the crystallization zone can be collected by carefully removing the inner glass sleeves. Most of this work was done in with mentorship and assistance from Professor Alex Briseño using home-made CVD apparatus.

9.5 General Synthetic and Purification Procedures

Copper Purification Procedure

I₂ (0.4 g, 3.15 mmol) was dissolved in 40 mL of acetone with stirring. Cu powder (2.0 g, 31.5 mmol, mesh size not available) was added and the mixture stirred for 15 min. During this time, the mixture becomes grayish in color and the Cu settles to the bottom when stirring is stopped. The solids were filtered and were twice stirred in 50 mL of 1:1 concentrated HCl/acetone for 15 min with subsequent filtration. The final filtered solids were washed with acetone, and dried under vacuum. This purified copper retained catalytic effectiveness for a couple of weeks when stored in a desiccator with no special efforts taken to ensure inert atmosphere.

General Procedure for the Oxidation of Fluorene Derivatives:

This procedure was adapted from the literature.³ A fluorene derivative was combined with sufficient acetic anhydride to make a 0.1 M solution. Then, 2.5 eq of CrO₃ was slowly added and the reaction mixture stirred at room temperature overnight, during which it turned from a dark brown slurry to a dark green slurry with yellowish particulates. The mixture was poured into excess 1:1 ice/H₂O, acidified with conc. HCl, and stirred until the ice was melted. Vacuum filtration yielded a powdery yellow solid which was thoroughly washed with water to give the product. Recrystallization from 95% EtOH afforded pure product if the crude material was impure after filtering and washing (generally only necessary for large-scale reactions, e.g. 10 g).

Alternative Procedure for the Oxidation of Fluorene Derivatives (via Cs₂CO₃):

A 9-*H*-fluorene derivative and 2.5 eq of Cs₂CO₃ were added sequentially to sufficient dry DMSO to make a 0.5 M solution, and dry air was passed over the briskly stirred reaction mixture overnight. The reaction mixture was then poured into water, filtered, and the aqueous layer extracted with solvents such as DCM or EtOAc. The organic layers were combined, dried over anhydrous MgSO₄, filtered, and the solvent evaporated; the crude product is purified as described if necessary. Yield is typically quantitative.

General Procedure for Heck Coupling:

Aryl halide (ArX; X = Br or I), a styrene derivative, 0.2 eq of P(*o*-tolyl)₃ plus 0.07 eq of Pd(OAc)₂ (with respect to ArX) were combined under nitrogen atmosphere. Dry DMF (5 mL per 1 mmol of ArX) was added and the reaction mixture was heated to 80 °C under nitrogen. After stirring at 80 °C for 30 min, freshly nitrogen-sparged triethylamine (1 mL per 1 mmol of ArX) was added and the reaction stirred until complete by TLC. The reaction mixture was then allowed to cool to room temperature, poured into approximately aqueous 1 M HCl and stirred for 15 min. Any resulting solids were separated by filtration and dissolved in CHCl₃; the filtrate was also extracted using CHCl₃. The combined organic layers were filtered through Celite, dried over anhydrous MgSO₄, and concentrated *in vacuo*. The resulting solids were purified as described.

General Procedure for Buchwald-Hartwig Amination:

Aryl halide (ArX; X = Br, I), aryl amine, 0.02 eq of P(*t*-butyl)₃, 0.02 eq of Pd₂dba₃, and 1.06 eq of *t*-BuONa were combined under nitrogen. Toluene (5 mL per 1 mmol of ArX) was added and the reaction mixture was heated at 110 °C until complete by TLC. The reaction mixture was allowed to cool to room temperature, filtered through Celite, and concentrated *in vacuo*. The resulting solids were purified as described below for each specific compound prepared using this procedure.

General Procedure for Knoevenagel Condensation Reactions between Fluorenone Derivatives and Malononitrile:

This procedure was adapted from the literature.⁴ A mixture of 1 eq of fluorenone derivative and 6 eq of malononitrile were added to a flask under nitrogen atmosphere, enough dry DMSO added to make a 0.1 M solution, and the reaction mixture heated with stirring at 110 °C under nitrogen until complete by TLC. The reaction was then cooled to room temperature, and worked up and purified as described below for each specific compound prepared using this procedure.

General Procedure for Buchwald/Ullmann-Goldberg Amidation:

This procedure was adapted from the literature.^{5,6} Aryl halide (ArX; X = Br, I), BOC-aniline derivative, 0.2 eq of *N,N'*-dimethylethylenediamine (DMEDA), 0.1 eq of CuI, and 1.5 eq of K₂CO₃ were placed in a flask under nitrogen, toluene (freshly distilled from potassium, 5 mL per 1 mmol ArX) was added and the reaction mixture heated at 110 °C until complete by TLC. [CAUTION: potassium metal is very hazardous if exposed to even small amounts of water, alcohols, or organohalides! Appropriate precautions are required!] The reaction mixture was allowed to cool to room temperature, filtered through Celite, and concentrated *in vacuo*. The resulting solids were purified as described below for each specific compound prepared using this procedure.

General Procedure for Ullmann Coupling:

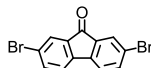
Arylamine, 3 eq of aryl iodide, 0.2 eq of Cu (freshly purified using the above procedure), 0.1 eq of anhydrous CuSO₄, 0.1 eq of sodium ascorbate, and 2.3 eq of anhydrous K₂CO₃ were placed in a flask under nitrogen, *o*-dichlorobenzene (5 mL per 1 mmol arylamine) was added, and the reaction mixture heated at 230 °C until complete by TLC. The reaction mixture was allowed to cool to room temperature, filtered through Celite, and concentrated *in vacuo*. The resulting *o*-DCB solution/suspension was purified as described below for each specific compound prepared using this procedure.

General Procedure for Demethylation:

A methoxybenzene derivative was dissolved in dry DCM under nitrogen and cooled to -78 °C. BBr₃ (1 eq per -OCH₃ group) was added dropwise and the reaction mixture stirred at room temperature overnight. The reaction mixture was poured onto ice, neutralized with saturated aq. Na₂CO₃ (caution: foaming), and extracted with DCM. The combined organic layers were dried over anhydrous MgSO₄, filtered, and concentrated *in vacuo*. Crude product was typically acceptable to use in subsequent steps without further purification.

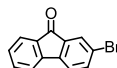
9.6 Specific Synthetic and Purification Procedures

2,7-Dibromo-9H-fluoren-9-one:



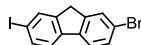
Prepared using the general procedure for fluorene derivative oxidation from 2,7-dibromofluorene (Aldrich). Mp = 202-203 °C (lit mp = 202-203 °C).³ ¹H-NMR (400 MHz, CDCl₃): 7.40 (d, 2H, J = 8 Hz), 7.64 (dd, J = 8 Hz, 2 Hz, 2H), 7.77 (d, J = 2 Hz, 2H).

2-Bromo-9H-fluoren-9-one:



Prepared using the general procedure for fluorene derivative oxidation from 2-bromofluorene (Aldrich). Mp = 147-149 °C (lit mp = 146-148 °C).⁷ ¹H-NMR (400 MHz, CDCl₃): 7.31 (s, 1H), 7.40-7.42 (d, 1H, J = 8 Hz), 7.50-7.52 (m, 2H), 7.61-7.63 (dd, 1H, J = 8 Hz, 2 Hz), 7.66-7.68 (d, 1H, J = 8 Hz), 7.77 (d, 1H, J = 2 Hz).

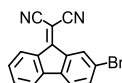
2-Bromo-7-iodo-9H-fluorene:



2-Bromofluorene (1.00 g, 4.08 mmol), I₂ (0.434 g, 1.71 mmol), and KIO₃ (0.210 g, 0.979 mmol) were added to a round bottom flask under nitrogen atmosphere. Upon addition of a solution of 1.2 mL H₂SO₄ in 22 mL of acetic acid, the resulting suspension turned dark red and the mixture was heated at 90 °C for 2 h. The reaction was cooled to room temperature and the

resulting yellow precipitate was vacuum filtered and washed sequentially with acetic acid and then H₂O. The filtered solid was recrystallized from DCM/MeOH to give 1.03 g (68% yield) of white crystalline solid. Mp = 184-185°C (lit mp = 178-180 °C).^{8,9} ¹H-NMR (400 MHz, CDCl₃): 3.86 (s, 2H), 7.48-7.51 (m, 2H), 7.60-7.62 (d, 1H, J = 8 Hz), 7.67 (s, 1H), 7.69-7.71 (d, 1H, J = 8 Hz), 7.88 (s, 1H).

2-Bromo-9H-fluorylinene malononitrile:



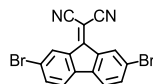
Prepared using the general procedure for Knoevenagel condensation from 2-bromo-fluorenone. 85% yield. Mp = 297-299 °C (no lit mp). ¹H-NMR (400 MHz, CDCl₃): 7.36 (m, 1H), 7.44 (d, 1H, J = 8 Hz), 7.53 (m, 1H), 7.64 (dd, 1H, J = 8 Hz, 2 Hz), 8.39 (d, 1H, J = 8 Hz), 8.50 (d, 1H, J = 2 Hz).

9H-fluorylinene malononitrile:



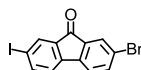
Prepared using the general procedure for Knoevenagel condensation from fluorenone. 97% yield. Mp = 231-233 °C (lit mp = 230-232 °C).¹⁰ ¹H-NMR not obtained.

2,7-Dibromo-9H-fluorylinene malononitrile:



Prepared using the general procedure for Knoevenagel condensation from 2,7-dibromofluorenone. 96% yield. Mp not obtained. ¹H-NMR not obtained.

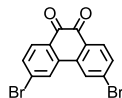
2-Bromo-7-iodo-9H-fluorenone:



Prepared using the general procedure for fluorene derivative oxidation from 2-bromo-7-iodofluorene. 97 % yield. Mp = 198-200 °C (no lit mp) ¹H-NMR (400 MHz, CDCl₃): 7.28 (d,

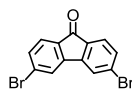
1H, J = 8 Hz), 7.39-7.41 (d, 1H, J = 8 Hz), 7.62-7.64 (dd, 1H, J = 8 Hz, 2 Hz), 7.77 (d, 1H, J = 2 Hz), 7.83-7.86 (dd, 1H, J = 8 Hz, 2 Hz), 7.97 (d, 1H, J = 2 Hz).

Dibromophenanthrenequinone [3,6-dibromophenanthrene-9,10-dione]:



This procedure was modified from the literature.¹¹ 9,10-phenanthraquinone (10.4 g, 50.0 mmol) and benzoyl peroxide (0.400 g, 1.66 mmol) were dissolved in 50 mL of nitrobenzene. The solution was heated to 110 °C while stirring. Br₂ (5.57 mL, 108 mmol) was slowly dripped into the reaction mixture using an addition funnel, while exposing the vessel to light using a simple desktop incandescent lamp. The mixture was heated at 110 °C for another 2 h, then cooled to room temperature, poured into 100 mL of cold methanol, and the resulting precipitate filtered. Recrystallization from hot nitrobenzene afforded 11.84 g of product as yellow-orange needles (65% yield). Mp = 294-296 °C (lit mp = 278-279 °C).¹² ¹H NMR (DMSO-*d*₆, 400 MHz): 7.85-7.78 (dd, 2H, J = 8 Hz, 2 Hz), 7.92-7.94 (d, 2H, J = 8 Hz), 8.67 (s, 2H).

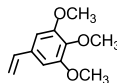
3,6-Dibromofluorenone [3,6-dibromo-9H-fluoren-9-one]:



This procedure was modified from the literature.¹¹ In a three-necked round-bottom flask, KOH (5.98 g, 107 mmol) was dissolved in about 15 mL of H₂O and heated to 130 °C. Next, 3,6-dibromophenanthrenequinone (3.00 g, 8.20 mmol) was added and the reaction heated with stirring for 30 min, during which it became viscous and darker in color. Then, KMnO₄ (6.87 g, 43.4 mmol) was slowly added to the reaction mixture over 2 h, which was allowed to react for an additional hour at 130 °C. The mixture was cooled to room temperature and treated with several drops of conc. H₂SO₄. Solid sodium bisulfite was slowly added to quench excess KMnO₄ until the solution became pale yellow in color. The resulting solids were filtered, washed liberally with cold water, and thoroughly air-dried. Recrystallization from hot 95% ethanol gave 1.86 g of

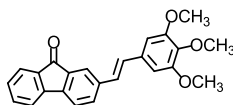
product as a yellow powder (67 % yield). Mp = 258-261 °C (lit mp = 320-323 °C).¹³ ¹H NMR (CDCl₃, 300 MHz): 7.50-7.58 (m, 2H), 7.67-7.71 (m, 2H), 8.08-8.14 (m, 2H).

Trimethoxystyrene (1,2,3-trimethoxy-5-vinylbenzene):



This procedure was modified from the literature.¹⁴ CH₃PPh₃Br (9.64 g, 27 mmol) was added to a three-neck round bottom flask under nitrogen atmosphere. Dry THF (150 mL) was added and the suspension cooled to 0 °C. n-BuLi (14.4 mL, 2.5 M in hexanes 30.6 mmol) was added dropwise and the solution allowed to warm to room temperature for 10 min to give a yellow ylide solution. [CAUTION: n-BuLi is a fire hazard and extremely reactive with even small amounts of water or alcohols! Appropriate precautions are required!] 3,4,5-Trimethoxybenzaldehyde (4.00 g, 20.4 mmol) was dissolved in 50 mL of dry THF under nitrogen atmosphere and then added dropwise to the ylide solution. The reaction mixture was allowed to stir overnight, after which the resulting light yellow milky suspension was poured into H₂O stirred for 10 min. The organic layer was separated, and the aqueous layer was extracted with Et₂O. The combined organic extracts were dried over anhydrous MgSO₄, concentrated *in vacuo*, and purified on silica eluted with Et₂O to yield 3.33 g (84%) of clear yellow oil. ¹H-NMR (400 MHz, CDCl₃): 3.84 (s, 3H), 3.87 (s, 6H), 5.20 (d, 1H, J = 12 Hz), 5.657 (d, 1H, J = 16 Hz), 6.63 (m, 3H).

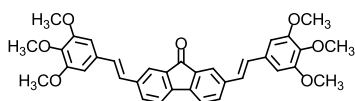
FOS (*E*)-2-(3,4,5-trimethoxystyryl)-9H-fluoren-9-one:¹⁵



Prepared using the general procedure for Heck coupling using 0.500 g (1.93 mmol) of 2-bromofluorenone and 0.431 g (2.22 mmol) of 3,4,5-trimethoxystyrene after a 3 day reaction time. The reaction mixture was poured into acidified water, stirred for 10 min, extracted with DCM, and filtered through Celite to give an orange-red solution. The filtrate was washed with H₂O,

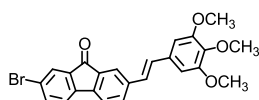
dried over anhydrous MgSO_4 , and concentrated *in vacuo* to give an orange-red pasty solid. The crude material was recrystallized from 100 % EtOH and further purified by flash chromatography on silica eluted with 1:3 ethyl acetate/hexanes to give 0.121 g of orange solid (17 % yield). Mp = 147-149 °C; ATR-IR (neat, cm^{-1}) 1703 (s, C=O str); $^1\text{H-NMR}$ (400 MHz, CDCl_3): 3.88 (s, 3H), 3.93 (s, 6H), 6.75 (s, 2H), 6.99-7.03 (d, 1H, J = 16 Hz), 7.10-7.14 (d, 1H, J = 16 Hz), 7.30-7.31 (td, 1H, J = 16 Hz, J' = 8 Hz, J'' = 1.6 Hz), 7.48-7.53 (m, 3H), 7.56-7.57 (dd, 1H, J = 16 Hz, J' = 8 Hz), 7.66-7.68 (d, 1H, J = 8 Hz), 7.87 (s, 1H); MS (FAB, m/z): found 372.1362, calculated for $\text{C}_{24}\text{H}_{20}\text{O}_4$ 372.1362.

FODS (2,7-(*E,E*)-bis(3,4,5-trimethoxystyryl)-9*H*-fluoren-9-one):



Prepared using the general procedure for Heck Coupling using 2.50 g (7.40 mmol) of 2,7-dibromo-9*H*-fluoren-9-one and 3.30 g (17.0 mmol) of trimethoxystyrene. After three days, the product mixture was worked up as described in the general procedure. The resulting red solid was further triturated with ethanol, then recrystallized from boiling 95% ethanol to yield 3.42 g (82 %) of product. Mp = 170-172 °C (lit mp = 168-172 °C).³ $^1\text{H-NMR}$ (400 MHz, CDCl_3): 3.88 (s, 6H), 3.93 (s, 12H), 6.75 (s, 4H), 6.98-7.03 (d, 2H, J = 16 Hz), 7.10-7.14 (d, 2H, J = 16 Hz), 7.48-7.50 (d, 2H, J = 8 Hz), 7.56-7.58 (dd, 2H, J = 8 Hz, 2 Hz), 7.86 (s, 2H).

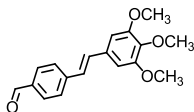
2-BrFOPV [(*E*)-2-bromo-7-(3,4,5-trimethoxystyryl)-9*H*-fluoren-9-one]:¹⁵



Prepared using the general procedure for Heck Coupling using 1.00 g (2.60 mmol) of 2-bromo-7-iodo-9*H*-fluorenone and 0.504 g (2.60 mmol) of 1,2,3-trimethoxy-5-vinylbenzene (trimethoxystyrene). After three days, the product mixture was worked up as described in the general procedure. The resulting red solid was triturated with ethanol, then recrystallized from boiling DCM/MeOH to yield 0.515 g (44 %) of product. Mp = 218-220 °C. $^1\text{H-NMR}$ (400 MHz,

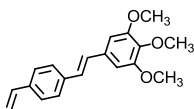
CDC13): 3.88 (s, 3H), 3.93 (s, 6H), 6.75 (s, 2H), 6.98-7.02 (d, 1H, J = 16 Hz), 7.09-7.13 (d, 1H, J = 16 Hz) 7.50-7.52 (d, 1H, J = 8 Hz), 7.55-7.59 (t, 2H, J = 7 Hz), 7.74-7.76 (dd, 1H, J = 8 Hz, 2 Hz), 7.86 (s, 1H), 7.89 (s, 1H).

TMSBA (trimethoxystyrylbenzaldehyde) [(E)-4-(3,4,5-trimethoxystyryl)benzaldehyde]:



Prepared using the general procedure for Heck Coupling using 2.28 g (11.7 mmol) trimethoxystyrene and 3.09 g (10.7 mmol) *p*-bromobenzaldehyde. After three days the reaction mixture was worked up as described in the general procedure. The resulting orange solid was purified on silica eluted with EtOAc/hexanes (1:9 increasing in polarity to 9:1) to yield 1.94 g (61 %) of product as a yellow-orange solid. Mp not determined. ¹H-NMR (400 MHz, CDCl₃): 3.89 (s, 3H), 3.93 (s, 6H), 6.78 (s, 2H), 7.03-7.07 (d, 1H, J = 16 Hz), 7.18-7.22 (d, 1H, J = 16 Hz), 7.64-7.66 (d, 2H, J = 8 Hz), 7.86-7.88 (d, 2H, J = 8 Hz), 10.0 (s, 1H).

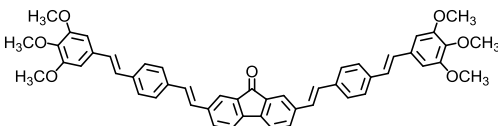
TMSS (trimethoxystyrylstyrene) [(E)-1,2,3-trimethoxy-5-(4-vinylstyryl)benzene]:



CH₃PPh₃Br (4.00 g, 11.2 mmol) was added to a three-neck round bottom flask under nitrogen atmosphere. Dry THF (70 mL) was added and the suspension cooled to 0 °C. *n*-BuLi (5.2 mL, 2.5 M in hexanes, 12.9 mmol) was added dropwise and the solution allowed to warm to room temperature for 10 min. [CAUTION: *n*-BuLi is a fire hazard and extremely reactive with even small amounts of water or alcohols! Appropriate precautions are required!]] Solid TMSBA (2.57 g, 8.62 mmol) was added in portions and the reaction mixture was allowed to stir overnight. The resulting yellowish-brown reaction mixture was poured into 150 mL H₂O and the organic layer separated. The aqueous layer was extracted with CHCl₃, then the combined organic extracts were dried over MgSO₄, concentrated *in vacuo*, and purified on silica eluted with Et₂O/hexanes (9:1) to yield 1.69 g (66%) of light yellow crystalline solid. Mp not determined. ¹H-NMR (400

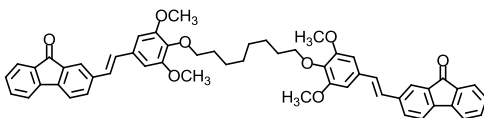
MHz, CDCl₃): 3.87 (s, 3H), 3.92 (s, 6H), 5.24-5.27 (d, 1H, J = 12 Hz), 5.75-5.79 (d, 1H, J = 16 Hz), 6.64-6.75 (m, 3H), 6.97-7.01 (d, 1H, J = 16 Hz), 7.03-7.07 (d, 1H, J = 16 Hz), 7.40-7.42 (d, 2H, J = 8 Hz), 7.46-7.48 (d, 2H, J = 8 Hz).

FODS2 [2,7-bis(4-(3,4,5-trimethoxystyryl)styryl)-9H-fluoren-9-one]:



Prepared using the general procedure for Heck Coupling using 0.272 g (0.805 mmol) 2,7-dibromo-9H-fluoren-9-one and 0.500 g (1.69 mmol) TMSS. After three days the reaction mixture was worked up as described in the general procedure. Crude product was extracted with CHCl₃, dried over anhydrous MgSO₄, concentrated *in vacuo*, and purified on silica eluted with EtOAc/hexanes (1:9 ratio increasing in polarity to 100% EtOAc), and then eluted further with DCM/EtOAc (1:1) to yield 0.141 g (24%) of dark red crystalline solid. Mp = 254-256 °C. ¹H-NMR (400 MHz, CDCl₃): 3.88 (s, 6H), 3.93 (s, 12H), 6.76 (s, 4H), 6.99-7.03 (d, 2H, J = 16 Hz), 7.05-7.09 (d, 2H, J = 16 Hz), 7.08-7.12 (d, 2H, J = 16 Hz), 7.15-7.19 (d, 2H, J = 16 Hz), 7.47-7.49 (d, 2H, J = 8 Hz), 7.51 (s, 8H), 7.55-7.57 (d, 2H, J = 8 Hz), 7.85 (s, 2H); MS (FAB, *m/z*): found 769.314, calculated for C₅₁H₄₄O₇ 768.3087.

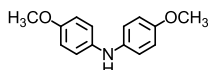
FOS-n-octyl-FOS (2,2'-((1E,1'E)-((octane-1,8-diylbis(oxy))bis(3,5-dimethoxy-4,1-phenylene))bis(ethene-2,1-diyl))bis(9H-fluoren-9-one)):



Prepared using the general procedure for Heck Coupling using 0.319 g (1.23 mmol) of 2-bromofluorenone and 0.289 g (0.614 mmol) of 1,8-bis(2,6-dimethoxy-4-vinylphenoxy)octane (provided by Jeffrey Lucas). After three days the reaction mixture was worked up using the general method. The product was crudely purified on silica eluted with 35 % ethyl acetate/hexanes, and the resulting yellowish-orange solid was dissolved in minimal boiling MeOH/DCM, cooled to -20 °C, and precipitated in hexanes to yield 0.105 g (21 %) of orange

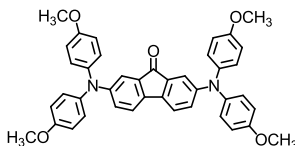
solid. ¹H-NMR (400 MHz, CDCl₃): 1.38 (m, 4H), 1.48 (m, 4H), 1.74-1.81 (p, 4H), 3.90 (s, 12H), 3.98-4.01 (t, 4H, J = 7 Hz), 6.74 (s, 4H), 6.98-7.02 (d, 2H, J = 16 Hz), 7.09-7.13 (d, 2H, J = 16 Hz), 7.28-7.30 (dd, 2H, J = 7 Hz, J' = 2 Hz), 7.46-7.51 (m, 6H), 7.54-7.56 (dd, 2H, J = 8 Hz, J' = 1 Hz), 7.65-7.67 (d, 2H, J = 7 Hz), 7.85 (s, 2H). Further development of this compound was done by Jeffrey Lucas, who will report those results subsequently.

DAA (Dianisylamine) [bis(4-methoxyphenyl)amine]:

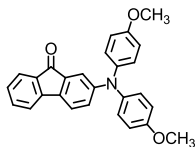


Prepared using the general procedure for Buchwald-Hartwig amination using 2.99 g (16.0 mmol) of *p*-bromoanisole and 2.47 g (20.0 mmol) of *p*-anisidine in 40 mL of toluene. After three days, the reaction mixture was worked up as described in the general procedure. The resulting reddish-brown solid was recrystallized twice from heptane to yield 2.72 g (74 %) of flaky gray solid. Mp = 96-97 °C, lit mp = 98 °C.¹⁶ ¹H-NMR (DMSO-*d*₆): δ 3.68 (s, 6H), 6.79-6.81 (d, 4H), 6.90-6.92 (d, 4H), 7.51 (s, 1H).

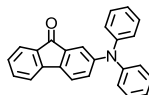
FOBDAA27 (2,7-bis(bis(4-methoxyphenyl)amino)-9H-fluoren-9-one):¹⁵



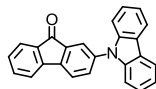
Prepared using the general procedure for Buchwald-Hartwig amination using 0.250 g (1.48 mmol) of 2,7-dibromo-9H-fluoren-9-one and 0.424 g (3.70 mmol) of DAA. After three days, the reaction mixture was worked up as described in the general procedure. The resulting dark blue solid was purified by dry-column chromatography on silica gel eluted with EtOAc/hexanes (20:80). The resulting dark blue crystalline solid was collected to yield 0.470 g (50 %) of product. Mp = 202-203 °C (d). ¹H-NMR (400 MHz, DMSO-*d*₆): 3.75 (s, 12H), 6.78 (d, 2H, J = 2.0 Hz), 6.82-6.85 (dd, 2H, J = 8.0 Hz, 2.5 Hz), 6.93-6.95 (d, 8H, J = 8.8 Hz), 7.05-7.07 (d, 8H, J = 8.8 Hz), 7.34-7.36 (d, 2H, J = 8.1 Hz); MS (FAB, *m/z*): found 634.2468, calculated for C₄₁H₃₄N₂O₄ 634.2468.

FODAA [2-(bis(4-methoxyphenyl)amino)-9H-fluoren-9-one]:¹⁵

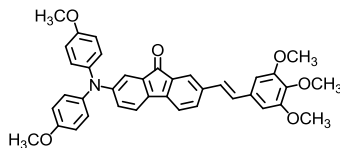
Prepared using the general procedure for Buchwald-Hartwig amination using 0.250 g (0.965 mmol) of 2,7-dibromo-9H-fluoren-9-one and 0.277 g (1.21 mmol) of DAA. After two days, the reaction mixture was worked up as described in the general procedure. The resulting magenta oil (thick) was purified by dry-column chromatography on basic alumina eluted with EtOAc/hexanes (15:85). The resulting dark magenta oil was collected to yield 0.275 g (70 %) of product. After a few days the thick oil formed a solid. Mp = 57-59 °C. ¹H-NMR (400 MHz, DMSO-*d*₆): 3.75 (s, 6H), 6.84-6.86 (d, 2H, J = 10.9 Hz), 6.94-6.96 (d, 4H, J = 8.6 Hz), 7.08-7.10 (d, 4H, J = 8.6 Hz), 7.20-7.23 (t, 1H, J = 7.2 Hz), 7.48-7.52 (m, 3H), 7.56-7.58 (d, 1H, J = 7.3 Hz). MS (FAB⁺, *m/z*): found 407.1521, calculated for C₂₇H₂₃NO₃ 407.1520.

FODPA [2-(diphenylamino)-9H-fluoren-9-one]:¹⁵

Prepared using the general procedure for Buchwald-Hartwig amination using 0.250 g (0.965 mmol) of 2-bromo-9H-fluoren-9-one and 0.205 g (1.21 mmol) of diphenylamine. After 1 h, the reaction mixture was worked up as described in the general procedure. The resulting red solid was purified by dry-column chromatography on silica eluted with hexanes. The resulting powdery red solid was collected to yield 0.222 g (66 %) of product. Mp = 122-124 °C; ATR-IR (neat, cm⁻¹) 1706 (s, C=O str); ¹H NMR (400 MHz, DMSO-*d*₆) 7.03-7.04 (d, 1H, J = 1.5 Hz), 7.08-7.15 (m, 7H), 7.26-7.30 (t, 1H, J = 7.3 Hz), 7.34-7.38 (t, 4H, J = 7.7 Hz), 7.53-7.58 (m, 2H), 7.63-7.67 (t, 2H, 7.7 Hz); MS (FAB⁺, *m/z*): found 347.131, calculated for C₂₅H₁₇NO 347.13.

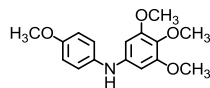
FOCz [2-(9H-carbazol-9-yl)-9H-fluoren-9-one]:¹⁵

Prepared using the general procedure for Buchwald-Hartwig amination using 0.250 g (0.965 mmol) 2-bromo-9H-fluoren-9-one and 0.202 g (1.21 mmol) carbazole. After 1 hour, the reaction mixture was worked up as described in the general procedure. The resulting yellow solid was purified by recrystallization from hot heptane/EtOAc to yield 0.170 g (51 %) of yellow crystalline solid. Mp = 196-197 °C; ATR-IR (neat, cm^{-1}) 1705-1716 (d, C=O str); ^1H NMR (400 MHz, $\text{DMSO-}d_6$, δ/ppm) 7.30-7.34 (m, 2H), 7.43-7.50 (m, 5H), 7.68-7.72 (m, 2H), 7.77-7.78 (d, 1H, $J = 1.8$ Hz), 7.88-7.90 (dd, 1H, $J = 8$ Hz, 1.8 Hz), 7.94-7.96 (d, 1H, $J = 7.6$ Hz), 8.10-8.12 (d, 1H, $J = 7.8$ Hz), 8.26-8.28 (d, 2H, $J = 7.8$ Hz); MS (FAB^+ , m/z): found 345.117, calculated for $\text{C}_{25}\text{H}_{17}\text{NO}$ 345.12.

FODAAS [(E)-2-(bis(4-methoxyphenyl)amino)-7-(3,4,5-trimethoxystyryl)-9H-fluoren-9-one]:¹⁵

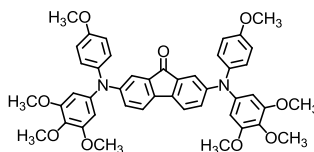
Prepared using the general procedure for Buchwald-Hartwig amination using 0.250 g (0.554 mmol) of 2-BrFOPV and 0.159 g (0.693 mmol) of dianisylamine. After 5 h, the reaction mixture was worked up as described in the general procedure. The resulting dark purple solid was purified by dry-column chromatography on silica eluted with EtOAc/hexanes (40:60). The resulting dark purple crystalline solid was collected to yield 0.110 g (33 %) of product. Mp = 99-101 °C. ^1H -NMR (400 MHz, $\text{DMSO-}d_6$): 3.67 (s, 3H), 3.77 (s, 6H), 3.83 (s, 6H), 6.84-6.85 (d, 1H, $J = 2$ Hz), 6.86-6.89 (dd, 1H, $J = 8.4$ Hz, 2.3 Hz), 6.95-6.98 (m, 6H), 7.11-7.13 (d, 4H, $J = 8.8$ Hz), 7.24-7.28 (d, 1H, $J = 16$ Hz), 7.29-7.33 (d, 1H, $J = 16$ Hz), 7.52-7.54 (d, 1H, $J = 8.1$ Hz), 7.58-7.60 (d, 1H, $J = 7.8$ Hz), 7.67-7.69 (dd, 1H, $J = 7.6$ Hz, 0.8 Hz), 7.78 (s, 1H); MS (FAB , m/z): found 599.2308, calculated for $\text{C}_{38}\text{H}_{33}\text{NO}_6$ 599.2308.

TMPMPA (Trimethoxyphenyl-methoxyphenylamine) [3,4,5-trimethoxy-*N*-(4-methoxyphenyl)aniline]:



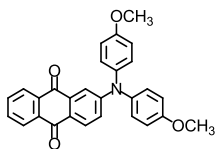
Prepared using the general procedure for Buchwald-Hartwig amination using 3.95 g (16.0 mmol) of 5-bromo-1,2,3-trimethoxybenzene and 2.47 g (20.0 mmol) of *p*-anisidine in 40 mL of toluene. After two days, the reaction mixture was worked up as described in the general procedure. The resulting tan solid was purified on silica eluted with diethyl ether to yield 3.90 g (84 %) of tan solid. Mp = 99-100 °C. ¹H-NMR (DMSO-*d*₆): δ 3.58 (s, 3H), 3.69 (s, 6H), 3.70 (s, 3H), 6.22 (s, 2H), 6.84-6.86 (d, 2H, J = 8 Hz), 7.03-7.05 (d, 2H, J = 8 Hz), 7.72 (s, 1H).

FOBTMPMPA [2,7-bis((4-methoxyphenyl)(3,4,5-trimethoxyphenyl)amino)-9*H*-fluoren-9-one]:¹⁵



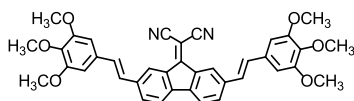
Prepared using the general procedure for Buchwald-Hartwig amination using 0.250 g (0.740 mmol) of 2,7-dibromo-9*H*-fluoren-9-one and 0.545 g (1.85 mmol) of TMPMPA. After 17 h, the reaction mixture was worked up as described in the general procedure. The resulting dark blue solid was purified by dry-column chromatography on silica gel eluted with Et₂O/hexanes (66:33). The resulting dark blue crystalline solid was collected to yield 0.117 g (21 %) of product. Mp = 68-70 °C. ¹H-NMR (400 MHz, DMSO-*d*₆): 3.63 (s, 12H), 3.65 (s, 6H), 3.76 (s, 6H), 6.35 (d, 4H, J = 2 Hz), 6.87 (d, 2H, J = 8 Hz), 6.94-6.97 (m, 6H), 7.10-7.12 (d, 4H, J = 8 Hz), 7.40-7.4 (d, 2H, J = 8 Hz); MS (FAB, *m/z*): found 754.2890, calculated for C₄₅H₄₂N₂O₉ 754.2892.

DAAAQ [2-(bis(4-methoxyphenyl)amino)anthracene-9,10-dione]:

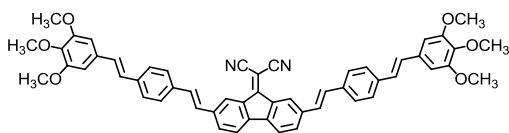


Prepared using the general procedure for Buchwald-Hartwig amination using 0.250 g (1.12 mmol) of 2-aminoanthraquinone and 0.31 mL (2.46 mmol, 2.2 eq) of 4-bromoanisole. After 17 h, the reaction mixture was worked up as described in the general procedure. The resulting dark red solid was purified by dry-column chromatography on silica gel eluted with 20 % ethyl acetate/hexanes to yield 0.059 g (12 %) of dark red solid. Mp not determined. ¹H-NMR (400 MHz, DMSO-*d*₆): 3.80 (s, 6H), 6.98-7.01 (dd, 1H, J = 8 Hz, J' = 40 Hz), 7.03-7.05 (d, 4H, J = 8 Hz), 7.27-7.29 (d, 5H, J = 8 Hz), 7.83-7.91 (m, 2H), 7.99-8.01 (d, 1H, J = 8 Hz), 8.09-8.11 (dd, 1H, J = 8 Hz, J' = 1 Hz), 8.15-8.17 (dd, 1H, J = 8 Hz, J' = 1 Hz).

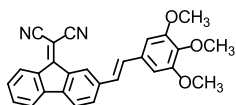
FMDS 2-(2,7-bis(3,4,5-trimethoxystyryl)-9H-fluoren-9-ylidene)malononitrile:¹⁷



Prepared using the general procedure for Knoevenagel condensation using 1.00 g (1.77 mmol) of FODS and 0.700 g (10.6 mmol) of malononitrile overnight, during which time the solution turned from bright red to dark greenish-blue. The reaction mixture was then cooled to room temperature and poured into 300 mL water. The precipitate was collected via suction filtration, dissolved in chloroform, dried over anhydrous MgSO₄, and concentrated *in vacuo*. The resulting blue solid was purified by crystallization from hot 95% ethanol to yield 0.900 g (83 %) of product. Mp = 267-269 °C (d); ATR-IR (neat, cm⁻¹) 2225 (s, C≡N str); ¹H-NMR (400 MHz, CDCl₃): 3.89 (s, 6H), 3.94 (s, 12H), 6.75 (s, 4H), 6.97-7.01 (d, 2H, J = 16 Hz), 7.07-7.11 (d, 2H, J = 16 Hz), 7.49-7.51 (d, 2H, J = 8 Hz), 7.61-7.63 (d, 2H, J = 8 Hz), 8.48 (s, 2H); MS (FAB, *m/z*): found 612.2260, calculated for C₃₈H₃₂N₂O₆ 612.2260.

FMDS2 [2-(2,7-bis(4-(3,4,5-trimethoxystyryl)styryl))-9H-fluoren-9-ylidene)malononitrile]:

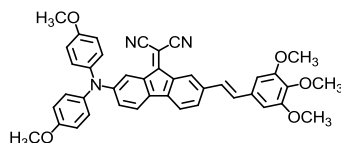
To a three-necked round-bottom flask were added 0.0400 g (0.0520 mmol) of FODS2 and 0.0206 g (0.312 mmol) of malononitrile under nitrogen atmosphere. Dry DMSO (10 mL) was added and the solution was heated at 110 °C overnight, during which time the solution turned from dark red to dark green. The reaction mixture was then cooled to room temperature and poured into 100 mL of water. The precipitate was collected via suction filtration and dissolved in chloroform. The filtrate was extracted with CHCl₃, and the combined organic solutions were dried over anhydrous MgSO₄ and concentrated *in vacuo*. The resulting greenish-gray solid was purified by crystallization from hot ethanol/acetone to give 0.045 g of product (81% yield). Mp not determined. ¹H-NMR (400 MHz, CDCl₃): 3.88 (s, 6H), 3.93 (s, 12H), 6.75 (s, 4H), 6.96-7.06 (m, 4H), 7.10-7.13 (m, 4H), 7.51-7.54 (m, 12H), 7.61-7.62 (m, 2H), 8.50 (s, 2H).

FMS (E)-2-(2-(3,4,5-trimethoxystyryl)-9H-fluoren-9-ylidene)malononitrile:¹⁷

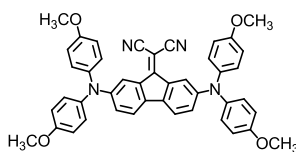
Prepared using the general procedure for Knoevenagel condensation using 0.100 g (0.269 mmol) FOS and 0.106 g (1.61 mmol) malononitrile after a 22 h reaction time. The reaction mixture was poured into water, stirred for 10 min, and extracted with DCM. The organic layers were combined, dried over anhydrous MgSO₄, and concentrated *in vacuo* to give a dark purple pasty solid. The crude material was recrystallized from 100 % EtOH to furnish 0.0810 g (72 % yield) of product as a dark purple crystalline solid. Recrystallization from DCM by slow evaporation yielded dark purple needles. Mp = 203-204 °C. ATR-IR (neat, cm⁻¹) 2220 (s, C≡N str); ¹H-NMR (400 MHz, DMSO-d₆): 3.68 (s, 3 H), 3.85 (s, 6H), 6.96 (s, 2H), 7.16-7.20 (d, 1H, J = 16 Hz), 7.29-7.33 (d, 1H, J = 16 Hz), 7.43-7.47 (t, 1H, J = 16 Hz, J' = 8 Hz), 7.61-7.65 (t, 1H, J

= 16 Hz, $J' = 8$ Hz), 7.86-7.89 (m, 3H), 8.22-8.24 (d, 1H, $J = 8$ Hz), 8.36 (s, 1H); $^1\text{H-NMR}$ (400 MHz, CDCl_3): 3.89 (s, 3 H), 3.94 (s, 6H), 6.76 (s, 2H), 6.99-7.03 (d, 1H, $J = 16$ Hz), 7.08-7.12 (d, 1H, $J = 16$ Hz), 7.29-7.33 (t, 1H, $J = 16$ Hz, $J' = 8$ Hz), 7.48-7.54 (m, 3H), 7.62-7.64 (d, 1H, $J = 8$ Hz), 8.36-8.38 (d, 1H, $J = 8$ Hz), 8.50 (s, 1H); MS (FAB, m/z): found 420.14606, calculated for $\text{C}_{27}\text{H}_{20}\text{N}_2\text{O}_3$ 420.14740.

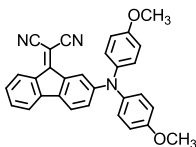
FMDAAS (E)-2-(2-(bis(4-methoxyphenyl)amino)-7-(3,4,5-trimethoxystyryl)-9H-fluoren-9-ylidene)malononitrile:¹⁷



Prepared using the general procedure for Knoevenagel condensation using 0.0670 g (0.112 mmol) of FODAAS and 0.0444 g (0.672 mmol) of malononitrile after an 18 h reaction time. The reaction mixture was poured into water, stirred for 10 min, and extracted with EtOAc. The organic layers were combined, dried over anhydrous MgSO_4 , and concentrated *in vacuo* to give a pasty green solid. The crude material was purified by a quick recrystallization from 100 % EtOH to remove malononitrile, then by flash chromatography on silica eluted with 40 % EtOAc/hexanes to furnish 0.060 g (83 % yield) of product as a greasy dark green film. Mp N/A (greasy film). ATR-IR (neat, cm^{-1}) 2222 (s, $\text{C}\equiv\text{N}$ str); $^1\text{H-NMR}$ (400 MHz, DMSO-d_6): 3.67 (s, 3 H), 3.75 (s, 6 H), 3.83 (s, 6 H), 6.85-6.87 (dd, 1 H, $J = 8$ Hz, $J' = 2$ Hz), 6.92-6.96 (m, 6 H), 7.08-7.11 (m, 5 H), 7.22-7.26 (d, 1 H, $J = 16$ Hz), 7.55-7.57 (d, 1 H, $J = 8$ Hz), 7.62-7.64 (d, 1 H, $J = 8$ Hz), 7.75-7.77 (dd, 2 H, $J = 8$ Hz, $J' = 1.6$ Hz), 8.24 (s, 1 H); MS (FAB, m/z): found 647.2413, calculated for $\text{C}_{41}\text{H}_{33}\text{N}_3\text{O}_5$ 647.24202.

FMBDAA27 2-(2,7-bis(bis(4-methoxyphenyl)amino)-9H-fluoren-9-ylidene)malononitrile:¹⁷

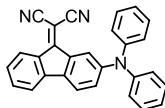
Prepared using the general procedure for Knoevenagel condensation using 0.250 g (0.394 mmol) of FOBDA and 0.156 g (2.36 mmol) of malononitrile after a 4 day reaction time. The reaction mixture was poured into water, stirred for 10 min, and extracted with EtOAc. The organic layers were combined, dried over anhydrous MgSO₄, and concentrated *in vacuo* to give a pasty black solid. The crude material was recrystallized from a gradient of hot acetone and 95 % EtOH to furnish 0.198 g (73 % yield) of black crystalline solid. Mp = 106-108 °C. ATR-IR (neat, cm⁻¹) 2221 (s, C≡N str); ¹H-NMR (400 MHz, DMSO-*d*₆): 3.73 (s, 12 H), 6.81-6.83 (dd, 2H, J = 8 Hz, J' = 2 Hz), 6.91-6.93 (d, 8H, J = 8 Hz), 7.03-7.05 (d, 8H, J = 8 Hz), 7.34-7.36 (d, 2H, J = 8 Hz), 7.68-7.69 (d, 2H, J = 2 Hz); MS (FAB, *m/z*): found 682.2580, calculated for C₄₄H₃₄N₄O₄ 682.2580.

FMDAA 2-(2-(bis(4-methoxyphenyl)amino)-9H-fluoren-9-ylidene)malononitrile:¹⁷

Prepared using the general procedure for Knoevenagel condensation using 0.250 g (0.614 mmol) of FODAA and 0.243 g (3.68 mmol) of malononitrile after a 2 day reaction time. The reaction mixture was poured into water, stirred for 10 min, and extracted with EtOAc. The organic layers were combined, dried over anhydrous MgSO₄, and concentrated *in vacuo* to give a dark green pasty solid. The crude material was recrystallized from 95 % EtOH to furnish 0.176 g (63 % yield) of product as fine green needles. Mp = 182-184 °C. ATR-IR (neat, cm⁻¹) 2224 (s, C≡N str); ¹H-NMR (400 MHz, DMSO-*d*₆): 3.75 (s, 6 H), 6.85-6.88 (dd, 1H, J = 8 Hz, J' = 2 Hz), 6.94-6.96 (d, 4H, J = 8 Hz), 7.09-7.11 (d, 4H, J = 8 Hz), 7.26-7.30 (t, 1H, J = 16 Hz, J' = 8 Hz), 7.50-7.54 (t, 1H, J = 16 Hz, J' = 8 Hz), 7.56-7.58 (d, 1H, J = 8 Hz), 7.62-7.63 (d, 1H, J = 2 Hz),

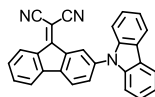
7.77 (d, 1H, J = 8 Hz), 8.09-8.11 (d, 1H, J = 8 Hz); MS (FAB, m/z): found 455.1634, calculated for $C_{30}H_{21}N_3O_2$ 455.1634.

FMDPA 2-(2-(diphenylamino)-9H-fluoren-9-ylidene)malononitrile:¹⁷



Prepared using the general procedure for Knoevenagel condensation using 0.250 g (0.720 mmol) of FODPA and 0.285 g (4.31 mmol) of malononitrile after a 22 h reaction time. The reaction mixture was poured into water, stirred for 10 min, and extracted with DCM. The organic layers were combined, dried over anhydrous $MgSO_4$, and concentrated *in vacuo* to give a dark blue pasty solid. The crude material was recrystallized from 100 % EtOH to furnish 0.203 g (71 % yield) of product as a dark blue crystalline solid. Crystallization from 1:1 EtOAc/DCM by slow evaporation yielded dark blue needles. Mp = 199-200 °C. ATR-IR (neat, cm^{-1}) 2219 (s, $C\equiv N$ str); 1H -NMR (400 MHz, DMSO- d_6): 7.09-7.15 (m, 7 H), 7.32-7.38 (m, 5H), 7.54-7.58 (t, 1H, J = 16 Hz, J' = 8 Hz), 7.68-7.72 (t, 2H, J = 16 Hz, J' = 8 Hz), 7.92 (s, 1H), 8.13-8.15 (d, 1H, J = 8 Hz); 1H -NMR (400 MHz, $CDCl_3$): 7.09-7.16 (m, 7 H), 7.18-7.22 (td, 1H, J = 16 Hz, J' = 8 Hz, J'' = 1.2 Hz), 7.29-7.35 (m, 5H), 7.40-7.45 (m, 2H), 8.06 (d, 1H, J = 1.6 Hz), 8.28-8.29 (d, 1H, J = 8 Hz); MS (FAB, m/z): found 395.14180, calculated for $C_{28}H_{17}N_3$ 395.14225.

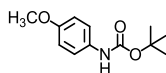
FMCz 2-(2-(9H-carbazol-9-yl)-9H-fluoren-9-ylidene)malononitrile:¹⁷



Prepared using the general procedure for Knoevenagel condensation using 0.100 g (0.290 mmol) of FOCz and 0.115 g (1.74 mmol) of malononitrile after a 5 h reaction time. The reaction mixture was poured into water, stirred for 10 min, and filtered to give an orange-red powdery solid. The solid was dissolved in DCM, washed with H_2O , dried over anhydrous $MgSO_4$, and concentrated *in vacuo* to give an orange-red pasty solid. The crude material was recrystallized from 100 % EtOH to furnish 0.0830 g (73 % yield) of product as an orange-red solid. Mp >260

°C. ATR-IR (neat, cm^{-1}) 2224 (s, $\text{C}\equiv\text{N}$ str); $^1\text{H-NMR}$ (400 MHz, $\text{DMSO-}d_6$): 7.32-7.36 (t, 2H, $J = 16$ Hz, $J' = 8$ Hz), 7.46-7.55 (m, 5H), 7.70-7.74 (t, 1H, $J = 16$ Hz, $J' = 8$ Hz), 7.94-7.96 (dd, 1H, $J = 8$ Hz, $J' = 1.2$ Hz), 8.02-8.04 (dd, 1H, $J = 8$ Hz, $J' = 0.4$ Hz), 8.18-8.20 (d, 1H, $J = 8$ Hz), 8.28-8.31 (t, 3H, $J = 12$ Hz, $J' = 8$ Hz), 8.45 (s, 1H); $^1\text{H-NMR}$ (400 MHz, CDCl_3): 7.32 (m, 2 H), 7.39-7.45 (m, 5H), 7.58-7.60 (t, 1H, $J = 16$ Hz, $J' = 8$ Hz), 7.64-7.66 (d, 1H, $J = 8$ Hz), 7.71-7.73 (d, 1H, $J = 8$ Hz), 7.78-7.80 (d, 1H, $J = 8$ Hz), 8.14-8.16 (d, 2H, $J = 8$ Hz), 8.44-8.46 (d, 1H, $J = 8$ Hz), 8.64 (s, 1H); MS (FAB, m/z): found 393.12562, calculated for $\text{C}_{28}\text{H}_{15}\text{N}_3$ 393.12660.

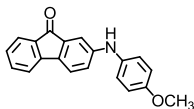
BOC-AA (tert-butyl (4-methoxyphenyl)carbamate):¹⁷



This procedure was adapted from the literature.¹⁸ Indium tribromide (0.035 g, 0.100 mmol) was added to 2.18 g (10.0 mmol) of di-*t*-butylcarbonate with stirring. 4-Anisylamine (1.24 g, 10.0 mmol) was added to the reaction mixture in one portion, and the mixture stirred for 30 min. Hexane was added during the reaction as needed to prevent clumping. When complete, the reaction was diluted with EtOAc and washed with water. The organic layer was separated and dried over anhydrous MgSO_4 , then concentrated *in vacuo* to give a gray-brown solid.

Recrystallization from hot heptane yielded 2.14 g (96 %) of large, gun-metal gray needles (two crops). Mp = 94-96 °C. $^1\text{H-NMR}$ (400 MHz, acetone- d_6): 1.47 (s, 9H), 3.75 (s, 3 H), 6.84-6.86 (d, 2H, $J = 8$ Hz), 7.44-7.46 (d, 2H, $J = 8$ Hz), 8.18 (s, 1H).

FOAA (2-((4-methoxyphenyl)amino)-9H-fluoren-9-one):¹⁷

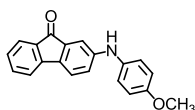


Prepared using the general procedure for Buchwald/Goldberg amidation using 0.250 g (0.965 mmol) of 2-bromofluorenone and 0.259 g (1.16 mmol) of BOC-AA after a 3 day reaction time. The dark orange-brown reaction mixture was worked up as described in the general procedure, and crudely purified on silica eluted with 20 % EtOAc/hexanes to give a yellow-

orange solid. The solid was dissolved in EtOAc at room temperature and a few mL of conc. HCl was added. The mixture was stirred for about 2 h and then quenched with saturated aq. Na₂CO₃ (caution: foaming). The organic layer was separated, washed again with saturated aq. Na₂CO₃, dried over anhydrous Na₂SO₄, and concentrated *in vacuo* to give a red-purple solid.

Crystallization from hot heptane yielded a combined 0.261 g (67 %) of analytically pure (HPLC) product as dark red-purple crystalline solid from two crops. Mp = 152-154 °C. ATR-IR (neat, cm⁻¹) 3355 (N-H str), 1704 (s, C=O str); ¹H-NMR (400 MHz, DMSO-*d*₆): 3.74 (s, 3 H), 6.92-6.96 (d, 2H, J = 8 Hz), 7.00-7.02 (dd, 1H, J = 8 Hz, J' = 1.6 Hz), 7.06-7.10 (m, 3H), 7.17-7.21 (t, 1H, J = 8 Hz), 7.47-7.56 (m, 4H), 8.31 (s, 1H) MS (FAB, *m/z*): found 302.1171 (M+H), calculated for C₂₀H₁₅NO₂ 301.11028.

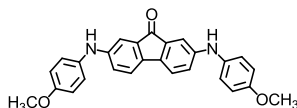
FOAA (2-((4-methoxyphenyl)amino)-9H-fluoren-9-one) (Alternate Route):¹⁷



Prepared in two steps via Buchwald-Hartwig amination between 2-aminofluorene and 4-bromoanisole, followed by the general oxidation procedure in dry DMSO. For the amination reaction, 0.131 g (0.725 mmol) of 2-aminofluorene, 0.1 mL (0.797 mmol, 1.1 eq) of 4-bromoanisole, 0.0402 g (0.0725 mmol, 0.1 eq) of DPPF, 0.0166 g (0.0181 mol, 0.025 eq) of Pd₂dba₃, and 0.0836 g (0.870 mmol, 1.2 eq) of *t*-BuONa were added to 5 mL dry toluene under nitrogen and heated at 160 °C in a CEM MARS Organic Reactor (microwave reactor) at 200 W for 30 min. The yellowish-brown reaction mixture was worked up as described in the general procedure, and crudely purified on silica eluted with 20 % EtOAc/hexanes to give 0.105 g (51 %) of *N*-(4-methoxyphenyl)-9H-fluoren-2-amine as a tan solid. ¹H-NMR (400 MHz, acetone-*d*₆): 3.78 (s, 3 H), 3.81 (s, 2H), 6.89-6.91 (d, 2H, J = 8 Hz), 6.99-7.01 (d, 1H, J = 8 Hz), 7.14-7.16 (m, 3H), 7.19-7.23 (m, 2H), 7.28-7.31 (t, 1H), 7.47-7.48 (d, 1H), 7.65-7.69 (overlapping doublets, 2H, J₁ = 8 Hz, J₂ = 8 Hz). The product was then oxidized via the general fluorene oxidation procedure using 0.118 g (0.411 mmol) of 2-anisylaminofluorene and 0.670 g (2.05 mmol, 5 eq) of

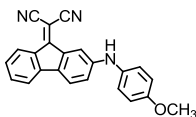
Cs₂CO₃ in 10 mL of dry DMSO at 40 °C over 3 h. The reaction then was cooled to room temperature, poured into water, extracted with ethyl acetate, dried over anhydrous MgSO₄, and concentrated *in vacuo* to give dark red solid in quantitative yield (0.123 g). Mp = 152-154 °C. See the previous entry for characterization data.

FOBAA (2,7-bis((4-methoxyphenyl)amino)-9H-fluoren-9-one):¹⁷



Prepared using the general procedure for Buchwald/Ullmann-Goldberg amidation using 0.250 g (0.740 mmol) of 2,7-dibromofluorenone and 0.397 g (1.78 mmol) of BOC-AA after a 3 day reaction time. The dark red-brown reaction mixture was worked up as described in the general procedure, and crudely purified on silica eluted with 20 % EtOAc/hexanes to give a red solid. The solid was dissolved in EtOAc at room temperature and a few mL of conc. HCl was added. The reaction was allowed to stir for about 2 h and then quenched with saturated Na₂CO₃. The dark blue organic layer was separated, washed with saturated Na₂CO₃, dried over anhydrous Na₂SO₄, and concentrated *in vacuo* to give a shiny gold-colored solid. Recrystallization from hot heptane yielded a combined 0.149 g (48 %) analytically pure (HPLC) product as shiny gold-colored crystalline solid after two crops. Mp = 214-216 °C. ATR-IR (neat, cm⁻¹) 3329-3394 (N-H str), 1714 (s, C=O str); ¹H-NMR (400 MHz, DMSO-d₆): 3.74 (s, 3 H), 6.92-6.96 (d, 2H, J = 8 Hz), 7.00-7.02 (dd, 1H, J = 8 Hz, J' = 1.6 Hz), 7.06-7.10 (m, 3H), 7.17-7.21 (t, 1H, J = 8 Hz), 7.47-7.56 (m, 4H), 8.31 (s, 1H) MS (FAB, *m/z*): found 422.1596, calculated for C₂₇H₂₂N₂O₃ 422.16304.

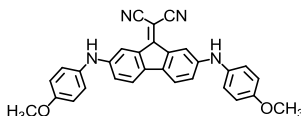
FMAA (2-(2-((4-methoxyphenyl)amino)-9H-fluoren-9-ylidene)malononitrile):¹⁷



Prepared using the general procedure for Knoevenagel condensation using 0.100 g (0.332 mmol) of FOAA and 0.132 g (1.99 mmol) of malononitrile after a 16 h reaction time. The dark

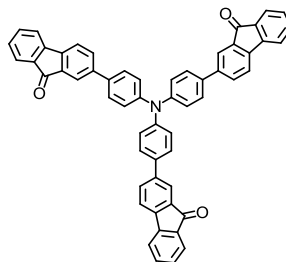
aqua-blue reaction mixture was cooled to room temperature, poured into water, stirred for 10 min, and filtered to get a purple solid. The solid was dissolved in DCM to give an aqua-blue solution, washed sequentially with water and brine, dried over anhydrous MgSO_4 , and concentrated *in vacuo* to give a dark purple pasty solid. The crude material was crystallized from hot 95% EtOH to yield 0.0790 g (68 %) of black/green crystalline solid. Mp = 187-188 °C. ATR-IR (neat, cm^{-1}) 3337 (N-H str), 2222 (sh, $\text{C}\equiv\text{N}$ str); $^1\text{H-NMR}$ (400 MHz, $\text{DMSO-}d_6$): 3.73 (s, 3 H), 6.89-6.91 (d, 2H, $J = 8$ Hz), 7.01-7.03 (dd, 1H, $J = 8$ Hz, $J' = 2$ Hz), 7.09-7.11 (d, 2H, $J = 8$ Hz), 7.22-7.26 (t, 1H, $J = 8$ Hz), 7.47-7.51 (t, 1H, $J = 8$ Hz), 7.55-7.59 (t, 2H, $J = 8$ Hz), 7.89 (dd, 1H, $J = 2$ Hz), 8.08-8.10 (d, 1H, $J = 8$ Hz), 8.49 (s, 1H) MS (FAB, m/z): found 372.1087 (M+Na), calculated for $\text{C}_{23}\text{H}_{15}\text{N}_3\text{O}$ 349.12151.

FMBA (2-(2,7-bis((4-methoxyphenyl)amino)-9H-fluoren-9-ylidene)malononitrile):¹⁷



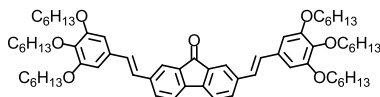
Prepared using the general procedure for Knoevenagel condensation using 0.0500 g (0.119 mmol) of FOBAA and 0.0469 g (0.710 mmol) of malononitrile after a 16 h reaction time. The reaction mixture was cooled to room temperature, poured into water, stirred for 10 min, and extracted with Et_2O . The organic layers were combined, dried over anhydrous MgSO_4 , and concentrated *in vacuo* to give a pasty reddish solid. The crude material was column purified on silica eluted with 20 % EtOAc/hexanes to give a dark green/gray solution which when concentrated yielded 0.039 g (70 %) of dark green/black solid. Slow crystallization from elution solvent yielded fine, long, green/gray needles. Mp = 204-205 °C. ATR-IR (neat, cm^{-1}) 3344 (N-H str), 2225 (sh, $\text{C}\equiv\text{N}$ str); $^1\text{H-NMR}$ (400 MHz, $\text{DMSO-}d_6$): 3.72 (s, 6 H), 6.86-6.88 (d, 4H, $J = 8$ Hz), 6.94-6.96 (dd, 2H, $J = 8$ Hz, $J' = 1.6$ Hz), 7.04-7.06 (d, 4H, $J = 8$ Hz), 7.30-7.32 (d, 2H, $J = 8$ Hz), 7.80-7.81 (d, 2H, $J = 1.6$ Hz), 8.26 (s, 2H); MS (FAB, m/z): found 471.1793 (M+H), calculated for $\text{C}_{30}\text{H}_{22}\text{N}_4\text{O}_2$ 470.17428.

Tris(FOPh)Amine (2,2',2''-(nitriлотris(benzene-4,1-diyl))tris(9H-fluoren-9-one):



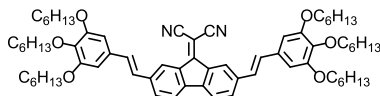
Tris-4-bromophenylamine (0.250 g, 0.519 mmol) was dissolved in 20 mL of dry Et₂O and cooled to -78 °C under nitrogen. t-BuLi (1.2 mL, 1.6 M, 1.87 mmol, 3.6 eq) was added carefully dropwise, and the reaction was stirred 1 h with continued cooling. [CAUTION: t-BuLi is a severe fire hazard, is extremely reactive with even small amounts of water or alcohols, and is pyrophoric in air! Appropriate precautions are required!] SnBu₃Cl (0.5 mL, 1.71 mmol, 3.33 eq) was added dropwise while keeping the stirred reaction at -78 °C, following which the mixture was allowed to warm to room temperature. After 16 h, the reaction mixture was poured into 150 mL of H₂O, extracted with Et₂O, dried over anhydrous MgSO₄, and conc. *in vacuo* to give the stannane intermediate as a yellowish oil which was used immediately without purification. 2-Bromofluorenone (0.606 g, 2.34 mmol, 4.5 eq) and Pd(PPh₃)₄ (0.060 g, 0.0519 mmol, 0.1 eq) were dissolved in toluene and combined with the stannane obtained in the previous steps. The reaction mixture was heated at 110 °C for 3 days and then cooled to room temperature. Aqueous KF (0.1 g/mL) was added, and the reaction mixture stirred 2.5 h to remove tin impurities. The reaction mixture was poured into H₂O, extracted with DCM, dried over anhydrous MgSO₄, and concentrated *in vacuo* to give an orange-red solid. The crude material was column purified on silica eluted with 30 % EtOAc/hexanes to give 0.100 g (25 % overall) of powdery orange-red solid. Mp = 196-198 °C. ATR-IR not obtained. ¹H-NMR (400 MHz, DMSO-*d*₆): 7.20-7.22 (d, 6H, J = 8 Hz), 7.37-7.41 (t, 3H, J = 7 Hz), 7.62-7.65 (m, 6H), 7.78-7.80 (m, 6H), 7.83-7.85 (m, 3H), 7.88-7.89 (m, 6H), 7.94-7.96 (m, 3H). MS (FAB, *m/z*): found *m/z* = 779.2444, calculated for C₅₇H₃₃NO₃ *m/z* = 779.24604.

FODS-Hex (2,7-bis(*E*)-3,4,5-tris(hexyloxy)styryl)-9*H*-fluoren-9-one):



Prepared using the general procedure for Heck Coupling using 0.362 g (1.07 mmol) of 2,7-dibromo-9*H*-fluoren-9-one and 1.00 g (2.47 mmol, 2.3 eq) of trihexyloxystyrene (provided by Timothy Gehan). After three days, the reaction mixture was worked up as described in the general procedure. The resulting aqueous suspension was extracted with DCM, dried over MgSO₄, and concentrated *in vacuo* to give an orange-red solid. Recrystallization from 95 % ethanol yielded 0.782 g (75 %) of product. Mp = 81-83 °C. ATR-IR not obtained. ¹H-NMR (400 MHz, CDCl₃): 0.91-0.94 (m, 18 H), 1.33-1.37 (m, 24 H), 1.49-1.51 (m, 12 H), 1.72-1.78 (p, 4H), 1.80-1.87 (p, 8H), 3.97-4.01 (t, 4H, J = 6 Hz), 4.02-4.05 (t, 8H, J = 6 Hz), 6.72 (s, 4H), 6.95-6.99 (d, 2H, J = 16 Hz), 7.07-7.11 (d, 2H, J = 16 Hz), 7.47-7.49 (d, 2H, J = 8 Hz), 7.54-7.56 (d, 2H J = 8 Hz), 7.85 (s, 2H). MP = 81-83 °C. MS (FAB, *m/z*): found *m/z* = 984.680, calculated for C₆₅H₉₂O₇ *m/z* = 984.68431.

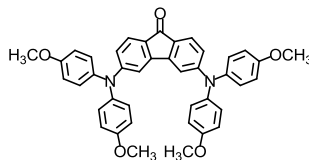
FMDS-Hex (2-(2,7-bis(*E*)-3,4,5-tris(hexyloxy)styryl)-9*H*-fluoren-9-ylidene)malononitrile):



Prepared using the general procedure for Knoevenagel condensation using 0.100 g (0.102 mmol) of FODS-Hex and 0.0400 g (0.612 mmol) of malononitrile overnight, during which time the solution turned from bright red to dark greenish-blue. The reaction mixture was cooled to room temperature, poured into 100 mL water, extracted with EtOAc, dried over anhydrous MgSO₄, and concentrated *in vacuo*. The resulting blue-green solid was purified by crystallization from hot ethanol to yield 0.0851 g (81 %) of sticky blue-green product. Mp N/A greasy. ATR-IR not obtained. ¹H-NMR (400 MHz, CDCl₃): 0.91-0.93 (m, 18 H), 1.33-1.36 (m, 24 H), 1.47-1.53 (m, 12 H), 1.72-1.80 (p, 4H), 1.80-1.87 (p, 8H), 3.97-4.00 (t, 4H, J = 7 Hz), 4.02-4.05 (t, 8H, J = 7 Hz), 6.73 (s, 4H), 6.94-6.98 (d, 2H, J = 16 Hz), 7.04-7.08 (d, 2H, J = 16 Hz), 7.47-7.49 (d, 2H, J

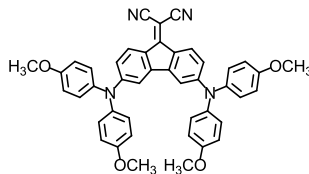
= 8 Hz), 7.59-7.61 (d, 2H, J = 8 Hz), 8.47 (s, 2H); MS (FAB, m/z): found 1033.7074, calculated for $C_{68}H_{92}N_2O_6$ 1032.69554.

FOBDAA36 (3,6-bis(bis(4-methoxyphenyl)amino)-9H-fluoren-9-one):¹⁷



Prepared using the general procedure for Buchwald-Hartwig amination using 0.250 g (0.740 mmol) of 3,6-dibromofluorenone and 0.442 g (1.85 mmol) of dianisylamine. After 2 days, the red reaction mixture was worked up as described in the general procedure. The crude mixture was purified on silica eluted with 30:70 EtOAc/hexanes to yield 0.306 g (65 %) of dark red crystalline solid. Mp = 119-120 °C. ATR-IR (neat, cm^{-1}) 1684 (s, C=O str); ¹H-NMR (400 MHz, DMSO- d_6): 3.75 (s, 12 H), 6.42-6.44 (dd, 2H, J = 8 Hz, J' = 2 Hz), 6.58-6.59 (d, 2H, J = 1.6 Hz), 6.94-6.96 (d, 8H, J = 8 Hz), 7.12-7.14 (d, 8H, J = 8 Hz), 7.30-7.32 (d, 2H, J = 8 Hz); MS (FAB, m/z): found 634.2455, calculated for $C_{41}H_{34}N_2O_5$ 634.24677.

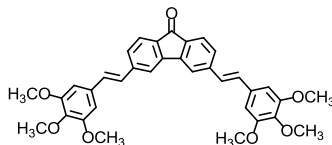
FMBDAA36 (2-(3,6-bis(bis(4-methoxyphenyl)amino)-9H-fluoren-9-ylidene)malononitrile):¹⁷



Prepared using the general procedure for Knoevenagel condensation using 0.0183 g (0.0288 mmol) of FOBDAA36 and 0.0114 g (0.173 mmol) of malononitrile after a 2 day reaction time. The reaction mixture was poured into water, stirred for 10 min, and extracted with Et₂O. The organic layers were combined, dried over anhydrous MgSO₄, and concentrated *in vacuo* to give a pasty purple solid. The crude material was recrystallized from hot 95% EtOH to yield 0.013 g (66 %) of purple powdery solid. Mp = 178-180 °C. ATR-IR (neat, cm^{-1}) 2212 (s, C≡N str); ¹H-NMR (400 MHz, DMSO- d_6): 3.76 (s, 12 H), 6.48-6.51 (dd, 2H, J = 8 Hz, J' = 2 Hz),

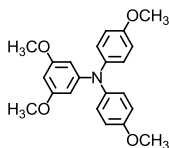
6.54-6.55 (d, 2H, J = 1.6 Hz), 6.96-6.98 (d, 8H, J = 8 Hz), 7.16-7.18 (d, 8H, J = 8 Hz), 7.90-7.92 (d, 2H, J = 8 Hz); MS (FAB, m/z): found 682.2580, calculated for $C_{44}H_{34}N_4O_4$ 682.25801.

FODS36 (3,6-bis(bis(4-methoxyphenyl)amino)-9H-fluoren-9-one):



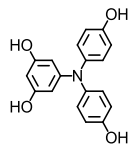
Prepared using the general procedure for Heck Coupling using 0.250 g (0.740 mmol) of 3,6-dibromo-9H-fluoren-9-one and 0.359 g (1.85 mmol, 2.5 eq) of trimethoxystyrene. After two days the reaction mixture was worked up as described in the general procedure. The resulting aqueous suspension was extracted with DCM, dried over anhydrous $MgSO_4$, and concentrated *in vacuo* to give an reddish orange solid. The crude mixture was purified on silica eluted with 30→50 % EtOAc/hexanes to yield 0.063 g (15 %) of reddish orange solid. Mp = 228-230 °C. ATR-IR not obtained. 1H -NMR (400 MHz, $CDCl_3$): 3.90 (s, 6H), 3.95 (s, 12H), 6.80 (s, 4H), 7.05-7.09 (d, 2H, J = 16 Hz), 7.21-7.25 (d, 2H, J = 16 Hz), 7.40-7.42 (d, 2H, J = 8 Hz), 7.66-7.68 (d, 2H, J = 8 Hz), 7.75 (s, 2H).

Dianisylamino-3,5-dimethoxybenzene (3,5-dimethoxy-N,N-bis(4-methoxyphenyl)aniline):¹⁹



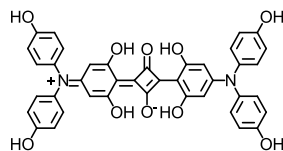
Prepared using the general procedure for Ullmann Coupling using 0.554 g (3.62 mmol) of 3,5-dimethoxyaniline and 2.54 g (10.9 mmol, 3 eq) of iodoanisole. After three days, the reaction mixture was worked up as described in the general procedure. The crude mixture was purified on silica eluted with 100 % hexanes → 100 % DCM to yield 0.850 g (64 %) tan-white solid. Mp not obtained. ATR-IR (neat, cm^{-1}) 1200 (s, Ar-O, Ar-N str); 1H -NMR (400 MHz, $DMSO-d_6$): 3.59 (s, 6H), 3.73 (s, 6H), 5.84-5.85 (d, 2H, J = 2 Hz), 6.02 (t, 1H, J = 2 Hz), 6.88-6.90 (d, 4H, J = 8 Hz), 7.00-7.02 (d, 4H, J = 8 Hz). MS (FAB, m/z): found 365.2, calculated for $C_{22}H_{23}NO_4$ 365.16271.

Diphenolyl-3,5-dihydroxybenzene (5-(bis(4-hydroxyphenyl)amino)benzene-1,3-diol):¹⁹



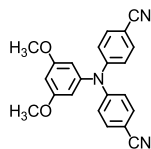
Prepared using the general procedure for demethylation using 1.20 g (3.29 mmol) of dianisylamino-3,5-dimethoxybenzene and 1.25 mL (13.2 mmol, 4 eq) of BBr₃ in 16 mL of dry DCM. The reaction mixture turned bright red upon BBr₃ addition, and gave an orange-red slurry after time. The reaction was worked up as described in the general procedure to give a tan-white solid in quantitative yield (1.01 g). Product was used in the next step without further purification. Mp not obtained. ATR-IR (neat, cm⁻¹) 3293 (br, O-H str), 1219-1258 (s, Ar-O, Ar-N str); ¹H-NMR (400 MHz, DMSO-*d*₆): 5.56-5.57 (d, 2H, J = 2 Hz), 5.61-5.62 (t, 1H, J = 2 Hz), 6.69-6.71 (d, 4H, J = 8 Hz), 6.87-6.90 (d, 4H, J = 8 Hz) 8.84 (s, 2H), 9.26 (s, 2H). MS (FAB, *m/z*): found 309.1, calculated for C₁₈H₁₅NO₄ 309.10011.

SQ-OH (2,4-bis-(4-(bis(4-hydroxyphenyl)amino)-2,6-dihydroxyphenyl)-3-oxocyclobut-1-enolate):¹⁹



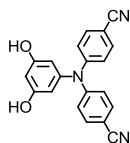
Diphenolyl-3,5-dihydroxybenzene (1.18 g, 3.81 mmol) and) squaric acid (0.218 g, 1.91 mmol, 0.5 eq) were dissolved in 25 mL of 1:1 toluene/n-butanol under nitrogen and heat at reflux overnight. After just 30 min the reaction mixture turned from clear tan to very dark green/blue. After 16 h the reaction was cooled to -20 °C and filtered to collect the dark green precipitate, which was washed thoroughly with toluene, then hexanes to give 1.00 g (75 %) of green solid. Mp > 260 °C. ATR-IR (neat, cm⁻¹) 1208 (s, C-O, C-N str), 3342-3459 (s/br, O-H str); ¹H-NMR (400 MHz, DMSO-*d*₆): 5.47 (s, 4H), 6.81-6.83 (d, 8H, J = 8 Hz), 7.13-7.15 (d, 8H, J = 8 Hz), 9.76 (s, 4H) 11.3 (s, 4H). MS (FAB, *m/z*): found 696.2, calculated for C₄₀H₂₈N₂O₁₀ 696.17440.

Bis-*N,N*-(*p*-cyanophenyl)amino-3,5-dimethoxybenzene (4,4'-((3,5-dimethoxyphenyl)azanediyl)dibenzonitrile):



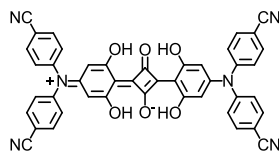
Prepared using the general procedure for Ullmann Coupling using 0.554 g (3.62 mmol) of 3,5-dimethoxyaniline and 2.49 g (10.9 mmol, 3 eq) of *p*-iodobenzonitrile. After three days, the reaction mixture was worked up as described in the general procedure. The crude mixture was purified on silica eluted with 100 % hexanes → 100 % DCM → 10 % MeOH/DCM to yield 1.02 g (78 %) of white solid. Mp = 158-159 °C. ATR-IR (neat, cm⁻¹) 2216 (s, C≡N str); ¹H-NMR (400 MHz, DMSO-*d*₆): 3.70 (s, 6H), 6.31-6.32 (d, 2H, J = 2 Hz), 6.47-6.48 (d, 1H, J = 2 Hz), 7.12-7.14 (d, 4H, J = 8 Hz), 7.72-7.74 (d, 4H, J = 8 Hz).

Bis-*p*-cyanophenylamino-3,5-dihydroxybenzene (4,4'-((3,5-dihydroxyphenyl)azanediyl)dibenzonitrile):



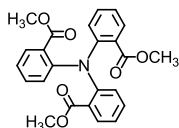
Prepared using the general procedure for demethylation using 1.16 g (3.26 mmol) of *N,N*-bis-(*p*-cyanophenyl)amino-3,5-dimethoxybenzene and 1.25 mL (13.2 mmol, 4 eq) of BBr₃ (required 2 eq per -OCH₃) in 32 mL of dry DCM. The reaction mixture turned bright red upon BBr₃ addition, and gave an orange-red slurry after time. The reaction was worked up as described in the general procedure to give a tan solid in quantitative yield (1.06 g). Product used in the next step without further purification. Mp not obtained. ATR-IR (neat, cm⁻¹) 2228 (s, C≡N str), 3349 (br, O-H str); ¹H-NMR (400 MHz, DMSO-*d*₆): 5.56-5.57 (d, 2H, J = 2 Hz), 5.61-5.62 (t, 1H, J = 2 Hz), 6.69-6.71 (d, 4H, J = 8 Hz), 6.87-6.90 (d, 4H, J = 8 Hz) 8.84 (s, 2H), 9.26 (s, 2H).

Attempted synthesis of SQ-CN (2,4-bis-(4-(bis(4-cyanophenyl)amino)-2,6-dihydroxyphenyl)-3-oxocyclobut-1-enolate):



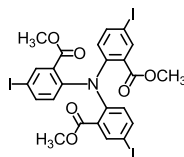
Bis-p-cyanophenylamino-3,5-dihydroxybenzene (0.710 g, 3.81 mmol) and 0.124 g (1.09 mmol, 0.5 eq) of squaric acid were dissolved in 25 mL of 1:1 toluene/n-butanol under nitrogen and heated at reflux for 3 days. The reaction was cooled to -20 °C to maximize precipitate, filtered, and the solid washed with toluene followed by hexanes to give a dark violet powdery product. ¹H-NMR was inconclusive, and product impure by TLC. Column chromatography failed, crystallization does not give pure product by NMR, dark blue filtrates decomposed into light brown solutions.

TAA-Triester (trimethyl 2,2',2''-nitrilotribenzoate):



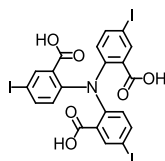
This procedure was modified from the literature.^{20,21} Prepared using the general procedure for Ullmann Coupling using 1.0 mL (1.17 g, 7.74 mmol) of methyl 2-aminobenzoate and 3.4 mL (6.08 g, 20.3 mmol, 3 eq) of methyl 2-iodobenzoate. (Note: Reaction should be carried out in the dark, since methyl 2-aminobenzoate is light-sensitive.) After three days, the reaction mixture was worked up as described in the general procedure. The crude mixture was poured into hexanes and cooled at -20 °C for 30-60 minutes to give 2.02 g of powdery yellow precipitate (62 %). The filtrate was concentrated in vacuo, and purified on silica eluted with 100 % hexanes → 100 % DCM → 10-20 % MeOH/DCM giving 2.63 g (81 %) of product. Mp = 134-135 °C (lit mp 130.0-130.8).²² ¹H-NMR (400 MHz, DMSO-*d*₆): 3.26 (s, 9H), 6.93-6.95 (d, 3H, J = 8 Hz), 7.13-7.17 (dt, 3H, J = 8 Hz), 7.43-7.47 (dt, 3H, J = 8 Hz), 7.49-7.52 (dd, 3H, J = 8 Hz, J' = 2 Hz).

TriIodo-TAA-Triester (trimethyl 2,2',2''-nitritotribenzoate):



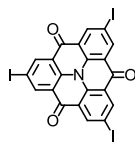
The procedure was modified from the literature.²¹ TAA-triester (0.250 g, 0.596 mmol) was combined with I₂ (0.454 g, 1.79 mmol, 3 eq) and of Ag₂SO₄ (0.558 g, 1.79 mmol, 3 eq). 95% EtOH (40 mL) was added, and the reaction stirred overnight at room temperature. The resulting yellow precipitate was filtered away, the solids were washed with DCM, and combined organic layers was concentrated *in vacuo* to give a powdery yellow solid, 0.433 g (92 %). No further purification was deemed necessary, and this product used immediately for the next step (hydrolysis). ¹H-NMR (400 MHz, DMSO-*d*₆): 3.31 (s, 9H), 6.72-6.74 (d, 3H, J = 8 Hz), 7.78-7.81 (m, 6H).

TriIodo-TAA-Triacid (trimethyl 2,2',2''-nitritotribenzoate):



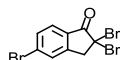
This procedure was modified from the literature.²¹ Triiodo-TAA-Triester (0.250 g, 0.314 mmol) was combined with KOH (0.264 g, 4.71 mmol, 15 eq) in 15 mL of 4:1 MeOH/H₂O. The reaction mixture was heated overnight at 50 °C, cooled to room temperature, poured into 80 mL of H₂O, and acidified with 1 M aq HCl to pH ≈ 3 to produce a white precipitate. The solids were filtered away, dissolved in EtOAc, and dried over anhydrous MgSO₄ to give 0.204 g (86 %) of off-white solid. ¹H-NMR indicates some minor impurity, but the product was used anyway without further purification. ¹H-NMR (400 MHz, DMSO-*d*₆): 3.33 (s, broad with H₂O peak, 3H), 6.65-6.67 (m, 3H), 7.75-7.91 (m, 6H).

TriIodo-Heterotriangulene (2,6,10-triiodo-12c-aza-dibenzo[cd,mn]pyrene-4,8,12-trione):



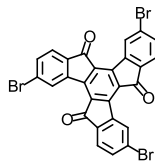
This procedure was modified from the literature.^{20,21} TriIodo-TAA-Triacid (0.500 g, 0.662 mmol) was dissolved in 13 mL of dry DCM under nitrogen. SOCl₂ (1.5 mL, of ~20 mmol, ~30 eq) and 0.5 mL of dry DMF were added, and the reaction mixture heated at reflux for 3 h. SnCl₄ (1.4 mL, 11.9 mmol, 18 eq) was then added dropwise (slowly!) with continued heating to give a bright red solution with some red precipitate. After 24 h, the reaction was allowed to cool to room temperature and poured carefully into ice cold 1 M aq NaOH. Red chunks were broken up with stirring to give a yellow solid. The solids were then filtered away, washed with H₂O, and then thoroughly with acetone. The aqueous filtrate was extracted with DCM, dried over anhydrous MgSO₄, and concentrated *in vacuo*. The resulting solids were combined with the filtered solids to give 0.214 g yellow solid (46% yield). ¹H-NMR (400 MHz, CDCl₃/TFA): 9.32 (s, 6H), peak very small due to low solubility.

Tribromoindanone (2,2,5-tribromo-2,3-dihydro-1H-inden-1-one):



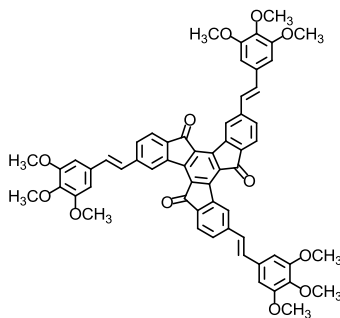
Procedure adapted from the literature.²³ 5-Bromoindan-1-one (7.00 g, 4.74 mmol) was dissolved in chloroform and cooled to 0 °C, and Br₂ (3.5 mL, 68.7 mmol, 2.07 eq) added slowly. The reaction mixture was stirred for 1 h at room temperature, and then nitrogen was bubbled in to remove excess Br₂. The reaction mixture was concentrated *in vacuo* and recrystallized from boiling methanol to give 10.8 g (88 %) of product after two crops. ¹H-NMR (400 MHz, CDCl₃/TFA): 4.26 (s, 1H), 7.59 (s, 1H), 7.63-7.65 (d, 1H, J = 8 Hz), 7.79-7.81 (d, 1H, J = 8Hz). Mp = 93-95 °C (lit mp = 93 °C).¹⁹

4,9,14-Tribromotru xenone (3,8,13-tribromo-5H-diindeno[1,2-a:1',2'-c]fluorene-5,10,15-trione):



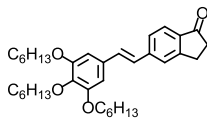
This procedure was adapted from the literature.²³ 2,2,5-tribromoindanone (23.9 g, 64.7 mmol) was heated at 220 °C in a preheated oil bath for 1.5 h during which time a vapor evolved (presumably HBr). After vapor evolution ceased, the crude blackish-brown solid was suspended in chloroform, sonicated for 15 min, filtered, and washed with chloroform until the filtrate was not sludgy; the remaining crude solid weighted 2.15 g (16 % yield). Recrystallization from nitrobenzene, filtration, chloroform washing, and air drying gave 0.644 g (4.8 %) of tan solid that was not soluble enough for NMR. ATR-IR (neat, cm⁻¹) 1706 (s, C=O str).

Attempted synthesis of 4,9,14-Tris-(trimethoxystyryl)truxenone (3,8,13-tris((E)-3,4,5-trimethoxystyryl)-5H-diindeno[1,2-a:1',2'-c]fluorene-5,10,15-trione):



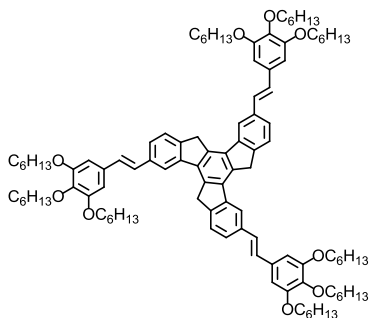
Attempted using the general procedure for Heck Coupling using 0.250 g (0.403 mmol) of 4,9,14-tribromotru xenone and 0.293 g (1.51 mmol, 3.75 eq) of 3,4,5-trimethoxystyrene. After three days, the dark red reaction mixture was worked up as described in the general procedure. The resulting aqueous suspension was extracted with DCM, dried over anhydrous MgSO₄, and concentrated *in vacuo* to give a dark red solid. Attempts to purify by column or crystallization did not succeed. Crude MS (FAB, *m/z*): found *m/z* = 961.3, calculated for C₆₀H₄₈O₁₂ *m/z* = 960.31458.

5-Trihexyloxystyrylindan-1-one ((E)-5-(3,4,5-tris(hexyloxy)styryl)-2,3-dihydro-1H-inden-1-one):



Prepared using the general procedure for Heck Coupling using 0.476 g (2.25 mmol) of 5-bromoindan-1-one and 1.00 g (2.47 mmol, 1.1 eq) of 3,4,5-trihexyloxystyrene (provided by Timothy Gehan). After three days, the reaction mixture was worked up as described in the general procedure. The resulting aqueous suspension was extracted with DCM, dried over $MgSO_4$, and concentrated *in vacuo* to give crude tan solid. Purification on silica eluted with 5 → 20 % EtOAc/hexanes yielded 0.825 g (70 %) of tan solid that fluoresces teal-white under long-wave UV. Mp = 62-64 °C. ATR-IR not obtained; 1H -NMR (400 MHz, $CDCl_3$): 0.90-0.93 (m, 9H), 1.33-1.36 (m, 12H), 1.46-1.52 (m, 6H), 1.72-1.80 (m, 2H), 1.80-1.87 (m, 4H), 2.70-2.73 (t, 2H, J = 6 Hz), 3.13-3.16 (t, 2H, J = 6 Hz), 3.97-4.00 (t, 2H, J = 7 Hz), 4.00-4.05 (t, 4H, J = 7 Hz), 6.74 (s, 2H), 7.00-7.04 (d, 1H, J = 8 Hz), 7.14-7.18 (d, 1H, J = 8 Hz), 7.49-7.51 (d, 1H, J = 4 Hz), 7.56 (s, 1H), 7.72-7.74 (d, 1H, J = 8 Hz). MS (FAB, m/z): found 534.4, calculated for $C_{35}H_{50}O_4$ 534.76910.

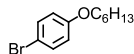
4,9,14-Tris-(trihexyloxystyryl)truxene (3,8,13-tris((E)-3,4,5-tris(hexyloxy)styryl)-10,15-dihydro-5H-diindeno[1,2-a:1',2'-c]fluorene):



5-Trihexyloxystyrylindan-1-one (0.250 g, 0.468 mmol) and p-toluene sulfonic acid (0.282 g, 1.64 mmol, 3.5 eq) were combined under nitrogen atmosphere in 0.1 mL of acetic acid and 0.35 mL of *o*-dichlorobenzene. The mixture was sparged with nitrogen and heated at 105 °C overnight. This reaction seems never to go to completion, always showing starting material by

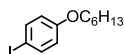
TLC (20 % ethyl acetate/hexanes), with a second spot having higher R_f . Isolation of the crude reaction mixture gave inconclusive $^1\text{H-NMR}$.

1-Bromo-4-hexyloxybenzene:



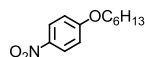
This procedure was modified from the literature.²⁴ 4-Bromophenol (5.00 g, 29.0 mmol) was combined with K_2CO_3 (4.00 g, 29.0 mmol, 1 eq) and NaI (0.435 g, 2.90 mmol, 0.1 eq) in 60 mL of 2-butanone under nitrogen. The reaction mixture was heated to 80 °C 5 mL (32.0 mmol, 1.1 eq) of n-bromohexane was added, and the reaction stirred with heating overnight. The reaction was cooled to room temperature, filtered, and washed with H_2O . The organic layer was separated and dried over anhydrous MgSO_4 , and concentrated *in vacuo*. The crude product was purified by running through a pad of silica gel with hexanes to give 7.28 g (98 %) of yellowish oil. $^1\text{H-NMR}$ (400 MHz, CDCl_3): 0.89-0.92 (m, 3H), 1.31-1.36 (m, 4H), 1.41-1.48 (m, 2H), 1.72-1.80 (p, 2H, $J = 7$ Hz), 3.89-3.92 (t, 2H, $J = 7$ Hz), 6.76-6.78 (d, 2H $J = 8$ Hz), 7.34-7.36 (d, 2H, $J = 8$ Hz).

1-Hexyloxy-4-iodobenzene:



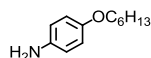
This procedure was modified from the literature.²⁴ 4-Iodophenol (5.00 g, 22.8 mmol) was combined with anhydrous K_2CO_3 (3.15 g, 22.8 mmol, 1 eq) and NaI (0.337 g, 2.28 mmol, 0.1 eq) in 50 mL of 2-butanone under nitrogen. The reaction mixture was heated to 80 °C, 3.9 mL (25.1 mmol, 1.1 eq) of n-bromohexane was added, and the reaction heated with stirring overnight. The reaction was cooled to room temperature, filtered, and washed with H_2O . The organic layer was separated and dried over anhydrous MgSO_4 , and concentrated *in vacuo*. The crude product was purified by running through a pad of silica with 20 % ethyl acetate/hexanes to give 6.80 g (99 %) of yellowish oil.

1-Hexyloxy-4-nitrobenzene:



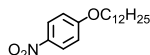
This procedure was modified from the literature.^{25,26} 4-Nitrophenol (1.00 g, 7.40 mmol) was combined with 1.99 g anhydrous K_2CO_3 (14.4 mmol, 2 eq) and NaI (0.108 g, 0.720 mmol, 0.1 eq) in 24 mL of 2-butanone under nitrogen. The reaction mixture was heated to 80 °C, 1.1 mL (7.92 mmol, 1.1 eq) n-bromohexane was added, and the reaction heated with stirring overnight. The reaction was cooled to room temperature, filtered, and washed with H_2O . The organic layer was separated and extracted with ethyl acetate, dried over anhydrous $MgSO_4$, and concentrated *in vacuo*. The crude product was purified over silica with 20 % ethyl acetate/hexanes to give 1.54 g (96 %) of yellowish oil. 1H -NMR (400 MHz, acetone- d_6): 0.89-0.92 (m, 3H), 1.34-1.38 (m, 4H), 1.45-1.53 (m, 2H), 1.79-1.86 (p, 2H, J = 8 Hz), 4.14-4.18 (t, 2H, J = 8 Hz), 7.12-7.14 (d, 2H, J = 8 Hz), 8.20-8.22 (d, 2H, J = 8 Hz).

4-Hexyloxyaniline:



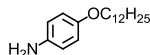
This procedure was adapted from the literature.²⁷ 1-(Hexyloxy)-4-nitrobenzene (10.9 g, 48.8 mmol) was dissolved in 80 mL of 95 % ethanol under nitrogen. The reaction mixture was heated to 50 °C, and a few milligrams of 10 % Pd/C was added, followed by 3 mL of hydrazine hydrate, followed by another few milligrams of 10 % Pd/C, at which time the reaction mixture began to bubble vigorously. The reaction was heated at 50 °C overnight, cooled to room temperature, and filtered. The solid was washed with H_2O , the filtrate was extracted with DCM, and the combined organic layers were dried over anhydrous $MgSO_4$, filtered and concentrated *in vacuo* to give 8.57 g (90 %) of brown crystalline solid. 1H -NMR (400 MHz, DMSO- d_6): 0.85-0.88 (t, 3H, J = 8 Hz), 1.26-1.30 (m, 4H), 1.34-1.39 (m, 2H), 1.59-1.66 (p, 2H, J = 8 Hz), 3.77-3.80 (t, 2H, J = 8 Hz), 4.56 (s, 2 H), 6.47-6.49 (d, 2H, J = 8 Hz), 6.71-6.93 (d, 2H, J = 8 Hz).

1-(Dodecyloxy)-4-nitrobenzene:

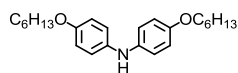


This procedure was modified from the literature.^{25,26} 4-Nitrophenol (5.00 g, 35.9 mmol) was combined with anhydrous K_2CO_3 (9.92 g, 71.8 mmol, 2 eq) and NaI (0.538 g, 3.59 mmol, 0.1 eq) in 120 mL of 2-butanone under nitrogen. The reaction mixture was heated to 80 °C and n-bromododecane (13.0 mL, 53.9 mmol, 1.5 eq) was added, and the mixture was heated with stirring overnight. The reaction was cooled to room temperature and filtered. The solid was washed with H_2O , the filtrate was extracted with DCM, and the combined organic layers were dried over anhydrous $MgSO_4$, filtered, and concentrated *in vacuo* to give a yellowish oil in quantitative yield (11.0 g). 1H -NMR (400 MHz, $DMSO-d_6$): 0.83-0.86 (t, 3H, J = 6 Hz), 1.24 (m, 16H), 1.37-1.42 (m, 2H), 1.70-1.75 (p, 2H), 4.09-4.13 (t, 2H, J = 6 Hz), 7.12-7.15 (d, 2H, J = 9 Hz), 8.18-8.21 (d, 2H, J = 9 Hz).

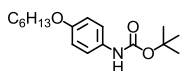
4-Dodecyloxyaniline:



This procedure was adapted from the literature.²⁷ 1-(dodecyloxy)-4-nitrobenzene (0.345 g, 2.48 mmol) was dissolved in 80 mL of 95 % ethanol under nitrogen. The reaction mixture was heated to 50 °C and a few milligrams of 10 % Pd/C was added, followed by 1 mL of hydrazine hydrate, followed by another few milligrams of 10 % Pd/C, at which time the reaction mixture began to bubble vigorously. The reaction was heated at 50 °C overnight, cooled to room temperature, and filtered. The solid was washed with H_2O , the filtrate was extracted with DCM, and the combined organic layers were dried over anhydrous $MgSO_4$, filtered, and concentrated *in vacuo* to give 0.0830 g (23 %) of tan solid after crystallization from boiling heptane. Mp not obtained. 1H -NMR (400 MHz, $DMSO-d_6$): 0.84-0.87 (m, 3H), 1.25-1.39 (m, 18H), 1.59-1.66 (p, 2H), 3.77-3.81 (t, 2H, J = 6 Hz), 4.57 (s, 2H), 6.47-6.49 (d, 2H, J = 8 Hz), 6.61-6.63 (d, 2H, J = 8 Hz).

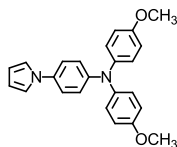
BHPA [bis(4-(hexyloxy)phenyl)amine]:

Prepared via Buchwald-Hartwig amination using 0.500 g (1.94 mmol) of *p*-bromohexyloxybenzene, 0.470 g (2.43 mmol, 1.25 eq) of *p*-hexyloxyaniline, 0.108 g (0.194 mmol, 0.1 eq) of DPPF, 0.0444 g (0.0485 mmol, 0.025 eq) of Pd₂dba₃, and 0.361 g (2.72 mmol, 1.4 eq) of *t*-BuONa in 4 mL of dry toluene. After reacting 2 h the reaction mixture was worked up as described in the general procedure. The resulting reddish-brown solid was recrystallized in two crops from heptane to yield 0.469 g (65 %) of brown solid. ¹H-NMR (DMSO-*d*₆): δ 0.86-0.89 (t, 6H, J = 7 Hz), 1.29-1.31 (m, 8 H), 1.36-1.43 (p, 4H), 1.63-1.70 (p, 4H), 3.85-3.88 (t, 4H, J = 7 Hz), 6.78-6.80 (d, 4H, J = 8 Hz), 6.87-6.89 (d, 4H, J = 8 Hz), 7.48 (s, 1H). Mp not obtained (lit mp = 77-79 °C).²⁸

BOC-HexOAniline (*tert*-butyl 4-(hexyloxy)phenylcarbamate):

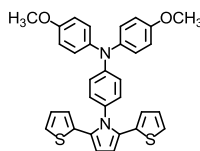
This procedure was adapted from the literature.¹⁸ indium tribromide (0.018 g, 0.0500 mmol, 0.01 eq) was added to di-*t*-butyl carbonate (1.09 g, 5.00 mmol, 1 eq) with stirring. 4-(Hexyloxy)aniline (0.966 g, 5.00 mmol) was added to the reaction mixture in one portion, and the mixture stirred for 30 min at room temperature. Hexane was added during the reaction as needed to prevent clumping. When complete, the reaction mixture was diluted with EtOAc and washed with water. The organic layer was dried over anhydrous MgSO₄, filtered, and concentrated *in vacuo* to give a gray-brown solid. Recrystallization from hot heptane yielded 1.12 g (76 %) of small, light gray needles after two crops. Mp not obtained. ¹H-NMR (400 MHz, DMSO-*d*₆): 0.85-0.89 (m, 3H), 1.27-1.31 (m, 4H), 1.37-1.41 (m, 2H), 1.45 (s, 9H), 1.63-1.70 (m, 2H), 3.86-3.89 (t, 2H, J = 6 Hz), 6.79-6.82 (d, 2H, J = 8 Hz), 7.30-7.32 (d, 2H, J = 8 Hz), 9.10 (s, 1H).

DAAPP (4-Dianisylamino-*N*-phenylpyrrole) (N-(4-(1H-pyrrol-1-yl)phenyl)-4-methoxy-N-(4-methoxyphenyl)aniline):



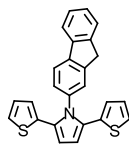
Prepared using the general procedure for Buchwald-Hartwig amination using 0.250 g (1.13 mmol) of 4-bromo-*N*-phenylpyrrole and 0.312 g (1.36 mmol, 1.2 eq) of DAA. After 2 h, the reaction mixture was worked up as described in the general procedure. The crude mixture was purified on silica eluted with hexanes → 10:90 EtOAc/hexanes to yield 0.293 g (70 %) of sticky clear yellowish oil. ¹H-NMR (400 MHz, DMSO-*d*₆): 3.73 (s, 3 H), 6.21 (s, 2H), 6.83-6.85 (d, 2H, J = 8 Hz), 6.89-6.91 (d, 4H, J = 8 Hz), 6.99-7.01 (d, 4H, J = 8 Hz), 7.20 (s, 2H), 7.35-7.37 (d, 2H, J = 8 Hz); MS (FAB, *m/z*): found 370.2, calculated for C₂₄H₂₂N₂O₂ 370.16813.

DAAPDTP (Dianisylaminophenyl-dithienylpyrrole) (4-(2,5-di(thiophen-2-yl)-1H-pyrrol-1-yl)-*N,N*-bis(4-methoxyphenyl)aniline):



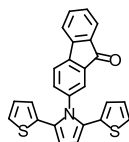
Prepared under Buchwald-Hartwig amination conditions using 0.229 g (0.593 mmol) of 4-bromo-*N*-phenyl-2,5-(dithiophen-2-yl)pyrrole (provided by Jonathan Tinkham), 0.148 g (0.652 mmol, 1.1 eq) of dianisylamine, 0.0359 g (0.0647 mmol, 0.1 eq) of DPPF, 0.0148 g (0.0162 mmol, 0.025 eq) of Pd₂dba₃, and 0.0871 g (0.906 mmol, 1.4 eq) of *t*-BuONa in 3 mL of dry toluene. After 3 days, the reaction mixture was worked up as described in the general procedure. The crude mixture was purified on silica eluted with 5 % → 20 % EtOAc/hexanes to yield 0.265 g (84 %) of brown sticky solid. ¹H-NMR (400 MHz, DMSO-*d*₆): 3.80 (s, 6H), 6.53 (s, 2H), 6.70-6.71 (dd, 2H, J = 4 Hz, J' = 1 Hz), 6.84-6.89 (m, 6H), 6.91-6.93 (d, 2H, J = 8 Hz), 7.06-7.12 (m, 8H). This material was subjected to further use and testing by Jonathan Tinkham, who will report those results subsequently.

***N*-Fluorenyl-dithienylpyrrole (1-(9H-fluoren-2-yl)-2,5-di(thiophen-2-yl)-1H-pyrrole):**

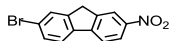


1,4-Di(thiophen-2-yl)butane-1,4-dione (0.0500 g, 0.200 mmol, 1 eq) and (0.181 g, 1.00 mmol, 5 eq) of 2-aminofluorene were combined in 3.5 mL acetic acid. The reaction mixture was heating using a CEM MARS Organic Reactor (microwave reactor) at 180 °C for 15 min. The product was precipitated into water, washed with water, air-dried, and purified by silica gel chromatography eluting with 10 % ethyl acetate/hexanes to give 0.0540 g (68 %) of tan solid product. Mp = 220-222 °C. ¹H-NMR (400 MHz, CDCl₃): 3.93 (s, 2H), 6.56-6.57 (m, 4H), 6.77-6.79 (m, 2H), 7.00-7.01 (d, 2H, J = 4 Hz), 7.34-7.38 (m, 2H), 7.41-7.45 (t, 1H, J = 8 Hz), 7.48 (s, 1H), 7.57-7.59 (d, 1H, J = 8 Hz), 7.83-7.86 (m, 2H). MS (FAB, *m/z*): found 395.1, calculated for C₂₅H₁₇NS₂ 395.08024.

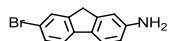
***N*-Fluorenonyl-dithienylpyrrole (2-(2,5-di(thiophen-2-yl)-1H-pyrrol-1-yl)-9H-fluoren-9-one):**



Prepared using the general fluorene oxidation procedure using 0.0250 g (0.0632 mmol, 1 eq) of *N*-fluorenyl-dithienylpyrrole and 0.103 g (0.316 mmol, 5 eq) of Cs₂O₃ in 4 mL of dry DMSO at 40 °C. After 3 h, the reaction was worked up as described in the general procedure to give 0.0255 g (99 %) of yellow solid. Mp not obtained. ¹H-NMR (400 MHz, acetone-*d*₆): 6.58 (s, 2H), 6.78-6.79 (dd, 2H, J = 4 Hz, J' = 1 Hz), 6.87-6.89 (dd, 2H, J = 4 Hz, J' = 1 Hz), 7.24-7.25 (dd, 2H, J = 5 Hz, J' = 1 Hz), 7.45-7.49 (t, 1H, J = 8 Hz), 7.52-7.56 (m, 2H), 7.66-7.70 (m, 2H), 7.87-7.91 (t, 2H, J = 8 Hz). This material was subjected to further use and testing by Jonathan Tinkham, who will report those results subsequently.

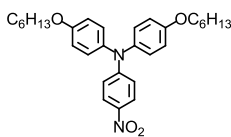
BrNO₂Fl (2-bromo-7-nitro-9H-fluorene):

This procedure was adapted from the literature.²⁹ 2-Bromofluorene (8.82 g, 36.0 mmol) was suspended in 100 mL of acetic acid and heated to 100 °C until dissolved, then cooled to 50 °C. Concentrated HNO₃ (8 mL) was added dropwise, as the reaction mixture fumed with white vapor. The reaction was allowed to stir with heating at 50 °C overnight, as a yellow precipitate formed. The reaction was then cooled to room temperature, filtered, and the precipitate washed with acetic acid until the washings were colorless. The solids were then washed thoroughly with water to give 8.00 g (77 %) of yellowish-white solid. Mp = 235-237 °C, lit. 233-234 °C);³⁰ ¹H-NMR (400 MHz, CDCl₃): 4.01 (s, 2H), 7.58-7.60 (dd, 1H, J = 8 Hz, J' = 1 Hz), 7.72-7.74 (d, 1H, J = 8 Hz), 7.72 (s, 1H), 7.84-7.86 (d, 1H, J = 8 Hz), 8.29-8.32 (dd, 1H, J = 8 Hz, J' = 2 Hz), 8.40 (s, 1H).

BrAF1 (7-bromo-9H-fluoren-2-amine):

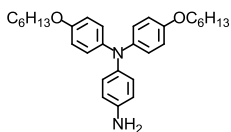
BrNO₂Fl (1.50 g, 5.17 mmol) was suspended in 17 mL of 100 % ethanol under nitrogen, and the reaction mixture vigorously boiled. Iron powder (0.866 g, 15.5 mmol, 3 eq) was added, followed by careful addition of 22 mL of concentrated HCl (4.2 mL/mmol of starting material) over 20 min, during which time the reaction mixture became yellow and chunky. The reaction mixture was heated at 90 °C overnight, cooled to room temperature, and the precipitate was filtered and washed with ethanol and conc. aq. Na₂CO₃. The white solid was column purified over silica eluted with DCM → 10 % MeOH/DCM to give 0.490 g (37 %) of white powdery solid. Mp not obtained. ¹H-NMR (400 MHz, DMSO-d₆): 3.76 (s, 2H), 5.29 (s, 2H), 6.57-6.59 (d, 1H, J = 8 Hz), 6.75 (s, 1H), 7.41-7.43 (d, 1H, J = 8 Hz), 7.51-7.56 (overlapping doublets, 2H, J₁ = J₂ = 8 Hz), 8.60 (s, 1H).

Bis-hexyloxyphenylamino-nitrobenzene (*N,N*-Bis-(4-(hexyloxy)phenyl)-4-nitroaniline):



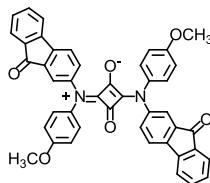
Prepared using the general procedure for Ullmann Coupling using 0.250 g (1.81 mmol) 4-nitroaniline and 1.65 g (5.44 mmol, 3 eq) 1-(hexyloxy)-4-iodobenzene. After three days, the reaction mixture was worked up as described in the general procedure. The crude mixture was purified on silica eluted with 100 % hexanes → 20 % ethyl acetate/hexanes to yield 0.886 g (96 %) of a sticky reddish-orange oil. ¹H-NMR (400 MHz, DMSO-*d*₆): 0.86-0.89 (m, 6H), 1.29 (m, 8H), 1.40 (m, 4H), 1.68-1.71 (m, 4H), 3.95 (m, 4H), 6.60-6.62 (d, 2H, J = 8 Hz), 6.97-6.99 (d, 4H, J = 8 Hz), 7.21-7.23 (d, 4H, J = 8 Hz), 7.99-8.01 (d, 2H, J = 8 Hz).

4-[Bis-*N,N*-(p-hexyloxyphenyl)amino]aniline:



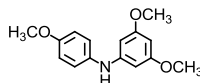
N,N-Bis-hexyloxyphenylamino-*N*-nitrobenzene (0.250 g, 0.510 mmol) was dissolved in 1 mL of 95 % ethanol under nitrogen. The reaction mixture was heated to 50 °C and a few milligrams of 10 % Pd/C was added, followed by 0.05 mL of hydrazine hydrate, followed by another few milligrams of 10 % Pd/C, at which time the reaction mixture began to bubble vigorously. The reaction was heated at 50 °C for 12 h with a few 50 microliter extra additions of hydrazine hydrate. Subsequently, it was allowed to cool to room temperature and filtered. The solids were filtered and washed with DCM to collect the organic product, and the DCM filtrate was washed with water, dried over anhydrous MgSO₄, and concentrated *in vacuo* to give a crude brown sticky oil in quantitative yield (0.230 g). Column purification attempts resulted in decomposition, crude ¹H-NMR too messy for characterization.

SQ-OH (2,4-bis-((4-methoxyphenyl)(9-oxo-9H-fluoren-3-yl)amino)-3-oxocyclobut-1-enolate):



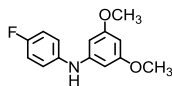
Anisylaminofluorenone (FOAA, 0.100 g, 0.332 mmol) and squaric acid (0.189 g, 0.166 mmol, 0.5 eq) were dissolved in 10 mL of 1:1 toluene/n-butanol under nitrogen and heated at reflux for 3 days. The reaction was cooled to -20 °C and filtered to collect a bright orange precipitate (fluorescent yellowish orange under long wave UV). The precipitate was washed thoroughly with toluene, then hexanes to give an orange solid (mass not obtained). Much of the FOAA starting material was not consumed even after 3 days and did not precipitate with the product. Mp not obtained. ATR-IR not obtained. ¹H-NMR (400 MHz, DMSO-*d*₆): 3.80-3.81 (d, 6H), 5.75-5.76 (d, 7.77H??), 6.99-7.02 (dd, 4H, J = 9 Hz, J' = 2 Hz), 7.28-7.30 (d, 2H, J = 8 Hz), 7.34 (s, 2H), 7.37-7.41 (m, 2H), 7.46-7.48 (d, 2H, J = 8 Hz), 7.62-7.66 (m, 4H), 7.82-7.87 (m, 4H). NMR peaks are well defined, but the results are inconclusive. MS not obtained.

AAPh(OMe)₂ (Anisylamino-dimethoxybenzene) (3,5-dimethoxy-N-(4-methoxyphenyl)aniline):



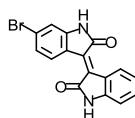
Prepared using the general procedure for Buchwald-Hartwig amination using 0.800 g (5.22 mmol, 1.25 eq) of 3,5-dimethoxyaniline and 0.52 mL (4.18 mmol, 1 eq) of 4-bromoanisole. The mixture was reacted overnight and worked up as described in the general procedure. The crude brown oil was purified on silica eluted with hexanes → 20 % EtOAc/hexanes to yield 0.880 g (82 %) of sticky clear yellowish-tan oil. ¹H-NMR (400 MHz, DMSO-*d*₆): 3.66 (s, 6H), 3.71 (s, 3H), 5.89 (s, 1H), 6.06-6.07 (d, 2H, J = 4 Hz), 6.86-6.88 (d, 2H, J = 8 Hz), 7.04-7.06 (d, 2H, J = 8 Hz), 7.84 (s, 1H).

FPhA₂(OMe)₂ (Fluorophenylamino-dimethoxybenzene) (*N*-(4-fluorophenyl)-3,5-dimethoxyaniline):



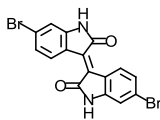
Prepared using the general procedure for Buchwald-Hartwig amination using 0.800 g (5.22 mmol, 1.25 eq) of 3,5-dimethoxyaniline and 0.46 mL (4.18 mmol, 1 eq) of 1-bromo-4-fluorobenzene. The mixture was reacted overnight and worked up as described in the general procedure. The crude brown oil was purified on silica eluted with hexanes → 20 % EtOAc/hexanes to yield 0.939 g (91 %) of sticky clear yellowish-tan oil. ¹H-NMR (400 MHz, DMSO-*d*₆): 3.68 (s, 6H), 5.98 (s, 1H), 6.14-6.15 (d, 2H, J = 2 Hz), 7.08-7.10 (m, 4H), 8.10 (s, 1H).

6-Bromoisindigo [(*E*)-6-bromo-[3,3'-biindolinylidene]-2,2'-dione]:



This procedure was adapted from Reynolds and coworkers.³¹ Indolin-2-one (1.47 g, 11.1 mmol) and 6-bromoindoline-2,3-dione (2.50 g, 11.1 mmol) were refluxed with 0.2 mL concentrated hydrochloric acid in 40 mL of glacial acetic acid for 24 h. The reaction mixture was then allowed to cool to room temperature and the purplish red solids were filtered and washed liberally with 95 % ethanol followed by ethyl acetate to give 3.12 g (82% yield) pure purplish red powdery solid. ¹H-NMR (400 MHz, DMSO-*d*₆): 6.83-6.86 (d, 1H, J = 8 Hz), 6.95-6.99 (m, 2H), 7.16-7.19 (dd, 1H, J = 8 Hz, 2Hz), 7.34-7.37 (t, 1H, J = 8 Hz), 8.99-9.05 (2 doublets, 2H, J = 8 Hz), 10.9 (s, 1H), 11.0 (s, 1H).

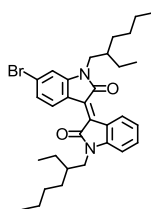
6,6'-Dibromoisindigo [(*E*)-6,6'-dibromo-[3,3'-biindolinylidene]-2,2'-dione]:



This procedure was adapted from Reynolds and coworkers.³¹ 6-bromoindolin-2-one (2.13 g, 9.43 mmol) and 6-bromoindoline-2,3-dione (2.00 g, 9.43 mmol) were refluxed with 0.4 mL

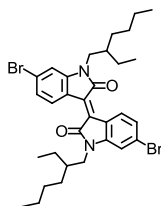
concentrated hydrochloric acid in 80 mL of glacial acetic acid for 24 h. The reaction mixture was then allowed to cool to room temperature and the purplish red solids were filtered and washed liberally with 95 % ethanol followed by ethyl acetate to give 3.54 g (89% yield) pure purplish red powdery solid. ¹H-NMR (400 MHz, DMSO-*d*₆): 6.83-6.86 (d, 1H, J = 8 Hz), 6.95-6.99 (m, 2H), 7.16-7.19 (dd, 1H, J = 8 Hz, 2Hz), 7.34-7.37 (t, 1H, J = 8 Hz), 8.99-9.05 (2 doublets, 2H, J = 8 Hz), 10.9 (s, 1H), 11.0 (s, 1H).

6-Bromoisindigo-ethylhexyl [(*E*)-6-bromo-1,1'-bis(2-ethylhexyl)-[3,3'-biindolinylidene]-2,2'-dione]:



This procedure was adapted from Reynolds and coworkers.³¹ 6-bromoisindigo (1.00 g, 2.93 mmol) and potassium carbonate (2.43 g, 17.6 mmol) were combined under nitrogen. Dry DMF (20 mL) was added, followed by 1-bromo-2-ethylhexane (1.70 g, 8.79 mmol). The reaction mixture heated at 100 °C overnight, cooled to room temperature, and poured into 500 mL water. The product was extracted with DCM, dried over anhydrous MgSO₄, and concentrated *in vacuo*. The crude reddish brown solid was purified over silica eluted with 40% DCM/hexanes to give 0.497 g (30% yield) pure reddish brown powdery solid. ¹H-NMR (400 MHz, DMSO-*d*₆): 0.81-0.90 (m, 12H), 1.23-1.36 (m, 18H), 3.65-3.69 (t, 4H, J = 8Hz), 7.01-7.07 (m, 2H), 7.25-7.27 (m, 2H), 7.44-7.48 (t, 1H, J = 7 Hz), 9.03-9.10 (m, 2H).

6,6'-Dibromoisoidigo-ethylhexyl [(E)-6,6'-dibromo-1,1'-bis(2-ethylhexyl)-[3,3'-biindolinylidene]-2,2'-dione]:



This procedure was adapted from Reynolds and coworkers.³¹ 6,6'-dibromoisoidigo (2.10 g, 5.00 mmol) and potassium carbonate (3.46 g, 25.0 mmol) were combined under nitrogen. Dry DMF (100 mL) was added, followed by 1-bromo-2-ethylhexane (2.0 mL, 11.0 mmol). The reaction mixture was heated at 100 °C overnight, cooled to room temperature, and poured into 1 L water. The product was extracted with DCM, dried over anhydrous MgSO₄, and concentrated *in vacuo*. The crude reddish brown solid was recrystallized from ethanol to give 1.66 g (52% yield) pure reddish brown powdery solid. ¹H-NMR (400 MHz, DMSO-*d*₆): 0.78-0.91 (m, 12H), 1.19-1.33 (m, 16H), 1.79-1.82 (m, 2H), 3.65-3.67 (t, 4H, J = 8Hz), 7.24-7.25 (d, 2H J = 4 Hz), 7.27 (s, 2H), 9.01-9.03 (d, 2H, J = 8 Hz).

9.7 Acknowledgements

This work was supported as part of Polymer-Based Materials for Harvesting Solar Energy (PHaSE), an Energy Frontier Research Center funded by the U.S. Department of Energy, Office of Basic Energy Sciences under Award Number DE-SC0001087.

9.8 References

- (1) Homnick, P. J.; Tinkham, J. S.; Lahti, P. M. Radical Cations from Diarylamino-Substituted Fluorenones. *Tetrahedron Lett.* **2013**, *54*, 35–39.
- (2) Liu, S.; Wang, W. M.; Briseno, A. L.; Mannsfeld, S. C. B.; Bao, Z. Controlled Deposition of Crystalline Organic Semiconductors for Field-Effect-Transistor Applications. *Adv. Mater.* **2009**, *21*, 1217–1232.
- (3) Rathnayake, H. P.; Cirpan, A.; Karasz, F. E.; Odoi, M. Y.; Hammer, N. I.; Barnes, M. D.; Lahti, P. M. Luminescence of Molecular and Block Copolymeric 2,7-Bis(phenylethynyl)-Fluorenones; Identifying Green-Band Emitter Sites in a Fluorene-Based Luminophore. *Chem. Mater.* **2007**, *19*, 3265–3270.
- (4) Wong, W.-Y.; Lu, G.-L.; Choi, K.-H.; Lin, Z. Functionalization of 9-(Dicyanomethylene)fluorene Derivatives with Substituted Acetylenes. *European J. Org. Chem.* **2003**, *2003*, 365–373.
- (5) Klapars, A.; Huang, X.; Buchwald, S. L. A General and Efficient Copper Catalyst for the Amidation of Aryl Halides. *J. Am. Chem. Soc.* **2002**, *124*, 7421–7428.
- (6) Klapars, A.; Antilla, J. C.; Huang, X.; Buchwald, S. L. A General and Efficient Copper Catalyst for the Amidation of Aryl Halides and the N-Arylation of Nitrogen Heterocycles. *J. Am. Chem. Soc.* **2001**, *123*, 7727–7729.
- (7) Zhang, X.; Ji, X.; Jiang, S.; Liu, L.; Weeks, B. L.; Zhang, Z. Highly Efficient Synthesis of 9-Fluorenones from 9H-Fluorenes by Air Oxidation. *Green Chem.* **2011**, *13*, 1891–1896.
- (8) Peterson, J. J.; Simon, Y. C.; Coughlin, E. B.; Carter, K. R. Polyfluorene with P-Carborane in the Backbone. *Chem. Commun.* **2009**, 4950–4952.
- (9) Promarak, V.; Punkvung, A.; Sudyoadsuk, T.; Junguttiwong, S.; Saengsuwan, S.; Keawin, T.; Sirithip, K. Synthesis and Characterization of N-Carbazole End-Capped Oligofluorene-Thiophenes. *Tetrahedron* **2007**, *63*, 8881–8890.
- (10) Ghandi, M.; Rezaei, S. J. T.; Yari, A.; Taheri, A. Cycloaddition Reactions of Azomethine Ylides with a 9-Fluorenone-Malononitrile Knöevenagel Adduct. *Tetrahedron Lett.* **2008**, *49*, 5899–5901.
- (11) Kobin, B.; Grubert, L.; Blumstengel, S.; Henneberger, F.; Hecht, S. Vacuum-Processable Ladder-Type Oligophenylenes for Organic–inorganic Hybrid Structures: Synthesis, Optical and Electrochemical Properties upon Increasing Planarization as Well as Thin Film Growth. *J. Mater. Chem.* **2012**, 4383–4390.
- (12) Shirai, Y.; Osgood, A. J.; Zhao, Y.; Yao, Y.; Saudan, L.; Yang, H.; Yu-Hung, C.; Alemany, L. B.; Sasaki, T.; Morin, J.-F.; *et al.* Surface-Rolling Molecules. *J. Am. Chem. Soc.* **2006**, *128*, 4854–4864.

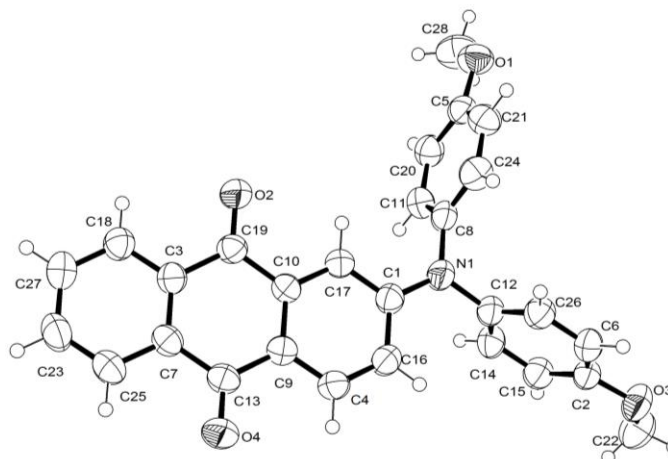
- (13) Brunner, K.; van Dijken, A.; Börner, H.; Bastiaansen, J. J. A. M.; Kigger, N. M. M.; Langeveld, B. M. W. Carbazole Compounds as Host Materials for Triplet Emitters in Organic Light-Emitting Diodes: Tuning the HOMO Level without Influencing the Triplet Energy in Small Molecules. *J. Am. Chem. Soc.* **2004**, *126*, 6035–6042.
- (14) Sierra, C. a.; Lahti, P. M. A Photoluminescent, Segmented Oligo-Polyphenylenevinylene Copolymer with Hydrogen-Bonding Pendant Chains. *Chem. Mater.* **2004**, *16*, 55–61.
- (15) Homnick, P. J.; Lahti, P. M. Modular Electron Donor Group Tuning of Frontier Energy Levels in Diarylamino-fluorenone Push-Pull Molecules. *Phys. Chem. Chem. Phys.* **2012**, *14*, 11961–11968.
- (16) Hill, L. L.; Moore, L. R.; Huang, R.; Craciun, R.; Vincent, A. J.; Dixon, D. A.; Chou, J.; Woltermann, C. J.; Shaughnessy, K. H. Bulky Alkylphosphines with Neopentyl Substituents as Ligands in the Amination of Aryl Bromides and Chlorides. *J. Org. Chem.* **2006**, *71*, 5117–5125.
- (17) Homnick, P. J.; Tinkham, J. S.; Devaughn, R.; Lahti, P. M. Engineering Frontier Energy Levels in Donor-Acceptor Fluorene-9-Ylidene Malononitriles versus Fluorenones. *J. Phys. Chem. A* **2014**, *118*, 475–486.
- (18) Chankeshwara, S.; Chakraborti, A. Indium(III) Halides as New and Highly Efficient Catalysts for N - Tert -Butoxycarbonylation of Amines. *Synthesis (Stuttg.)* **2006**, *2006*, 2784–2788.
- (19) Della Pelle, A. M.; Homnick, P. J.; Bae, Y.; Lahti, P. M.; Thayumanavan, S. Effect of Substituents on Optical Properties and Charge-Carrier Polarity of Squaraine Dyes. *J. Phys. Chem. C* **2014**, *118*, 1793–1799.
- (20) Field, J. E.; Venkataraman, D. Heterotriangulenes Structure and Properties. *Chem. Mater.* **2002**, *14*, 962–964.
- (21) Zhang, H.; Wang, S.; Li, Y.; Zhang, B.; Du, C.; Wan, X.; Chen, Y. Synthesis, Characterization, and Electroluminescent Properties of Star Shaped Donor–acceptor Dendrimers with Carbazole Dendrons as Peripheral Branches and Heterotriangulene as Central Core. *Tetrahedron* **2009**, *65*, 4455–4463.
- (22) Fang, Z.; Teo, T.-L.; Cai, L.; Lai, Y.-H.; Samoc, A.; Samoc, M. Bridged Triphenylamine-Based Dendrimers: Tuning Enhanced Two-Photon Absorption Performance with Locked Molecular Planarity. *Org. Lett.* **2009**, *11*, 1–4.
- (23) Lambert, C.; Nöll, G.; Schmäzlin, E.; Meerholz, K.; Bräuchle, C. Synthesis, (Non)Linear Optical and Redox Properties of a Donor-Substituted Truxenone Derivative. *Chem. - A Eur. J.* **1998**, *4*, 2129–2135.
- (24) Huang, W.; Su, L.; Bo, Z. Hyperbranched Polymers with a Degree of Branching of 100% Prepared by Catalyst Transfer Suzuki-Miyaura Polycondensation. *J. Am. Chem. Soc.* **2009**, *131*, 10348–10349.

- (25) Jeong, M. J.; Park, J. H.; Lee, C.; Chang, J. Y. Discotic Liquid Crystalline Hydrazone Compounds: Synthesis and Mesomorphic Properties. *Org. Lett.* **2006**, *8*, 2221–2224.
- (26) Kim, S.; Oehlhof, A.; Beile, B.; Meier, H. Donor-Acceptor-Substituted Oligo(1,4-Phenylene)s. *Helv. Chim. Acta* **2009**, *92*, 1023–1033.
- (27) Bavin, P. M. G.; Sheehan, J. C.; Chandler, R. E. 2-AminoFluorene. *Org. Synth.* **1973**, *5*, 30–31.
- (28) Shellaiah, M.; Rajan, Y. C.; Lin, H.-C. Synthesis of Novel Triarylamine-Based Dendrimers with N4{,}N6-Dibutyl-1{,}3{,}5-Triazine-4{,}6-Diamine Probe for Electron/energy Transfers in H-Bonded Donor-Acceptor-Donor Triads and as Efficient Cu²⁺ Sensors. *J. Mater. Chem.* **2012**, *22*, 8976–8987.
- (29) Kuhn, W. E.; Fieser, L. F.; Walker, J. T. 2-Nitrofluorene and 2-Aminofluorene. In *Organic Syntheses*; pp. 447–448.
- (30) Berkovic, S. 7-Halogeno-2-Vinylfluorenes and Related Compounds. *Isr. J. Chem.* **1963**, *1*, 1–11.
- (31) Mei, J.; Graham, K. R.; Stalder, R.; Reynolds, J. R. Synthesis of Isoindigo-Based Oligothiophenes for Molecular Bulk Heterojunction Solar Cells. *Org. Lett.* **2010**, *12*, 660–663.

CHAPTER 10
SUPPLEMENTARY DATA

10.1 Crystallographic Data

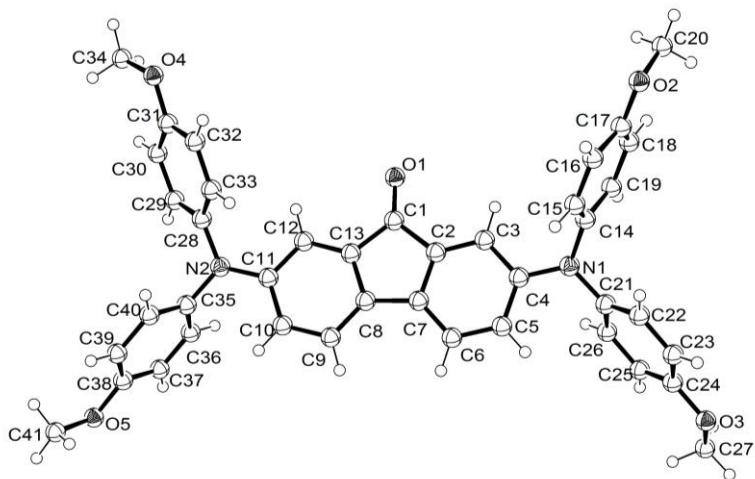
10.1.1. Crystallographic Summary for DAAAQ



Chemical Formula	C ₂₈ H ₂₁ NO ₄
Molecular Weight	435.46
Temperature	293 K
Cell Setting, Space Group	Monoclinic, <i>P</i> 2 ₁ / <i>c</i>
a, b, c (Angstroms)	9.925, 18.681, 12.195
α , β , γ (Degrees)	90, 106.81, 90
V (Å ³)	2164.5
Z	4
D _{calc} (g/cm)	1.336
Color	Dark Red Prisms
R-Factor (%)	4.05

CIF Location: XRD\DAAAQ\DAAAQ.cif

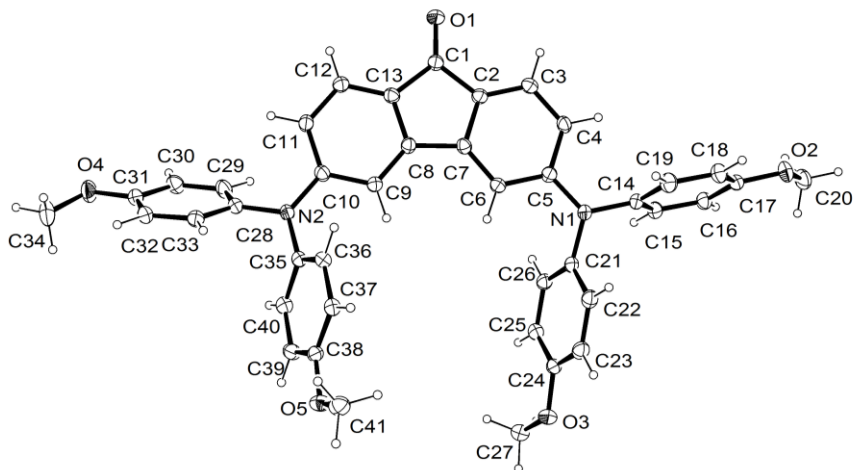
10.1.2. Crystallographic Summary for FOBDAA



Chemical Formula	$C_{41}H_{34}N_2O_5$
Molecular Weight	634.70
Temperature	293 K
Cell Setting, Space Group	Monoclinic, $P2_1/c$
a, b, c (Angstroms)	16.4812(2), 10.1301(1), 20.0948(2)
α , β , γ (Degrees)	90, 2.1331(6), 90
V (\AA^3)	3352.71(6)
Z	4
D _{calc} (g/cm)	1.257
Color	Dark Blue-Green Prisms
R-Factor (%)	3.97

CIF Location: XRD\FOBDAA27\PH1.cif

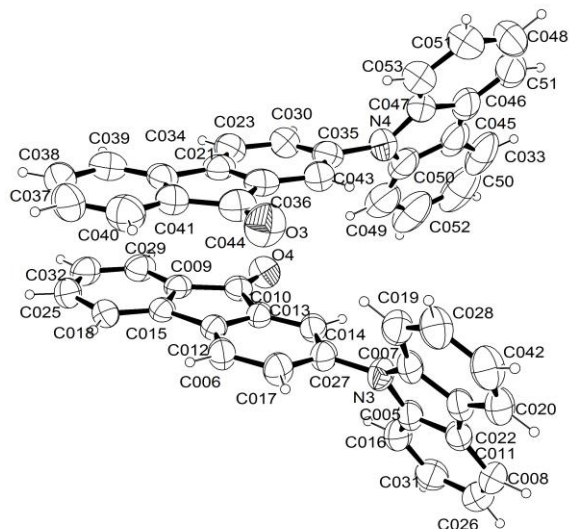
10.1.3. Crystallographic Summary for FOBDAA36



Chemical Formula	$C_{41}H_{34}N_2O_5$
Molecular Weight	634.70
Temperature	100 K
Cell Setting, Space Group	Triclinic, <i>P</i> -1
a, b, c (Angstroms)	11.5095(7), 12.0831(8), 14.0025(9)
α , β , γ (Degrees)	65.322(1), 67.184(1), 59.931(1)
V (\AA^3)	1600.73(18)
Z	2
D _{calc} (g/cm ³)	1.317
Color	Dark Red Blocks
R-Factor (%)	4.39

CIF Location: XRD\FOBDAA36\pml031_0m.cif

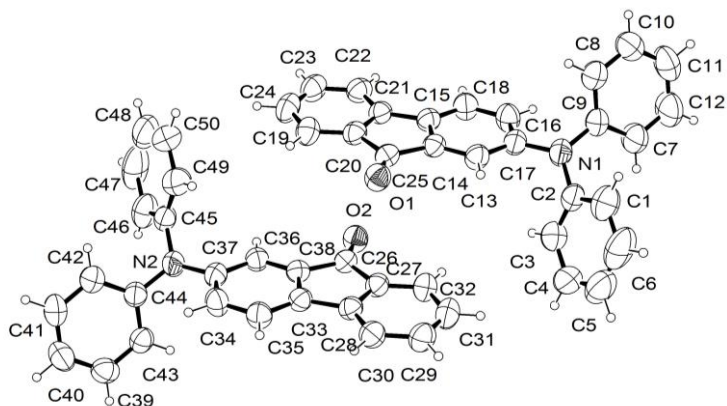
10.1.4. Crystallographic Summary for FOCz



Chemical Formula	C ₂₅ H ₁₅ NO
Molecular Weight	345.38
Temperature	293 K
Cell Setting, Space Group	Monoclinic, <i>P2₁/c</i>
a, b, c (Angstroms)	11.884(5), 16.903(5), 18.435(5)
α , β , γ (Degrees)	90.000(5), 107.859(5), 90.000(5)
V (Å ³)	3525(2)
Z	4
D _{calc} (g/cm)	1.302
Color	Orange Needles
R-Factor (%)	7.74

CIF Location: XRD\FOCz\New folder (2)\import (4).cif

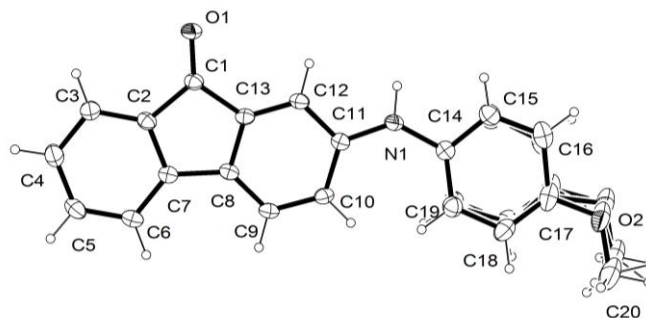
10.1.5. Crystallographic Summary for FODPA



Chemical Formula	C ₂₅ H ₁₇ NO
Molecular Weight	347.42
Temperature	293 K
Cell Setting, Space Group	Orthorhombic, <i>P2₁ 2₁ 2₁</i>
a, b, c (Angstroms)	7.6226(3), 15.9411(7), 30.0752(13)
α , β , γ (Degrees)	90, 90, 90
V (Å ³)	3654.5(3)
Z	8
D _{calc} (g/cm)	1.263
Color	Bright Red Needles
R-Factor (%)	5.5

CIF Location: XRD\FODPA\GOOD\FODPA.cif

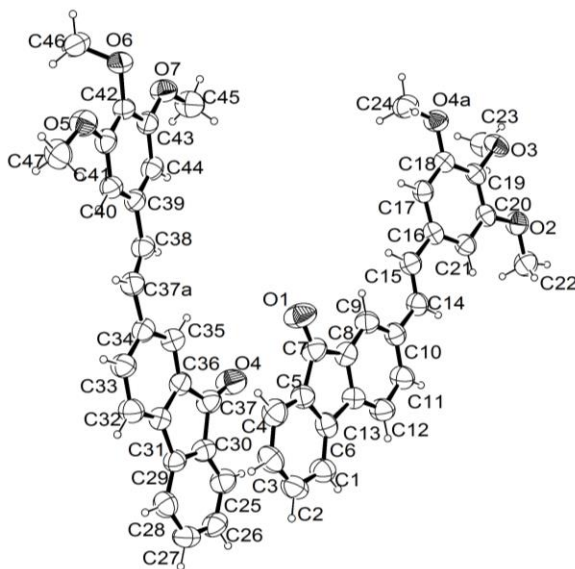
10.1.6. Crystallographic Summary for FOAA



Chemical Formula	C ₂₀ H ₁₅ NO ₂
Molecular Weight	301.33
Temperature	100 K
Cell Setting, Space Group	Monoclinic, <i>P2₁/c</i>
a, b, c (Angstroms)	16.338(2), 5.5322(7), 16.807(2)
α , β , γ (Degrees)	90, 105.592(2), 90
V (\AA^3)	1463.2(3)
Z	4
D _{calc} (g/cm ³)	1.368
Color	Dark Red Plates
R-Factor (%)	4.71

CIF Location: XRD\FOAA\PML022_0m.cif

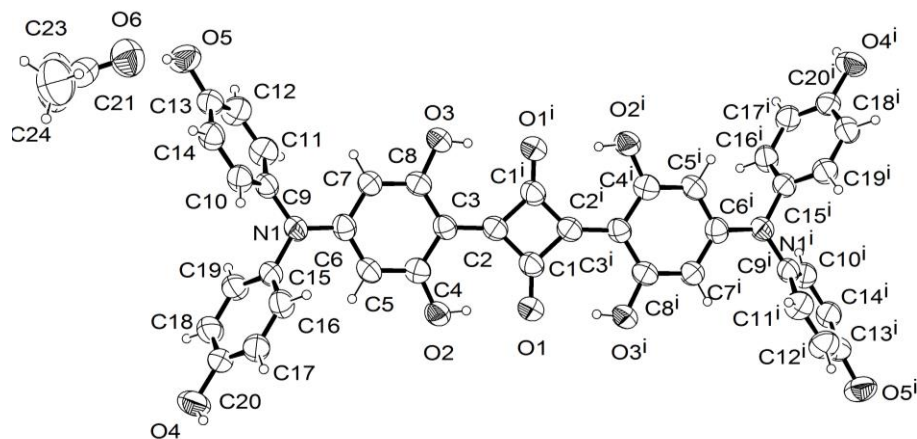
10.1.7. Crystallographic Summary for FOS



Chemical Formula	C ₂₄ H ₂₀ O ₄
Molecular Weight	372.42
Temperature	293 K
Cell Setting, Space Group	Not Determined, Not Determined
a, b, c (Angstroms)	7.7616(2), 8.5241(2), 28.0497(8)
α, β, γ (Degrees)	90, 90, 90
V (Å ³)	1855.79
Z	Not Determined
D _{calc} (g/cm)	Not Determined
Color	Orange-Red Needles
R-Factor (%)	Not Determined

RES Location (No CIF – crystal twinned, complicated to solve): XRD\FOS GOOD\FOS.res

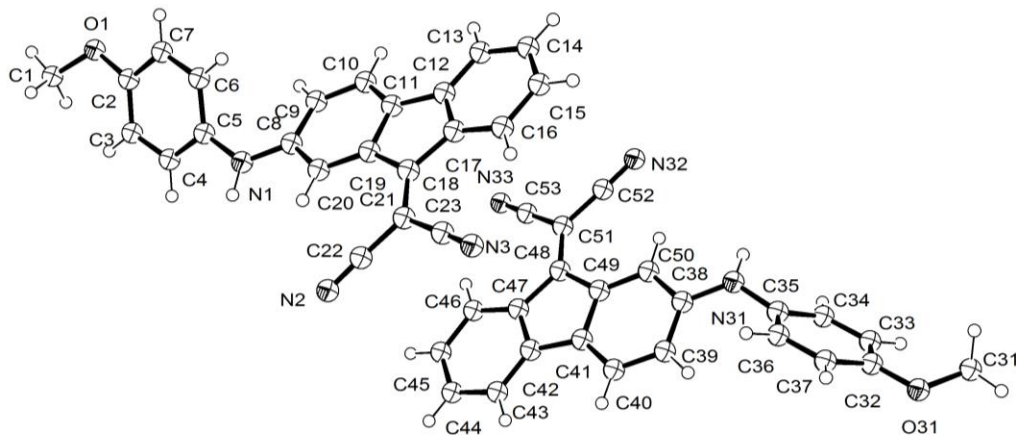
10.1.8. Crystallographic Summary for SQ-TAA-OH



Chemical Formula	$C_{46}H_{40}N_2O_{12}$
Molecular Weight	812.83
Temperature	293 K
Cell Setting, Space Group	Monoclinic, $P2_1/n$
a, b, c (Angstroms)	12.5208(10), 10.0602(5), 16.3679(14)
α, β, γ (Degrees)	90, 103.221(3), 90
V (\AA^3)	2007.1(3)
Z	2
D_{calc} (g/cm ³)	1.346
Color	Dark Green-Blue Prisms
R-Factor (%)	6.73

CIF Location: XRD\SQ-OH\Good\SQ-OH.cif

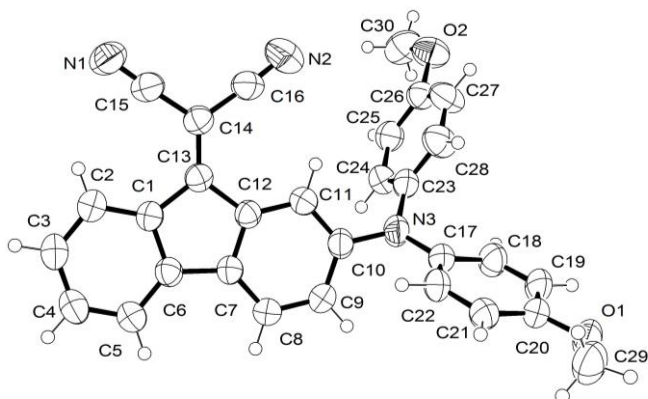
10.1.9. Crystallographic Summary for FMAA



Chemical Formula	C ₂₃ H ₁₅ N ₃ O
Molecular Weight	349.3930
Temperature	100 K
Cell Setting, Space Group	Monoclinic, <i>P</i> 2 ₁
a, b, c (Angstroms)	5.4188(2), 33.7580(13), 9.5644(4)
α, β, γ (Degrees)	90, 102.858(2), 90
V (Å ³)	1708.72
Z	Not Determined
D _{calc} (g/cm)	Not Determined
Color	Dark Green Needles
R-Factor (%)	Not Determined

CIF Location: XRD\FMAA\100kdata.cif

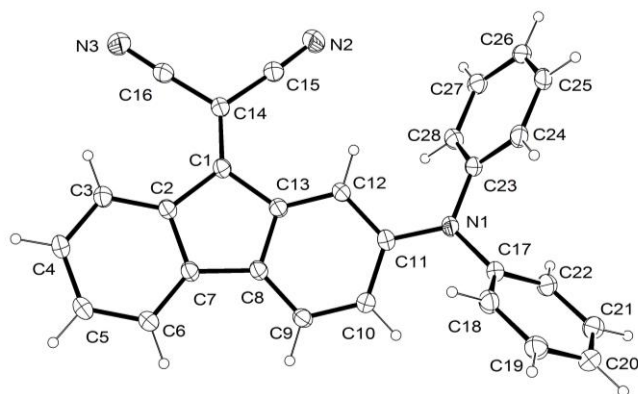
10.1.10. Crystallographic Summary for FMDAA



Chemical Formula	C ₃₀ H ₂₁ N ₃ O ₂
Molecular Weight	455.50
Temperature	293 K
Cell Setting, Space Group	Monoclinic, <i>P2₁/c</i>
a, b, c (Angstroms)	17.3506(5), 7.0892(1), 19.1145(5)
α , β , γ (Degrees)	90, 92.4911(12), 90
V (\AA^3)	2348.90(10)
Z	4
D _{calc} (g/cm ³)	1.288
Color	Dark Green Needles
R-Factor (%)	4.37

CIF Location: XRD\FMDAA\ph2.cif

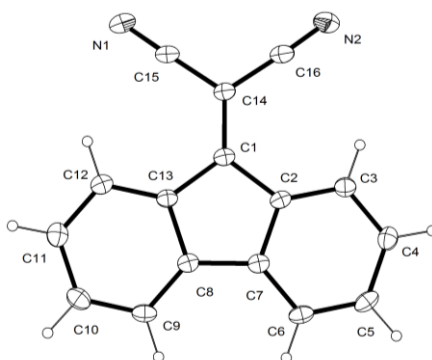
10.1.11. Crystallographic Summary for FMDPA



Chemical Formula	C ₂₈ H ₁₇ N ₃
Molecular Weight	395.45
Temperature	100 K
Cell Setting, Space Group	Monoclinic, <i>P2₁/c</i>
a, b, c (Angstroms)	10.7809(11), 18.3482(19), 10.4690(10)
α , β , γ (Degrees)	90, 107.8470(10), 90
V (\AA^3)	1971.22
Z	4
D _{calc} (g/cm)	1.332
Color	Dark Blue Needles
R-Factor (%)	4.46

CIF Location: XRD\FMDPA\pml025_1m.cif

10.1.12. Crystallographic Summary for FM

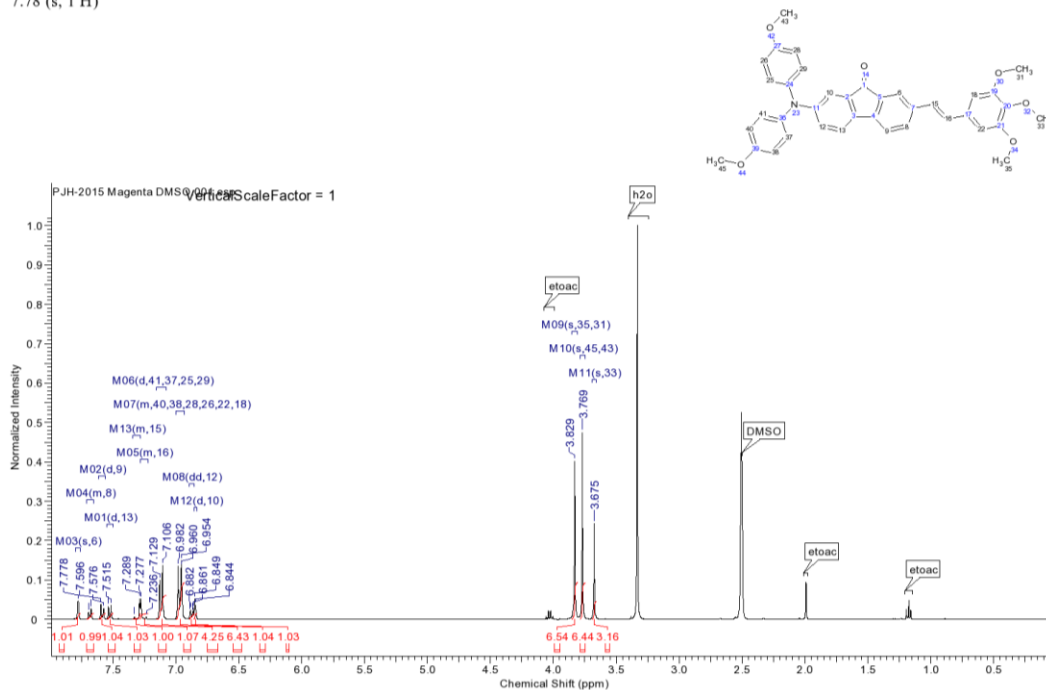


Chemical Formula	C ₁₆ H ₈ N ₂
Molecular Weight	228.24
Temperature	100 K
Cell Setting, Space Group	Orthorhombic, <i>P2₁2₁2₁</i>
a, b, c (Angstroms)	3.8456(4), 9.2678(9), 30.666(3)
α , β , γ (Degrees)	90, 90, 90
V (Å ³)	1092.95(19)
Z	4
D _{calc} (g/cm ³)	1.387
Color	Orange Plates
R-Factor (%)	4.28

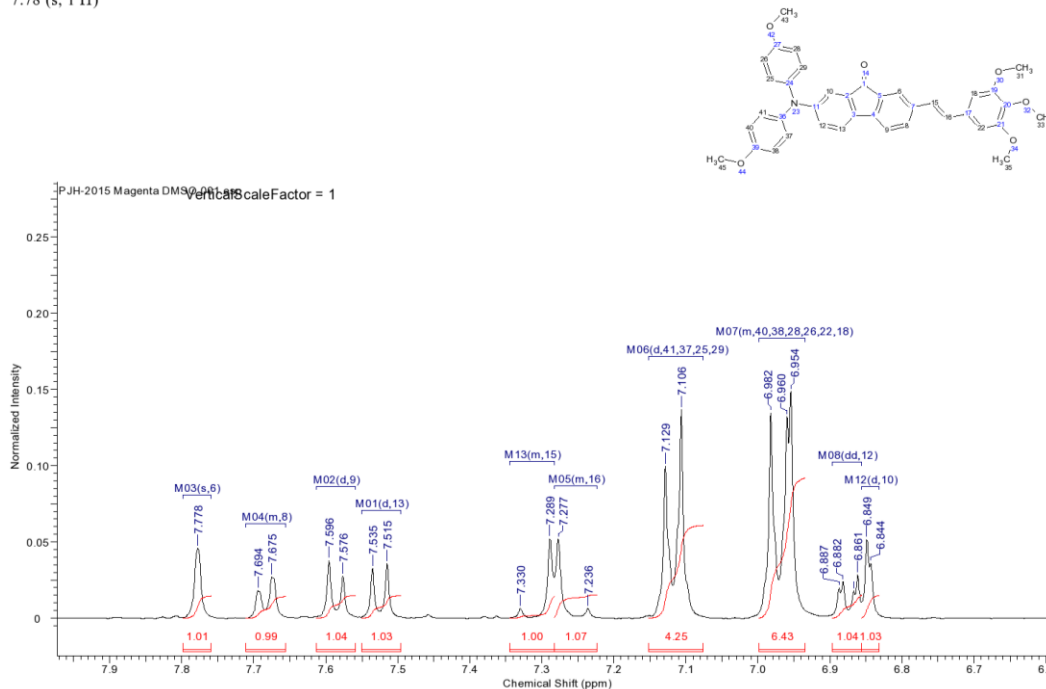
CIF Location: XRD\FM\pml023_0m.cif

10.2 $^1\text{H-NMR}$ Spectrum for FODAAS, Peak Assignments Amended from Homnick, P. J.; Lahti, P. M. *Phys. Chem. Chem. Phys.* 2012, 11961-11968.

$^1\text{H NMR}$ (400 MHz, $\text{DMSO}-d_6$) δ ppm 3.67 (s, 3 H) 3.77 (s, 6 H) 3.83 (s, 6 H) 6.85 (d, $J=2.02$ Hz, 1 H) 6.87 (dd, $J=8.21, 2.15$ Hz, 1 H) 6.93 - 7.00 (m, 6 H) 7.12 (d, $J=8.84$ Hz, 6 H) 7.22 - 7.28 (m, 1 H) 7.28 - 7.34 (m, 1 H) 7.53 (d, $J=8.08$ Hz, 1 H) 7.59 (d, $J=7.83$ Hz, 1 H) 7.66 - 7.71 (m, 1 H) 7.78 (s, 1 H)



$^1\text{H NMR}$ (400 MHz, $\text{DMSO}-d_6$) δ ppm 3.67 (s, 3 H) 3.77 (s, 6 H) 3.83 (s, 6 H) 6.85 (d, $J=2.02$ Hz, 1 H) 6.87 (dd, $J=8.21, 2.15$ Hz, 1 H) 6.93 - 7.00 (m, 6 H) 7.12 (d, $J=8.84$ Hz, 6 H) 7.22 - 7.28 (m, 1 H) 7.28 - 7.34 (m, 1 H) 7.53 (d, $J=8.08$ Hz, 1 H) 7.59 (d, $J=7.83$ Hz, 1 H) 7.66 - 7.71 (m, 1 H) 7.78 (s, 1 H)



BIBLIOGRAPHY

- Aida, T.; Meijer, E. W.; Stupp, S. I. Functional Supramolecular Polymers. *Science* . **2012**, *335*, 813–817.
- Aihara, J. Anomalous Solvatochromism of Charge-Transfer Absorption Bands. *Bull. Chem. Soc. Jpn.* **1981**, *54*, 1561–1562.
- Ananda Rao, B.; Yesudas, K.; Siva Kumar, G.; Bhanuprakash, K.; Jayathirtha Rao, V.; Sharma, G. D.; Singh, S. P. Application of Solution Processable Squaraine Dyes as Electron Donors for Organic Bulk-Heterojunction Solar Cells. *Photochem. Photobiol. Sci.* **2013**, *12*, 1688–1699.
- Anderson, P. A.; Strouse, G. F.; Treadway, J. A.; Keene, F. R.; Meyer, T. J. Black MLCT Absorbers. *Inorg. Chem.* **1994**, *33*, 3863–3864.
- Andrew, T. L.; Bulović, V. Bulk Heterojunction Solar Cells Containing 6,6-Dicyanofulvenes as N-Type Additives. *ACS Nano* **2012**, *6*, 4671–4677.
- Andrews, L. J.; Deroulede, A.; Linschitz, H. Photophysical Processes in Fluorenone. *J. Phys. Chem.* **1978**, *82*, 2304–2309.
- Anslyn, E. V.; Dougherty, D. A. *Modern Physical Organic Chemistry*; University Science Books: Sausalito, CA, 2006.
- Anthony, J. E. The Larger Acenes: Versatile Organic Semiconductors. *Angew. Chem. Int. Ed. Engl.* **2008**, *47*, 452–483.
- Anthony, J. E.; Facchetti, A.; Heeney, M.; Marder, S. R.; Zhan, X. N-Type Organic Semiconductors in Organic Electronics. *Adv. Mater.* **2010**, *22*, 3876–3892.
- Arathi Rani, S.; Sobhanadri, J.; Prasada Rao, T. . Determination of the Excited State Dipole Moment of Fluorenone Using the Method of Solvatochromism. *Spectrochim. Acta Part A Mol. Biomol. Spectrosc.* **1995**, *51*, 2473–2479.
- Bavin, P. M. G.; Sheehan, J. C.; Chandler, R. E. 2-AminoFluorene. *Org. Synth.* **1973**, *5*, 30–31.
- Beaujuge, P. M.; Fréchet, J. M. J. Molecular Design and Ordering Effects in Π -Functional Materials for Transistor and Solar Cell Applications. *J. Am. Chem. Soc.* **2011**, *133*, 20009–20029.
- Becke, A. D. Density-Functional Exchange-Energy Approximation with Correct Asymptotic Behavior. *Phys. Rev. A* **1988**, *38*, 3098–3100.
- Becke, A. D. Density-Functional Thermochemistry. III. The Role of Exact Exchange. *J. Chem. Phys.* **1993**, *98*, 5648.
- Behrendt, A.; Screttas, C. G.; Bethell, D.; Schiemann, O.; Steele, B. R. Magnetic and Electrochemical Investigations on Anions Derived from Oligoketones Containing Fl Uorenone and Benzophenone Units . An Approach to the Design of Stable Multiradical Organic Materials. **1998**, 2039–2045.

- Berkovic, S. 7-Halogeno-2-Vinylfluorenes and Related Compounds. *Isr. J. Chem.* **1963**, *1*, 1–11.
- Bian, L.; Zhu, E.; Tang, J.; Tang, W.; Zhang, F. Recent Progress in the Design of Narrow Bandgap Conjugated Polymers for High-Efficiency Organic Solar Cells. *Prog. Polym. Sci.* **2012**, *37*, 1292–1331.
- Biczók, L.; Bérces, T.; Inoue, H. Effects of Molecular Structure and Hydrogen Bonding on the Radiationless Deactivation of Singlet Excited Fluorenone Derivatives †. *J. Phys. Chem. A* **1999**, *103*, 3837–3842.
- Boschloo, G.; Häggman, L.; Hagfeldt, A. Quantification of the Effect of 4-Tert-Butylpyridine Addition to I-/I³⁺- Redox Electrolytes in Dye-Sensitized Nanostructured TiO₂ Solar Cells. *J. Phys. Chem. B* **2006**, *110*, 13144–13150.
- Boudreault, P.-L. T.; Najari, A.; Leclerc, M. Processable Low-Bandgap Polymers for Photovoltaic Applications †. *Chem. Mater.* **2010**, 101012131424030.
- Brédas, J.-L.; Norton, J. E.; Cornil, J.; Coropceanu, V. Molecular Understanding of Organic Solar Cells: The Challenges. *Acc. Chem. Res.* **2009**, *42*, 1691–1699.
- Briseno, A. L.; Aizenberg, J.; Han, Y.-J.; Penkala, R. a; Moon, H.; Lovinger, A. J.; Kloc, C.; Bao, Z. Patterned Growth of Large Oriented Organic Semiconductor Single Crystals on Self-Assembled Monolayer Templates. *J. Am. Chem. Soc.* **2005**, *127*, 12164–12165.
- Briseno, A. L.; Tseng, R. J.; Ling, M.-M.; Falcao, E. H. L.; Yang, Y.; Wudl, F.; Bao, Z. High-Performance Organic Single-Crystal Transistors on Flexible Substrates. *Adv. Mater.* **2006**, *18*, 2320–2324.
- Brunner, K.; van Dijken, A.; Börner, H.; Bastiaansen, J. J. A. M.; Kikken, N. M. M.; Langeveld, B. M. W. Carbazole Compounds as Host Materials for Triplet Emitters in Organic Light-Emitting Diodes: Tuning the HOMO Level without Influencing the Triplet Energy in Small Molecules. *J. Am. Chem. Soc.* **2004**, *126*, 6035–6042.
- Bundgaard, E.; Krebs, F. Low Band Gap Polymers for Organic Photovoltaics. *Sol. Energy Mater. Sol. Cells* **2007**, *91*, 954–985.
- Bushby, R. J.; McGill, D. R.; Ng, K. M.; Taylor, N. Disjoint and Coextensive Diradical Diions. *J. Chem. Soc. Perkin Trans. 2* **1997**, 1405–1414.
- C. Ego, A.C. Grimsdale, F. Uckert, G. Yu, G. Srdanov, K. M. Triphenylamine-Substituted Polyfluorene—A Stable Blue-Emitter with Improved Charge Injection for Light-Emitting Diodes. *Adv. Mater.* **2002**, *14*, 809–811.
- Cardona, C. M.; Li, W.; Kaifer, A. E.; Stockdale, D.; Bazan, G. C. Electrochemical Considerations for Determining Absolute Frontier Orbital Energy Levels of Conjugated Polymers for Solar Cell Applications. *Adv. Mater.* **2011**, *23*, 2367–2371.
- Cardona, C. M.; Li, W.; Kaifer, A. E.; Stockdale, D.; Bazan, G. C. Electrochemical Considerations for Determining Absolute Frontier Orbital Energy Levels of Conjugated Polymers for Solar Cell Applications. *Adv. Mater.* **2011**, *23*, 2367–2371.

- Chang, C.-C.; Yueh, H.; Chen, C.-T. Generation and Spectroscopic Profiles of Stable Multiarylammonium Radical Cations Bridged by Fluorenes. *Org. Lett.* **2011**, *13*, 2702–2705.
- Chankeshwara, S.; Chakraborti, A. Indium Halides as New and Highly Efficient Catalysts for N-Tert-Butoxycarbonylation of Amines. *Synthesis*. **2006**, *2006*, 2784–2788.
- Chapin, D. M.; Fuller, C. S.; Pearson, G. L. A New Silicon P-N Junction Photocell for Converting Solar Radiation into Electrical Power. *J. Appl. Phys.* **1954**, *25*, 676.
- Charvet, R.; Yamamoto, Y.; Sasaki, T.; Kim, J.; Kato, K.; Takata, M.; Saeki, A.; Seki, S.; Aida, T. Segregated and Alternately Stacked Donor/acceptor Nanodomains in Tubular Morphology Tailored with Zinc Porphyrin-C60 Amphiphilic Dyads: Clear Geometrical Effects on Photoconduction. *J. Am. Chem. Soc.* **2012**, *134*, 2524–2527.
- Chen, G.; Sasabe, H.; Wang, Z.; Wang, X.-F.; Hong, Z.; Yang, Y.; Kido, J. Co-Evaporated Bulk Heterojunction Solar Cells with >6.0% Efficiency. *Adv. Mater.* **2012**, *24*, 2768–2773.
- Chen, G.; Yokoyama, D.; Sasabe, H.; Hong, Z.; Yang, Y.; Kido, J. Optical and Electrical Properties of a Squaraine Dye in Photovoltaic Cells. *Appl. Phys. Lett.* **2012**, *101*, -.
- Chen, Y.-H.; Lin, L.-Y.; Lu, C.-W.; Lin, F.; Huang, Z.-Y.; Lin, H.-W.; Wang, P.-H.; Liu, Y.-H.; Wong, K.-T.; Wen, J.; *et al.* Vacuum-Deposited Small-Molecule Organic Solar Cells with High Power Conversion Efficiencies by Judicious Molecular Design and Device Optimization. *J. Am. Chem. Soc.* **2012**, *134*, 13616–13623.
- Cheng, Y.-J.; Yang, S.-H.; Hsu, C.-S. Synthesis of Conjugated Polymers for Organic Solar Cell Applications. *Chem. Rev.* **2009**, *109*, 5868–5923.
- Chi, L.-C.; Chen, H.-F.; Hung, W.-Y.; Hsu, Y.-H.; Feng, P.-C.; Chou, S.-H.; Liu, Y.-H.; Wong, K.-T. Donor-Acceptor Small Molecule with Coplanar and Rigid Π -Bridge for Efficient Organic Solar Cells. *Sol. Energy Mater. Sol. Cells* **2013**, *109*, 33–39.
- Cho, M.; Choi, D.; Sullivan, P.; Akelaitis, a; Dalton, L. Recent Progress in Second-Order Nonlinear Optical Polymers and Dendrimers. *Prog. Polym. Sci.* **2008**, *33*, 1013–1058.
- Cho, Y. J.; Lee, J. Y.; Chin, B. D.; Forrest, S. R. Polymer Bulk Heterojunction Photovoltaics Employing a Squaraine Donor Additive. *Org. Electron.* **2013**, *14*, 1081–1085.
- Chudomel, J. M.; Yang, B.; Barnes, M. D.; Achermann, M.; Mague, J. T.; Lahti, P. M. Highly Twisted Triarylamines for Photoinduced Intramolecular Charge Transfer. *J. Phys. Chem. A* **2011**, *115*, 8361–8368.
- Creutz, C. Mixed Valence Complexes of d5-d6 Metal Centers. In *Progress in Inorganic Chemistry*; John Wiley & Sons, Inc., 2007; pp. 1–73.
- Crutchley, R. J. Intervalence Charge Transfer and Electron Exchange Studies of Dinuclear Ruthenium Complexes. *Advances in Inorganic Chemistry*, 1994, *41*, 273–325.

- Daeneke, T.; Kwon, T.-H.; Holmes, A. B.; Duffy, N. W.; Bach, U.; Spiccia, L. High-Efficiency Dye-Sensitized Solar Cells with Ferrocene-Based Electrolytes. *Nat. Chem.* **2011**, *3*, 211–215.
- Dalton, L. R.; Sullivan, P. a; Bale, D. H. Electric Field Poled Organic Electro-Optic Materials: State of the Art and Future Prospects. *Chem. Rev.* **2010**, *110*, 25–55.
- De Boer, R. W. I.; Gershenson, M. E.; Morpurgo, A. F.; Podzorov, V. Organic Single-Crystal Field-Effect Transistors. *Phys. status solidi* **2004**, *201*, 1302–1331.
- Della Pelle, A. M.; Homnick, P. J.; Bae, Y.; Lahti, P. M.; Thayumanavan, S. Effect of Substituents on Optical Properties and Charge-Carrier Polarity of Squaraine Dyes. *J. Phys. Chem. C* **2014**, *118*, 1793–1799.
- Demadrille, R.; Delbosc, N.; Kervella, Y.; Firon, M.; De Bettignies, R.; Billon, M.; Rannou, P.; Pron, A. Conjugated Alternating Copolymer of Dialkylquaterthiophene and Fluorenone: Synthesis, Characterisation and Photovoltaic Properties. *J. Mater. Chem.* **2007**, *17*, 4661.
- Deng, P.; Zhang, Q. Recent Developments on Isoindigo-Based Conjugated Polymers. *Polym. Chem.* **2014**.
- Dennler, G.; Scharber, M. C.; Brabec, C. J. Polymer-Fullerene Bulk-Heterojunction Solar Cells. *Adv. Mater.* **2009**, *21*, 1323–1338.
- Ding, X.; Guo, J.; Feng, X.; Honsho, Y.; Guo, J.; Seki, S.; Maitarad, P.; Saeki, A.; Nagase, S.; Jiang, D. Synthesis of Metallophthalocyanine Covalent Organic Frameworks That Exhibit High Carrier Mobility and Photoconductivity. *Angew. Chem. Int. Ed. Engl.* **2011**, *50*, 1289–1293.
- Dogru, M.; Handloser, M.; Auras, F.; Kunz, T.; Medina, D.; Hartschuh, A.; Knochel, P.; Bein, T. A Photoconductive Thienothiophene-Based Covalent Organic Framework Showing Charge Transfer towards Included Fullerene. *Angew. Chem. Int. Ed. Engl.* **2013**, *52*, 2920–2924.
- Dollish, F. R.; Hall, W. K. On the Interaction of Triphenylamine with Iodine and with Silica—Alumina Catalysts. *J. Phys. Chem.* **1965**, *69*, 2127–2129.
- dye-sensitized-solar-cells.com <http://dye-sensitized-solar-cells.com/new-record-efficiency-for-dye-sensitized-solar-cells/#more-619> .
- Eakins, G. L.; Alford, J. S.; Tiegs, B. J.; Breyfogle, B. E.; Stearman, C. J. Tuning HOMO-LUMO Levels: Trends Leading to the Design of 9-Fluorenone Scaffolds with Predictable Electronic and Optoelectronic Properties. *J. Phys. Org. Chem.* **2011**, *24*, 1119–1128.
- Estrada, L. A.; Cai, X.; Neckers, D. C. Nonradiative Decay Mechanism of Fluoren-9-Ylidene Malononitrile Ambipolar Derivatives. *J. Phys. Chem. A* **2011**, *115*, 2184–2195.
- Estrada, L. A.; Neckers, D. C. Synthesis and Photophysics of Ambipolar Fluoren-9-Ylidene Malononitrile Derivatives. *J. Org. Chem.* **2009**, *74*, 8484–8487.

- Estrada, L. A.; Stalder, R.; Abboud, K. A.; Risko, C.; Brédas, J.-L.; Reynolds, J. R. Understanding the Electronic Structure of Isoindigo in Conjugated Systems: A Combined Theoretical and Experimental Approach. *Macromolecules* **2013**, *46*, 8832–8844.
- Estrada, L. A.; Yarnell, J. E.; Neckers, D. C. Revisiting Fluorenone Photophysics via Dipolar Fluorenone Derivatives. *J. Phys. Chem. A* **2011**, *115*, 6366–6375.
- Etgar, L.; Park, J.; Barolo, C.; Lesnyak, V.; Panda, S. K.; Quagliotto, P.; Hickey, S. G.; Nazeeruddin, M. K.; Eychmuller, A.; Viscardi, G.; *et al.* Enhancing the Efficiency of a Dye Sensitized Solar Cell due to the Energy Transfer between CdSe Quantum Dots and a Designed Squaraine Dye. *RSC Adv.* **2012**, *2*, 2748–2752.
- Facchetti, A.; Yoon, M.-H.; Stern, C. L.; Katz, H. E.; Marks, T. J. Building Blocks for N-Type Organic Electronics: Regiochemically Modulated Inversion of Majority Carrier Sign in Perfluoroarene-Modified Polythiophene Semiconductors. *Angew. Chemie Int. Ed.* **2003**, *42*, 3900–3903.
- Fang, Z.; Teo, T.-L.; Cai, L.; Lai, Y.-H.; Samoc, A.; Samoc, M. Bridged Triphenylamine-Based Dendrimers: Tuning Enhanced Two-Photon Absorption Performance with Locked Molecular Planarity. *Org. Lett.* **2009**, *11*, 1–4.
- Feng, X.; Chen, L.; Honsho, Y.; Saengsawang, O.; Liu, L.; Wang, L.; Saeki, A.; Irle, S.; Seki, S.; Dong, Y.; *et al.* An Ambipolar Conducting Covalent Organic Framework with Self-Sorted and Periodic Electron Donor-Acceptor Ordering. *Adv. Mater.* **2012**, *24*, 3026–3031.
- Feng, X.; Liu, L.; Honsho, Y.; Saeki, A.; Seki, S.; Irle, S.; Dong, Y.; Nagai, A.; Jiang, D. High-Rate Charge-Carrier Transport in Porphyrin Covalent Organic Frameworks: Switching from Hole to Electron to Ambipolar Conduction. *Angew. Chem. Int. Ed. Engl.* **2012**, *51*, 2618–2622.
- Ferenczi, T. a M.; Sims, M.; Bradley, D. D. C. On the Nature of the Fluorenone-Based Emission in Oxidized Polys. *J. Phys. Condens. Matter* **2008**, *20*, 045220.
- Field, J. E.; Venkataraman, D. Heterotriangulenes - Structure and Properties. *Chem. Mater.* **2002**, *14*, 962–964.
- Frisch, M. J.; Trucks, G. W.; Schlegel, H. B.; Scuseria, G. E.; Robb, M. A.; Cheeseman, J. R.; Scalmani, G.; Barone, V.; Mennucci, B.; Petersson, G. A.; Nakatsuji, H.; Caricato, M.; Li, X.; Hratchian, H. P.; Izmaylov, A. F.; Bloino, J.; Zheng, G.; Sonnenb, D. J. Gaussian 09, Revision D.01, 2009.
- Gao, X.; Hu, Y. Development of N-Type Organic Semiconductors for Thin Film Transistors: A Viewpoint of Molecular Design. *J. Mater. Chem. C* **2014**.
- Ghandi, M.; Rezaei, S. J. T.; Yari, A.; Taheri, A. Cycloaddition Reactions of Azomethine Ylides with a 9-Fluorenone-Malononitrile Knöevenagel Adduct. *Tetrahedron Lett.* **2008**, *49*, 5899–5901.

- Głowacki, E. D.; Irimia-Vladu, M.; Bauer, S.; Sariciftci, N. S. Hydrogen-Bonds in Molecular Solids – from Biological Systems to Organic Electronics. *J. Mater. Chem. B* **2013**, *1*, 3742.
- Głowacki, E. D.; Leonat, L.; Voss, G.; Bodea, M.; Bozkurt, Z.; Irimia-Vladu, M.; Bauer, S.; Sariciftci, N. S. Natural and Nature-Inspired Semiconductors for Organic Electronics. In *Organic Semiconductors in Sensors and Bioelectronics IV*; Shinar, R.; Kymissis, I., Eds.; San Diego, California, 2011; Vol. 8118, p. 81180M–81180M–10.
- Głowacki, E. D.; Leonat, L.; Voss, G.; Bodea, M.-A.; Bozkurt, Z.; Ramil, A. M.; Irimia-Vladu, M.; Bauer, S.; Sariciftci, N. S. Ambipolar Organic Field Effect Transistors and Inverters with the Natural Material Tyrian Purple. *AIP Adv.* **2011**, *1*, 042132.
- Głowacki, E. D.; Voss, G.; Leonat, L.; Irimia-Vladu, M.; Bauer, S.; Sariciftci, N. S. Indigo and Tyrian Purple - From Ancient Natural Dyes to Modern Organic Semiconductors. *Isr. J. Chem.* **2012**, *52*, 540–551.
- Gong, X.; Iyer, P. K.; Moses, D.; Bazan, G. C.; Heeger, a. J.; Xiao, S. S. Stabilized Blue Emission from Polyfluorene-Based Light-Emitting Diodes: Elimination of Fluorenone Defects. *Adv. Funct. Mater.* **2003**, *13*, 325–330.
- Grabowski, Z. R.; Rotkiewicz, K.; Rettig, W. Structural Changes Accompanying Intramolecular Electron Transfer: Focus on Twisted Intramolecular Charge-Transfer States and Structures. *Chem. Rev.* **2003**, *103*, 3899–4032.
- Graham, K. R.; Stalder, R.; Wieruszewski, P. M.; Patel, D. G. D.; Salazar, D. H.; Reynolds, J. R. Tailor-Made Additives for Morphology Control in Molecular Bulk-Heterojunction Photovoltaics. *ACS Appl. Mater. Interfaces* **2013**, *5*, 63–71.
- Grätzel, M. Recent Advances in Sensitized Mesoscopic Solar Cells. *Acc. Chem. Res.* **2009**, *42*, 1788–1798.
- Grimsdale, A. C.; Müllen, K. The Chemistry of Organic Nanomaterials. *Angew. Chem. Int. Ed. Engl.* **2005**, *44*, 5592–5629.
- Guan, Z.; Yu, J.; Huang, J.; Zhang, L. Power Efficiency Enhancement of Solution-Processed Small-Molecule Solar Cells Based on Squaraine via Thermal Annealing and Solvent Additive Methods. *Sol. Energy Mater. Sol. Cells* **2013**, *109*, 262–269.
- Guo, X.; Zhou, N.; Lou, S. J.; Smith, J.; Tice, D. B.; Hennek, J. W.; Ortiz, R. P.; Navarrete, J. T. L.; Li, S.; Strzalka, J.; *et al.* Polymer Solar Cells with Enhanced Fill Factors. *Nat. Photonics* **2013**, *7*, 825–833.
- Hagfeldt, A.; Boschloo, G.; Sun, L.; Kloo, L.; Pettersson, H. Dye-Sensitized Solar Cells. *Chem. Rev.* **2010**, *110*, 6595–6663.
- Hardin, B. E.; Hoke, E. T.; Armstrong, P. B.; Yum, J.-H.; Comte, P.; Torres, T.; Fréchet, J. M. J.; Nazeeruddin, M. K.; Grätzel, M.; McGehee, M. D. Increased Light Harvesting in Dye-Sensitized Solar Cells with Energy Relay Dyes. *Nat. Photonics* **2009**, *3*, 406–411.

- Hardin, B. E.; Snaith, H. J.; McGehee, M. D. The Renaissance of Dye-Sensitized Solar Cells. *Nat. Photonics* **2012**, *6*, 162–169.
- Heckmann, A.; Lambert, C. Neutral Organic Mixed-Valence Compounds: Synthesis and All-Optical Evaluation of Electron-Transfer Parameters. *J. Am. Chem. Soc.* **2007**, *129*, 5515–5527.
- Helgesen, M.; Søndergaard, R.; Krebs, F. C. Advanced Materials and Processes for Polymer Solar Cell Devices. *J. Mater. Chem.* **2010**, *20*, 36.
- Heliatek Newscenter http://www.heliatek.com/newscenter/latest_news/neuer-weltrekord-fur-organische-solarzellen-heliatek-behauptet-sich-mit-12-zelleffizienz-als-technologiefuhrer/?lang=en .
- Hernandez, V.; Castiglioni, C.; Del Zoppo, M.; Zerbi, G. Confinement Potential and Π -Electron Delocalization in Polyconjugated Organic Materials. *Phys. Rev. B* **1994**, *50*, 9815–9823.
- Hill, L. L.; Moore, L. R.; Huang, R.; Craciun, R.; Vincent, A. J.; Dixon, D. A.; Chou, J.; Woltermann, C. J.; Shaughnessy, K. H. Bulky Alkylphosphines with Neopentyl Substituents as Ligands in the Amination of Aryl Bromides and Chlorides. *J. Org. Chem.* **2006**, *71*, 5117–5125.
- Hoffmann, R. How Chemistry and Physics Meet in the Solid State. *Angew. Chemie Int. Ed. English* **1987**, *26*, 846–878.
- Homnick, P. J.; Lahti, P. M. Modular Electron Donor Group Tuning of Frontier Energy Levels in Diarylamino-fluorenone Push-Pull Molecules. *Phys. Chem. Chem. Phys.* **2012**, 11961–11968.
- Homnick, P. J.; Tinkham, J. S.; Devaughn, R.; Lahti, P. M. Engineering Frontier Energy Levels in Donor-Acceptor Fluorene-9-Ylidene Malononitriles versus Fluorenones. *J. Phys. Chem. A* **2014**, *118*, 475–486.
- Homnick, P. J.; Tinkham, J. S.; Lahti, P. M. Radical Cations from Diarylamino-Substituted Fluorenones. *Tetrahedron Lett.* **2013**, *54*, 35–39.
- Hu, R.; Lager, E.; Aguilar-Aguilar, A.; Liu, J.; Lam, J. W. Y.; Sung, H. H. Y.; Williams, I. D.; Zhong, Y.; Wong, K. S.; Peña-Cabrera, E.; *et al.* Twisted Intramolecular Charge Transfer and Aggregation-Induced Emission of BODIPY Derivatives. *J. Phys. Chem. C* **2009**, *113*, 15845–15853.
- Hu, W.; Tao, Y.-T.; Sirringhaus, H. Organic Electronics-New Physical Chemistry Insight. *Phys. Chem. Chem. Phys.* **2012**, *14*, 14097–14098.
- Huang, W.; Su, L.; Bo, Z. Hyperbranched Polymers with a Degree of Branching of 100% Prepared by Catalyst Transfer Suzuki-Miyaura Polycondensation. *J. Am. Chem. Soc.* **2009**, *131*, 10348–10349.
- Hush, N. S. Intervalence-Transfer Absorption. Part 2. Theoretical Considerations and Spectroscopic Data. In *Progress in Inorganic Chemistry*; John Wiley & Sons, Inc., 2007; pp. 391–444.

- Irimia-Vladu, M.; Głowacki, E. D.; Troshin, P. a; Schwabegger, G.; Leonat, L.; Susarova, D. K.; Krystal, O.; Ullah, M.; Kanbur, Y.; Bodea, M. a; *et al.* Indigo - A Natural Pigment for High Performance Ambipolar Organic Field Effect Transistors and Circuits. *Adv. Mater.* **2011**, 375–380.
- Irimia-Vladu, M.; Troshin, P. a.; Reisinger, M.; Shmygleva, L.; Kanbur, Y.; Schwabegger, G.; Bodea, M.; Schwödiauer, R.; Mumyatov, A.; Fergus, J. W.; *et al.* Biocompatible and Biodegradable Materials for Organic Field-Effect Transistors. *Adv. Funct. Mater.* **2010**, 20, 4069–4076.
- Isoda, K.; Yasuda, T.; Kato, T. Truxene-Based Columnar Liquid Crystals: Self-Assembled Structures and Electro-Active Properties. *Chem. Asian J.* **2009**, 4, 1619–1625.
- Ito, S.; Wehmeier, M.; Brand, J. D.; Kubel, C.; Epsch, R.; Rabe, J. P.; Müllen, K. Synthesis and Self-Assembly of Functionalized Hexa-Peri-Hexabenzocoronenes. *Chem. - A Eur. J.* **2000**, 6, 4327–4342.
- Jenekhe, S. A.; Lu, L.; Alam, M. M. New Conjugated Polymers with Donor–Acceptor Architectures: Synthesis and Photophysics of Carbazole–Quinoline and Phenothiazine–Quinoline Copolymers and Oligomers Exhibiting Large Intramolecular Charge Transfer. *Macromolecules* **2001**, 34, 7315–7324.
- Jeong, M. J.; Park, J. H.; Lee, C.; Chang, J. Y. Discotic Liquid Crystalline Hydrazone Compounds: Synthesis and Mesomorphic Properties. *Org. Lett.* **2006**, 8, 2221–2224.
- Jin, S.; Ding, X.; Feng, X.; Supur, M.; Furukawa, K.; Takahashi, S.; Addicoat, M.; El-Khouly, M. E.; Nakamura, T.; Irle, S.; *et al.* Charge Dynamics in a Donor-Acceptor Covalent Organic Framework with Periodically Ordered Bicontinuous Heterojunctions. *Angew. Chem. Int. Ed. Engl.* **2013**, 52, 2017–2021.
- Johansson, T.; Mammo, W.; Svensson, M.; Andersson, M. R.; Inganas, O. Electrochemical Bandgaps of Substituted Polythiophenes. *J. Mater. Chem.* **2003**, 13, 1316.
- Jones, B. A.; Ahrens, M. J.; Yoon, M.-H.; Facchetti, A.; Marks, T. J.; Wasielewski, M. R. High-Mobility Air-Stable N-Type Semiconductors with Processing Versatility: Dicyanoperylene-3,4:9,10-Bis. *Angew. Chemie Int. Ed.* **2004**, 43, 6363–6366.
- Józefowicz, M.; Heldt, J. R. Dipole Moments Studies of Fluorenone and 4-Hydroxyfluorenone. *Spectrochim. Acta. A. Mol. Biomol. Spectrosc.* **2007**, 67, 316–320.
- K. Nazeeruddin, M.; Pechy, P.; Gratzel, M. Efficient Panchromatic Sensitization of Nanocrystalline TiO₂ Films by a Black Dye Based on a Trithiocyanato-Ruthenium Complex. *Chem. Commun.* **1997**, 1705–1706.
- Kamin, J.; Heldt, J. R.; Heldt, J.; Jo, M. Spectroscopic Studies of Fluorenone Derivatives. **2001**, 11.
- Kanibolotsky, A. L.; Perepichka, I. F.; Skabara, P. J. Star-Shaped Pi-Conjugated Oligomers and Their Applications in Organic Electronics and Photonics. *Chem. Soc. Rev.* **2010**, 39, 2695–2728.

- Karak, S.; Homnick, P. J.; Della Pelle, A. M.; Bae, Y.; Duzhko, V.; Liu, F.; Russell, T. P.; Lahti, P. M.; Thayumanavan, S. Morphological Size Scale Correlations with Performance in Solvent-Processed Solar Cells with a Triarylamine Substituted Squaraine. *Manuscr. Prep.* **2014**.
- Keppner, H.; Meier, J.; Torres, P.; Fischer, D.; Shah, A. Microcrystalline Silicon and Micromorph Tandem Solar Cells. *Appl. Phys. A Mater. Sci. Process.* **1999**, *69*, 169–177.
- Kim, S.; Oehlhof, A.; Beile, B.; Meier, H. Donor-Acceptor-Substituted Oligos. *Helv. Chim. Acta* **2009**, *92*, 1023–1033.
- Kim, Y.; Cook, S.; Tuladhar, S. M.; Choulis, S. A.; Nelson, J.; Durrant, J. R.; Bradley, D. D. C.; Giles, M.; McCulloch, I.; Ha, C.-S.; *et al.* A Strong Regioregularity Effect in Self-Organizing Conjugated Polymer Films and High-Efficiency Polythiophene:fullerene Solar Cells. *Nat. Mater.* **2006**, *5*, 197–203.
- Kim, Y.-G.; Walker, J.; Samuelson, L. a.; Kumar, J. Efficient Light Harvesting Polymers for Nanocrystalline TiO₂ Photovoltaic Cells †. *Nano Lett.* **2003**, *3*, 523–525.
- Kippelen, B.; Bredas, J.-L. Organic Photovoltaics. *Energy Environ. Sci.* **2009**, *2*, 251–261.
- Kippelen, B.; Brédas, J.-L. Organic Photovoltaics. *Energy Environ. Sci.* **2009**, *2*, 251.
- Kirtman, B.; Champagne, B. Nonlinear Optical Properties of Quasilinear Conjugated Oligomers, Polymers and Organic Molecules. *Int. Rev. Phys. Chem.* **1997**, *16*, 389–420.
- Klapars, A.; Antilla, J. C.; Huang, X.; Buchwald, S. L. A General and Efficient Copper Catalyst for the Amidation of Aryl Halides and the N -Arylation of Nitrogen Heterocycles. *J. Am. Chem. Soc.* **2001**, *123*, 7727–7729.
- Klapars, A.; Huang, X.; Buchwald, S. L. A General and Efficient Copper Catalyst for the Amidation of Aryl Halides. *J. Am. Chem. Soc.* **2002**, *124*, 7421–7428.
- Kobayashi, T.; Nagakura, S. Picosecond Time-Resolved Spectroscopy and the Intersystem Crossing Rates of Anthrone and Fluorenone. *Chem. Phys. Lett.* **1976**, *43*, 429–434.
- Kobin, B.; Grubert, L.; Blumstengel, S.; Henneberger, F.; Hecht, S. Vacuum-Processable Ladder-Type Oligophenylenes for Organic–inorganic Hybrid Structures: Synthesis, Optical and Electrochemical Properties upon Increasing Planarization as Well as Thin Film Growth. *J. Mater. Chem.* **2012**, 4383–4390.
- Köhler, J.; Quast, T.; Buback, J.; Fischer, I.; Brixner, T.; Nuernberger, P.; Geiss, B.; Mager, J.; Lambert, C. Ultrafast Charge-Transfer Dynamics of Donor-Substituted Truxenones. *Phys. Chem. Chem. Phys.* **2012**, *14*, 11081–11089.
- Kokil, A.; Chudomel, J. M.; Homnick, P. J.; Lahti, P. M.; Kumar, J. Push–pull Triarylamine Additives That Enhance Dye Sensitized Solar Cell Performance. *RSC Adv.* **2013**, *3*, 15626.
- Kuboyama, A. Similarity between the Pi, Pi* Absorption Spectra of Fluorenone and 9, 10-Phenanthrenequinone. *Chem. Phys. Lett.* **1976**, *41*, 544–546.

- Kuhn, W. E.; Fieser, L. F.; Walker, J. T. 2-Nitrofluorene and 2-Aminofluorene. In *Organic Syntheses*; pp. 447–448.
- Kurata, T.; Koshika, K.; Kato, F.; Kido, J.; Nishide, H. An Unpaired Electron-Based Hole-Transporting Molecule: Triarylamine-Combined Nitroxide Radicals. *Chem. Commun.* **2007**, *1*, 2986–2988.
- Kylberg, W.; Zhang, Y.; Aebersold, A.; de Castro, F. A.; Geiger, T.; Heier, J.; Kuster, S.; Ma, C.-Q.; Bäuerle, P.; Nüesch, F.; *et al.* Oligothiophene Dendron-Decorated Squaraine Dyes: Synthesis, Thin Film Formation, and Performance in Organic Solar Cells. *Org. Electron.* **2012**, *13*, 1204–1212.
- Lambert, C.; Nöll, G. The Class II/III Transition in Triarylamine Redox Systems. *J. Am. Chem. Soc.* **1999**, *121*, 8434–8442.
- Lambert, C.; Nöll, G.; Schmäzlin, E.; Meerholz, K.; Bräuchle, C. Synthesis, Linear Optical and Redox Properties of a Donor-Substituted Truxenone Derivative. *Chem. - A Eur. J.* **1998**, *4*, 2129–2135.
- Lancaster, K.; Odom, S. a; Jones, S. C.; Thayumanavan, S.; Marder, S. R.; Brédas, J.-L.; Coropceanu, V.; Barlow, S. Intramolecular Electron-Transfer Rates in Mixed-Valence Triarylaminines: Measurement by Variable-Temperature ESR Spectroscopy and Comparison with Optical Data. *J. Am. Chem. Soc.* **2009**, *131*, 1717–1723.
- Lee, C.; Yang, W.; Parr, R. G. Development of the Colle-Salvetti Correlation-Energy Formula into a Functional of the Electron Density. *Phys. Rev. B* **1988**, *37*, 785–789.
- Leriche, P.; Frère, P.; Cravino, A.; Alévêque, O.; Roncali, J. Molecular Engineering of the Internal Charge Transfer in Thiophene-Triphenylamine Hybrid Pi-Conjugated Systems. *J. Org. Chem.* **2007**, *72*, 8332–8336.
- Lewis, N. S. Toward Cost-Effective Solar Energy Use. *Science* **2007**, *315*, 798–801.
- Li, G.; Zhu, R.; Yang, Y. Polymer Solar Cells. *Nat. Photonics* **2012**, *6*, 153–161.
- Li, R.; Hu, W.; Liu, Y.; Zhu, D. Micro- and Nanocrystals of Organic Semiconductors. *Acc. Chem. Res.* **2010**, *43*, 529–540.
- Lincker, F.; Delbosc, N.; Bailly, S.; De Bettignies, R.; Billon, M.; Pron, A.; Demadrille, R. Fluorenone-Based Molecules for Bulk-Heterojunction Solar Cells: Synthesis, Characterization, and Photovoltaic Properties. *Adv. Funct. Mater.* **2008**, *18*, 3444–3453.
- Lincker, F.; Heinrich, B.; De Bettignies, R.; Rannou, P.; Pécaut, J.; Grévin, B.; Pron, A.; Donnio, B.; Demadrille, R. Fluorenone Core Donor–acceptor–donor Π -Conjugated Molecules End-Capped with Dendritic Oligos: Synthesis, Liquid Crystalline Behaviour, and Photovoltaic Applications. *J. Mater. Chem.* **2011**, *21*, 5238.
- Liu, S.; Wang, W. M.; Briseno, A. L.; Mannsfeld, S. C. B.; Bao, Z. Controlled Deposition of Crystalline Organic Semiconductors for Field-Effect-Transistor Applications. *Adv. Mater.* **2009**, *21*, 1217–1232.

- Liu, Y.; Chen, C.-C.; Hong, Z.; Gao, J.; Michael Yang, Y.; Zhou, H.; Dou, L.; Li, G.; Yang, Y. Solution-Processed Small-Molecule Solar Cells: Breaking the 10% Power Conversion Efficiency. *Sci. Rep.* **2013**, *3*, 3356.
- Liu, Y.; Tao, X.; Wang, F.; Shi, J.; Sun, J.; Yu, W.; Ren, Y.; Zou, D.; Jiang, M. Intermolecular Hydrogen Bonds Induce Highly Emissive Excimers: Enhancement of Solid-State Luminescence. *J. Phys. Chem. C* **2007**, *111*, 6544–6549.
- Lloyd, M. T.; Anthony, J. E.; Malliaras, G. G. Photovoltaics from Soluble Small Molecules. *Mater. Today* **2007**, *10*, 34–41.
- Lu, Y.-M.; Wong, J.-S.; Hsu, L.-C. Characterization of Indigo-Doped poly:[6,6]-Phenyl C61-Butyric Acid Methyl Ester Bulk Heterojunction Solar Cells. *Thin Solid Films* **2013**, *529*, 58–61.
- MacDiarmid, A. G. “Synthetic Metals”: A Novel Role for Organic Polymers. *Angew. Chemie Int. Ed.* **2001**, *40*, 2581–2590.
- Maeda, T.; Tsukamoto, T.; Seto, A.; Yagi, S.; Nakazumi, H. Synthesis and Characterization of Squaraine-Based Conjugated Polymers With Phenylene Linkers for Bulk Heterojunction Solar Cells. *Macromol. Chem. Phys.* **2012**, *213*, 2590–2597.
- Magnani, L.; Rumbles, G.; Samuel, I. D. W.; Murray, K.; Moratti, S. C.; Holmes, A. B.; Friend, R. H. Photoluminescence Studies of Chain Interactions in Electroluminescent Polymers. *Synth. Met.* **1997**, *84*, 899–900.
- Mahmood, K.; Liu, Z.-P.; Li, C.; Lu, Z.; Fang, T.; Liu, X.; Zhou, J.; Lei, T.; Pei, J.; Bo, Z. Novel Isoindigo-Based Conjugated Polymers for Solar Cells and Field Effect Transistors. *Polym. Chem.* **2013**, *4*, 3563.
- Maldonado, J.-L.; Bishop, M.; Fuentes-Hernandez, C.; Caron, P.; Domercq, B.; Zhang, Y.; Barlow, S.; Thayumanavan, S.; Malagoli, M.; Brédas, J.-L.; *et al.* Effect of Substitution on the Hole Mobility of Bisbiphenyl Derivatives Doped in Poly. *Chem. Mater.* **2003**, *15*, 994–999.
- Martinez-Martinez, V.; Lim, J.; Banuelos, J.; Lopez-Arbeloa, I.; Miljanic, O. S. Strong Intramolecular Charge Transfer Emission in Benzobisoxazole Cruciforms: Solvatochromic Dyes as Polarity Indicators. *Phys. Chem. Chem. Phys.* **2013**, *15*, 18023–18029.
- McKee, J. R.; Zanger, M. A Microscale Synthesis of Indigo: Vat Dyeing. *J. Chem. Educ.* **1991**, *68*, A242.
- Mei, J.; Diao, Y.; Appleton, A. L.; Fang, L.; Bao, Z. Integrated Materials Design of Organic Semiconductors for Field-Effect Transistors. *J. Am. Chem. Soc.* **2013**, *135*, 6724–6746.
- Mei, J.; Graham, K. R.; Stalder, R.; Reynolds, J. R. Synthesis of Isoindigo-Based Oligothiophenes for Molecular Bulk Heterojunction Solar Cells. *Org. Lett.* **2010**, *12*, 660–663.

- Meier, H. Conjugated Oligomers with Terminal Donor-Acceptor Substitution. *Angew. Chem. Int. Ed. Engl.* **2005**, *44*, 2482–2506.
- Meier, H.; Stalmach, U.; Kolshorn, H. Effective Conjugation Length and UV/vis Spectra of Oligomers. *Acta Polym.* **1997**, *48*, 379–384.
- Meiss, J.; Merten, A.; Hein, M.; Schuenemann, C.; Schäfer, S.; Tietze, M.; Urich, C.; Pfeiffer, M.; Leo, K.; Riede, M. Fluorinated Zinc Phthalocyanine as Donor for Efficient Vacuum-Deposited Organic Solar Cells. *Adv. Funct. Mater.* **2012**, *22*, 405–414.
- Meyers, F.; Bredas, J. L. Electronic Structure and Nonlinear Optical Properties of Push-Pull Conjugated Molecules. *Int. J. Quantum Chem.* **1992**, *42*, 1595–1614.
- Mishra, A.; Bäuerle, P. Small Molecule Organic Semiconductors on the Move: Promises for Future Solar Energy Technology. *Angew. Chem. Int. Ed. Engl.* **2012**, *51*, 2020–2067.
- Miyajima, D.; Araoka, F.; Takezoe, H.; Kim, J.; Kato, K.; Takata, M.; Aida, T. Ferroelectric Columnar Liquid Crystal Featuring Confined Polar Groups within Core-Shell Architecture. *Science* **2012**, *336*, 209–213.
- Montilla, F.; Mallavia, R. On the Origin of Green Emission Bands in Fluorene-Based Conjugated Polymers. *Adv. Funct. Mater.* **2007**, *17*, 71–78.
- Morley, J. Calculated Hyperpolarisabilities of Polythiophenes, Polyfurans and Polypyrroles. *J. Chem. Soc., Faraday Trans.* **1991**, *87*, 3009–3013.
- Morton, O. Solar Energy: A New Day Dawning? Silicon Valley Sunrise. *Nature* **2006**, *443*, 19–22.
- Murata, H.; Lahti, P. M. Synthesis and Oxidation of Triarylamine Derivatives Bearing Hydrogen-Bonding Groups. *J. Org. Chem.* **2007**, *72*, 4974–4977.
- Murata, H.; Takahashi, M.; Namba, K.; Takahashi, N.; Nishide, H. A High-Spin and Durable Polyradical: poly. *J. Org. Chem.* **2004**, *69*, 631–638.
- National Center for Photovoltaics Home Page <http://www.nrel.gov/ncpv> .
- Nawn, G.; McDonald, R.; Hicks, R. G. Synthesis and Characterization of Heterobimetallic Nindigo Complexes and Comparisons to Their Homobimetallic Analogues. *Inorg. Chem.* **2013**, *52*, 10912–10919.
- Nawn, G.; Oakley, S. R.; Majewski, M. B.; McDonald, R.; Patrick, B. O.; Hicks, R. G. Redox-Active, near-Infrared Dyes Based on “Nindigo” Boron Chelate Complexes. *Chem. Sci.* **2013**, *4*, 612.
- Nazeeruddin, M. K.; Kay, A.; Rodicio, I.; Humphry-Baker, R.; Mueller, E.; Liska, P.; Vlachopoulos, N.; Graetzel, M. Conversion of Light to Electricity by Cis-X2bisruthenium Charge-Transfer Sensitizers on Nanocrystalline Titanium Dioxide Electrodes. *J. Am. Chem. Soc.* **1993**, *115*, 6382–6390.

- Negi, Y. S.; Adhyapak, P. V. Development in Polyaniline Conducting Polymers. *J. Macromol. Sci. Part C Polym. Rev.* **2002**, *42*, 35–53.
- Newman, C. R.; Frisbie, C. D.; da Silva Filho, D. A.; Brédas, J.-L.; Ewbank, P. C.; Mann, K. R. Introduction to Organic Thin Film Transistors and Design of N-Channel Organic Semiconductors. *Chem. Mater.* **2004**, *16*, 4436–4451.
- Ning, Z.; Tian, H. Triarylamine: A Promising Core Unit for Efficient Photovoltaic Materials. *Chem. Commun.* **2009**, 5483–5495.
- Oakley, S. R.; Nawn, G.; Waldie, K. M.; MacInnis, T. D.; Patrick, B. O.; Hicks, R. G. “Nindigo”: Synthesis, Coordination Chemistry, and Properties of Indigo Diimines as a New Class of Functional Bridging Ligands. *Chem. Commun.* **2010**, *46*, 6753–6755.
- Oliva, M. M.; Casado, J.; Navarrete, J. T. L.; Berridge, R.; Skabara, P. J.; Kanibolotsky, A. L.; Perepichka, I. F. Electronic and Molecular Structures of Trigonal Truxene-Core Systems Conjugated to Peripheral Fluorene Branches. Spectroscopic and Theoretical Study. *J. Phys. Chem. B* **2007**, *111*, 4026–4035.
- Ooyama, Y.; Oda, Y.; Mizumo, T.; Ohshita, J. Specific Solvatochromism of D- π -A Type Pyridinium Dyes Bearing Various Counter Anions in Halogenated Solvents. *Tetrahedron* **2013**, *69*, 1755–1760.
- Patwardhan, S.; Kocherzhenko, A. a.; Grozema, F. C.; Siebbeles, L. D. a. Delocalization and Mobility of Charge Carriers in Covalent Organic Frameworks. *J. Phys. Chem. C* **2011**, *115*, 11768–11772.
- Péchy, P.; Renouard, T.; Zakeeruddin, S. M.; Humphry-Baker, R.; Comte, P.; Liska, P.; Cevey, L.; Costa, E.; Shklover, V.; Spiccia, L.; *et al.* Engineering of Efficient Panchromatic Sensitizers for Nanocrystalline TiO₂-Based Solar Cells. *J. Am. Chem. Soc.* **2001**, *123*, 1613–1624.
- Peet, J.; Heeger, A. J.; Bazan, G. C. “Plastic” Solar Cells: Self-Assembly of Bulk Heterojunction Nanomaterials by Spontaneous Phase Separation. *Acc. Chem. Res.* **2009**, *42*, 1700–1708.
- Pérez, E. M.; Capodilupo, A. L.; Fernández, G.; Sánchez, L.; Viruela, P. M.; Viruela, R.; Ortí, E.; Bietti, M.; Martín, N. Weighting Non-Covalent Forces in the Molecular Recognition of C. Relevance of Concave-Convex Complementarity. *Chem. Commun.* **2008**, 4567–4569.
- Pérez, E. M.; Illescas, B. M.; Herranz, M. Á.; Martín, N. Supramolecular Chemistry of Π -Extended Analogues of TTF and Carbon Nanostructures. *New J. Chem.* **2009**, *33*, 228.
- Pérez, E. M.; Martín, N. Curves Ahead: Molecular Receptors for Fullerenes Based on Concave-Convex Complementarity. *Chem. Soc. Rev.* **2008**, *37*, 1512–1519.
- Pérez, E. M.; Sierra, M.; Sánchez, L.; Torres, M. R.; Viruela, R.; Viruela, P. M.; Ortí, E.; Martín, N. Concave Tetrathiafulvalene-Type Donors as Supramolecular Partners for Fullerenes. *Angew. Chem. Int. Ed. Engl.* **2007**, *46*, 1847–1851.

- Peterson, J. J.; Simon, Y. C.; Coughlin, E. B.; Carter, K. R. Polyfluorene with P-Carborane in the Backbone. *Chem. Commun.* **2009**, 4950–4952.
- Pommerehne, J.; Vestweber, H.; Guss, W. Efficient Two Layer LEDs on a Polymer Blend Basis. *Adv. Mater.* **1995**, *7*, 551–554.
- Porzio, W.; Destri, S.; Pasini, M.; Giovanella, U.; Ragazzi, M.; Scavia, G.; Kotowski, D.; Zotti, G.; Vercelli, B. Synthesis and Characterisation of Fluorenone–thiophene-Based Donor–acceptor Oligomers: Role of Moiety Sequence upon Packing and Electronic Properties. *New J. Chem.* **2010**, *34*, 1961.
- Prasad, P. N.; Williams, D. J. *Introduction to Nonlinear Optical Effects in Molecules & Polymers*; John Wiley & Sons: New York, 1991.
- Promarak, V.; Punkvuang, A.; Sudyoadsuk, T.; Jungstittiwong, S.; Saengsuwan, S.; Keawin, T.; Sirithip, K. Synthesis and Characterization of N-Carbazole End-Capped Oligofluorene-Thiophenes. *Tetrahedron* **2007**, *63*, 8881–8890.
- Qi, D.; Zhang, L.; Jiang, J. Toward Panchromatic Organic Functional Molecules: Density Functional Theory Study on the Nature of the Broad UV–Vis–NIR Spectra of Substituted Tetraporphyrins. *J. Mol. Graph. Model.* **2012**, *38*, 304–313.
- Ragoussi, M.-E.; Ince, M.; Torres, T. Recent Advances in Phthalocyanine-Based Sensitizers for Dye-Sensitized Solar Cells. *European J. Org. Chem.* **2013**, *2013*, 6475–6489.
- Raimundo, J.; Blanchard, P.; Gallego-Planas, N.; Mercier, N.; Ledoux-Rak, I.; Hierle, R.; Roncali, J. Design and Synthesis of Push–Pull Chromophores for Second-Order Nonlinear Optics Derived from Rigidified Thiophene-Based Π -Conjugating Spacers. *J. Org. Chem.* **2002**, *67*, 205–218.
- Ratera, I.; Veciana, J. Playing with Organic Radicals as Building Blocks for Functional Molecular Materials. *Chem. Soc. Rev.* **2012**, *41*, 303–349.
- Rathnayake, H. P.; Cirpan, A.; Karasz, F. E.; Odoi, M. Y.; Hammer, N. I.; Barnes, M. D.; Lahti, P. M. Luminescence of Molecular and Block Copolymeric 2,7-Bis-Fluorenes; Identifying Green-Band Emitter Sites in a Fluorene-Based Luminophore. *Chem. Mater.* **2007**, *19*, 3265–3270.
- Rathnayake, H. P.; Cirpan, A.; Lahti, P. M.; Karasz, F. E. Optimizing LED Properties of 2,7-Bisfluorenes. *Chem. Mater.* **2006**, *18*, 560–566.
- Reed, A. E.; Curtiss, L. a.; Weinhold, F. Intermolecular Interactions from a Natural Bond Orbital, Donor-Acceptor Viewpoint. *Chem. Rev.* **1988**, *88*, 899–926.
- Reese, C.; Bao, Z. Organic Single-Crystal Field-Effect Transistors. *Mater. Today* **2007**, *10*, 20–27.
- Rettig, W. Charge Separation in Excited States of Decoupled Systems—TICT Compounds and Implications Regarding the Development of New Laser Dyes and the Primary Process of Vision and Photosynthesis. *Angew. Chemie Int. Ed. English* **1986**, *25*, 971–988.

- Riede, M.; Mueller, T.; Tress, W.; Schueppel, R.; Leo, K. Small-Molecule Solar Cells-Status and Perspectives. *Nanotechnology* **2008**, *19*, 424001.
- Robb, M. J.; Ku, S.-Y.; Brunetti, F. G.; Hawker, C. J. A Renaissance of Color: New Structures and Building Blocks for Organic Electronics. *J. Polym. Sci. Part A Polym. Chem.* **2013**, *51*, 1263–1271.
- Robin, M. B.; Day, P. Mixed Valence Chemistry-A Survey and Classification. *Adv. Inorg. Chem. Radiochem.* **1968**, *10*, 247–422.
- Roncali, J. Molecular Bulk Heterojunctions: An Emerging Approach to Organic Solar Cells. *Acc. Chem. Res.* **2009**, *42*, 1719–1730.
- Roncali, J. Synthetic Principles for Bandgap Control in Linear Pi-Conjugated Systems. *Chem. Rev.* **1997**, *97*, 173–206.
- Roquet, S.; Cravino, A.; Leriche, P.; Alévêque, O.; Frère, P.; Roncali, J. Triphenylamine-Thienylenevinylene Hybrid Systems with Internal Charge Transfer as Donor Materials for Heterojunction Solar Cells. *J. Am. Chem. Soc.* **2006**, *128*, 3459–3466.
- Rumbles, G.; Samuel, I. D. W.; Magnani, L.; Murray, K. A.; DeMello, A. J.; Crystall, B.; Moratti, S. C.; Stone, B. M.; Holmes, A. B.; Friend, R. H. Chromism and Luminescence in Regioregular poly. *Synth. Met.* **1996**, *76*, 47–51.
- Sanguinet, L.; Williams, J. C.; Yang, Z.; Twieg, R. J.; Mao, G.; Singer, K. D.; Wiggers, G.; Petschek, R. G. Synthesis and Characterization of New Truxenones for Nonlinear Optical Applications. *Chem. Mater.* **2006**, *18*, 4259–4269.
- Sariciftci, N. S.; Braun, D.; Zhang, C.; Srdanov, V. I.; Heeger, A. J.; Stucky, G.; Wudl, F. Semiconducting Polymer-buckminsterfullerene Heterojunctions: Diodes, Photodiodes, and Photovoltaic Cells. *Appl. Phys. Lett.* **1993**, *62*.
- Sariciftci, N. S.; Smilowitz, L.; Heeger, A. J.; Wudl, F. Photoinduced Electron Transfer from a Conducting Polymer to Buckminsterfullerene. *Science* . **1992**, *258*, 1474–1476.
- Scalmani, G.; Frisch, M. J.; Mennucci, B.; Tomasi, J.; Cammi, R.; Barone, V. Geometries and Properties of Excited States in the Gas Phase and in Solution: Theory and Application of a Time-Dependent Density Functional Theory Polarizable Continuum Model. *J. Chem. Phys.* **2006**, *124*, 94107.
- Scott, J. L.; Yamada, T.; Tanaka, K. Guest Specific Solid-State Fluorescence Rationalised by Reference to Solid-State Structures and Specific Intermolecular Interactions. *New J. Chem.* **2004**, *28*, 447.
- Shang, H.; Fan, H.; Liu, Y.; Hu, W.; Li, Y.; Zhan, X. A Solution-Processable Star-Shaped Molecule for High-Performance Organic Solar Cells. *Adv. Mater.* **2011**, *23*, 1554–1557.
- Shankar, K.; Feng, X.; Grimes, C. A. Enhanced Harvesting of Red Photons in Nanowire Solar Cells: Evidence of Resonance Energy Transfer. *ACS Nano* **2009**, *3*, 788–794.

- Shellaiah, M.; Rajan, Y. C.; Lin, H.-C. Synthesis of Novel Triarylamine-Based Dendrimers with N4-, N6-Dibutyl-1,3,5-Triazine-4,6-Diamine Probe for Electron/energy Transfers in H-Bonded Donor-Acceptor-Donor Triads and as Efficient Cu²⁺ Sensors. *J. Mater. Chem.* **2012**, *22*, 8976–8987.
- Shigeta, M.; Morita, M.; Konishi, G.-I. Selective Formation of Twisted Intramolecular Charge Transfer and Excimer Emissions on 2,7-bis-Fluorenone by Choice of Solvent. *Molecules* **2012**, *17*, 4452–4459.
- Shirai, Y.; Osgood, A. J.; Zhao, Y.; Yao, Y.; Saudan, L.; Yang, H.; Yu-Hung, C.; Alemany, L. B.; Sasaki, T.; Morin, J.-F.; *et al.* Surface-Rolling Molecules. *J. Am. Chem. Soc.* **2006**, *128*, 4854–4864.
- Sierra, C. a.; Lahti, P. M. A Photoluminescent, Segmented Oligo-Polyphenylenevinylene Copolymer with Hydrogen-Bonding Pendant Chains. *Chem. Mater.* **2004**, *16*, 55–61.
- Silvestri, F.; Irwin, M. D.; Beverina, L.; Facchetti, A.; Pagani, G. A.; Marks, T. J. Efficient Squaraine-Based Solution Processable Bulk-Heterojunction Solar Cells. *J. Am. Chem. Soc.* **2008**, *130*, 17640–17641.
- Snaith, H. J. Estimating the Maximum Attainable Efficiency in Dye-Sensitized Solar Cells. *Adv. Funct. Mater.* **2010**, *20*, 13–19.
- So, S.; Choi, H.; Ko, H. M.; Kim, C.; Paek, S.; Cho, N.; Song, K.; Lee, J. K.; Ko, J. Novel Unsymmetrical Push–pull Squaraine Chromophores for Solution Processed Small Molecule Bulk Heterojunction Solar Cells. *Sol. Energy Mater. Sol. Cells* **2012**, *98*, 224–232.
- Spanggaard, H.; Krebs, F. C. A Brief History of the Development of Organic and Polymeric Photovoltaics. *Sol. Energy Mater. Sol. Cells* **2004**, *83*, 125–146.
- Spitler, E. L.; Colson, J. W.; Uribe-Romo, F. J.; Woll, A. R.; Giovino, M. R.; Saldivar, A.; Dichtel, W. R. Lattice Expansion of Highly Oriented 2D Phthalocyanine Covalent Organic Framework Films. *Angew. Chem. Int. Ed. Engl.* **2012**, *51*, 2623–2627.
- Spitler, E. L.; Dichtel, W. R. Lewis Acid-Catalysed Formation of Two-Dimensional Phthalocyanine Covalent Organic Frameworks. *Nat. Chem.* **2010**, *2*, 672–677.
- Sreenath, K.; Suneesh, C. V.; Kumar, V. K. R.; Gopidas, K. R. Cu-Mediated Generation of Triarylamine Radical Cations and Their Dimerization. an Easy Route to Tetraarylbenzidines. *J. Org. Chem.* **2008**, *73*, 3245–3251.
- Stalder, R.; Mei, J.; Graham, K. R.; Estrada, L. A.; Reynolds, J. R. Isoindigo, a Versatile Electron-Deficient Unit For High-Performance Organic Electronics. *Chem. Mater.* **2014**, *26*, 664–678.
- Stalder, R.; Mei, J.; Reynolds, J. R. Isoindigo-Based Donor–Acceptor Conjugated Polymers. *Macromolecules* **2010**, *43*, 8348–8352.
- Stamires, D. N.; Turkevich, J. Electron Paramagnetic Resonance in Some Molecular Charge Transfer Complexes. *J. Am. Chem. Soc.* **1963**, *85*, 2557–2561.

- Stephens, P. J.; Devlin, F. J.; Chabalowski, C. F.; Frisch, M. J. Ab Initio Calculation of Vibrational Absorption and Circular Dichroism Spectra Using Density Functional Force Fields. *J. Phys. Chem.* **1994**, *98*, 11623–11627.
- Subbiah, J.; Amb, C. M.; Reynolds, J. R.; So, F. Effect of Vertical Morphology on the Performance of Silole-Containing Low-Bandgap Inverted Polymer Solar Cells. *Sol. Energy Mater. Sol. Cells* **2012**, *97*, 97–101.
- Sun, Q.; Wang, H.; Yang, C.; Li, Y. Synthesis and Electroluminescence of Novel Copolymers Containing Crown Ether Spacers. *J. Mater. Chem.* **2003**, *13*, 800–806.
- Sun, X.; Liu, Y.; Xu, X.; Yang, C.; Yu, G.; Chen, S.; Zhao, Z.; Qiu, W.; Li, Y.; Zhu, D. Novel Electroactive and Photoactive Molecular Materials Based on Conjugated Donor–Acceptor Structures for Optoelectronic Device Applications. *J. Phys. Chem. B* **2005**, *109*, 10786–10792.
- Sun, Y.; Welch, G. C.; Leong, W. L.; Takacs, C. J.; Bazan, G. C.; Heeger, A. J. Solution-Processed Small-Molecule Solar Cells with 6.7% Efficiency. *Nat. Mater.* **2011**, *11*, 44–48.
- Tanaka, H.; Shizu, K.; Nakanotani, H.; Adachi, C. Twisted Intramolecular Charge Transfer State for Long-Wavelength Thermally Activated Delayed Fluorescence. *Chem. Mater.* **2013**, *25*, 3766–3771.
- The Microscale Synthesis of Indigo Dye. In *Microscale Chemistry*; Skinner, J., Ed.; Education Division, Royal Society of Chemistry, 1997; pp. 188–189.
- Thelakkat, M. Star-Shaped, Dendrimeric and Polymeric Triarylamines as Photoconductors and Hole Transport Materials for Electro-Optical Applications. *Macromol. Mater. Eng.* **2002**, *287*, 442.
- Thompson, B. C.; Fréchet, J. M. J. Polymer-Fullerene Composite Solar Cells. *Angew. Chem. Int. Ed. Engl.* **2008**, *47*, 58–77.
- Uribe-Romo, F. J.; Doonan, C. J.; Furukawa, H.; Oisaki, K.; Yaghi, O. M. Crystalline Covalent Organic Frameworks with Hydrazone Linkages. *J. Am. Chem. Soc.* **2011**, *133*, 11478–11481.
- Usta, H.; Facchetti, A.; Marks, T. J. N-Channel Semiconductor Materials Design for Organic Complementary Circuits. *Acc. Chem. Res.* **2011**, *44*, 501–510.
- Usta, H.; Risko, C.; Wang, Z.; Huang, H.; Deliomeroğlu, M. K.; Zhukhovitskiy, A.; Facchetti, A.; Marks, T. J. Design, Synthesis, and Characterization of Ladder-Type Molecules and Polymers. Air-Stable, Solution-Processable N-Channel and Ambipolar Semiconductors for Thin-Film Transistors via Experiment and Theory. *J. Am. Chem. Soc.* **2009**, *131*, 5586–5608.
- Vasilev, A. A.; De Mey, K.; Asselberghs, I.; Clays, K.; Champagne, B.; Angelova, S. E.; Spassova, M. I.; Li, C.; Müllen, K. Enhanced Intramolecular Charge Transfer in New Type Donor–Acceptor Substituted Perylenes. *J. Phys. Chem. C* **2012**, *116*, 22711–22719.

- Vijayakumar, C.; Saeki, A.; Seki, S. Optoelectronic Properties of Dicyanofluorene-Based N-Type Polymers. *Chem. Asian J.* **2012**, *7*, 1845–1852.
- Völker, S. F.; Uemura, S.; Limpinsel, M.; Mingeback, M.; Deibel, C.; Dyakonov, V.; Lambert, C. Polymeric Squaraine Dyes as Electron Donors in Bulk Heterojunction Solar Cells. *Macromol. Chem. Phys.* **2010**, *211*, 1098–1108.
- Walker, B.; Kim, C.; Nguyen, T.-Q. Small Molecule Solution-Processed Bulk Heterojunction Solar Cells †. *Chem. Mater.* **2011**, *23*, 470–482.
- Wan, S.; Gándara, F.; Asano, A.; Furukawa, H.; Saeki, A.; Dey, S. K.; Liao, L.; Ambrogio, M. W.; Botros, Y. Y.; Duan, X.; *et al.* Covalent Organic Frameworks with High Charge Carrier Mobility. *Chem. Mater.* **2011**, *23*, 4094–4097.
- Wan, X.; Zhang, H.; Li, Y.; Chen, Y. Self-Assembly Based on Heterotriangulene Derivatives: From Nanowires to Microrods. *New J. Chem.* **2010**, *34*, 661.
- Wang, E.; Lam, J. W. Y.; Hu, R.; Zhang, C.; Zhao, Y. S.; Tang, B. Z. Twisted Intramolecular Charge Transfer{,} Aggregation-Induced Emission{,} Supramolecular Self-Assembly and the Optical Waveguide of Barbituric Acid-Functionalized Tetraphenylethene. *J. Mater. Chem. C* **2014**, *2*, 1801–1807.
- Wang, E.; Mammo, W.; Andersson, M. R. 25th Anniversary Article: Isoindigo-Based Polymers and Small Molecules for Bulk Heterojunction Solar Cells and Field Effect Transistors. *Adv. Mater.* **2014**, n/a–n/a.
- Wang, J.; Xiao, Q.; Pei, J. Benzothiadiazole-Based D-II-A-II-D Organic Dyes with Tunable Band Gap: Synthesis and Photophysical Properties. *Org. Lett.* **2010**, *12*, 4164–4167.
- Wang, M.; Chamberland, N.; Breau, L.; Moser, J.-E.; Humphry-Baker, R.; Marsan, B.; Zakeeruddin, S. M.; Grätzel, M. An Organic Redox Electrolyte to Rival Triiodide/iodide in Dye-Sensitized Solar Cells. *Nat. Chem.* **2010**, *2*, 385–389.
- Wang, P.; Zakeeruddin, S. M.; Moser, J. E.; Nazeeruddin, M. K.; Sekiguchi, T.; Grätzel, M. A Stable Quasi-Solid-State Dye-Sensitized Solar Cell with an Amphiphilic Ruthenium Sensitizer and Polymer Gel Electrolyte. *Nat. Mater.* **2003**, *2*, 402–407.
- Wang, S.; Hall, L.; Diev, V. V.; Haiges, R.; Wei, G.; Xiao, X.; Djurovich, P. I.; Forrest, S. R.; Thompson, M. E. N,N-Diarylanilinosquaraines and Their Application to Organic Photovoltaics. *Chem. Mater.* **2011**, *23*, 4789–4798.
- Wang, S.; Kivala, M.; Lieberwirth, I.; Kirchhoff, K.; Feng, X.; Pisula, W.; Müllen, K. Dip-Coating-Induced Fiber Growth of a Soluble Heterotriangulene. *Chemphyschem* **2011**, *12*, 1648–1651.
- Watson, M. D.; Fechtenkötter, a; Müllen, K. Big Is Beautiful--“Aromaticity” Revisited from the Viewpoint of Macromolecular and Supramolecular Benzene Chemistry. *Chem. Rev.* **2001**, *101*, 1267–1300.

- Wei, G.; Lunt, R. R.; Sun, K.; Wang, S.; Thompson, M. E.; Forrest, S. R. Efficient, Ordered Bulk Heterojunction Nanocrystalline Solar Cells by Annealing of Ultrathin Squaraine Thin Films. *Nano Lett.* **2010**, *10*, 3555–3559.
- Wei, G.; Wang, S.; Sun, K.; Thompson, M. E.; Forrest, S. R. Solvent-Annealed Crystalline Squaraine: PC70BM Solar Cells. *Adv. Energy Mater.* **2011**, *1*, 184–187.
- Wei, G.; Xiao, X.; Wang, S.; Sun, K.; Bergemann, K. J.; Thompson, M. E.; Forrest, S. R. Functionalized Squaraine Donors for Nanocrystalline Organic Photovoltaics. *ACS Nano* **2012**, *6*, 972–978.
- Wei, G.; Xiao, X.; Wang, S.; Zimmerman, J. D.; Sun, K.; Diev, V. V.; Thompson, M. E.; Forrest, S. R. Arylamine-Based Squaraine Donors for Use in Organic Solar Cells. *Nano Lett.* **2011**, *11*, 4261–4264.
- Wong, W.-Y.; Lu, G.-L.; Choi, K.-H.; Lin, Z. Functionalization of 9-fluorene Derivatives with Substituted Acetylenes. *European J. Org. Chem.* **2003**, *2003*, 365–373.
- Würthner, F.; Schmidt, R. Electronic and Crystal Engineering of Acenes for Solution-Processible Self-Assembling Organic Semiconductors. *ChemPhysChem* **2006**, *7*, 793–797.
- Xiao, X.; Wei, G.; Wang, S.; Zimmerman, J. D.; Renshaw, C. K.; Thompson, M. E.; Forrest, S. R. Small-Molecule Photovoltaics Based on Functionalized Squaraine Donor Blends. *Adv. Mater.* **2012**, *24*, 1956–1960.
- Yang, D.; Guan, Z.; Yang, L.; Huang, Y.; Wei, Q.; Lu, Z.; Yu, J. Novel High-Performance Photovoltaic D–A Conjugated Polymers Bearing 1,2-Squaraine Moieties as Electron-Deficient Units. *Sol. Energy Mater. Sol. Cells* **2012**, *105*, 220–228.
- Yang, Z.; Xu, B.; He, J.; Xue, L.; Guo, Q.; Xia, H.; Tian, W. Solution-Processable and Thermal-Stable Triphenylamine-Based Dendrimers with Truxene Cores as Hole-Transporting Materials for Organic Light-Emitting Devices. *Org. Electron.* **2009**, *10*, 954–959.
- Yatsushashi, T.; Nakajima, Y.; Shimada, T.; Inoue, H. Photophysical Properties of Intramolecular Charge-Transfer Excited Singlet State of Aminofluorenone Derivatives. *J. Phys. Chem. A* **1998**, *102*, 3018–3024.
- Yoshihara, K. Spectroscopic Properties of the Lower-Lying Excited States of Fluorenone. *J. Chem. Phys.* **1966**, *45*, 1991.
- Yum, J.-H.; Hardin, B. E.; Moon, S.-J.; Baranoff, E.; Nüesch, F.; McGehee, M. D.; Grätzel, M.; Nazeeruddin, M. K. Panchromatic Response in Solid-State Dye-Sensitized Solar Cells Containing Phosphorescent Energy Relay Dyes. *Angew. Chemie Int. Ed.* **2009**, *48*, 9277–9280.
- Zhang, H.; Wang, S.; Li, Y.; Zhang, B.; Du, C.; Wan, X.; Chen, Y. Synthesis, Characterization, and Electroluminescent Properties of Star Shaped Donor–acceptor Dendrimers with Carbazole Dendrons as Peripheral Branches and Heterotriangulene as Central Core. *Tetrahedron* **2009**, *65*, 4455–4463.

- Zhang, J.; Yang, Y.; He, C.; He, Y.; Zhao, G.; Li, Y. Solution-Processable Star-Shaped Photovoltaic Organic Molecule with Triphenylamine Core and Benzothiadiazole–Thiophene Arms. *Macromolecules* **2009**, *42*, 7619–7622.
- Zhang, X.; Ji, X.; Jiang, S.; Liu, L.; Weeks, B. L.; Zhang, Z. Highly Efficient Synthesis of 9-Fluorenone from 9H-Fluorenes by Air Oxidation. *Green Chem.* **2011**, *13*, 1891–1896.
- Zhang, Z.; Wang, J. Structures and Properties of Conjugated Donor–Acceptor Copolymers for Solar Cell Applications. *J. Mater. Chem.* **2012**, *22*, 4178–4187.
- Zhao, K.-Q.; Chen, C.; Monobe, H.; Hu, P.; Wang, B.-Q.; Shimizu, Y. Three-Chain Truxene Discotic Liquid Crystal Showing High Charged Carrier Mobility. *Chem. Commun.* **2011**, *47*, 6290–6292.
- Zhao, Y.; Guo, Y.; Liu, Y. 25th Anniversary Article: Recent Advances in N-Type and Ambipolar Organic Field-Effect Transistors. *Adv. Mater.* **2013**, *25*, 5372–5391.
- Zhao, Y.; Truhlar, D. G. Density Functionals with Broad Applicability in Chemistry. *Acc. Chem. Res.* **2008**, *41*, 157–167.
- Zhao, Y.; Truhlar, D. G. The M06 Suite of Density Functionals for Main Group Thermochemistry, Thermochemical Kinetics, Noncovalent Interactions, Excited States, and Transition Elements: Two New Functionals and Systematic Testing of Four M06-Class Functionals and 12 Other Function. *Theor. Chem. Acc.* **2007**, *120*, 215–241.
- Zhou, H.; Yang, L.; You, W. Rational Design of High Performance Conjugated Polymers for Organic Solar Cells. *Macromolecules* **2012**, *45*, 607–632.
- Zimmerman, J. D.; Lassiter, B. E.; Xiao, X.; Sun, K.; Dolocan, A.; Gearba, R.; Vanden Bout, D. A.; Stevenson, K. J.; Wickramasinghe, P.; Thompson, M. E.; *et al.* Control of Interface Order by Inverse Quasi-Epitaxial Growth of Squaraine/Fullerene Thin Film Photovoltaics. *ACS Nano* **2013**, *7*, 9268–9275.
- Zyss, J. *Molecular Nonlinear Optics: Materials, Physics, and Devices*; Kelley, P.; Liao, P. F., Eds.; Academic Press: Boston, 1993.